Berkeley Seismological Laboratory

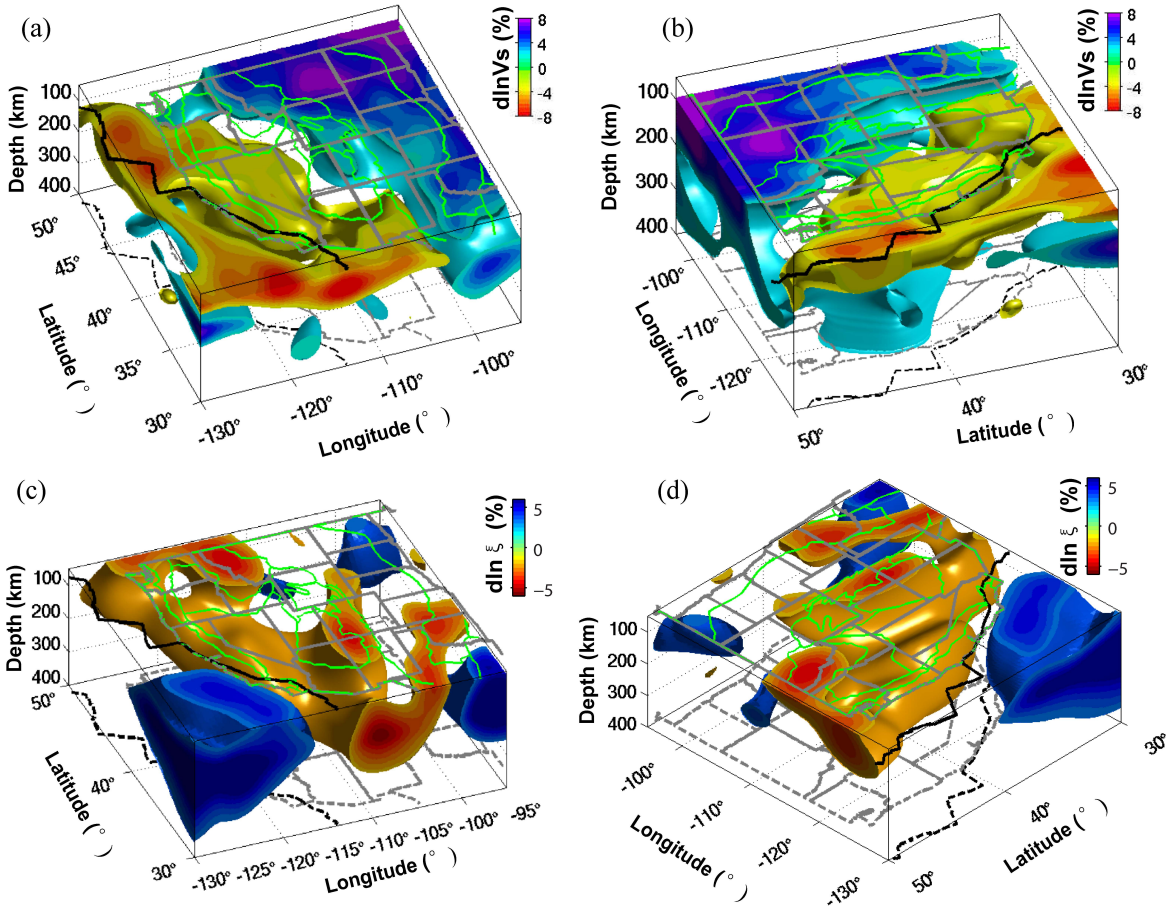

Annual Report
July 2009 - June 2010

Berkeley Seismological Laboratory

Annual Report

July 2009 - June 2010

Cover Picture

3-D rendering of the North American isotropic and radially anisotropic shear wave model *SVEMum_NA2* (Research Section 11) in the western US, viewing from the southwest (a and c), and the northwest (b and d). The velocity variations are with respect to the NA regional average. The isosurfaces in a) and b) are drawn at -1.5% and 3% for the slow and fast velocities, respectively. For radial anisotropy (c and d), the isosurface values are -2% and 4%. Green lines at the top of each plot indicate the western US physiographic regions. Thick black line is the plate boundary between the North American and the Pacific plates.

Contents

1 Director's Report **1**

1 Introduction . . . 1
2 History and Facilities . . . 1
3 BSL staff news . . . 3
4 Acknowledgements . . . 3

2 Research Studies **5**

1 Global Effective Elastic Thickness, Mechanical Anisotropy and the Supercontinent Cycle . . . 6
2 New Terrestrial LIDAR and Cosmogenic Radionuclide Constraints on the Little Lake Fault, Eastern California Shear Zone . . . 8
3 Using Geodetic Data to Understand Postseismic Processes following the Sumatra-Andaman Earthquake 10
4 Interseismic Creep on the Concord Fault from PS-InSAR and SBAS . . . 12
5 Probing the Deep Rheology of Tibet Constraints from 2008 M_w 7.9 Wenchuan, China Earthquake . . . 14
6 Tidal Triggering of LFEs near Parkfield, CA . . . 16
7 Monitoring Slow Moving Landslides in the Berkeley Hills with TerraSAR-X Data . . . 18
8 Slab-Plume Interaction Beneath the Pacific Northwest . . . 20
9 Imaging Shallow Cascadia Structure with Ambient Noise Tomography . . . 22
10 Anisotropic Layering of the North American Craton . . . 24
11 3-D Shear Wave Radially and Azimuthally Anisotropic Velocity Model of the North American Upper Mantle . . . 26
12 Depth Dependent Azimuthal Anisotropy in the Western US Upper Mantle . . . 28
13 Seismic Signature of Perovskite and Postperovskite in the D" . . . 30
14 Using the SEM to Simulate Random Wavefields and Improve Noise Tomography . . . 32
15 Toward the Future of Global Waveform Tomography: Scalable Gauss-Newton and Alternative Data-Partitioning Schemes . . . 34
16 Towards Constraining Lateral Variation of Attenuation Structure With Low-Degree Normal Modes Splitting Coefficients . . . 36
17 Efficient Computation of NACT Seismograms: Toward Application in Imagining Upper Mantle Discontinuities . . . 38
18 Modeling of the Byerly's False S Phase . . . 40
19 ShakeAlert: A Unified EEW System for California . . . 42
20 January 10, 2010 M_w6.5 Gorda Plate Earthquake: Automated Finite-Source Modeling . . . 44
21 Towards a Real-time Earthquake Source Determination and Tsunami Early Warning in Northern California . . . 46
22 Seismic Constraints on Fault-Zone Frictional Properties at Seismogenic Depth on the San Andreas Fault, Parkfield . . . 48
23 Postseismic Variations in Seismic Moment and Recurrence Interval of Repeating Earthquakes at Parkfield 50
24 Identification of Nonvolcanic Tremors Triggered by Regional Earthquakes in the Parkfield, California Region . . . 52
25 Locating Nonvolcanic Tremors Beneath the San Andreas Fault Using a Station-pair Double-Difference Location Method . . . 54

3 BSL Operations **57**
1 Berkeley Digital Seismic Network 59
2 California Integrated Seismic Network 67
3 Northern Hayward Fault Network 72
4 Parkfield Borehole Network (HRSN) 81
5 Bay Area Regional Deformation Network 91
6 Northern California Earthquake Data Center 97
7 Data Acquisition and Quality Control 107
8 Northern California Earthquake Monitoring 112
9 Outreach and Educational Activities 118

Glossary **120**

Appendix I Publications, Presentations, Awards, and Panels 2009-2010 **122**

Appendix II Seminar Speakers 2009-2010 **135**

Appendix III Organization Chart 2009-2010 **137**

Chapter 1

Director's Report

1 Introduction

As in previous years, I am pleased to introduce the 2009-10 Berkeley Seismological Laboratory Annual Report. This report covers two interrelated activities at BSL: basic research and real time earthquake monitoring operations. Chapter 2 describes the research accomplishments; Chapter 3 details progress in our development of infrastructure and facilities.

The basic research spans many topics in seismology and tectonics. They range from studies of the earth's deep structure and dynamics to various aspects of earthquake physics; from microearthquakes and tremor studies to studies of earthquake mechanisms and rupture spanning different times scales; and from slow tectonic deformation to real time seismology and earthquake early warning. These are described in 25 "two-page" contributions in Chapter 2 of this report. Highlights this year include a collection of studies at different scales of the upper mantle seismic isotropic and anisotropic structure beneath North America, taking advantage of the new broadband seismic dataset provided by the USArray component of the NSF funded national Earthscope program (Chapter 2, Research Sections 8, 9, 10, 12, and 11).

This year has been quite busy on the operational side of the BSL, owing to significant funding received through the USGS, in the framework of ARRA, to upgrade the recording systems at many of our broadband and borehole stations. We have already upgraded two-thirds of our broadband stations with state of the art Quanterra Q330 dataloggers, and we are starting to upgrade those at our borehole stations. These upgrades were much needed, as many of the recording systems were 15-20 years old, well beyond the expected lifetime of computer hardware. We have also received funding to upgrade receivers at our 26 BARD stations and to add GPS receivers at 7 of our existing BDSN stations. The new receivers will allow us to stream high rate (1Hz sampling) GPS data and to start implementing the use of GPS data in our real-time earthquake analysis procedures. Much effort has also gone into redesigning the data processing procedures and the web presentation for the continuous GPS data from the BARD network.

We have continued our involvement in the redesign of the STS-1 very broad band seismometer, under Metrozet's leadership, and with funding from the NSF EAR-Instruments and Facilities Program. The development phase is practically finished, and the new instruments are now being tested and fine-tuned not only at our Byerly Vault but also at Harvard (HRV) and the Albuquerque Seismological Laboratory.

The following sections give a brief historical overview of the BSL, and finally some BSL staff news.

2 History and Facilities

The Berkeley Seismological Laboratory (BSL), formerly the Berkeley Seismographic Stations (BSS), is the oldest Organized Research Unit (ORU) on the UC Berkeley campus. Its mission is unique in that, in addition to research and education in seismology and earthquake-related science, it is responsible for providing timely information on earthquakes (particularly those that occur in Northern and Central California) to the UC Berkeley constituency, to the general public, and to various local and state government and private organizations. The BSL is therefore both a research center and a facility/data resource, which sets it apart from most other ORUs. A major component of our activities is focused on developing and maintaining several regional observational networks, and participating, along with other agencies, in various aspects of the collection, analysis, archival, and distribution of data pertaining to earthquakes, while maintaining a vigorous research program on earthquake processes and Earth structure. In addition, the BSL staff spends considerable time on public relations activities, including tours, talks to public groups, responding to public inquiries about earthquakes, and, more recently, World-Wide-Web presence (`http://seismo.berkeley.edu/`).

UC Berkeley installed the first seismograph in the Western Hemisphere at Mount Hamilton (MHC) in 1887. Since then, it has played a leading role in the operation

of state-of-the-art seismic instruments and in the development of advanced methods for seismic data analysis and interpretation. Notably, the installation, starting in 1927, of Wood-Anderson seismographs at 4 locations in Northern California (BKS, ARC, MIN, and MHC) allowed the accurate determination of local earthquake magnitude (M_L) from which a unique historical catalog of regional earthquakes has been maintained to this day, providing crucial input to earthquake probabilities studies.

Over the years, the BSS continued to keep apace of technological improvements. The first centrally telemetered network using phone lines in an active seismic region was installed by BSS in 1960. The BSS was the first institution in California to operate a 3-component "broadband" system (1963). It played a major role in the early characterization of earthquake sources using "moment tensors" and source-time functions. The BSS also made important contributions to the early definitions of detection/discrimination of underground nuclear tests and, jointly with UCB Engineering, to earthquake hazards work. Starting in 1986, the BSS acquired 4 state-of-the-art broadband instruments (STS-1), while simultaneously developing PC-based digital telemetry, albeit with limited resources. As telecommunication and computer technologies made rapid progress, in parallel with broadband instrument development, paper record reading was completely abandoned in favor of largely automated analysis of digital data.

The current facilities of BSL have been built progressively over the last two decades, efforts initiated by significant "upgrade" funding from UC Berkeley in 1991-1995. The BSL currently operates and acquires data, continuously and in real-time, from over 60 regional observatories. These house a combination of broadband and strong motion seismic instrumentation installed in vaults, borehole seismic instrumentation, the permanent GPS stations of the Bay Area Regional Deformation (BARD) network, and electromagnetic sensors. The seismic data are fed into the BSL real-time processing and analysis system. Since 1996, they are used in conjunction with data from the USGS NCSN network in the joint earthquake notification program for Northern California. This program capitalizes on the complementary capabilities of the networks operated by each institution to provide rapid and reliable information on the location, size and other relevant source parameters of regional earthquakes. In recent years, a major emphasis in BSL instrumentation has been in densifying the state-of-the-art seismic and geodetic networks. At the same time, research efforts have been directed toward the development of robust methods for quasi-real time, automatic determination of earthquake source parameters and predicted strong ground motion, using a sparse network combining broadband and strong motion seismic sensors, as well as permanent geodetic GPS receivers. Recently, research emphasis has been directed toward the development of "earthquake early warning" capabilities

The Berkeley Digital Seismic Network (BDSN), a regional network of 32 digital broadband and strong motion seismic stations with continuous telemetry to UC Berkeley, is the backbone of the BSL operations. This network contributes basic regional data for real-time estimation of location, size and rupture parameters for earthquakes in Central and Northern California. It is the Berkeley contribution to the California Integrated Seismic Network (CISN). In June 2009, our operational software, the Rapid Eathquake Data Integration (REDI) program, was replaced by the CISN, now AQMS, software (see Chapter 3, Operational Section 8). The data from the BDSN also provide a fundamental database for the investigation of three-dimensional crustal structure and its effects on regional seismic wave propagation. This is ultimately crucial for estimating ground shaking for future earthquakes. Most stations also record auxiliary temperature/pressure channels, valuable in particular for background noise quality control. Complementing this network is a ~ 25 station "high-resolution" network of borehole seismic sensors located along the Hayward Fault (HFN) and under the Bay Area bridges, operated jointly with the USGS/Menlo Park and linked to the Bridge Safety Project of the California Department of Transportation (Caltrans). The latter has facilitated the installation of sensor packages at 15 bedrock boreholes along 5 East Bay bridges in collaboration with Lawrence Livermore National Laboratory (LLNL). A major science goal of this network is to collect high signal-to-noise data for micro-earthquakes along the Hayward Fault to gain insight into the physics that govern fault rupture and its nucleation. The BSL also operates and maintains the 13 element Parkfield borehole seismic array (HRSN). This array provides high quality data on micro-earthquakes, clusters and most recently tremors, and is an important reference for the San Andreas Fault Observatory at Depth (SAFOD). Since April 2002, the BSL collaborates with MBARI on the operation of a permanent broadband ocean bottom station, MOBB.

In addition to the seismic networks, the BSL operates, maintains and processes data from the 26 permanent geodetic stations of the BARD Network. It archives and distributes this data as well. Where possible, BARD sites are collocated with BDSN sites to minimize telemetry costs. In particular, sites are progressively being upgraded to 1 Hz sampling. This will support one focus of BSL research, the development of analysis methods which combine seismic and geodetic data to rapidly estimate source parameters of significant earthquakes.

Finally, two of the BDSN stations (PKD, SAO) also share data acquisition and telemetry with 5-component electromagnetic sensors installed with the goal of investi-

gating the possibility of detection of tectonic signals. In 2002-2003, automated quality control software was implemented to monitor the electromagnetic data.

Archival and distribution of data from these and other regional networks is performed at the Northern California Earthquake Data Center (NCEDC), operated at the BSL in collaboration with USGS/Menlo Park. The data reside on a mass-storage device (current holdings $\sim$ 50 terabytes), and are accessible "on-line" over the Internet (`http://www.ncedc.org`). Among others, data from the USGS Northern California Seismic Network (NCSN), are archived and distributed through the NCEDC. The NCEDC also maintains, archives and distributes the ANSS earthquake catalog.

Core University funding to our ORU has until now provided salary support for one staff scientist and several technical and administrative staff members, representing about 30% of the total infrastructure support. The remaining support comes from extra-mural grants and contracts, primarily from the USGS, NSF, and the State of California, through its Emergency Management Agency (CalEMA, formerly OES). We acknowledge valuable recent contributions from other sources such as Caltrans and PEER, as well as our Earthquake Research Affiliates. The effects of drastic budget cuts in FY09-10 are temporarily being offset by ARRA funding from the USGS.

3 BSL staff news

Changes in BSL staff in 2009-10 are as follows.

In the past year, the following graduate students associated with BSL completed their PhD's: Ved Lekic graduated in December 2009 and joined Brown University in May on an NSF post-doctoral fellowship. Trey Apel completed his doctorate in April 2010, and Gilead Wurman in May 2010. They are now working in industry at AMEC Geomatrix and Seismic Warning Systems, respectively.

There has been one new arrival: Andrea Chiang joined the BSL as a graduate student in the Fall of 2010.

BSL hosted the following visiting scientists in 09-10: Dr. Joshi Karra from the National Geophysical Research Institute, Hyderabad, India, and Yann Capdeville, from IPGP in France.

As a result of a campus-wide reorganization of the research administration of Organized Research Units, our four administrative staff were laid off, effective November 30, 2009. Tina and Yolanda were rehired at RES (Research Enterprise Services), the agency which provided business administration for BSL from December 2009 thru June 2010. After a brief sojourn at RES, Kristen Jensen, our former manager, joined EFA. They are very fortunate to have her! All three have been outstanding members of the BSL team, and we are sorry to see them go despite all our efforts. Fortunately, we were able to rehire Kate Lewis in March 2010 as Executive Assistant, to coordinate the programmatic aspects of BSL administration during the RES tenure. Kate has also played a major role in helping organize the 6 week long CIDER-2010 summer program in Santa Barbara, CA (`http:/www.deep-earth.org/summer10.html`) and the international SEDI 2010 symposium that followed from July 18-23, 2010. Since July 2010, BSL administration has been consolidated with that of the Earth and Planetary Science department, and Kate is now in charge of the coordination of all funds and transactions related to the BSL operations, as well as handling many everyday tasks while we wait for the hire of two additional administrative staff, jointly with EPS.

Finally, Rick McKenzie retired in June 2010. We miss him!

The greater BSL family has continued to grow in the past year, with the arrival of Audrey Lewis in October 2009. She was followed by Freeman McCarty and Arieh Wurman-Fenton in November 2009, Henry Allen in April 2010, and Rebekah Zheng in June 2010.

4 Acknowledgements

I wish to thank our technical and administrative staff, scientists and students for their efforts throughout the year and their contributions to this Annual Report. Individual contributions to activities and report preparation are mentioned in the corresponding sections, except for the Appendix section, which was prepared by Jennifer Taggart.

I also wish to specially thank the individuals who have regularly contributed to the smooth operation of the BSL facilities: Mario Aranha, Rich Clymer, Doug Dreger, John Friday, Jarrett Gardner, Peggy Hellweg, Ingrid Johanson, Bill Karavas, Oleg Khainovski, Rick Lellinger, Pete Lombard, Rick McKenzie, Bob Nadeau, Doug Neuhauser, Charley Paffenbarger, Jennifer Taggart, Taka'aki Taira, Bob Uhrhammer, and Stephane Zuzlewski, and in the administrative office, Kristen Jensen, Kate Lewis, Tina Barber-Riggins, and Yolanda Andrade. I also wish to thank our undergraduate assistants, Chris Rawles, Danny Feucht, Josef Matlak, Eric Winchell, and Amanda Truyol, for their contributions to our research and operations activities.

I am particularly grateful to Jennifer Taggart and Peggy Hellweg for their help in putting together this Annual Report and bringing it to completion.

The Annual Report of the Berkeley Seismological Laboratory is available on the Web at `http://seismo.berkeley.edu/annual_report`.

Chapter 2

Research Studies

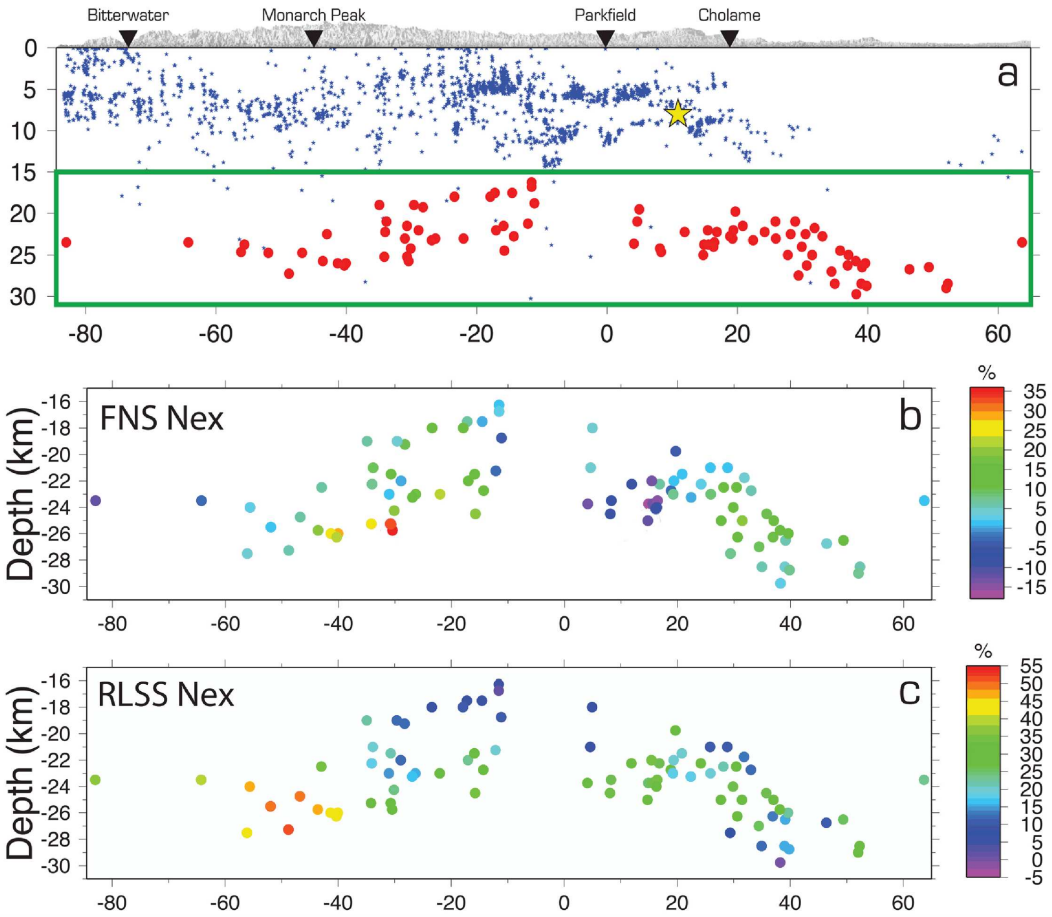

Figure 2.1: (a) Along-fault cross section of the SAF viewed from the south-west. Vertically exaggerated topography is shown in grey. Local towns are marked by inverted triangles. Hypocenters of SAF seismicity, the 2004 Parkfield earthquake, and LFE locations are shown as blue dots, yellow star, and red circles respectively. Panels (b) and (c) are delineated by the green box. (b) LFE locations color coded by their FNS Nex (percent excess = [actual number of LFEs during times of positive FNS - expected number of LFEs during times of positive FNS]/expected number of LFEs during times of positive FNS). (c) LFE locations color coded by the RLSS Nex values. (Figure from Research Section 6)

1 Global Effective Elastic Thickness, Mechanical Anisotropy and the Supercontinent Cycle

Pascal Audet and Roland Bürgmann

1.1 Introduction

The Earth experienced several supercontinent cycles since 2.7 Ga, the last one ending with the breakup of Pangaea into the current plate configuration. The driving mechanism is associated with vertical motion of the convective mantle from both subduction of ocean basins during supercontinent assembly and warm mantle upwelling causing breakup and the creation of new ocean floor (*Gurnis*, 1988). Although the details of the dynamics are still debated, it is generally agreed that continental margins are repeatedly deformed within weak, diffuse zones, and that stronger cratonic lithosphere remains intact during this process. Most cratonic cores within continents show crustal ages greater than 2.0 Gyr, are depleted in basaltic constituents, and have conductively cooled through time, thus acquiring a thick, high-viscosity thermo-chemical root (*Jordan*, 1978). Continental margins, in contrast, are much younger ($<$ 0.5 Gyr), have been thermally rejuvenated and structurally reactivated, and are much thinner. Such large differences in structure imply comparably large gradients in rheological properties of the lithosphere. These factors, combined with numerical simulations of coupled mantle convection and continental plates, suggest that deformation during supercontinent cycles is controlled by pre-existing structure acquired from past tectonic events. There is little observational constraint, however, on the spatial variability of rheological properties of the lithosphere because it cannot be observed directly.

1.2 Method

A useful proxy for the the long-term strength of the lithosphere is given by the flexural rigidity, $D = ET_e/12(1-\nu^2)$, where E is Young's modulus and ν is Poisson's ratio, which governs the resistance to flexure (*Watts*, 2001). The strong dependence of D on T_e implies that the magnitude and spatial variations of T_e can have a significant influence on the degree and style of deformation due to long-term tectonic loads. In particular, it is expected that spatial variations and gradients in T_e can prescribe where strain may localize and consequently determine the locus of deformation as manifested by brittle (e.g. seismicity, faulting) and thermal processes (e.g. volcanism, rifting). T_e is estimated by comparing the spectral coherence between topography and Bouguer gravity anomalies with that predicted for an equivalent elastic plate bending under surface and internal loading. The plate response is modeled either as isotropic or anisotropic, and the coherence is inverted for a single parameter, T_e, or the three parameters of an orthotropic elastic plate (i.e. having different rigidities in two perpendicular directions), T_{min}, T_{max}, and ϕ_e, the direction of weakest rigidity. Here we use the wavelet transform method to calculate the coherence and estimate T_e and T_e anisotropy (*Audet and Mareschal*, 2007) and apply the technique to all major continents, with the exception of Greenland and Antarctica where thick ice caps complicate the analysis and data coverage is incomplete. We account for possible bias in T_e estimation by considering the effect of gravitational "noise" and masking regions where the model fails.

1.3 Results

Figure 2.2 shows the azimuthal variations of the weak direction of T_e superposed on the pattern of T_e variations. In general, the T_e pattern correlates with age since the last thermo-tectonic event. T_e is high ($>$ 100 km) in Early to Late Proterozoic and Archean cratonic provinces, with the largest values found in the North American, West African, and East European shields. Some cratons (e.g. South Africa, North China, South India) exhibit lower T_e ($50 < T_e < 100$ km) where lithosphere has been thinned by plume-related magmatism or delamination. Low T_e ($<$ 40 km) is found in young Phanerozoic orogens (e.g. American Cordillera, Alpide belt) and tectonically active provinces (e.g. western North America, Afar Triple Junction and most of central-eastern Asia). T_e is also generally low in the hanging wall of past and present subduction zones and along most continental margins, possibly due to thermal and fluid-related weakening as a consequence of subduction and rifting processes. T_e anisotropy varies over short spatial scales ($\sim 200-500$ km) in both magnitude and direction (Figure 2.2), thus ruling out a deep, sub-lithospheric mantle-flow origin. Magnitude of T_e anisotropy is inversely correlated with T_e as young, low-T_e provinces display larger magnitude than older, high-T_e cratons. Directions of weak rigidity are oriented normal to most continental margins and tectonic boundaries. T_e anisotropy reflects directional variations in the flexural compensation of the lithosphere and has been speculated to originate from either dynamical or structural effects.

These results allow us to clarify the role of rheological heterogeneity and mechanical anisotropy in continental evolution and deformation. That T_e varies according to age since the last thermo-tectonic event and is parti-

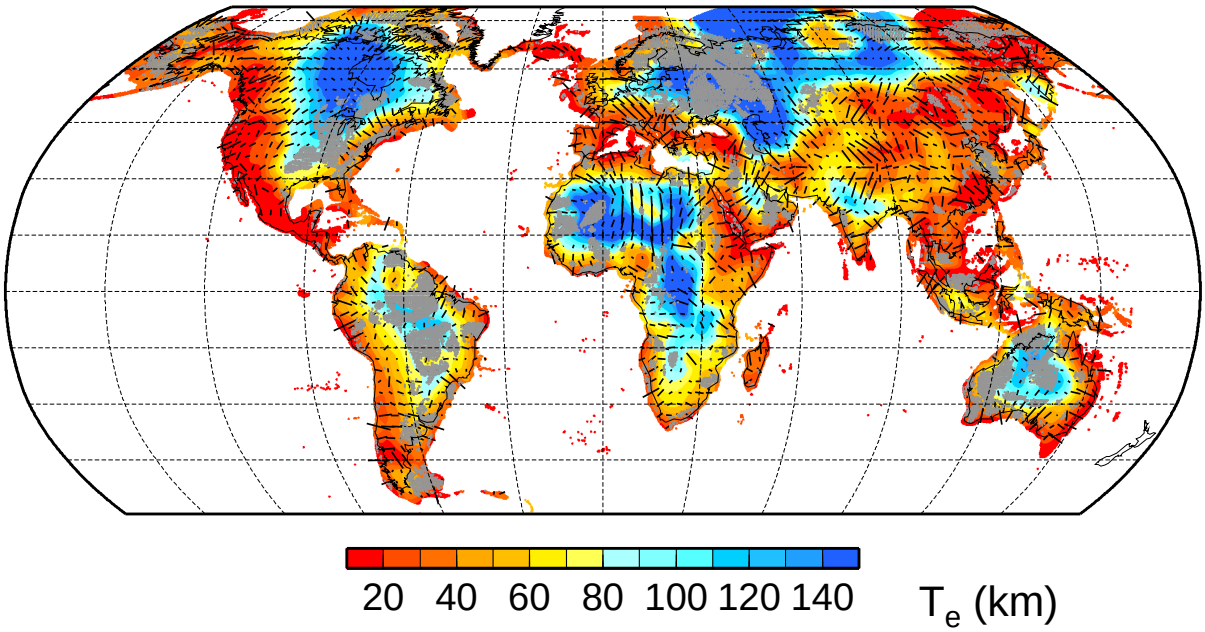

Figure 2.2: Global effective elastic thickness over continents calculated from the coherence between Bouguer gravity and topography using a wavelet transform. T_e anisotropy (sampled on a $3° \times 3°$ grid) is superposed on filtered (using a Gaussian function of width 900 km) and color-contoured T_e over continents and continental shelves (depth shallower than 500 m below sea level). Shaded areas correspond to regions where T_e estimation is biased by gravitational "noise." The length of black bars is given by the magnitude of T_e anisotropy from the ratio $(T_{max} - T_{min})/(T_{max} - T_{min})$.

tioned between continental cores and margins is consistent with the episodic thermal rejuvenation of continental margins and resetting of lithosphere strength during thermo-tectonic events. These episodes originate from large-scale vertical convective motion of the mantle during continental assembly and breakup and are accompanied by margin-wide faulting and fault reactivation (either from rifting or thrusting) that further weakens marginal lithosphere and induces significant mechanical anisotropy. A weak and faulted lithosphere may enhance deformation by concentrating strain at pre-existing structures. Over time, these factors isolate continental interiors from deformation due to plate boundary forces during continental assembly, thus creating positive feedback and allowing only a small fraction of continental lithosphere to be recycled. Only in rare cases do plumes or delamination events de-stabilize cratonic cores. This model is consistent with numerical models of continental evolution that simulate the stability of cratonic crust and longevity of deeper roots as a consequence of higher yield strength with respect to oceanic lithosphere, and the buffering effect of weak mobile belts and margins that absorb stresses during repeated supercontinent cycles. This, in turn, implies that the inherited weakness of marginal lithosphere is relatively long-lived, despite its tendency to get recycled into the mantle during orogeny, possibly due to continuous accretion of terranes and plateaus that further enhances mechanical weakness and anisotropy.

1.4 Acknowledgements

This work was funded by the Miller Institute for Basic Research in Science (UC Berkeley).

1.5 References

Audet, P., and J.-C. Mareschal, Wavelet analysis of the coherence between gravity and topography: Application to the elastic thickness anisotropy in the Canadian Shield, *Geophys. J. Int., 168*, 287-298, 2007.

Gurnis, M. Large-scale mantle convection and the aggregation and dispersal of supercontinents, *Nature, 332*, 695-699, 1988.

Jordan, T. H., Composition and development of the continental tectosphere, *Nature, 274*, 544-548, 1978.

Watts, A. B., Isostasy and Flexure of the lithosphere, Cambridge University Press, Cambridge, UK, 2001.

2 New Terrestrial LIDAR and Cosmogenic Radionuclide Constraints on the Little Lake Fault, Eastern California Shear Zone

Colin Amos, Roland Bürgmann, G. Burch Fisher (UCSB), Dylan Rood (LLNL), Angela Jayko (USGS)

2.1 Introduction

An ever-expanding inventory of fault slip-rates spanning various time intervals reveals contrasting spatial and temporal patterns of strain for active faults within the eastern California shear zone (ECSZ). Comparison of these data, derived from geologic, geomorphic, and paleoseismic records, with geodetic estimates of fault loading affords unparalleled opportunity to investigate the dynamics of earthquake processes and the evolution of an intracontinental plate boundary fault system. This work focuses on the Little Lake fault, which occurs along the western margin of the ECSZ between the Sierra Nevada and the Coso Range in east-central California. The fault accommodates 10-20% of the total dextral motion within the ECSZ at this latitude and a smaller fraction of the relative motion between the Pacific and North American plates. Relatively high rates of decadal fault loading described for the Little Lake fault zone from GPS measurements and InSAR data (7 ± 3 mm/yr; *Peltzer et al.*, 2001) suggest potential discrepancies with longer, late Quaternary records of geologic strain. To address this inconsistency, we targeted a series of previously unrecognized fluvial terraces related to overtopping and outflow from pluvial Owens Lake that cross the fault and record dextral offset since Late-Pleistocene time.

2.2 Methods

Geologic constraints on displaced Quaternary geomorphic features along the Little Lake fault zone come from geologic and geomorphic mapping and high-resolution digital topography collected using a Riegl LMS-Z420i terrestrial laser scanner (TLS).

Constraints on the age of offset terrace surfaces and risers come from cosmogenic ^{10}Be samples (currently being processed) from intact, meter-scale outwash boulders preserved on terrace treads bounding each riser. Slip rates were computed using the methods and code outlined by *Zechar and Frankel* (2009) from probability distributions of displacement and correlated surface age.

2.3 Findings

Initial results from TLS measurements of Late-Pleistocene geomorphic surfaces on the Little Lake fault zone suggest between 33 and 38 m of reconstructed right-lateral displacement over this time period. Preliminary correlation of terrace surfaces with exposure dating of fluvially scoured basalt upstream at Fossil Falls (∼16 ka; *Cerling*, 1990) suggests a right-lateral displacement-rate on the order of ∼2 mm/yr at 95% confidence.

Although more than double the previously reported rate estimate ($\geq$ 1 mm/yr; *Roquemore*, 1988) based on older, poorly constrained basalt flows, this result tentatively suggests that decadal rates of loading ($\leq \sim 5$ mm/yr) on the Little Lake fault zone are not sustained geologically over the ∼10,000 year timescale. Future work will explore the implications of this rate variation for the ECSZ and fault networks in general.

2.4 Acknowledgements

This work is supported by NSF award EAR 0847990 to Amos.

2.5 References

Cerling, T.E., Dating geomorphologic surfaces using cosmogenic He-3: *Quaternary Research, 33(2)*, 148-156, 1990.

Peltzer, G., Crampe, F., Hensley, S., and Rosen, P., Transient strain accumulation and fault interaction in the Eastern California shear zone: *Geology 29(11)*, 975-978, 2001.

Roquemore, G.R., Revised estimates of the slip rate on the Little Lake fault, California: *Geological Society of America Abstracts with Programs, 20(3)*, 225, 1988.

Zechar, J.D., and Frankel, K.L., 2009, Incorporating and reporting uncertainties in fault slip rates: *Journal of Geophysical Research-Solid Earth, 114*, DOI 10.1029/2009JB006325.

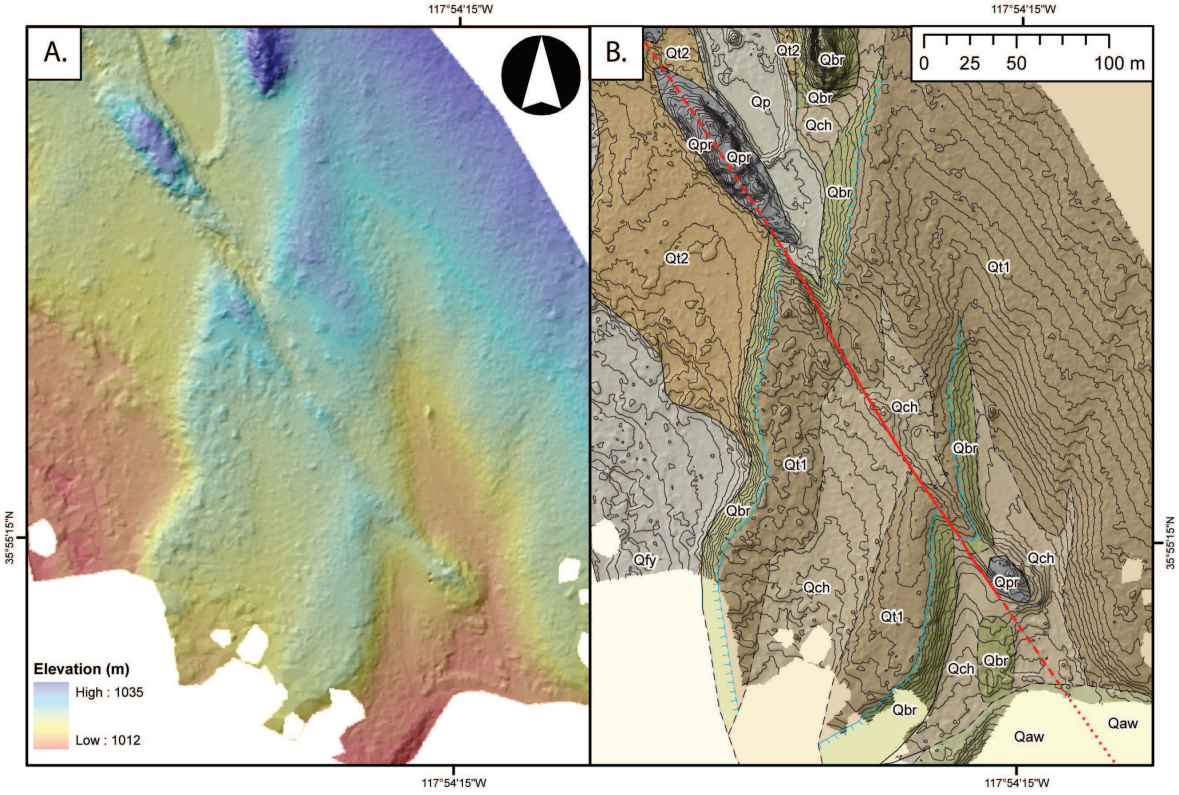

Figure 2.3: A) 50-cm DEM of lower Little Lake wash overlain on a hillshade image, both computed from high-resolution terrestrial laser scanning (TLS) surveys. B) Geologic mapping and 50-cm elevation contours of the same area as (A), highlighting right-lateral displacement of the Qt1/Qt2 terrace riser by the Little Lake fault.

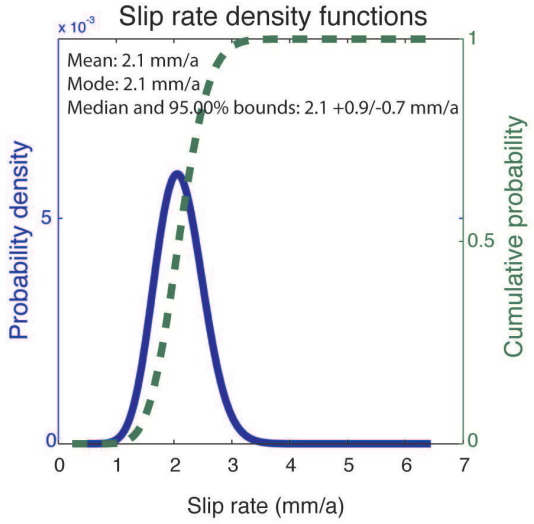

Figure 2.4: Probability density functions of fault slip rates computed from offset terrace risers and cosmogenic age constraints at Fossil Falls (*Cerling*, 1990).

3 Using Geodetic Data to Understand Postseismic Processes following the Sumatra-Andaman Earthquake

Kelly Grijalva, Roland Bürgmann, and Paramesh Banerjee (Earth Observatory of Singapore)

3.1 Introduction

Investigations of postseismic deformation are often plagued by ambiguities between fundamental deformation mechanisms that can be expected to contribute to the deformation, including viscous flow, localized afterslip and poroelastic rebound. Previous studies have explained the near-field postseismic deformation following the Sumatra-Andaman earthquake with afterslip or poroelastic rebound, and the far-field postseismic deformation with viscoelastic relaxation from both the 2004 M_w 9.2 and 2005 M_w 8.7 events. We aim to fit both the near and far-field data, spanning years 2005-2007, with a combination of postseismic mechanisms. We utilize campaign GPS data from *Gahalaut et al.* (2008) and continuous GPS data from the regional networks: NICT, SuGAr, and THAI.

3.2 Poroelastic Rebound

The strain field resulting from a coseismic dislocation produces changes in pore fluid pressure in the brittle upper crust. The subsequent decay of the excess pore-fluid-pressure gradients will lead to fluid flow and poroelastic deformation. We approximate the fully relaxed poroelastic response by subtracting the undrained solution for coseismic deformation from the drained solution for coseismic deformation. Based on earlier studies (e.g. *Masterlark*, 2003), the crust is assumed to be fluid-saturated down to 15 km depth. However, *Ogawa and Heki* (2007) propose that the downgoing slab releases fluids into the mantle wedge in sufficiently high quantities, with sufficiently large pore pressure diffusivities, to contribute to the poroelastic rebound during the early postseismic period. We therefore test a range of earth models, with undrained Poisson's ratio values 0.05 above the drained value for the top 15 km to 60 km of the lithosphere (Figure 2.5a).

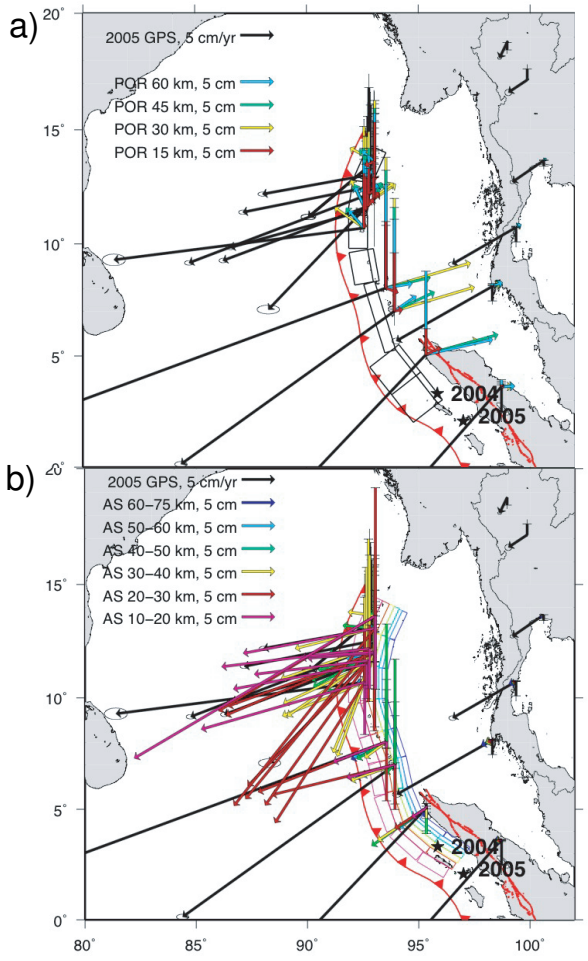

Figure 2.5: a) Modeled surface deformation due to a) poroelastic rebound and b) afterslip on the Sunda megathrust. The modeled displacements are compared with geodetic measurements over the year 2005.

3.3 Afterslip

We test afterslip models that range in depth from 10 km to 75 km, spanning the coseismic rupture planes and the downdip portion of the megathrust (Figure 2.5b). In general, the horizontal deformation is oriented towards the trench and magnitude of the deformation in the far-field increases with increased afterslip plane depth. When the afterslip plane is placed trenchward of the GPS site, there is vertical subsidence. Conversely, when the GPS site is located trenchward of the afterslip plane, there is vertical uplift. Afterslip can be optimized to fit the near-field vertical and horizontal data with 1-2 m of slip. However, in order to fit the far-field sites in Thailand, it is necessary to have approximately 10 m of afterslip at 60-75 km depth.

3.4 Viscoelastic Relaxation

Deep-seated transient postseismic relaxation can produce time dependent deformation exceeding that from the earthquake itself in the intermediate-to-far field

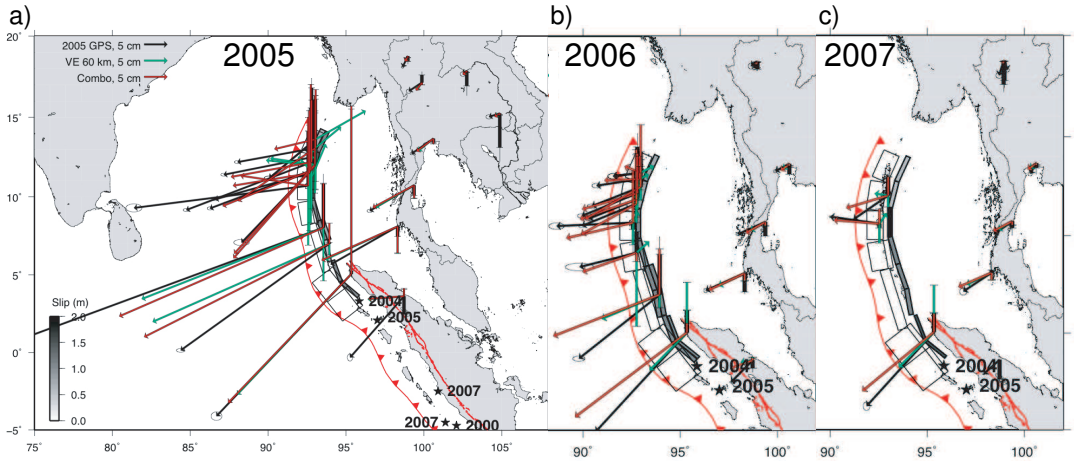

Figure 2.6: Comparison of a) 2005, b) 2006, and c) 2007 geodetic data with the preferred viscoelastic relaxation model and a combination model. The coseismic rupture planes for the Sumatra-Andaman earthquake are outlined in black (*Banerjee et al.*, 2007).

range. We test a range of earth models with the lithosphere-asthenosphere boundary (LAB) increasing from 50 km to 80 km in depth. Increasing the LAB decreases the magnitude of the surface deformation. The viscoelastic models can be optimized to fit the far-field data, but they poorly fit the near-field data. Our preferred LAB is 60 km because it is similar to previously published results (*Pollitz et al.*, 2006) and the subsidence in the Nicobar Islands helps to offset the modeled uplift from poroelastic rebound and afterslip. We find that our viscoelastic model fits the rate of decay at the Thai sites best with a transient asthenospheric viscosity of $2.5x10^{17}$ Pa s and a steady-state viscosity of $5x10^{18}$ Pa s.

3.5 Discussion

We discovered that the vertical component is more important than the horizontal component for diagnosing the near-field postseismic processes. For the Sumatra-Andaman earthquake, poroelastic rebound always has uplift in the near-field, afterslip can have either uplift or subsidence depending on the slip location, and viscoelastic relaxation always has both uplift and subsidence. Our preferred postseismic model for 2005 includes a combination of the 15 km-poroelastic rebound model, the 60 km-viscoelastic relaxation model, and between 0.5-1.5 m of afterslip (Figure 2.6a). For 2006 and 2007, we did not include poroelastic rebound in our preferred combination model. The 2006 combination model includes between 0.7-1.0 m of afterslip (Figure 2.6b) and the sparser 2007 data suggest that the afterslip location is continuing further downdip along the megathrust with cumulative slip magnitude of between 0.5-2.0 m (Figure 2.6c). The afterslip magnitude does not appear to have decayed significantly during our observation period from 2005-2007. Overall, we find that the near-field and far-field data can not be fit by just one postseismic process and the vertical component is especially necessary for properly diagnosing the near-field postseismic deformation.

3.6 Acknowledgments

This work is supported by the National Science Foundation grant EAR 0738299. The GPS data is provided by the Tectonics Observatory, LIPI and SOPAC. The modeling programs are provided by Fred Pollitz.

3.7 References

Banerjee et al., Coseismic slip distributions of the 26 December 2004 Sumatra-Andaman and 28 March 2005 Nias earthquakes from GPS static offsets, *Bull. Seism. Soc. Am.*, *97*, S86-S102, 2007.

Gahalaut et al., GPS measurements of postseismic deformation in the Andaman-Nicobar region following the giant 2004 Sumatra-Andaman earthquake, *J. Geophys. Res.*, *113*, 10.1029/2007JB005511, 2008.

Masterlark, T., Finite element model predictions of static deformation from dislocation sources in a subduction zone: Sensitivities to homogenous isotropic, Poisson-solid, and half-space assumptions, *J. Geophys. Res.*, *108*, doi:10.1029/2002JB002296, 2003.

Ogawa, R. and K. Heli, Slow postseismic recovery of geoid depression formed by the 2004 Sumatra-Andaman Earthquake by mantle water diffusion, *Geophys. Res. Lett.*, *34*, doi:10.1029/2007/GL029340, 2007.

Pollitz et al., Post-seismic relaxation following the great 2004 Sumatra-Andaman earthquake on a compressible self-gravitating Earth, *Geophys. J. Int.*, *167*, 397-420, 2006.

4 Interseismic Creep on the Concord Fault from PS-InSAR and SBAS

Ingrid Johanson, Roland Bürgmann, Alessandro Ferretti (TRE, Milan) and Fabrizio Novali (TRE, Milan)

4.1 Introduction

The Concord fault (CF) is part of the San Andreas fault (SAF) system in California's San Francisco Bay Area. Its long-term slip rate of 7 ± 2 mm/yr (geodetically determined) represents about one-fifth of the total SAF system rate. The Concord fault also creeps at a rate of 2.5-3.5 mm/yr, determined from measurements at two alinement arrays (*McFarland et al.*, 2009). The alinement arrays also showed time-variable slip, with creep events occurring every 3-5 years. Measuring creep and its variability on the CF is important, not just for understanding the fault's earthquake potential, but also because it may give us insight into how slip is transferred onto the Concord fault. The similarity in creep rate between the Northern Calaveras Fault (NCF) and CF, noted by *Galehouse and Lienkamper* (2003) is one line of evidence for linking the two.

We use PS-InSAR (Permanent Scatterer Interferometric Synthetic Aperture Radar) and the SBAS (Small Baseline Subset) technique to construct time series of ground motion around the CF and measure the creep rate along several profiles (Figure 2.7). The analysis is possible because of the extensive set of ERS data available through the WInSAR and GeoEarthScope archives. The PS-InSAR method identifies and integrates individual points that act like point scatterers and have stable phase measurements in a set of interferograms with a common master scene (starting date) (*Ferretti et al.*, 2001) . The SBAS technique uses a set of interferograms with various master and slave scenes and provides time series of deformation at any consistently coherent pixel (*Berardino*, 2002).

4.2 Measuring creep from InSAR time series

We use 2 PS-InSAR datasets from descending tracks 70 and 342 from the European Space Agency's ERS1 & 2 satellites, using 46 and 30 acquisitions, respectively, and spanning from 1992 through 2001. The data were processed using the PS-InSAR method of *Ferretti et al.* (2001) to produce time series of range change (change in distance between the ground and satellite) for each point as shown in Figure 2.7B & C. We also use a set of 22 ERS scenes from ascending track 478, arranged into a time series using the SBAS technique (Figure 2.7D).

To measure creep on the Concord fault, we look at motion along several profiles crossing the Concord fault. We use swath averaging to construct a profile at each time step of the InSAR time series (e.g. Figure 2.8).

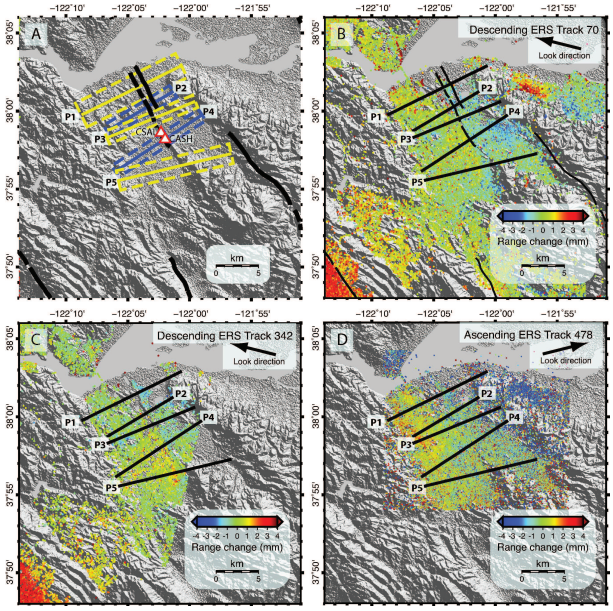

Figure 2.7: Overview map showing mean velocity of each PS-InSAR and SBAS dataset (B,C,D). Dashed boxes in subfigure A are the areas included in the swath averages, which are then projected onto the solid black centerlines. White triangles are alinement arrays CSAL and CASH.

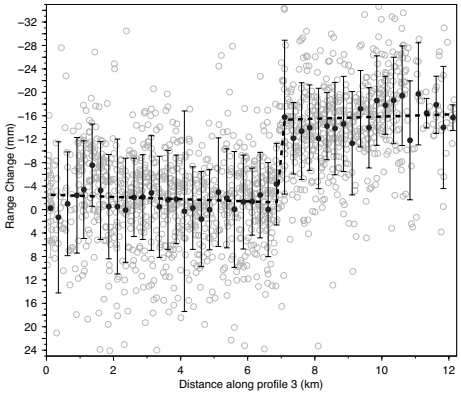

Figure 2.8: An example of a swath average profile for descending Track 70. Grey circles are the actual PS-InSAR points within the swath. Black circles are the calculated swath averages, with one sigma error bars. The dashed black line and offset is fit to the data by minimizing the least-squares residuals.

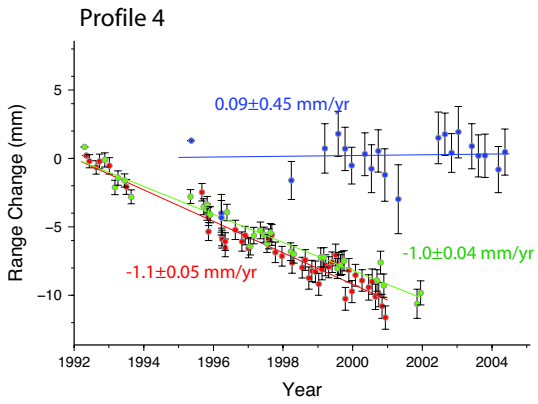

Figure 2.9: Range change across the trace of the Concord fault through time for all three datasets for one profile. Track 70 is shown in red, track 342 in green and track 478 is shown in blue. The secular creep rate as determined from a weighted linear inversion is printed next to each series.

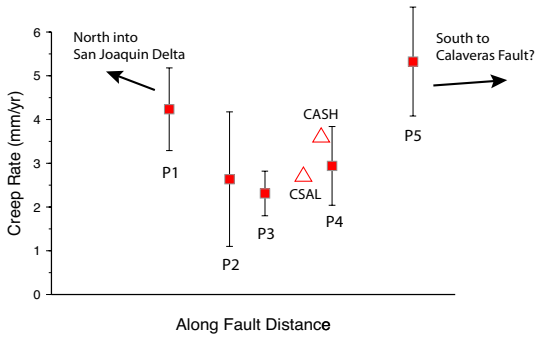

Figure 2.10: Calculated creep rates at each profile are shown according to their location along strike (red squares). Creep rates from alinement array measurements are shown as triangles.

Within each swath, shown as dashed lines in Figure 2.7A, points within 0.25 km bins perpendicular to the fault are averaged together and projected onto the centerline. For example, all points between 0.5 and 0.75 km west of the fault are averaged together to provide one point on the profile, and their standard deviation provides an estimate of the profile point's uncertainty.

A swath average profile is constructed for all acquisition dates in the three datasets and on each of the five profiles, for a total of 490 profiles. A linear inversion is performed on each profile to obtain the offset at the fault trace, produced by the shallowly creeping fault (dashed line in Figure 2.8). Each offset value represents the amount of creep on the Concord fault since the beginning of the time series.

4.3 Long-term creep rates

By fitting a line to the offsets, we can obtain a measurement of the secular range change rate at each profile (Figure 2.9). Using multiple viewing geometries (descending and ascending tracks) allows us to uniquely separate the range change into horizontal and vertical components. We assume horizontal motions are due to fault creep (Figure 2.10) and vertical motions represent hydrologic processes. All horizontal motion is taken to be parallel to the local strike of the Concord fault at each profile, as would be the case for pure strike-slip. The inversion of fault creep rate (V_{SS}) is set up as shown below.

$$RC = V_{SS}\left[\sin^2\theta\cos\alpha + \cos\theta\sin\theta\sin\alpha\right] + V_V\left[\cos\theta\right]$$

$$RC = V_{SS}G_{SS} + V_V G_V$$

$$\begin{bmatrix} V_{SS} \\ V_V \end{bmatrix} = \begin{bmatrix} G_{SS\ T70} & G_{V\ T70} \\ G_{SS\ T342} & G_{V\ T324} \\ G_{SS\ T478} & G_{V\ T478} \end{bmatrix}^{-1} \begin{bmatrix} RC_{T70} \\ RC_{T342} \\ RC_{T478} \end{bmatrix} \tag{2.1}$$

The results for secular creep-rate (V_{SS}) for each profile are shown in Figure 2.10. The results are very consistent with the long-term creep rates obtained from the alinement array surveys. It would appear that creep rates increase toward the ends of the Concord fault trace; however all the creep rate measurements from InSAR profiles are within uncertainty of the alinement array derived rates (2.5-3.5 mm/yr).

4.4 References

Berardino, P., G. Fornaro, R. Lanari, and E. Sansosti, A new algorithm for surface deformation monitoring based on small baseline differential SAR interferograms. *IEEE Trans. Geo. Rem. S., 40* 2375-2383, 2002.

Ferretti, A., C. Prati, and F. Rocca, Permanent scatterers in SAR interferometry, *IEEE Trans. Geosci. Remote Sens., 39*, 8-20, 2001.

Galehouse, J.S. and J. J. Lienkaemper, Inferences drawn from two decades of alinement array measurements of creep on faults in the San Francisco Bay Region. *Bull. Seismol. Soc. Am., 93(6)*, 2415-2433, 2003.

McFarland, F., J. Lienkaemper, and S. J. Caskey, Data from theodolite measurements of creep rates on San Francisco Bay region faults, California; 1979-2009, *USGS Open file report 09-1119*, 2009.

5 Probing the Deep Rheology of Tibet Constraints from 2008 M_w 7.9 Wenchuan, China Earthquake

Mong-Han Huang and Roland Bürgmann

5.1 Introduction

Debate over the fundamental geological shape of the Tibetan Plateau has been running for many years. There are mainly two end-member models proposed: [1] The deformation in Tibet is diffuse and distributed, associated with ductile flow in the mantle and in the middle or lower crust (e.g., *Royden et al.*, 1997); [2] Tibet results from interactions among rigid blocks with localization of deformation along major faults (e.g., *Avouac and Tapponnier*, 1993). Both have major implications for the dynamics of plateau borders with different mechanisms for building up and supporting the mountain ranges. On 12 May 2008, a M_w 7.9 Earthquake occurred at Wenchuan in Sichuan Province, China, generating about 280 km of surface rupture (*Shen et al.*, 2009). More than 80,000 people were killed and over 4.8 million people became homeless due to this disastrous earthquake. The major faults involved in this event include the Pengguan fault in the east along the mountain front, the Beichuan fault about 10-15 km further to the west, and the Wenchuan-Maowen fault that lies about 30 km northwest of the Beichuan fault. They are all part of the Longmen Shan fault zone, which is located in the zone of crustal shortening between the Tibetan Plateau and the Sichuan Basin. The postseismic deformation is at least an order of magnitude less than the coseismic slip. The most significant postseismic deformation recorded at a continuous GPS station about 25 km away from the maximum rupture on the Beichuan fault shows 0.7 m coseismic offset but merely 0-6 mm of postseismic displacement in the 5 months following the event.

Postseismic deformation is considered to be a motion which is a response to the redistribution of stresses induced by an earthquake. In other words, the motion is evidence of the relaxation stress somewhere in the upper part of the lithosphere (*Ryder et al*, 2007). There are various hypotheses suggesting the relaxation procedure, such as: afterslip on a discrete plane, creep in a viscous or viscoelastic shear zone, viscoelastic relaxation in the lower crust/upper mantle, and poroelastic rebound, etc. In this study, we will apply viscoelastic modeling using the VISCO1D code (*Pollitz*, 1992), and compare different rheological configurations with their responses to the postseismic surface deformation. The aim for doing numerical modeling is to find out a relevant rheological forward model that could explain the geodetic observations. In this way, we can understand the key parameters, especially the viscosity, which control the deformation process following an earthquake.

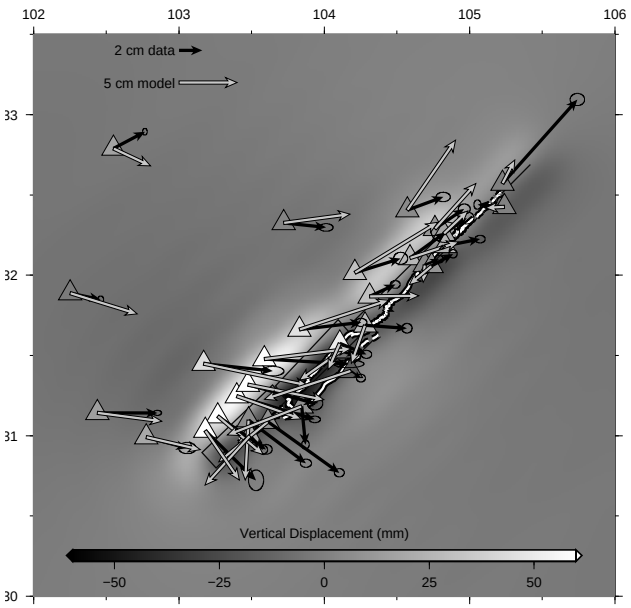

Figure 2.11: The GPS measurements and the forward modeling result of the Wenchuan postseismic deformation. The black arrows show the best fitting one year deformation from the GPS time series. The rectangles are the preferred earthquake fault model segments modified from Shen et al., 2009, and the white lines are the surface rupture. The white arrows are the forward modeling suing the Maxwell rheology according to Ryder et al., 2008. The background colors are the vertical forward modeling, and the colors in the triangles are the one year GPS vertical measurements.

5.2 Primary Result and Discussion

Shen et al., 2009 apply GPS and InSAR (Interferometric Synthetic Aperture Radar) inversion to find the best fault geometry and slip distribution. Here we simplify the Wenchuan coseismic fault geometry provided by *Shen et al.*, 2009 into 5 fault segments with different fault properties. According to coseismic studies (e.g., *Shen et al.*, 2009), all segments (Pengguan fault, Beichuan fault, and Wenchuan-Maowen fault) of the Longmenshen fault strike about 229°and dip to the NW. However, the dipping angle ranges from ∼43°in the SW to nearly vertical in the NE. Moreover, the sense of motion varies from thrusting in the SW to right lateral strike-slip in the

NE. Most of the GPS stations were installed just after the Wenchuan main shock. We estimate the one year postseismic slips in terms of linear least square fit to the GPS time series. In this study, we consider viscoelastic rebound to be the main driving force of the postseismic deformation. The viscoelastic model calculation is based on the software VISCO1D (*Pollitz*, 1992). This program can build up the earth model with either elastic or viscoelastic properties specified by users for Maxwell or Burgers rheological models. We consider the rheological model suggested by *Ryder et al.*, 2007 and *Godard et al.*, 2009 as the starting conditions. [1] *Ryder et al.*, 2007 study the post 1997 M_w 7.6 Manyi (Tibet) earthquake surface deformation in terms of SAR interferometry. They assume a 15 km elastic lid over a viscoelastic half-space, and the shear modulus is held constant at $5x10_{10}$ Pa. Their best fitting viscosity of the half-space (Maxwell rheology) is $7x10^{18}$ Pa s. [2] *Godard et al.*, 2009 explore the viscoelastic properties of the borders of Tibetan Plateau (the Sichuan and Tarim basins, for example) in terms of thermomechanical modeling of continental lithosphere coupled with fluvial denudation. They propose a viscoelastic model that has a 15 km elastic lid over the lower crust (viscosity: 10^{20} Pa s) and the upper mantle with viscosity decreasing in depth. We simplify their proposed viscosity model to include 4 layers: elastic lid, lower crust (viscosity: 10^{21} Pa s), upper-most mantle (viscosity: 10^{22} Pa s), and upper mantle (viscosity: 10^{18} Pa s).

Afterslip and poroelastic rebound are additional important mechanisms that contribute to postseismic deformation. Poroelastic rebound generally shows relatively localized postseismic slips near the fault rupture zone and is related to Poisson's ratio and shear modulus, etc. (*Freed et al.*, 2006). Afterslip represents accelerated aseismic slip on and adjacent to the main shock rupture. In this study, we also test for contributions from these two processes to the postseismic deformation. The afterslip distribution inverted from the postseismic GPS data can explain the near-field postseismic displacement in terms of afterslip on the deeper part of the Beichuan fault. However, this model is not able to fit the far-field transients, which might be dominated by the viscoelastic deformation. A first-order model of poroelastic rebound in terms of changing the Poisson's ratio in coseismic forward dislocation models from 0.29 (undrained) to 0.25 (drained) leads to surface deformation with only up to 6 mm horizontal and 1 mm vertical deformation at near-field GPS stations. The modeled poroelastic rebound can only contribute about 1/5 of the observed postseismic deformation and thus cannot be the primary source of the postseismic deformation. Our future work will involve careful exploration of how a combination of viscoelastic flow, poroelastic rebound and afterslip produces the observed transients, so that we will be able to characterize the relative importance of each mechanism at different scales of postseismic deformation and quantify the rheological parameters of the underlying processes.

5.3 Acknowledgements

We thank Z.K. Shen for providing the GPS time series. This work is supported by NSF grant (EAR 0738298).

5.4 References

Avouac, J.P. and Tapponnier, P., Kinematic model of active deformation in Central Asia, *Geophys. Res. Lett., 20,* 895-898, 1993.

Bürgmann, R. and Dresen, G., Rheology of the Lower Crust and Upper Mantle: Evidence from Rock Mechanics, Geodesy, and Field Observations, *Annu. Rev. Earth Planet. Sci., 36,* 531-67, doi:10.1146/annurev.earth.36.031207.124326., 2008.

Freed, A., Bürgmann, R., Calais, E., Freymueller, J., and Hreinsdottir, S., Implications of deformation following the 2002 Denali, Alaska, earthquake for postseismic relaxation processes and lithospheric rheology, *J. Geophys. Res., 111,*, B01401, doi:10.1029/2005JB003894.i, 2006.

Godard, V., Cattin, R., and Lave, J., Erosional control on the dynamics of low-convergence rate continental plateau margins. *Geophys. J. Int., 179,* 763-777, doi: 10.1111/j.1365-246X.2009.04324.x., 2009.

Pollitz, F., Postseismic relaxation theory on a spherical earth. *Bull. Seism. Soc. Am., 82(1),* 422-453, 1992.

Royden, L.H., Burchfiel, B.C., King, R.W., Wang, E., Chen, Z.L., Shen, F., and Liu, Y.P., Surface deformation and lower crustal flow in eastern Tibet, *Science, 276,* 788-790, 1997.

Ryder, I., Parsons B., Wright T.J., and Funning G., Postseismic motion following the 1997 Manyi (Tibet) earthquake: InSAR observations and modeling, *Geophys. J. Int., 169,* 1009-1027, doi: 10.1111/j.1365-1246X.2006.03312.x., 2007.

Shen, Z.K., J. Sun, P. Zhang, Y. Wan, M. Wang, R. Bürgmann, Y. Zeng, W. Gan, H. Hiao, and Q. Wang, Slip maxima at fault junctions and rupturing of bariers during the 2008 Wenchuan earthquake, *Nat. Geosci., 2,* 718-724, doi:10.1038/NGEO636, 2009.

6 Tidal Triggering of LFEs near Parkfield, CA

Amanda M. Thomas, Roland Bürgmann, and David Shelly

6.1 Introduction

Studies of nonvolcanic tremor (NVT) in Japan, Cascadia, and Parkfield, CA have established the significant impact small stress perturbations, such as the solid earth and ocean tides, have on NVT generation (*Thomas et al.*, 2009). Similar results irrespective of tectonic environment suggest that extremely high pore fluid pressures are required to produce NVT. Here we analyze the influence of the solid earth and ocean tides on a catalog of 500,000 low frequency earthquakes (LFE) distributed along a 150km section of the San Andreas Fault centered at Parkfield (*Shelly and Hardebeck*, 2010). LFEs comprising the tremor signal are grouped into families based on waveform similarity and precisely located using waveform cross-correlation. Analogous to repeating earthquakes, LFE families are thought to represent deformation on the same patch of fault. While the locations of repeating earthquakes are assumed to be coincident with the location of asperities in the fault zone, NVT occurs below the seismogenic zone, where fault zones behave ductilely. Here we explore the sensitivity of each of these LFE families to the tidally induced shear (right-lateral shear stress, RLSS), normal (fault-normal stress, FNS), and Coulomb (CS) stresses on the SAF.

6.2 Methods

Tidally induced strains are computed in the LFE source region using SPOTL. Assuming two-dimensional plane strain and linear elasticity, with an elastic modulus of 30 GPa and Poisson ratio of 0.25, strains are then converted to stresses and resolved into fault normal and parallel (shear) directions of the San Andreas fault (N°45W), and the volumetric strain is converted to pressure. Timeseries of the resolved stresses are then used to compute the percent excess [=(actual number of LFEs that occur under a particular loading condition-expected number)/expected number] for each stress constituent. We compute the percent excess, or Nex, for each stressing condition. Additionally, relative tremor rates during times when the tides are encouraging or retarding failure can be used to estimate the effective normal stress (*Dieterich*, 1986). The precisely relocated LFE families allow us to map spatial variation of the aforementioned quantities in the deep San Andreas fault.

6.3 Preliminary Results

Preliminary results indicate that extremely small stresses induced in the lithosphere by the tides are sufficient to trigger/modulate LFE families on the deep SAF. Additionally, precise LFE locations coupled with tidal influence on LFE families can be used to produce maps of along-fault spatial variability in tidal sensitivity, friction, and effective normal stress (Figure 2.12). The tidally induced RLSS has the most robust influence on LFE generation, however many families also show statistically significant correlation or anti-correlation with FNS. All families exhibit near-lithostatic pore pressure.

Future research efforts will focus on using tidal sensitivity of LFEs to place controls on the mechanical properties and behavior of deep fault zones.

6.4 Acknowledgements

This work is funded by the United States Geological Survey and a National Science Foundation Graduate Research Fellowship.

6.5 References

Dieterich, J.H., Nucleation and triggering of earthquake slip: effect of periodic stresses , *Tectonophysics, 144,* 127-139, 1986.

Shelly, D.R. and J.L. Hardebeck, Precise tremor source locations and amplitude variations along the lower-crustal central San Andreas Fault, *Geophys. Res. Lett., 37,* L14301, 2010.

Thomas, A.M., R.M. Nadeau, and R. Bürgmann, Tremor-tide correlations and near-lithostatic pore pressure on the deep San Andreas fault, *Nature, 462,* 1048-1051, 2009.

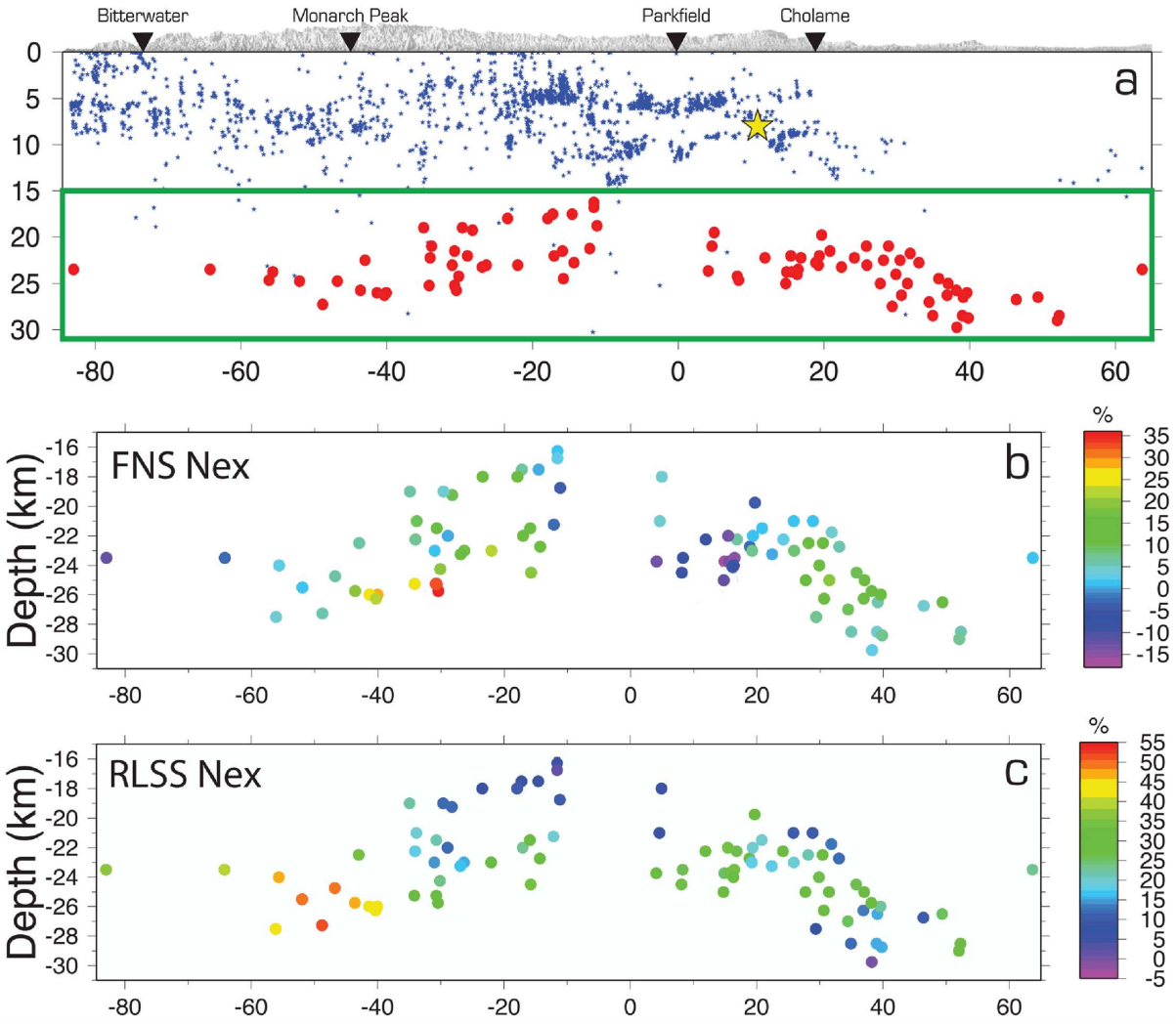

Figure 2.12: (a) Along-fault cross section of the SAF viewed from the south-west. Vertically exaggerated topography is shown in grey. Local towns are marked by inverted triangles. Hypocenters of SAF seismicity, the 2004 Parkfield earthquake, and LFE locations are shown as blue dots, yellow star, and red circles respectively. Panels (b) and (c) are delineated by the green box. (b) LFE locations color coded by their FNS Nex (percent excess = [actual number of LFEs during times of positive FNS - expected number of LFEs during times of positive FNS]/expected number of LFEs during times of positive FNS). (c) LFE locations color coded by the RLSS Nex values. (See color version of this figure at the front of the research chapter.)

7 Monitoring Slow Moving Landslides in the Berkeley Hills with TerraSAR-X Data

Ling Lei and Roland Bürgmann

7.1 Introduction

Resolving the kinematics of landslides is a prerequisite for improving our understanding of the mechanics of these potentially hazardous features. We need to better understand how landslides destabilize during large rainstorms and seismic events. In the Berkeley Hills there are four large, slow moving, deep-seated landslides. All the landslides extend through residential areas and move on the order of cm/year, each covering an area of roughly 0.25-1.00km^2. These slides are located in a rapidly uplifting zone adjacent to the Hayward fault (Figure 2.13). A lot of damage to homes, breakage of underground utility pipes, and confusion over property lines was caused by landslides over the years, although deformation on these landslides is typically small and slow. It is currently not well understood how the landslides respond to seismic activity on the Hayward fault. DInSAR (Differential Interferometric Synthetic Aperture Radar) is a powerful tool for measuring movements of ground by exploiting the phase difference of SAR images taken at different time instances. In this project, we aim to monitor the Berkeley Hills landslides using SAR data from a number of different satellites, especially TerraSAR-X.

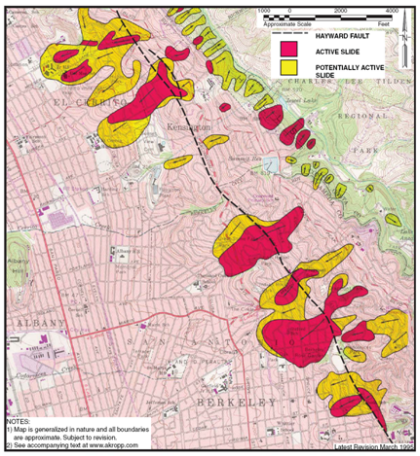

Figure 2.13: Map of active landslides of the Berkeley Hills (`http://www.akropp.com/resources`)

7.2 TerraSAR-X Data Set

The TerraSAR-X satellite, launched on June 15, 2007, carries an X-band SAR operating at 9.65 GHz. One of the main goals of the TerraSAR-X mission is to produce high resolution imagery with near optical quality. The antenna on TerraSAR-X can be steered in both elevation and azimuth and can be used to generate Spotlight, Stripmap and ScanSAR images. Spotlight images have a resolution of about 1 meter, while Stripmap data have a ground resolution between 2 meters and 6 meters, and ScanSAR images have a resolution of approximately 16 meters. The satellite operates in an 11 day repeat orbit at an altitude of 514 km. The rather short orbit repeat cycle and the electronically steerable antenna allow fast and frequent imaging of a particular site. The frequent interferometric coverage can help especially with monitoring events on shorter time scales. Fast events can be detected and atmospheric delay errors can be reduced by averaging many interferograms.

Up to now, we have ordered and received 90 TerraSAR-X Spotlight Single Look Complex (SLC) images and a few Stripmap SLC images delivered by DLR. The TerraSAR-X images were acquired over the active landslides, coastal subsidence and shallow Hayward fault creep near the city of Berkeley. The data acquisition interval is from November, 2008 till now. Four types of Spotlight images and one type of Stripmap images in time sequence were ordered and acquired: spot_012, spot_038, spot_049, spot_075 and strip_003, with HH polarization, different look angles, and different pass directions.

We use ROI_PAC to do the Interferometric processing. We used a two-pass differential interferometry approach using SRTM 1-arc-second DEM heights as a reference to calculate the topographic phase. From the analysis of a map of phase coherence values, we find high coherence values in urban areas but low values in the hills and more vegetated areas which caused phase unwrapping problems in the landslides area. Thus, a time series of interferograms was used for the atmospheric correction. We used sequential interferograms to do the stacking, which means that every image appears in two interferograms except the first and last image. We obtained preliminary results from Stripmap interferograms and standard stacking of Spotlight interferograms. The results are generally consistent with southwest motion of the landslides.

7.3 Persistent Scatterer Processing

While standard InSAR measurements that rely on one or a stack of several interferograms can resolve the motion of large landslides, this method is still often hampered by significant noise introduced by atmospheric delays and by loss of coherence in vegetated or high-relief terrain. The persistent scatterer approach can enhance the ability to find suitable scatterers in relatively low-coherence ter-

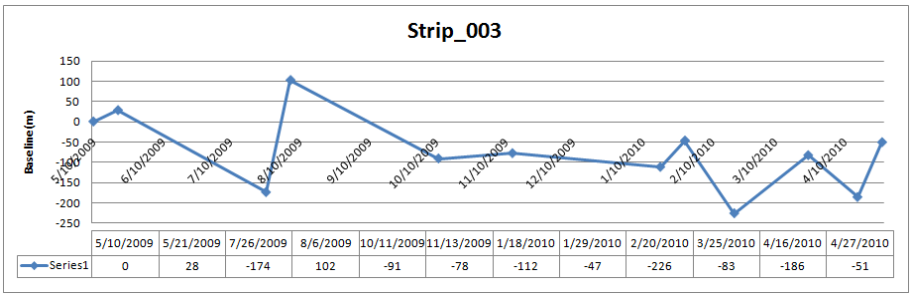

Figure 2.14: Acquisition dates and perpendicular baseline

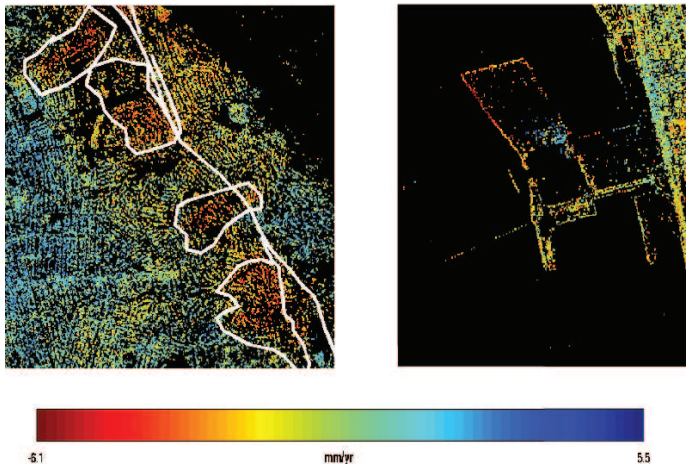

Figure 2.15: Mean LOS velocity of the landslides area and Berkeley Marina

rains. We use Stanford Method for Persistent Scatterers (StaMPS) which was developed at Stanford University by Dr. Andy Hooper (*Hooper et al.*, 2004). Since we do not have many Strimap acquisitions yet, we only used 12 scenes, which span the time interval from May 2009 to April 2010, for our analysis. We constructed eleven interferograms relative to the master scene of May 10, 2010 with Doris (Delft Object-oriented Radar Interferometric Software). All of these images were used to identify persistent and coherent pixels. Figure 2.14 shows the acquisition date and baseline information. The wrapped phase of the PS pixels is selected and the improved phase unwrapping algorithm is adopted.

The negative mean Line-of-sight (LOS) velocity in the landslides area (Figure 2.15) is consistent with landslide motion, moving away from the satellite. Also, the negative LOS velocity reveals subsidence of the Berkeley marina area. For our future work, we hope the four beams of TerraSAR-X Spotlight data from different viewing geometries will significantly improve our ability to fully characterize the kinematics and temporal patterns of the landslides. We are still in the early stages of this investigation and will acquire more data to do the PS processing. Results from TerraSAR data will be carefully compared and integrated with InSAR data from other spacecraft, including the ERS-1/2, Envisat, RADARSAT-1, and ALOS satellites.

7.4 Acknowledgements

We thank the German Aerospace Centre (DLR) for providing TerraSAR-X data for this project. We thank Paul Lundgren, Eric J. Fielding, and Paul Rosen for providing TerraSAR reading codes and beneficial discussions. We thank Andy Hooper for supporting StaMPS software.

7.5 References

Hilley, G., R. Bürgmann, A. Ferretti, F. Novali and F. Rocca, Dynamic of slow-moving landslides from permanent scatterer analysis, *Science, 304*, 1952-1955, 2004.

TerraSAR-X Ground Segment Basic Product Specification Document, TX-GS-DD-3302.

Bürgmann, R., E. Fielding, and J. Sukhatme, Slip along the Hayward fault, California, estimated from space-based synthetic aperture radar interferometry, *Geology, 26*, 559-562, 1998.

Eineder, M., N. Adam, and R. Bamler, Spaceborne Spotlight SAR Interferometry With TerraSAR-X, *IEEE Trans. Geosci. Remote Sense.*, 5, 1524-1535, 2009.

Hooper, A., H. Zebker, P. Segall and B. Kampes, A new method for measuring deformation on volcanoes and other natural terrains using InSAR persistent scatterers, *Geophys, 31*, 2004.

8 Slab-Plume Interaction Beneath the Pacific Northwest

Mathias Obrebski, Richard Allen, Mei Xue (Tongji University, China), Shu-Huei Hung (National Taiwan University)

8.1 Introduction

The Pacific Northwest of western North America is unusual in that both a subducting slab and a hotspot occur within 1000 km of one another. Globally, these geologic components are commonly separated into distinct provinces. The Juan de Fuca (JdF) plate that continues to subduct today is a remnant corner of the Farallon plate and is terminated to the south by the Mendocino Triple Junction (MTJ). Subduction beneath the Pacific Northwest has been continuous for more than 150 Ma. The westernmost US exibits several major Neogene to Quaternary volcanic provinces. The Columbia River Basalts (CRB) is the product of a phase of massive volcanic outpouring that occurred 17 Ma. The Yellowstone Snake River Plain (YSRP) hosts a bimodal volcanic trend that exhibits a time progressive sequence of volcanic centers. Two groups of hypotheses have been proposed to explain this surface geology: a stationary deep-seated whole mantle plume, or various lithospheric-driven processes of fracture and volcanism. Nevertheless, seismic imaging efforts to constrain the geometry of any Yellowstone plume anomaly through the mantle have been inconclusive. Here we take advantage of the Yellowstone region being now well covered by the dense USAarray deployment to provide constraints on the source of the hotspot, the process of subduction, and the inevitable interaction between the two in the mantle beneath the Pacific Northwest.

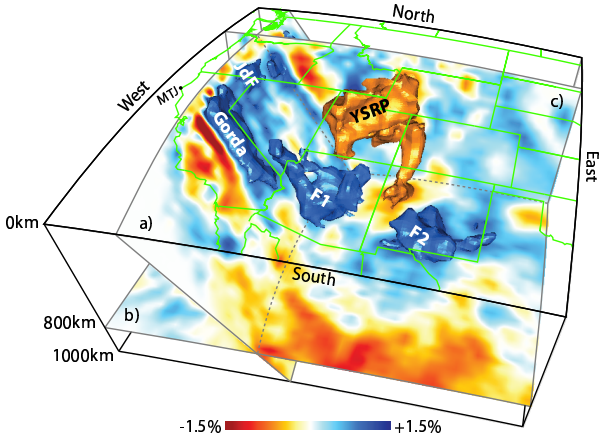

Figure 2.16: Tomographic 3D view of the DNA09 P-wave velocity structure of the mantle beneath the Pacific Northwest. a) is an oblique section through the currently subducting Gorda-Juan de Fuca slab (JdF) that clearly shows the southern edge of the slab beneath the Mendocino Triple Junction (MTJ). b) is a constant depth slice at 800km that illustrates the contrast between dominantly high velocity mantle to the north and slow velocities to the south where the Farallon slab is no longer present. c) is an E-W vertical slice at 46.5°N. 3D blue isosurfaces show strong fast anomalies linked to the Gorda-JdF slab and to possible Farallon fragments (F1-F2). The red isosurface depicts the 3D geometry of a large slow anomaly that extends from beneath the Yellowstone-Snake River Plain (YSRP) hotspot track to the bottom of our model at 1000km depth and that we interpret as a mantle plume.

8.2 Data and Method

To image the Earth's interior beneath the Pacific Northwest, we use all of the available Earthscope-USArray data recorded from January 2006 to July 2009. The station coverage extends from the west coast to 100°W and from the Mexican border to the Canadian border. We also processed the data from two Earthscope temporary arrays (FlexArray Along Cascadia Experiment for Segmentation [FACES] and the Mendocino Experiment) deployed along the Cascadia trench and permanent seismic networks in the western US. The velocity structure of the mantle is retrieved through body wave finite frequency tomographic inversion. The dataset of our multi-frequency compressional model DNA09-P is derived from 58,670 traveltimes of direct P from 127 earthquakes measured in four frequency bands. The dataset used for our shear model DNA09-S includes 38,750 traveltime measurements, 34,850 S-wave observations from 142 events and 3,900 SKS observations from 24 events.

8.3 Result and Interpretation

We interpret the low velocity anomaly beneath the YSRP as a mantle plume with a lower mantle origin. Our interpretation, based on geometrical observations of our P- and S-wave models, is also supported by the high He3/He4 isotopic ratio typical of the YSRP volcanism (*Graham et al.*, 2004), which is often interpreted as indicative of a lower mantle source. The low velocities are consistent with high temperatures and low density. A hot plume with a large volume of low density material, as observed in our models, accounts for the high heat flow, the broad topographic swell, the geoid high, and the large free air gravity anomaly observed in the YSRP area (*Smith et al.*, 2009 and references therein), and also

the 410km mantle discontinuity that deepens by 10km in this region (*Fee and Dueker*, 2004). The geometry and structure of the elongated slow anomaly observed in the upper 200km beneath the YSRP are consistent with the predictions of numerical models for the deflection of a plume head by the motion of an overlying lithospheric plate (*Steinberger et al.*, 2004). It is elongated in the SW-NE direction parallel to the motion of the North American plate, the amplitude of the slow anomalies decreases to the southwest with increasing age of the calderas, and the plume conduit today coincides with active volcanism in the Yellowstone Caldera.

The geometry of the Cascadia subduction zone, namely the length and amplitude of the slab anomaly, displays north-south variations (Figure 2.16). In particular, the slab is virtually absent deeper than 300 km beneath Oregon, and is thus too short to act as a mechanical barrier to upper-mantle flow. This gap in the trench may allow the mantle underlying the JdF plate to flow eastward beneath the plate margin as the North American plate moves southwestward above it. This provides a possible explanation for the trench-normal fast direction of anisotropy retrieved from SKS splitting analysis in central and northern Cascadia (*Eakin et al.*, 2010). The orientation of the fast direction in central and northern Cascadia differs from most other subduction zones where the fast direction is trench-parallel (*Long and Silver*, 2009). The Gorda-Juan de Fuca slab is thought to be in trench rollback, and it has been suggested that the Gorda slab plays a significant role. This is consistent with our model, where the Gorda slab dives deeper into the mantle and exhibits a faster anomaly, potentially indicative of cooler and denser material. Finally, the Cascadia subduction zone is also unusual due to the near-absence of deep seismicity. The fragmentation of the slab may play a role. There is no recorded seismicity deeper than 35km beneath Oregon, where the depth extent of the slab is only 300 km, thereby reducing the slab pull force usually responsible for intermediate depth down-dip-tension earthquakes. There is some sub-crustal seismicity beneath Northern California and beneath northern Washington, where the slab is imaged deeper into the mantle.

The analysis of the geometry of our tomographic models suggests that the arrival and emplacement of the large Yellowstone plume had a substantial impact on the nearby Cascadia subduction zone, promoting the tearing and weakening of the JdF slab. The existence of a whole-mantle plume and an active subduction zone within 1000km of one another as imaged in our models makes the tectonic setting of the Pacific Northwest unique. Also striking is the substantial fragmentation of the slab. The latitude where the slab is absent coincides with that of the Yellowstone plume (Figure 2.16). Around 19 Ma, there was a substantial change in the spreading rate at the Pacific-JdF ridge and also in the convergence rate of the Cascadia trench (*Wilson*, 1988). This change could result from a reduction in slab pull. The change also shortly predates the massive magma outpouring of the Columbia River Basalts and the onset of volcanism along the YSRP, which have been interpreted as the manifestation of Yellowstone plume head emplacement (*Smith et al.*, 2009) around 17 Ma. We thus propose that the ascent of the Yellowstone plume, and its necessary encounter with the JdF slab, contributed to a rupture of the slab (*Xue and Allen*, 2007) (Figure 2.16) and the subsequent reduction of slab pull in the Cascadia trench. The composition of the CRB requires the presence of oceanic crust in the source (*Takahahshi et al.*, 1998), which supports the hypothesis that the Yellowstone plume interacted with the JdF slab and carried fragments of oceanic crust back up to the melting zone. This interpretation also explains several intriguing geophysical properties of the Cascadia trench that contrast with most other subduction zones, such as the absence of deep seismicity and the trench-normal fast direction of mantle anisotropy.

8.4 Acknowledgements

We thank USArray TA for data collection and the IRIS DMC for data distribution. This work was supported by the National Science Foundation and a UC-National Laboratory Research program grant.

8.5 References

Eakin, C.M., M. Obrebski, R. M. Allen, D. C. Boyarko, M. R. Brudzinski, R. Porritt, Seismic anisotropy beneath Cascadia and the Mendocino triple junction: Interaction of the subducting slab with mantle flow, *Earth Planet. Sci. Lett.*, doi:10.1016/j.epsl.2010.07.015, 2010.

Fee, D. and K. Dueker, Mantle transition zone topography and structure beneath the Yellowstone hotspot, *Geophys. Res. Lett.*, 31, L18603, doi:10.1029/2004GL020636, 2004.

Graham, D. W., M. R. Reid, B. T. Jordan, A. L. Grunder, W. P. Leeman, and J. E. Lupton, Mantle source provinces beneath the Northwestern USA delimited by helium isotopes in young basalts, *J. Volcanol. Geotherm. Res.*, doi:10.1016/j.jvolgeores.2008.12.004, 2009.

Smith, R. B., M. Jordan, B. Steinberger, C. M. Puskas, J. Farrell, G. P. Waite, S. Husen, W. L. Chang, and R O'Connell, Geodynamics of the Yellowstone hotspot and mantle plume: Seismic and GPS imaging, kinematics, and mantle flow, *J. Volcanol. Geotherm. Res., 188*, 26-56, 2009

Steinberger, B., R. Sutherland, and R. J. O'Connell, Prediction of Emperor-Hawaii seamount locations from a revised model of global plate motion and mantle flow, *Nature, 430*, 167-173, 2004

Takahahshi, E., K. Nakajima, and T. L. Wright, Origin of the Columbia River basalts: Melting model of a heterogeneous mantle plume head, *Earth Planet. Sci. Lett., 162*, 63-80, 1998

9 Imaging Shallow Cascadia Structure with Ambient Noise Tomography

Robert W. Porritt and Richard M. Allen

9.1 Introduction

Along strike variation has been observed throughout the Cascadia Subduction Zone in multiple studies with a variety of data sets. Body-wave tomography shows a broad zone in the center of the slab beneath Oregon with a weak high velocity signal in an atypically quiescent seismic zone (*Obrebski and Allen*, 2009). Characteristics of primitive basalts found in the arc volcanoes change along strike, defining four distinct magma sources or plumbing systems (*Schmidt et al*, 2007). However, the most striking variation is in the recurrence rate of episodic tremor and slip throughout the region (*Brudzinski and Allen*, 2007). These separate observations may reflect lithospheric variations on a regional scale. This study seeks to connect these previous observations by developing a short period surface wave model of structure in the region using ambient seismic noise as the source.

9.2 Data Processing

Data for this study comes from the Berkeley Digital Seismic Network, the Southern California Earthquake Center, the Canadian National Seismic Network, and USArray with focus on two Flexible Array Experiments. The Flexible Array deployments, FlexArray Along Cascadia Experiment for Segmentation (FACES) and Mendocino Broadband, were deployed in 2007 and have completed their deployments as of summer 2010. This is one of the first studies utilizing the approximately one hundred stations in these broadband experiments.

Detailed processing flow for computing group and phase velocity maps can be found in *Benson et al* (2007). While the typical measurements from 7-40 seconds were well constrained from signal-to-noise ratio (SNR) and wavelength criterion, in order to obtain reliable longer period measurements (40-92) seconds, the empirical Green's functions and measured dispersion curves were checked manually to ensure that the measurements were reasonable and consistent with realistic Earth models. The inter-station dispersion curves were inverted with a ray theoretical approach onto a 0.1° by 0.1° grid with a smoothing radius of one wavelength for each period from 7-92 seconds. Initial models exhibited strongly biased maps with clear artifacts from the heterogeneous distribution of noise sources. This bias was removed by binning the paths into 15° bins, normalizing the number of paths in each bin, and applying post-inversion smoothing regularization. To estimate the uncertainties in the phase and group velocity maps, a bootstrapping procedure was applied by randomly choosing 70% of the paths to invert and repeating the process 30 times.

Dispersion curves over the model space and their corresponding uncertainties from the bootstrapping and a static value proportional to period are utilized in a Monte Carlo inversion scheme (*Shapiro and Ritzwoller*, 2002). The inversion used PREM (*Dziewonski and Anderson*, 1982) as a starting model in the mantle and GIL7 (*Dreger and Romanowicz*, 1994) in the crust. Crustal thickness was imposed from the receiver function model of *Levander et al.* (2008). Slab depth estimates from *Audet et al* (2009) were also used for better constaints in the subduction zone.

9.3 Results

It is not possible to discuss al the features of the model in this short summary; instead we discuss just two key areas of interest. Figure 2.17 details the crustal structure of the Klamath Mountain range. These mountains primarily overlay the Gorda plate portion of the Gorda-Juan de Fuca system, and the region has the shortest tremor recurrence interval of the Cascadia Subduction Zone at 10 months. The fastest velocities in the crust are around 3.6km/s and occur around 20km deep in the core of the mountains. The variability of the top of the Gorda slab with respect to the crustal variations implies some dynamic system of crust-mantle interaction in this zone.

Figure 2.18 details the three dimensional structure of the Siletzia terrain. This piece of accreted ocean terrain is often seen in high-resolution 2D active source studies (*Trehu et. al*, 1994), and anomalies in geochemical studies are often attributed to it. This study clearly illustrates the structure in a 3D capacity. From this it is clear the Siletzia terrain consists of high velocity material above the plate interface which may be driving the very long recurrence interval of episodic tremor and slip.

Comparing the structure of the two regions can provide insight into the observed variations. The Klamath range is overall slower than the Siletzia. While mapping velocity to rheology is a non-unique process, in general the low shear velocity could be due to a higher silicic or fluid content, or lower shear modulus, both of which imply a lower density and thus less compressive stress on the plate interface. Both of these factors are probable causes for an area to be more likely to have non-volcanic tremors. Future studies, such as receiver function analysis for V_p/V_s ratio and tomographic V_p and V_s studies will further improve our constraints on the region.

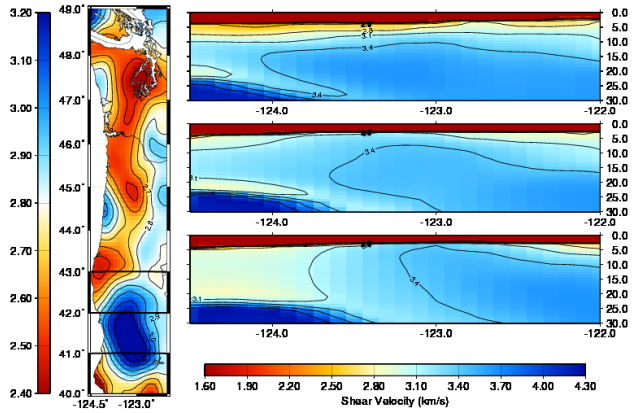

Figure 2.17: Slices to illustrate the structure of the Klamath terrain. Left: Map slice at sea level. Right: Sections of constant latitude showing high velocity mountain core and the top toe of the subducting slab.

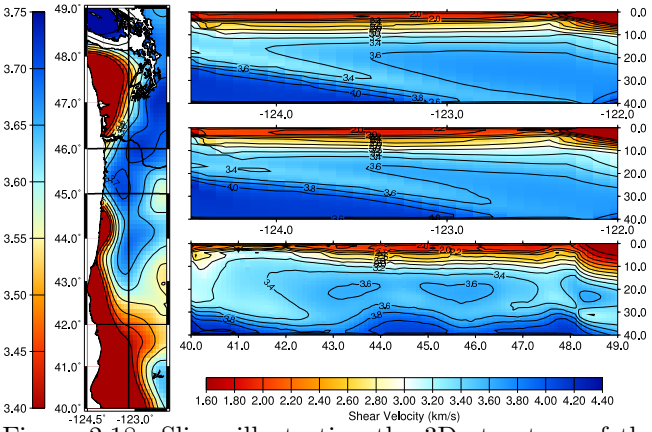

Figure 2.18: Slices illustrating the 3D structure of the Siletzia terrain. Left: Map slice at 15km. Right bottom: Cross section at 123°W longitude. Right top and middle: Cross sections at 46°N and 45°N respectively.

9.4 Acknowledgements

We would like to acknowledge our co-PIs and collaborators on the flexible array experiments. The Mendocino Broadband experiment was made possible through NSF grants EAR0643392 and EAR0745934, with help from Gene Humphreys, Leland O'Driscoll, Alan Levander, and Yongbo Zhao for fieldwork and discussions. The FlexArray Along Cascadia was funded through NSF grant EAR0643007 with co-PI Mike Brudzinksi and his students Devin Boyarko and Stefany Sit.

Data from this study came from the Earthscope USArray/Transportable Array, the Canadian National Seismic Network through the AutoDRM system, the Berkeley Digital Seismic Network, and the Southern California Earthquake Center.

This work has been made possible with the resources available through the PASSCAL instrument center at New Mexico Tech.

9.5 References

Audet, P., Bostock, M. G., Christensen, N. I., and Peacock, S. M., Seismic evidence for overpressured subducted oceanic crust and megathrust fault sealing. *Nature, 457*, 76-78, 2009

Benson, G.D., Ritzwoller, M.H., Barmin, M.P., Levshin, A.L., Lin, F., Moschetti, M. P., Shapiro, N.M., Yang, Y., Processing seismic ambient noise data to obtain reliable broadband surface wave dispersion measurements. *Geophysical Journal International, 169*, 1239-1260, 2007

Bostock, M.G., Hyndman, R.S., Rondenay, S., and Peacock, S. M., An inverted continental Moho and serpentinization of the forearc mantle. *Nature, 417*, 53-539, 2002

Brudzinksi, M. and Allen, R. M., Segmentation in Episodic Tremor and Slip All Along Cascadia. *Geology, 35(10)* 907-910, 2007

Dreger, D. S. and Romanowicz, B., Source characteristics of events in the San Francisco Bay region, *U. S. Geol. Surv. Open-File Report 94-176*, 301-309, 1994

Dziewonski and Anderson, Preliminary Reference Earth Model, *Phys. Earth. Planet. Int., 25*, 297-356, 1981

Levander, A., Niu, F., Miller, M.S., Zhai, Y. and Liu, K., USArray Receiver Function Images of the Lithosphere in the Western U.S.. *EOS Trans. AGU 82(52)*, Fall Meet. Suppl., Abstract S44B-01, 2007

Obrebski, M. J., and Allen, R. M., Plume Vs. Plate: Convection beneath the Pacific Northwest. *Berkeley Seismological Laboratory Annual Report*, 2008-2009

Schmidt, M. E., Grunder, A.L., and Rowe, M., Segmentation of the Cascades Arc as indicated by Sr and Nd isotopic variation among primitive basalts. *Earth and Planetary Science Letters, 266* 166-181, 2007

Shapiro, N. M., and Ritzwoller, M. H., Monte-Carlo inversion for a global shear velocity model of the crust and upper mantle, *Geophysical Journal International, 151*, 88-105, 2002

Trehu, A. M., Asudeh, I., Brocher, T. M., Luetgert, J. H., Mooney, W. D., Nabelek, J. L., and Nakamura, Y., Crustral Architecture of the Cascadia Forearc. *Science, 266*, 237-243, 1994

Xue, M., and Allen, R. M., The Fate of the Juan de Fuca Plate: Implications for a Yellowstone Plume Head. *Earth and Planetary Science Letters, 264*, 266-276, 2007

10 Anisotropic Layering of the North American Craton

Huaiyu Yuan and Barbara Romanowicz

10.1 Summary

Seismic anisotropy in the Earth's upper mantle is generally attributed to lattice-preferred orientation of anisotropic crystals in minerals such as olivine and pyroxene (e.g. *Nicolas and Christensen*, 1987) resulting from rock deformation in past and present mantle flow. Under continents, seismic anisotropy results from a combination of frozen-in lithospheric anisotropy from past deformation processes, shear coupling between the lithosphere and asthenosphere, and current flow in the asthenosphere (*Park and Levin*, 2002). Characterizing seismic anisotropy and relating it to past and present geodynamic processes thus provides insights into our understanding of the driving mechanisms of plate tectonics and lithospheric evolution.

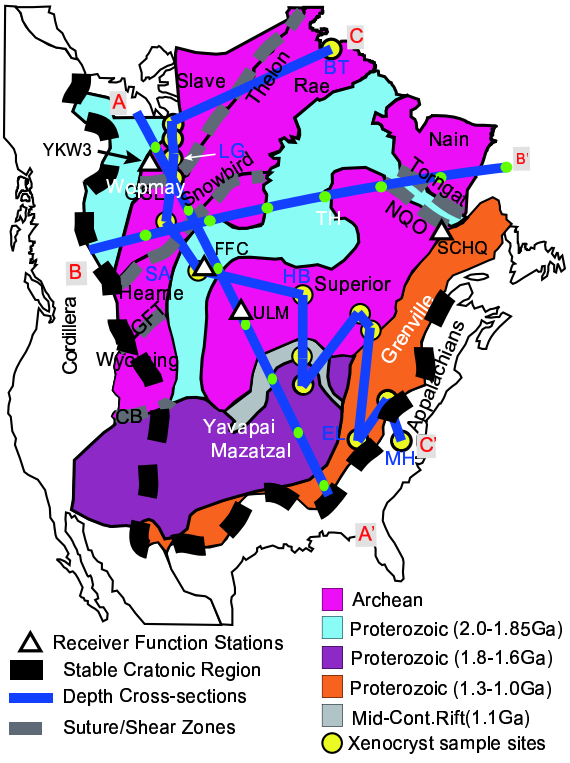

Figure 2.19: Precambrian basement of the North American continent. Precambrian province ages follow *Whitmeyer and Karlstrom* (2007). Labels are: BHT, the Buffalo Head Terrane; THO, Trans-Hudson Orogen; MH, Medicine Hat province; WY, Wyoming Province; CP, Colorado Plateau. Depth cross-section locations are shown as thick black lines with white circles for better correspondence with Figure 2.

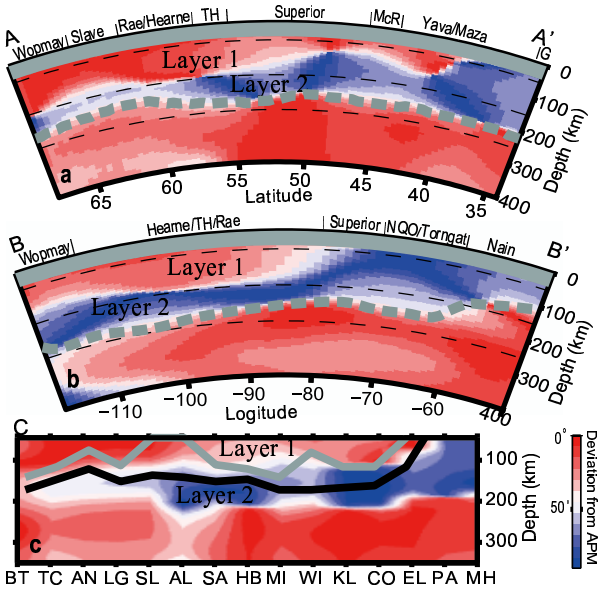

Figure 2.20: Upper mantle layering defined by changes in the direction of azimuthal anisotropy fast axis across three profiles in Figure 2.19: (a) AA', (b) BB' and (c) CC'. The fast axis direction is color coded as a deviation from the NA APM. Thick dashed line is our inferred LAB. Layer 1 and 2 are two lithospheric layers defined by the change of anisotropic fast axis directions. (a) Symbols are: TH, Trans-Hudson Orogen; Yava/Mazat/G: Yavapai, Mazatzal and Grenville provinces; and McR: Mid Continent Rift. (b) NQO: New Quebec Orogen. (c) This profile follows the sites where xenocryst samples have been obtained (yellow circles in Figure 2.19; *Griffin et al.*, [2004]). Sample sites are labeled at the bottom of (c). The boundary corresponding to Mg#93 is indicated by a grey line, and the black line corresponds to Mg#92.

The North American (NA) continent is in many ways an ideal target for this type of study due to its rich tectonic history (Figure 2.19; e.g. *Hoffman*, 1989; *Thomas*, 2006; *Whitmeyer and Karlstrom*, 2007). In this report, we show strong anisotropic layering in the stable North American craton upper mantle, inferred from our updated 3-D upper mantle SVEMum_NA2 model (*Yuan et al.*, 2010). This layering of anisotropy in the craton enables us to distinguish three domains of azimuthal anisotropy, two in the lithosphere and one in the asthenosphere (*Yuan and Romanowicz*, 2010). In particular, the boundary between the two lithospheric layers roughly corresponds to the negative velocity jump detected in receiver function studies (*Yuan et al.*, 2010).

10.2 Anisotropic Layering

In Figure 2.20, we present upper mantle layering defined by changes in the direction of azimuthal anisotropy fast axis, shown as depth cross sections across three profiles. We found that beneath the craton, the fast axis direction of anisotropy becomes systematically aligned with the absolute plate motion (APM; *Gripp and Gordon*, 2002) below the lithosphere-asthenosphere boundary (LAB), confirming our previous findings (*Marone and Romanowicz*, 2007). The changes with depth of azimuthal anisotropy define more accurately (to within ±20 km) the location of the LAB than depth profiles of isotropic shear velocity (V_s) or radial anisotropy ($\xi = (V_{sh}/V_{sv})^2$), which, in general, shows gradual decrease in amplitude across the LAB depth, and thus does not allow us to locate the LAB (*Yuan and Romanowicz*, 2010; *Yuan et al.*, 2010).

Moreover, a change in direction of the fast axis of azimuthal anisotropy at mid-lithospheric depths clearly defines two layers (Layer 1 and 2; Figure 2.20) within the cratonic lithosphere, separated by a boundary with large lateral variations in depth. Layer 1 is thick under the central part of the craton and tapers off at its boundaries with Paleozoic provinces (e.g. Figure 2.19). The thickest parts of Layer 1 are found in regions affected by orogenies in the Archean (e.g. the Trans-Hudson orogen). Layer 1 also thins in the Mid-continental rift zone (Figure 2.20a). The lateral variations in the thickness of Layer 1 are in good agreement with geochemical estimates from xenolith studies for the most depleted part of the craton, as defined in terms of Mg # (Figure 2.20c; *Griffin et al.*, 2004)

10.3 Tectonic Implications

Comparison with the geochemistry studies (Figure 2.20c) suggests that Layer 2 may represent a younger, less depleted, thermal boundary layer, possibly accreted at a later stage through processes influenced by the presence of a stagnant, chemically distinct lid (Layer 1). This scenario is supported by the excellent agreement between the lateral variations in the depth of the LAB inferred from our azimuthal anisotropy study and the variations predicted from the thickness of Layer 1 (Figure 4 in *Yuan and Romanowicz*, 2010), when applying the geodynamically inferred relationship between the thicknesses of the chemical and thermal lithospheres (e.g. *Cooper et al.*, 2004).

We suggest that receiver functions and long range seismic profiles preferentially detect the transition between the ancient Archean lithosphere (Layer 1) and the subsequently accreted thermal boundary layer (Layer 2). The details of this transition and its precise nature are likely to be complex, as indicated by the fine layering documented by long range seismic profile studies (*Thybo*, 2006), and may involve stacks of thin, low-velocity layers marking the trace of partial melting and dehydration (*Mierdel et al.*, 2007), possibly at the top of oceanic lithosphere that was welded onto the bottom of Layer 1. It could also result from kimberlite accumulation (*Sleep*, 2009) if the strong, chemically distinct, Archean Layer 1 acts as a barrier to their further ascent. Note that this mid-lithospheric anisotropic boundary zone must be a sharp high-to-low velocity horizon since it produces converted phases seen in receiver function studies, but it is barely detectable by isotropic velocity tomography, although we have noted the presence of a local minimum in the depth profile of shear velocity in some parts of our model. On the other hand, the LAB under cratons is likely more gradational, as it is hard to detect with receiver functions, which is consistent with a largely thermal, anisotropic boundary that likely does not involve any significant compositional changes or partial melting.

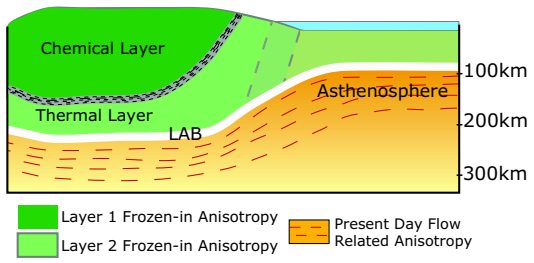

Figure 2.21: Cartoon illustrating the inferred stratification of the lithosphere. Beneath the craton, three layers of anisotropy are present: two in the lithosphere (Layers 1 and 2), and one in the asthenosphere. Layer 1 corresponds to the chemically distinct, depleted Archaean lithosphere, and Layer 2 is the thermal root, separated from the asthenosphere by the LAB, which is at relatively constant depth beneath the stable part of the continent, but rapidly shallows between the tectonic part of the continent and the oceans. The boundary between layers 1 and 2 is seismically sharp, but its fine-scale structure is likely to be complex.

Here, by using an approach based on seismic azimuthal anisotropy, we have documented the craton-wide presence of a mid-lithospheric boundary, separating a highly depleted chemical layer of laterally varying thickness, from a less depleted deeper layer bounded below by a relatively flat LAB (Figure 2.21). The change of fast-axis direction of azimuthal anisotropy with depth is a powerful tool for the detection of lithospheric layering under continents. Our study indicates that the "tectosphere" is no thicker than 200-240 km and that its chemically depleted part may bottom out around 160-170 km.

10.4 References

References are found in the References section of our paper: Yuan, H. and Romanowicz, B., Lithospheric layering in the North American Craton, *Nature*, 466, 1063-1068, 2010.

11 3-D Shear Wave Radially and Azimuthally Anisotropic Velocity Model of the North American Upper Mantle

Huaiyu Yuan, Barbara Romanowicz, Karen Fischer (Department of Geological Sciences, Brown University, Providence, Rhode Island, USA), and David Abt (ExxonMobil Exploration Company, Houston, Texas, USA)

11.1 Summary

Using a combination of long period seismic waveforms and SKS splitting measurements, we have developed a 3D upper mantle model (SAWum_NA2; *Yuan et al.* 2010) of North America that includes isotropic shear velocity (Figure 2.22) , with a lateral resolution of ∼200 km, as well as radial and azimuthal anisotropy (Figures 2.23, 2.24, respectively), with a lateral resolution of ∼400 km. Combining these results, we infer several key features of the lithosphere and asthenosphere structure.

A rapid change from thin (∼70-80km) lithosphere in the western US to thick lithosphere (∼200 km) in the central, cratonic part of the continent closely follows the Rocky Mountain Front (RMF; thick dashed line in Figure 2.22). Changes with depth of the fast axis direction of azimuthal anisotropy reveal the presence of two layers in the cratonic lithosphere, as shown in our companion paper (*Yuan and Romanowicz*, 2010a), and allow us to define the lithosphere-asthenosphere boundary (LAB) throughout the craton more precisely than from isotropic velocity tomography or the analysis of receiver function data, which, on the other hand, define the LAB consistently in the western US, where the boundary is sharper. The boundary between the two lithospheric layers in the craton varies significantly in depth and may correspond to the mid-lithospheric fast-to-slow discontinuity found in receiver function studies. Lateral variations in azimuthal and radial anisotropy in the cratonic lithosphere correspond to surface geological features marking tectonic events of the past.

Below the lithosphere, azimuthal anisotropy (Figure 2.23) manifests a maximum, stronger in the western US than under the craton, and the fast axis of anisotropy aligns with the absolute plate motion. In the western US, this zone is confined to between 70 and 150 km, decreasing in strength with depth from the top, from the RMF to the San Andreas Fault system and the Juan de Fuca/Gorda ridges. This result suggests that shear associated with lithosphere-asthenosphere coupling dominates mantle deformation down to this depth in the western part of the continent. The depth extent of the zone of increased azimuthal anisotropy below the cratonic lithosphere is not well resolved in our study, although it is peaked around 270 km, a robust result.

Radial anisotropy (Figure 2.24) is such that, predominantly, $\xi>1$, where $\xi=(V_{sh}/V_{sv})^2$, under the continent and its borders down to ∼200 km, with stronger ξ in the bordering oceanic regions. Across the continent and be-

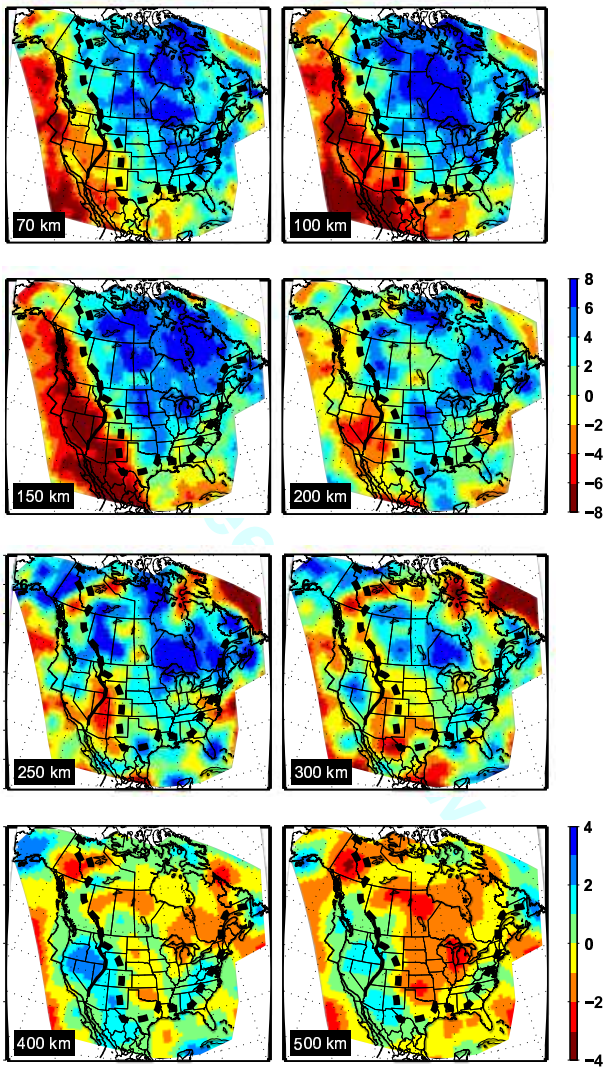

Figure 2.22: Isotropic velocity (V_s) perturbations, plotted with respect to the North America regional average shown (Figure 3 in *Yuan and Romanowicz*, 2010). Black dashed line approximately delineates the continent cratonic region, which approximately follows the Rocky Mountain front to the west, and the Ouachita and Appalachian fronts to the south and east. Velocity variations are saturated at -8% to 8% scale at ≤ 200 km depth, and -4% to 4% below 200km. The Paleozoic continent rift margin in the western US, which spatially correlates with the Sevier thrust and fold belt in the western US, is shown as a black line for reference.

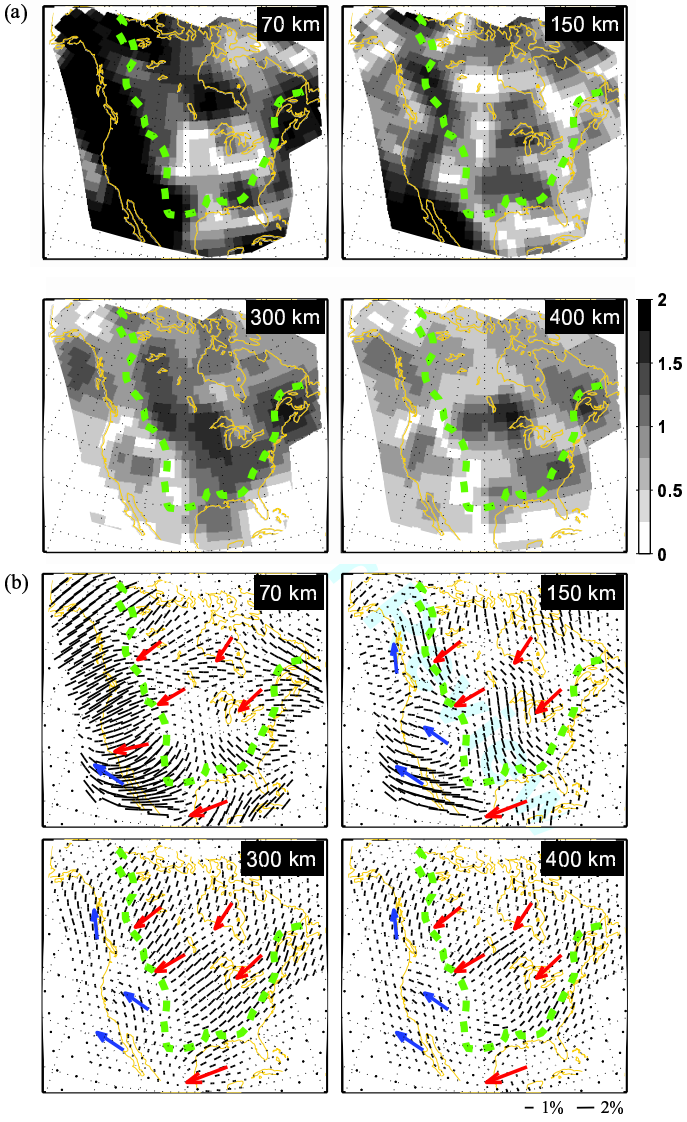

Figure 2.23: (a) Azimuthal anisotropy strength G. (b) Depth dependent fast axis direction. Red arrows show the absolute plate motion (APM) direction of the North American Plate, and blue arrows are those for the Pacific plate APM (Gripp and Gordon, 2002). Green dashed line approximately delineates the continent cratonic region as in Figure 2.22.

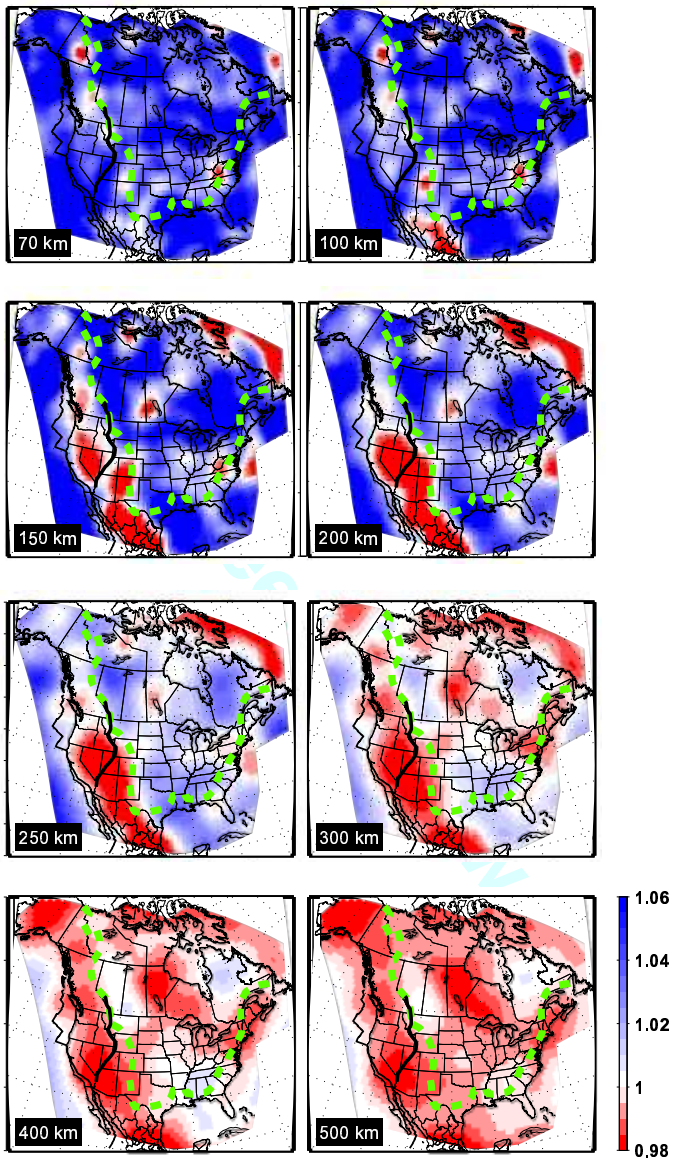

Figure 2.24: Radial anisotropy parameter ξ, plotted with respect to isotropy. Green dashed line approximately delineates the continent cratonic region, as in Figure 2.22. The Sevier thrust and fold belt in the western US is shown as a black line for reference.

low 200 km, alternating zones of weaker and stronger radial anisotropy, with predominantly ξ<1, correlate with zones of small lateral changes in the fast axis direction of anisotropy, and faster than average V_s below the LAB, suggesting the presence of small scale convection with a wavelength of ∼2000km.

11.2 References

Yuan, H. and Romanowicz, B., Lithospheric layering in the North American Craton, *Nature*, 466, 1063-1068, 2010a.

Yuan, H. and Romanowicz, B., Depth Dependent Azimuthal anisotropy in the western US upper mantle, *Earth Planet. Sci. Lett.*, doi:10.1016/j.epsl.2010.10.020, 2010b.

Yuan, H., Romanowicz, B., Fisher, K. and Abt, D., 3-D shear wave radially and azimuthally anisotropic velocity model of the North American upper mantle, *Geophys. J. Int.*, accepted, 2010.

12 Depth Dependent Azimuthal Anisotropy in the Western US Upper Mantle

Huaiyu Yuan and Barbara Romanowicz

12.1 Summary

We present the results of a joint inversion of long period seismic waveforms and SKS splitting measurements for 3D lateral variations of anisotropy in the upper mantle beneath the western US, incorporating recent datasets generated by the USArray deployment as well as other temporary stations in the region (*Yuan and Romanowicz*, 2010). We find that shallow azimuthal anisotropy closely reflects plate motion generated shear in the asthenosphere in the shallow upper mantle (70-150 km depth), whereas at depths greater than 150 km, it is dominated by northward and upward flow associated with the extension of the East-Pacific Rise under the continent, constrained to the east by the western edge of the North-American craton, and to the north by the presence of the east-west trending subduction zone. In particular, the depth integrated effects of this anisotropy explain the apparent circular pattern of SKS splitting measurements observed in Nevada without the need to invoke any local anomalous structures.

12.2 Circular pattern of the SKS splitting: Depth Integrated Effects

The recent deployment of the Transportable Array (TA) of EarthScope, as well as several other temporary broadband networks in the western US, have provided the opportunity to measure SKS splitting at a significantly larger number of locations in the region than was previously possible. Combined with previously available SKS splitting data, these measurements have revealed an intriguing apparent "circular" pattern in the distribution of fast axis directions and amplitude of anisotropy, centered in south-central Nevada, with vanishing strength in the center of the pattern (*Savage and Sheehan*, 2000; *Liu*, 2009; *West et al.*, 2009). Interestingly, some recent regional body wave tomographic studies also show the presence of a fast velocity anomaly extending into the transition zone, beneath the Cascades and High Lava Plains (e.g. *van der Lee and Nolet*, 1997; *Xue and Allen*, 2007; *Sigloch et al.*, 2008; *Burdick et al.*, 2009). Various geodynamic models have been proposed to address the mantle flow associated with these features, including: 1) initial impinging of the Yellowstone Plume into the lithosphere in the Basin and Range province (*Savage and Sheehan*, 2000; *Walker et al.*, 2004); 2) toroidal flow around the southern edge of the sinking Gorda-Juan de Fuca plate, associated with its retreating and the creation of a slab (*Zandt and Humphreys*, 2008); and 3) asthenospheric flow associated with a sinking lithospheric instability (or "drip") in the center of the Basin and Range (*West et al.*, 2009).

Our 3-D azimuthal anisotropy model (Figure 2.25; *Yuan and Romanowicz*, 2010) shows a strongly depth dependent azimuthal anisotropy pattern in the western US, with orientation of the fast axis controlled by plate motion related lithosphere-asthenosphere coupling at depths shallower than 150 km, and other processes at greater depths, likely representing the channeling of deep flow from the East Pacific Rise constrained by the presence of the craton margin to the west and subducted slabs to the north. We infer that all of these features combined significantly contribute to the circular pattern and large splitting times of the SKS splitting observations. The strong lateral and vertical variations throughout the western US revealed by our azimuthal anisotropy model reflect complex past and present tectonic processes. In particular, the depth integrated effects of this anisotropy (Figure 2.26) explain the apparent circular pattern of SKS splitting measurements observed in Nevada without the need to invoke any local anomalous structures (e.g. ascending plumes or sinking lithospheric instabilities; *Savage and Sheehan*, 2000; *West et al.*, 2009): the circular pattern results from the depth-integrated effects of the lithosphere-asthenosphere coupling to the North American, Pacific and Juan de Fuca plates at shallow depths, and in the depth range 200-400 km, northward flow from the East Pacific Rise channeled along the craton edge and deflected by the Juan de Fuca slab, and, more generally, slab-related anisotropy.

12.3 References

Burdick, S., van der Hilst, R.D., Vernon, F.L., Martynov, V., Cox, T., Eakins, J., Mulder, T., Astiz, L. and Pavlis, G.L., Model Update December 2008: Upper Mantle Heterogeneity beneath North America from P-wave Travel Time Tomography with Global and USArray Transportable Array Data, *Seismol. Res. Lett., 80*, 638-645, 2009.

Gripp, A.E. and Gordon, R.G., Young tracks of hotspots and current plate velocities, *Geophys. J. Int., 150*, 321-361, 2002.

Liu, K.H., NA-SWS-1.1: A uniform database of teleseismic shear wave splitting measurements for North America, *Geochem. Geophys. Geosyst., 10*, Q05011, doi:10.1029/2009GC002440, 2009.

Savage, M.K. and Sheehan, A.F., Seismic anisotropy and mantle flow from the Great Basin to the Great Plains, western United States, *J. Geophys. Res., 105(13)*, 715-713, 734, 2000.

Sigloch, K., McQuarrie, N. and Nolet, G., Two-stage subduction history under North America inferred from multiple-

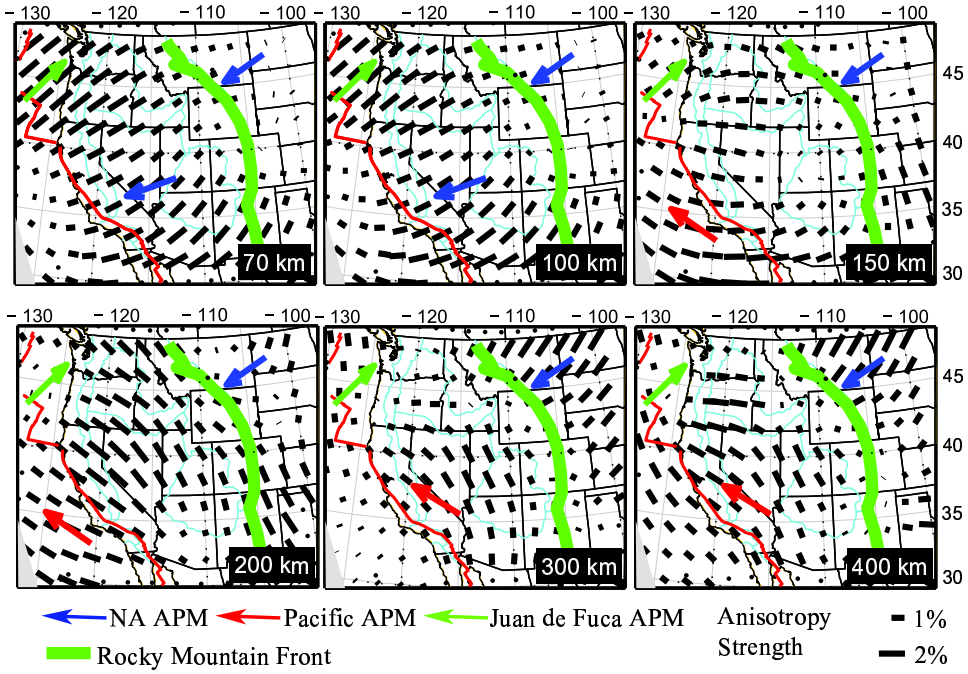

Figure 2.25: Azimuthal anisotropy variations with depth. Black bars indicate the fast axis direction and the bar length is proportional to the anisotropy strength. Blue, green and red arrows show the absolute plate motion (APM) directions of the North American, Juan de Fuca, and Pacific plates respectively, computed at each location using the HS3-NUVEL 1A model (*Gripp and Gordon*, 2002).

frequency tomography, *Nature Geosci., 1*, 458-462, 2008.

van der Lee, S. and Nolet, G., Upper mantle S velocity structure of North America, *J. Geophys. Res., 102*, 22815-22838, 1997.

Walker, K.T., Bokelmann, G.H.R. and Klemperer, S.L., Shear-wave splitting beneath the Snake River Plain suggests a mantle upwelling beneath eastern Nevada, USA, *Earth Planet. Sci. Lett., 222*, 529-542, 2004.

West, J.D., Fouch, M.J., Roth, J.B. and Elkins-Tanton, L.T., Vertical mantle flow associated with a lithospheric drip beneath the Great Basin, *Nature Geosci., 2*, 439-444, 2009.

Xue, M. and Allen, R.M., The fate of the Juan de Fuca plate: Implications for a Yellowstone plume head, *Earth Planet. Sci. Lett., 264*, 266-276, 2007.

Yuan, H. and Romanowicz, B., Depth Dependent Azimuthal anisotropy in the western US upper mantle, *Earth Planet. Sci. Lett.*, doi:10.1016/j.epsl.2010.10.020, 2010.

Zandt, G. and Humphreys, E., Toroidal mantle flow through the western US slab window, *Geology, 36*, 295-298, 2008.

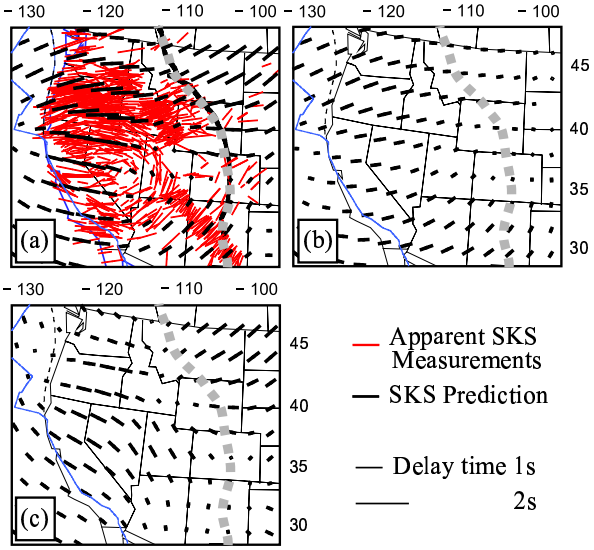

Figure 2.26: Comparison of observed and predicted station averaged SKS splitting direction and time. Red bars indicate observations and are shown in the left panels only, for clarity. Black bars indicate the model predictions. Predicted splitting is shown for integration of the models over, (a) the full depth range of the azimuthal anisotropy models, (b) the top 150 km of the models, and (c) the portion of the model between 150 and 500 km, respectively.

13 Seismic Signature of Perovskite and Postperovskite in the D"

Sanne Cottaar, Allen McNamara, Barbara Romanowicz and Rudy Wenk

13.1 Introduction

The D" zone at the base of the mantle is a boundary layer, both chemically and thermally. Complex dynamic processes are the cause of lateral heterogeneities, with sharp boundaries at the edge of superplumes (e.g. *Toh et al.*, 2005). Another characteristic of D" is the presence of strong and laterally varying anisotropy. A global long-wavelength model for S-wave velocity and radial anisotropy shows that, in general, SH phases are faster than SV phases (*Panning and Romanowicz*, 2006). This transverse isotropy is strongest in a ring around the Pacific, a.k.a. "the slab graveyard," and confirmed by a large number of regional studies. These observations lead to the idea that flow causes anisotropy by alignment of anisotropic minerals. This study combines geodynamics and mineral physics to investigate seismic heterogeneities and anisotropy in the D". Different seismic velocity models are created to constrain possible microscopic and macroscopic processes.

13.2 Method

The two-dimensional isochemical convection model is refined to emphasize deformation in D" (*McNamara and Zhong*, 2004). Lagrangian tracers travel through the lowermost part of the model providing strain information. Deformation is strong in the lowermost mantle, and if dislocation creep occurs, preferred orientation of minerals can cause seismic anisotropy. The exact resulting anisotropy depends on dominant deformation mechanisms and single crystal elastic constants. Using results from different experimental studies, we calculate the texturing of assemblages of perovskite and post-perovskite with periclase using VPSC (*Lebensohn and Tomé*, 1993). Averaging the single crystal elastic constants (*Stackhouse et al.*, 2005, *Wentzcovitch et al.*, 2007) over the orientation of the textured grains results in the prediction of a 2D, fully anisotropic model. Here we present a least squares fit of isotropic and transverse isotropic models to the fully anisotropic models.

13.3 Isotropic velocities

Results for the isotropic velocity models are presented in Figure 2.27A for 75% perovskite or 75% postperovksite with 25% periclase. Variations are mainly due to variations in pressure and temperature and are stronger than in typical inverted models. The temperature sensitivity of the shear modulus causes strong lateral S-wave velocity variations, while the bulk modulus, and thus the bulk sound velocity, have more sensitivity to vertical pressure variations. S-wave velocity variations are predicted to be stronger for post-perovskite than for perovskite. The occurrence of post-perovskite can thus explain the increase in $dlnV_s$ in the lowermost mantle in inverted models.

13.4 Transverse isotropic signature

Transversally isotropic models are shown in Figure 2.27B, in which the case for post-perovskite is expanded for three different dominant slip planes. Although all slip planes are activated during dislocation creep, different mineral physics experiments have concluded that different slip planes are dominant (*Merkel et al.*, 2007, *Miyagi et al.*, 2009, 2010). As the figures show, the different assemblages and deformation regimes result in different anisotropic signatures. The post-perovskite assemblage for dominant slip planes of [010] and [001] corresponds with these observations, while the perovskite assemblage has an opposite signature.

The results for dominant slip planes of [010] and [001] have opposite signatures for P-wave anisotropy. *Beghein et al.* (2006) find a likely anti-correlation between P and S wave anisotropy using normal modes, similar to the [001] case here. A number of local studies find anti-correlation between P and S wave velocities (*Wysession et al.*, 1999, *Tkalcic and Romanowicz*, 2002), as well as global studies, which find an anti-correlation between shear wave and bulk sound velocities (*Su and Dziewonski*, 1997). Possibly these measurements reveal the anti-correlation between SH and PH (or horizontal bulk sound velocity) caused by anisotropy, as isotropic variations (Figure 2.27A) cannot explain them.

The plumes on the right in the figures are more difficult to interpret as we use a 2D model for these 3D features, and it is more implausible for dislocation creep to occur at these higher temperatures.

13.5 Discussion and Conclusions

From a mineral physics point of view, the occurrence of the perovskite to post-perovksite transition a couple hundred kilometers above the D" is the subject of strong debate. *Shim et al.* (2009) show that adding Al and Fe causes the phase transition to broaden and shift to higher pressures.

From a seismological point of view, postperovskite can explain observations of strong S-wave heterogeneities, SH faster than SV in subduction regions, and anti-correlation between S and P wave anisotropy. Additionally, seismic

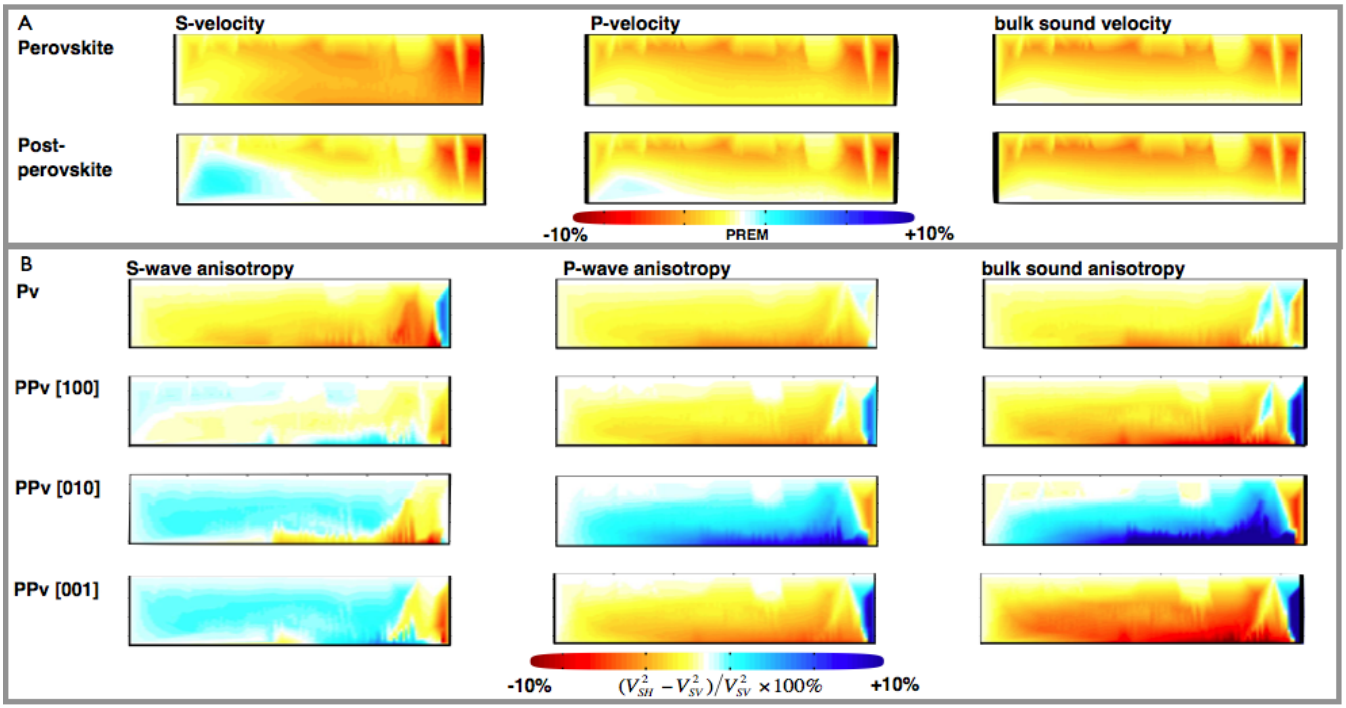

Figure 2.27: Best fitting isotropic and transversely isotropic models for the D". Figures are strongly vertically exaggerated: dimensions are ∼72 degrees horizontally to 300 km vertically above the core-mantle boundary (CMB). Slab subduction takes place on the left, and upwelling on the right. A. Isotropic velocities for perovskite and postperovskite plotted relative to PREM. B. Transversely isotropic models in which blue is SH faster than SV and red the opposite.

observations can constrain postperovskite to have a dominant slip plane along [001] as measured by *Miyagi et al.* (2010).

13.6 Acknowledgements

This project is funded by NSF's CSEDI program under grant number NSF EAR-0757608.

13.7 References

Beghein C., J. Trampert and H.J. van Heijst, Radial anisotropy in seismic reference models of the mantle, *J. Geophys. Res. 111*, B02303, 2006.

Lebensohn R.A., and C.N.Tomé, A self-consistent anisotropic approach for the simulation of plastic deformation and texture development of polycrystals, *Acta Metall. Mater. 41*, 2611-2624, 1993.

McNamara, A.K. and S. Zhong, The influence of thermochemical convection on the fixity of mantle plumes, *EPSL, 222*, 485-500, 2004.

Merkel S, A.K. McNamara, A. Kubo, S. Speziale, L. Miyagi, Y. Meng, T. S. Duffy, H.-R. Wenk, Deformation of (Mg,Fe)SiO3 post-perovskite and D anisotropy, *Science, 316*, 1729-1732, 2007.

Miyagi L., S. Merkel, T. Yagi, N. Sata, Y. Ohishi, H.-R. Wenk, Diamond anvil cell deformation of $CaSiO_3$ perovskite up to 49 GPa. *Phys. Earth Planet. Int., 174*, 159-164, 2009.

Miyagi L. et al., *in prep.*, 2010.

Panning, M. and B. Romanowicz, A three dimensional radially anisotropic model of shear velocity in the whole mantle,*Geophys. J. Int., 167*, 361-379, 2006.

Shim, S., K. Catalli, and V. Prakapenka, Seismic detectability of the postperovskite boundary, *AGU fall meeting*, abstract #DI21B-01, 2009.

Stackhouse, S., J.P. Brodholt, J. Wookey, J.-M. Kendall and G.D. Price, The effect of temperature on the seismic anisotropy of the perovskite and post-perovskite polymorphs of MgSiO3, *EPSL, 230*, 1-10, 2005.

Su W., and A.M. Dziwonski, Simultaneous inversion for 3-D variations in shear and bulk velocity in the mantle, *Phys. Earth Planet. Int., 100*, 135-156, 1997.

Thalcic H. and B. Romanowicz, Short Scale heterogeneity in the lowermost mantle: insights from PcP-P and ScS-S data, *EPSL, 201*, 57-68, 2002.

Toh, A., B. Romanowicz, Y. Capdeville and N. Takeuchi, 3D effects of sharp boundaries at the borders of the African and Pacific Superplumes: observation and modeling,*Earth and Planet. Sci. Lett., 233*, 137-153, 2005.

Wentzcovitch R.M., T. Tsuchiya, J. Tsuchiya, $MgSiO_3$ post-perovskite at D" conditions. *PNAS, 103*, 543-546, 2006.

Wysession, M.E., A. Langenhorst, M.J. Fouch, K.M. Fischer, G. I. Al-Eqabi, P.J. Shore, and T.J. Clarke, Lateral variations in compressional/ shear velocities at the base of the mantle, *Science, 284*, 120-125, 1999.

14 Using the SEM to Simulate Random Wavefields and Improve Noise Tomography

Paul Cupillard, Laurent Stehly and Barbara Romanowicz

14.1 Introduction

The correlation of a random wavefield recorded by distant receivers contains the Green's function (GF) of the medium. This makes the measurement of seismic wave travel times between any pair of receivers a possibility. These measurements can then be inverted to image the Earth's interior (e.g. *Shapiro et al*, 2005).

This result is valid in any medium but relies on a strong assumption: The wavefield has to be equipartitioned, that is, all the modes of the medium have to be excited with the same level of energy and a random phase (*Sánchez-Sesma and Campillo*, 2006). Equipartition is achieved, for instance, if there are white noise sources everywhere in the medium or if few sources are present in a highly scattering medium.

The seismic ambient noise comes from interactions between the atmosphere, the ocean and the sea floor. Even averaged over one year, the distribution of noise sources at the surface of the Earth is not homogeneous and does not completely match the requirements of the theories that relate noise correlations to the GF of the medium.

The uneven distribution of noise sources, the fact that one uses a finite amount of data to compute noise correlations, and the way noise correlations are inverted imply several limitations on ambient noise tomography. (i) In most of the noise tomographic studies, less than one interstation path out of three is used. Other paths are rejected because either surface waves cannot be identified unambiguously, or the surface wave travel times measured on the positive and negative side of the correlation are not consistent. This is mostly due to the uneven distribution of noise sources. (ii) The velocity of surface waves can be systematically over- or underestimated for certain azimuths, since noise sources are not evenly distributed. This could be erroneously interpreted as anisotropy of the medium. (iii) Most of the time, surface wave dispersion curves are inverted using the Path Average approximation. This procedure does not account for the complexity of the wave propagation within the Earth. When using noise correlations, this is an important problem because noise correlations are very sensitive to the crust, which is a very heterogeneous structure.

14.2 Simulating seismic ambient noise using the Spectral Element Method

In this work, we explore the possibility of taking into account the distribution of noise sources when inverting noise correlations. A first step towards such a goal is to perform a forward modeling which includes noise sources. To do so, we use the Spectral Element method (SEM). Computing synthetic correlations by simulating a random wavefield using the SEM would eliminate most of the biases arising from the uneven distribution of noise sources during the forward problem. We use the SEM instead of other methods such as the normal mode summation technique (*Cupillard and Capdeville*, 2010) because it enables us to solve the wave equation with no restriction on the velocity contrast of the model.

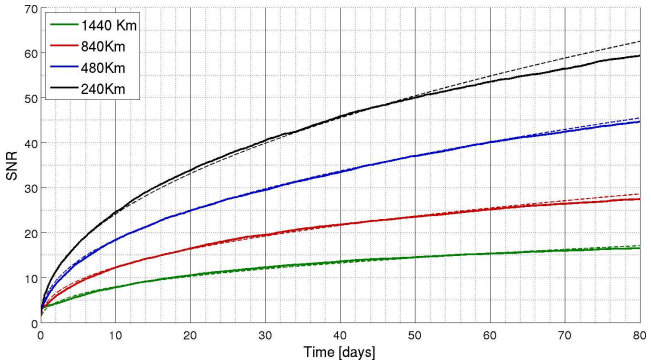

Figure 2.28: SNR of noise correlation surface waves as a function of the number of days of correlated noise (plain lines). Four interstation distances are considered. Each SNR curve is compared to the semi-empirical expression from *Larose et al* (2008) (dashed lines).

The code we use enables us to impose a three-component random traction on the top surface of the region. Because it makes the implementation very easy, the traction is discretized over the grid points of the spectral element mesh. For each grid point, three random signals are generated: one to define the normal traction and two to define the tangential traction. In the present work, we only use the normal component (the two tangential components are set to zero). All the random signals are filtered in the 25 - 80 s period band and are then used in the SEM simulation as an external surface force.

We start by investigating the easiest case: an homogeneous distribution of noise sources at the free surface of an attenuating and spherically symmetric Earth. Our simulation consists of 37 numerical runs computed in PREM and lasting 4 000 s each. We consider a 75x35 degree wide region surrounded by absorbing boundaries and a bottom lying at 600 km. An array of 40x5 receivers separated by 60 km records the vertical displacement. The

GF is retrieved between each station pair by correlating the background seismic noise records. No processing is performed on the noise records, such as frequency whitening or one-bit normalization.

Since we consider a 1D model, the GF only depends on the source-receiver distance. This implies that all correlations computed between station pairs separated by the same distance converge towards the same GF. Therefore, we consider that averaging the correlation over time T or over station pairs is equivalent. Since we perform 37 runs of 4 000 s, each receiver records $37 * 4\,000s = 1.7$ days of noise. As we have, for instance, 140 pairs of stations separated by 720 km, summing the corresponding correlations provides a result similar to correlating $37 * 140 * 4\,000\,s$ = 237 days of noise.

14.3 The convergence towards the GF

For scalar waves in a 2D homogeneous medium with a uniform source distribution, the signal-to-noise ratio (SNR) of the correlations is (*Larose et al*, 2008):

$$\mathrm{SNR}(T,r) = C\sqrt{\frac{n\,T\,\Delta f\,c}{r\,f}}, \qquad (2.2)$$

where r is the interstation distance, n the number of noise sources, c the velocity of the medium, f the frequency, Δf the bandwidth and C a constant.

We compare this theoretical prediction with our observations. Figure 2.28 shows how the SNR of the correlations evaluated in the 25-60 s period band evolves with the amount of data used for stations separated by 240, 480, 840, and 1440 km. For a short offset, less than two days are required to get a SNR > 10, and 20 days are required for stations separated by 1440 km. We fit this SNR vs time curve with a function of the form $a\left(\frac{n\,T\,\Delta f\,c}{r\,f}\right)^b$, a and b being two free parameters we want to determine. We find that our SNR measurements are best fitted with a=27.8 and b=0.45, i.e the SNR increases with $T^{0.45}$ whereas theoretically one expects $T^{0.5}$. However, this difference is only an artifact, coming from our assumption that averaging correlation over time is equivalent to averaging them over the interstation pairs.

14.4 Improving synthetic noise correlations using curvelet filters

Our numerical results show that (i) it takes only a few days to reconstruct accurately the surface wave part of the Green's function and (ii) several months of data are required for the random fluctuations of the correlation to disappear. If most of the information on the medium is already present in a correlation averaged over a few days, then it should be possible to isolate this information from the random fluctuations of the correlation. This would allow us to not only measure surface wave travel times more accurately, but also reconstruct the full waveform of the GF using a smaller amount of data. Figure 2.29 shows that curvelet filters achieve this goal very well.

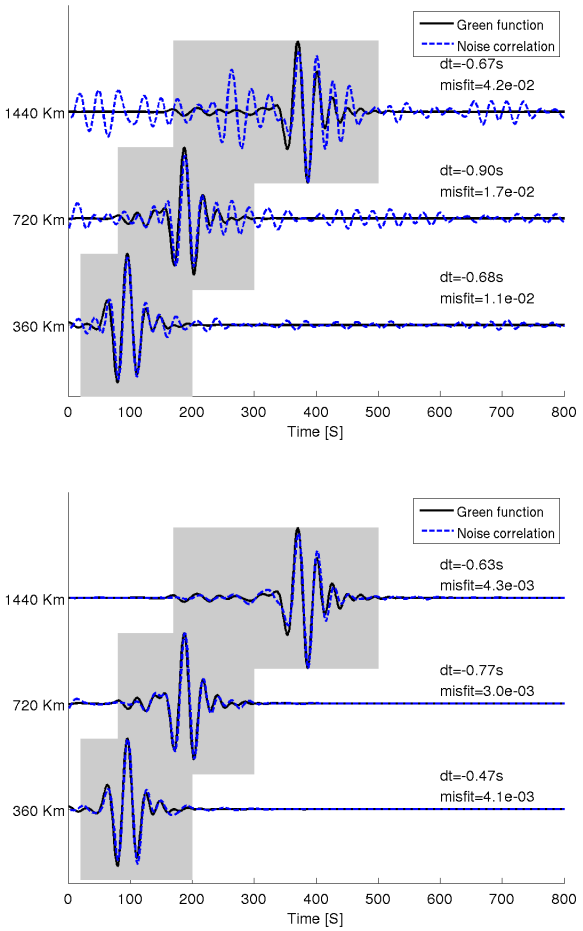

Figure 2.29: Correlations of 11 days of noise between stations separated by 320, 720 and 1440 km (dashed lines) vs corresponding GF (plain lines). For each comparison, we show the misfit of the correlation and GF waveforms measured in the shaded area and the surface wave travel time difference dt. Top: raw correlations. Bottom: correlations de-noised by curvelet filters.

14.5 References

Cupillard, P. and Y. Capdeville, On the amplitude of surface waves obtained by noise correlation and the capability to recover the attenuation: a numerical approach, *Geophys. J. Int., 181(3)*, 1687-1700, 2010.

Larose, E., P. Roux, M. Campillo and A. Derode, Fluctuations of correlations and Green's function reconstruction: role of scattering, *J. Appl. Phys., 103*, 114907, 2008.

Sánchez–Sesma, F. J. and M. Campillo, Retrieval of the Green's function from cross-correlation: The canonical elastic problem, *Bull. Seism. Soc. Am., 96*, 1182-1191, 2006.

Shapiro, N. M., M. Campillo, L. Stehly and M. H. Ritzwoller, High-resolution surface wave tomography from ambient seismic noise, *Science, 307*, 1615-1618, 2005

15 Toward the Future of Global Waveform Tomography: Scalable Gauss-Newton and Alternative Data-Partitioning Schemes

Scott French, Vedran Lekic, and Barbara Romanowicz

15.1 Introduction

With increasingly fine-scale parameterization of global tomographic models comes growth of the linear systems that underlie most iterative inversion schemes (e.g. SEMum: *Lekic and Romanowicz*, 2010). As assembly and solution of these systems becomes intractable on modern workstations, distributed-memory parallel solvers provide an attractive alternative. We summarize the development of a parallel solver tailored to the regularized Gauss-Newton scheme often used in global tomography.

In a separate effort, we explore alternative data-partitioning schemes for waveform inversion using a synthetic dataset. The SPICE tomographic benchmark was developed to evaluate the effects of inversion methodology on the resolving power of tomographic images (*Qin et al.*, 2008). We discuss our use of the simpler SPICE "preliminary" waveform dataset to examine data-partitioning schemes different from those employed in Berkeley global tomographic efforts to date.

15.2 A parallel Gauss-Newton solver for waveform tomography

In waveform tomography, we seek to invert a dataset of long-period waveforms $\mathbf{d}$ for a model of earth structure $\mathbf{m}$. The non-linear dependence of the wavefield upon $\mathbf{m}$ requires structural sensitivity to be linearized and $\mathbf{m}$ iteratively estimated. The generalized least-squares formalism is popular choice for such problems (e.g. *Tarantola*, 2005), and gives rise to the following regularized Gauss-Newton scheme:

$$\left(\mathbf{G}_k^T\mathbf{C}_d^{-1}\mathbf{G}_k + \epsilon^2\mathbf{C}_m^{-1}\right)\delta\mathbf{m}_k = \mathbf{G}_k^T\mathbf{C}_d^{-1}\delta\mathbf{d}_k + \epsilon^2\mathbf{C}_m^{-1}\delta\mathbf{m}_p$$

where $\mathbf{m}_k$ and $\mathbf{m}_{k+1}$ are current and updated model estimates, $\mathbf{m}_p$ and $\mathbf{C}_m$ are *a priori* model and covariance matrix estimates, $\mathbf{C}_d$ the data covariance matrix, and $\mathbf{G}_k$ the current waveform Jacobian matrix. Also, for clarity: $\delta\mathbf{m}_k = \mathbf{m}_{k+1} - \mathbf{m}_k$, $\delta\mathbf{d}_k = \mathbf{d} - g(\mathbf{m}_k)$, and $\delta\mathbf{m}_p = \mathbf{m}_p - \mathbf{m}_k$, where $g(\cdot)$ is the forward modeling operator.

While $\mathbf{G}_k$ possesses a sizable zero component, it is generally non-sparse. Thus, the m-by-m matrix $\mathbf{G}_k^T\mathbf{C}_d^{-1}\mathbf{G}_k + \epsilon^2\mathbf{C}_m^{-1}$, where m is the dimension of $\mathbf{m}$, is likely fully dense. In the case of the SEMum model of Lekic and Romanowicz (2010), where $m \simeq 38500$, wall-clock times of approximately one day were observed during assembly and sequential solution of the above system using MATLAB$^{\text{TM}}$ on a modern workstation. Further, repeated solution is required at each linearized iteration ($k \rightarrow k+1$) in order to evaluate model sensitivity to regularization. Thus, parallel solution for the regularized Gauss-Newton update described above is a desirable capability.

A parallel solver mimicking the functionality of the sequential code was developed and validated, utilizing the Scalable Linear Algebra PACKage (`ScaLAPACK`) - named for its attractive weak-scaling behavior on large dense problems such as these (*Choi et al.*, 1996). A robust parallel implementation of LU decomposition with partial pivoting was used. Benchmark tests were performed for realizations of the above system arising in the development of SEMum, and wall-clock solve times for a range of processor grids are shown in Table 2.1.

Processor Cores	4	16	64
Mean Wall-clock Time (s)	4388	1612	464.7

Table 2.1: Mean wall-clock times for a series of validation solves.

Perhaps most importantly, this savings in compute-time allows for faster and more detailed enumeration of model sensitivity to regularization - hopefully leading to greater flexibility in scheduling of compute resources for far heavier workloads, such as wavefield modeling with the Spectral Element Method (SEM: e.g. Komatitsch and Vilotte, 1998).

15.3 Synthetic tests of alternative data-partitioning schemes

The simple isotropic model underlying the SPICE "preliminary" benchmark contains three large ($r > 2500$ km) and five small ($r \simeq 1000$ km) columnar V_s perturbations of $\pm 2.5\%$ and $\pm 6\%$ respectively, from which V_p and ρ are scaled (*Qin et al.*, 2008). These structures have roughly Gaussian profile and extend from the surface to the CMB. The associated SEM synthetic dataset is valid to 50 s period, which we further bandpass filtered with corners at 80 and 250 s and cutoff at 60 and 400 s. Following the waveform partitioning and weighting scheme of Li and Romanowicz (1996), first and second orbit Rayleigh wave fundamental mode and overtone wavepackets were selected from vertical component waveforms for all 27 synthetic events recorded at the 256 stations in the dataset.

While maintaining a 1D crust, we inverted for mantle structure using the path-average approximation (PAVA:

Woodhouse and Dziewonski, 1984) and non-linear asymptotic coupling theory (NACT: *Li and Romanowicz*, 1995) for fundamental mode and overtone data, respectively. We partitioned the inversion at $\sim$ 300 km, below which the resolving power of fundamental mode data rapidly decreases, and adjusted the relative weight assigned to the fundamental mode and overtone datasets in each partition. We found that we could more effectively extend model sensitivity into the transition zone over simply merging the datasets with a uniform weighting. The cubic spline model parametrization was kept continuous across the partition so that the model would remain smooth. This represents a methodology broadly consistent with Berkeley tomographic studies to date.

To explore alternative approaches to optimizing depth sensitivity, we proposed a simple multi-frequency scheme. Overlapping filters with cutoff periods of 60/140 s, 120/200 s, and 180/260 s were applied to SPICE vertical component waveforms, which were further weighted according to path redundancy as in Li and Romanowicz (1996), as well as maximum waveform amplitude. As the filtered waveforms are dominated by fundamental mode surface waves, we chose to invert full waveforms using PAVA only. During the inversion, sensitivities of each of the filtered datasets were independently weighted to maximize smoothness of total sensitivity with depth. Unsurprisingly, resolution of structure through the transition zone, best constrained by overtone surface waves, was notably degraded relative to the wavepacket-partitioned inversion. A far more complex multi-frequency scheme (e.g. AMI: *Lebedev et al.*, 2005) would likely be required in order to compete with the wavepacket-based scheme.

As approximate forward modeling schemes are supplanted by SEM in waveform tomography (e.g. SEMum: *Lekic and Romanowicz*, 2010), mitigation of computational cost takes on new importance. One proposed solution is the source-stacking technique (*Capdeville et al.*, 2005). Linearity of the elastic wave equation with respect to source implies that SEM waveforms stacked over individual sources are equivalent to those resulting from simultaneous triggering of sources in a single simulation. Thus, inversion of source-stacked traces may provide a novel avenue for waveform tomography at vastly reduced cost. As a naïve test, we sought to invert the SPICE preliminary benchmark using PAVA for both the sensitivity kernels and as a stand-in for SEM.

Vertical component SPICE synthetic waveforms were bandpassed with corners at 120 and 250 s (cutoff at 100 and 400 s), aligned on event origin time, weighted by scalar moment magnitude, and stacked over all 27 events. PAVA sensitivity kernels and synthetics were similarly weighted and stacked. Using these approximate methods alone, the structure of the SPICE model became recognizable as early as the second inversion iteration (see Figure 2.30). Of course, while these results are highly preliminary and do not reflect realistic data reliability and noise conditions, they reiterate the promise of the source stacking method. Overcoming the shortcomings present in realistic datasets, as well as developing methods for optimized event-station clustering, are of primary concern moving forward.

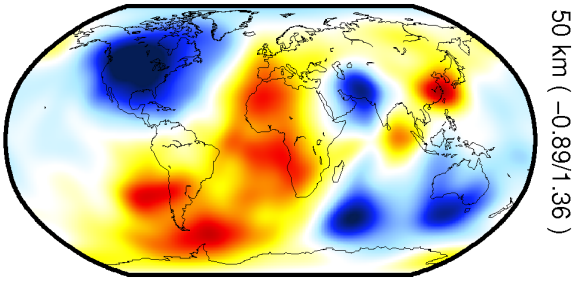

Figure 2.30: Depth snapshot at 50 km after stacked-waveform inversion iteration 2, PAVA only.

15.4 Acknowledgements

This research was supported by National Science Foundation grant NSF/EAR-0738284.

15.5 References

Capdeville, Y., Y. Gung, and B. Romanowicz, Towards global earth tomography using the spectral element method: a technique based on source stacking, *Geophys. J. Int, 162,* 541-554, 2005.

Choi, J., J. Demmel, I. Dhillon, J. Dongarra, S. Ostrouchov, A. Petitet, K. Stanley, D. Walker, and R.C. Whaley, ScaLAPACK: a portable linear algebra library for distributed memory computers - design issues and performance, *Comp. Phys. Comm., 97,* 1-15, 1996.

Komatitsch, D. and J. Vilotte, The spectral element method: an efficient tool to simulate the seismic responds of 2D and 3D geological structures, *Bull. Seism. Soc. Am., 88,* 368-392, 1998.

Lebedev, S., G. Nolet, T. Meier, and R.D. van der Hilst, Automated multimode inversion of surface and S waveforms, *Geophys. J. Int., 162,* 951-964, 2005.

Lekic, V. and B. Romanowicz, Inferring upper mantle structure by full waveform tomography with the Spectral Element Method, Submitted to *Geophys. J. Int.,* 2010.

Li, X.D. and B. Romanowicz, Comparison of global waveform inversions with and without considering cross-branch modal coupling, *Geophys. J. Int., 121,* 695-709, 1995.

Li, X.D. and B. Romanowicz, Global mantle shear-velocity model developed using nonlinear asymptotic coupling theory, *Geophys. J. R. Astr. Soc., 101,* 22,245-22,272, 1996.

Qin, Y., Y. Capdeville, V. Maupin, J.-P. Montagner, S. Lebedev, and E. Beucler, SPICE Benchmark for global tomographic methods, *Geophys. J. Int., 175,* 598-616, 2008.

Tarantola, A., *Inverse problem theory and methods for model parameter estimation,* SIAM, 2005.

Woodhouse, J.H. and A.M. Dziewonski, Mapping the upper mantle: Three dimensional modeling of earth structure by inversion of seismic waveforms, *J. Geophys. Res, 89,* 5953-5986, 1984.

16 Towards Constraining Lateral Variation of Attenuation Structure With Low-Degree Normal Modes Splitting Coefficients

Shan Dou and Barbara Romanowicz

16.1 Introduction

The study of attenuation is very challenging because of the complexity in its measurements and interpretation. However, attenuation is important for at least two reasons:

1) Attenuation is considerably more sensitive to temperature variations than elastic velocities. While elastic velocities have a quasi-linear dependence upon temperature variations, seismic attenuation depends exponentially on temperature (e.g., *Jackson*, 1993; *Karato*, 1993). Therefore, attenuation tomography is important for studying temperature variations within the Earth, and combining elastic and anelastic studies has the potential to separate different effects of chemical composition, water content, partial melting, etc.

2) Attenuation causes physical dispersion of seismic velocities, and this effect needs to be corrected for in velocity models.

16.2 Motivation and Theory

The two large regions of low shear velocity (Very Low Shear Velocity Provinces, denoted as LLSVPs in the following content) in the lowermost mantle located beneath the south-central Pacific Ocean and southern Africa/southern Atlantic/Southern Indian ocean regions are unusual deep structures that could offer important indications about the dynamic structures. Because these two LLSVPs each have a lateral extent that is much greater than what might be expected for a hot upwelling plume rising from a thermal boundary layer, they are usually referred to as "superplumes." However, resolving the dynamical significance of these large scale features is nontrivial as well as complicated: Low velocities may be caused by high temperatures or by chemical differences or the competing effects of the two. A variety of body wave studies have reported large velocity anomalies (varying from 1% to 10%) and strong lateral gradients (e.g. *Ritsema et al.*, 1998; *Ni and Helmberger*, 2003a, 2003b; *Wen et al.*, 2001; *Wang and Wen, 2004, 2006*; *Tanaka*, 2002; *Toh et al.*, 2005; *Ford et al.*, 2006; *He et al.*, 2006). Shear wave velocities tend to reduce at deep-mantle pressures, and thus lateral variations of $500 \sim 1000_{\circ}$ over ~ 100 km are needed to contribute to the observed velocity anomalies. Thermal anomalies to this extent could lead to the onset of partial melting that can generate strong velocity reductions. On the other hand, of chemical variations appear to be important in LLSVPs, the temperature contrasts may be far lower.

Comparing P-wave and S-wave velocities can offer important indications that LLSVPs involve chemical heterogeneities. One of the most important results from previous studies is that LLSVPs have a bulk-sound-velocity anomaly that is anti-correlated with the shear wave velocity anomalies (e.g. *Resovsky and Trampert*, 2003; *Trampert et al.*, 2004). Several normal modes studies *Ishii and Tromp*, 1999; *Trampert et al.*, 2004) also indicate that density heterogeneity exists at the base of the mantle, which is dominated by the two LLSVPs on a large scale. The anti-correlation between density and shear velocity anomalies that are proposed in these studies favors chemical heterogeneity. This remains a topic of controversy (e.g. *Romanowicz*, 2001; *Kuo and Romanowicz*, 2002), but at the same time, it is equally critical to better resolve the density and anelastic structure to assess the effect of thermal buoyancy and chemical negative buoyance. Nonetheless, resolving the attenuation signature of LLSVPs is quite challenging due to the contamination from the elasticity effect and strong lateral variations existing in the upper mantle. Because surface waves lose their sensitivity to such deep structures, lower mantle tomography mostly relies on deep-turning teleseismic body waves and normal mode data. Different from body wave datasets that could be degraded by uneven distribution of events and stations, the Earth's free oscillations involve the vibration of the whole planet and thus are much less likely to be biased by source-receiver geometry. In this way, information carried by normal modes signals can serve quite well for the purpose of exploring the physics properties of the large scale lateral variations in the lowermost mantle.

For normal mode multiplets well isolated in complex frequency, the effect of even-order aspherical structure on the splitting behavior of the spectra can be quantitatively represented by a discrete set of "splitting coefficients." These coefficients determine the coupling of the singlets within a multiplet. The splitting coefficients describe a radial average of three-dimensional heterogeneity, and can be related to internal properties by:

$$c_{st} = e_{st} + i a_{st}$$

$$e_{st} = \int_0^a \delta m_s^t(r) K_s(r) r^2 dr + \sum_d h_{sd}^t B_{sd} r_d^2$$

$$a_{st} = \int_0^a (\delta q_{\kappa s}^t K_{q\kappa} + \delta q_{\mu s}^t K_{q_\mu}) r^2 dr$$

Owing to the high quality digital data set assembled in the last 20 years on the global broadband seismic network, and owing to the occurrence of several very large earthquakes, putting new constraints on the large-scale attenuation in the lower mantle from normal modes is promising.

16.3 Preliminary Results and Prospective Work

We applied the Iterative Spectral Fitting (ISF) method (*Ritzwoller et al.* 1986, 1988) in the study. In the ISF approach, the technique breaks down naturally into two parts: A discrete regression for the interaction coefficients for a number of lower mantle sensitive modes followed by a continuous inverse problem to solve for the three-dimensional structure from the splitting coefficients. Figure 2.31 shows examples of elastic splitting functions obtained from the ISF approach, and we can clearly see the dominant degree-2 pattern in all of the mantle modes shown in the figure.

We applied the same technique to resolve anelastic splitting coefficients, but due to the data noise and very limited size of the dataset used in the study, the retrieved anelastic coefficients are generally below the error level, and appear to be quite unstable and strongly rely on the elastic starting model. With more data involved in the inversion, and more optimum regularization design, we hope to improve the stability of the anelastic splitting coefficients and then go further to invert for a three-dimensional anelastic model of the lower mantle from normal modes. Even if we can only resolve the longest wavelengths (degrees 2 or possibly up to 4), this will be important for the understanding of the nature of the two low velocity regions at the base of the mantle, commonly referred to as "superplumes," whose thermo-chemical nature is still under debate (e.g. *Masters et al.*, 1982; *Romanowicz*, 1998; *Bijwaard and Spakman*, 1999; *Ishii and Tromp*, 1999; *Romanowicz, 2001*; *Trampert et al.*, 2004; *Gung and Romanowicz*, 2004; *Anderson*, 2005).

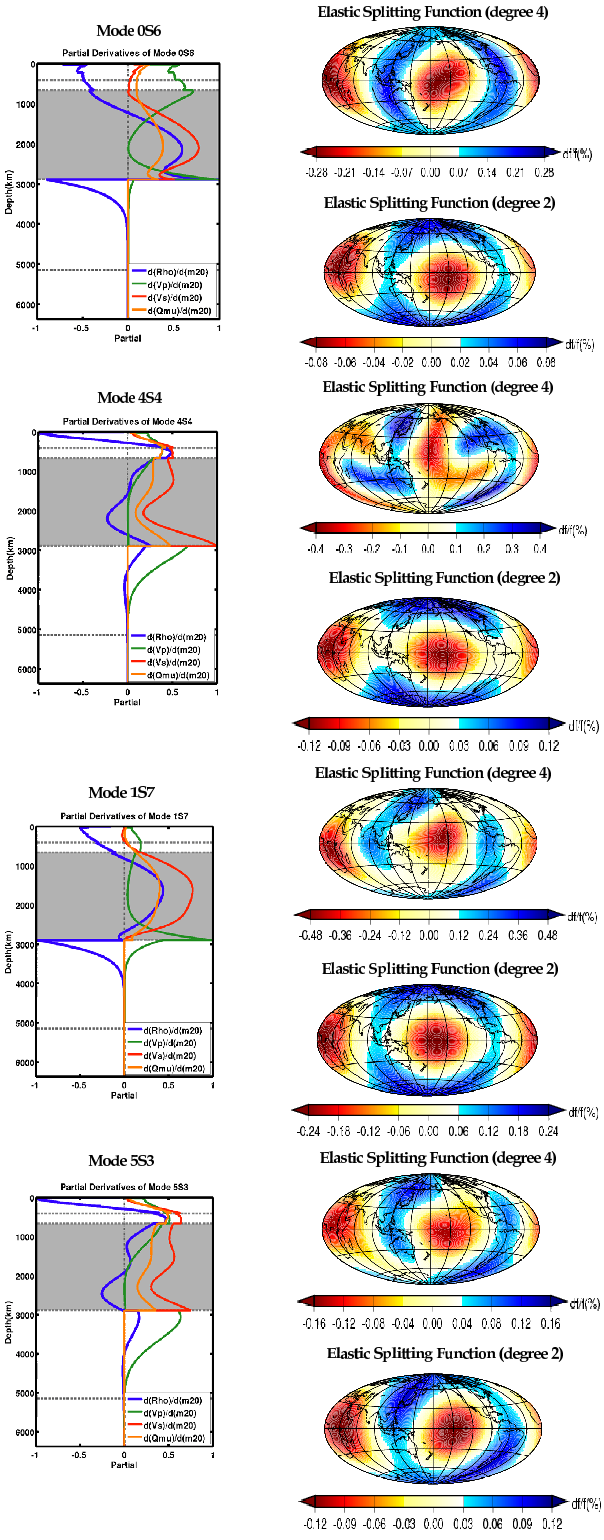

Figure 2.31: Examples of splitting function for mantle-sensitive modes ${}_0S_6$, ${}_4S_4$, ${}_1S_7$, and ${}_5S_3$

16.4 References

Ritzwoller M, Masters G, and Gilbert F, Observations of anomalous splitting and their interpretation in terms of aspherical structure with low frequency interaction coefficients: Application to uncoupled multiplets, *Journal of Geophysical Research*, *91*, 10203-10228, 1986.

Ritzwoller M, Masters G, and Gilbert F, Constraining aspherical structure with low frequency interaction coefficients: Application to uncoupled multiplets, *Journal of Geophysical Research*, *93*, 6369-6396, 1988.

Romanowicz B and Mitchell B, Deep Earth Structure — Q of the Earth from Crust to Core, *Treatise on Geophysics*, *Volume 1*, 775-803, 2007.

Widmer-Schnidrig R and Laske G, Theory and Observations — Normal Modes and Surface Wave Measurements, *Treatise on Geophysics*, *Volume 1*, 67-125, 2007.

17 Efficient Computation of NACT Seismograms: Toward Application in Imagining Upper Mantle Discontinuities

Zhao Zheng and Barbara Romanowicz

17.1 Introduction

The Berkeley Global Seismology group has been developing global mantle tomographic models (*Li and Romanowicz*, 1996; *Mégnin and Romanowicz*, 2000; *Panning and Romanowicz*, 2006) by inverting a dataset of surface waveforms down to 60 sec and long-period body waveforms down to 32 sec. A normal mode coupling method known as the Non-linear Asymptotic Coupling Theory (NACT; *Li and Romanowicz*, 1995) has been successfully applied to compute 3D synthetic seismogram and sensitivity kernels. It is an approximate approach which collapses sensitivity over the whole volume onto the vertical plane containing source and receiver. By taking into account the depth variation of sensitivity, NACT is able to bring out the ray character of body waves as well as the finite-frequency behavior of sensitivity kernels. On the other hand, as an approximate approach, it is computationally much faster than purely numerical methods such as the Spectral Element Method (SEM).

The frequency band ($\geq$ 32 sec) of the current tomographic dataset is too low to retrieve fine scale structures of upper mantle discontinuities, which place vital constraints on the temperature, composition and dynamics of the mantle. In order to retrieve them, it is necessary to incorporate phases such as the *SS* precursors.

Most *SS* precursor studies so far measure *SS-SdS* differential travel time and translate that to discontinuity depth, therefore suffering from the tradeoff between volumetric perturbation and discontinuity topography (for a review, see *Deuss*, 2009). Modeling the 3D waveforms of precursors will help to resolve this tradeoff. However, these precursor phases are typically peaked at a much shorter period ($\sim$10 sec), therefore presenting a great computational challenge to the current mode coupling scheme of NACT, in which the computational cost grows as f_{max}^4 with f_{max} being the cutoff frequency.

17.2 An Efficient NACT Formalism

In the NACT theory, the perturbed seismogram consists of an along-branch coupling term, which is computed under the well-known PAVA approximation (*Woodhouse and Dziewonski*, 1984), and an across-branch coupling term, which is computed under the linear Born approximation. In the classical formalism, the Born part is obtained by a double summation over all pairs of coupling modes (*Li and Romanowicz*, 1995):

$$\delta u(t) = \sum_k \sum_{k'} A_{kk'} \frac{exp(i\omega_k t) - exp(i\omega_{k'} t)}{\omega_k^2 - \omega_{k'}^2} \qquad (2.3)$$

where $k = (n, l)$ and $k' = (n', l')$ are indices for normal modes (n the radial and l the angular order), and

$$A_{kk'} = \sum_m \sum_{m'} R_k^m H_{kk'}^{mm'} S_{k'}^{m'} \qquad (2.4)$$

where R_k^m and $S_{k'}^{m'}$ (m being the azimuthal order of normal mode) are the receiver and source terms as defined in *Woodhouse and Girnius* (1982), and the coupling matrix $H_{kk'}$ due to perturbation in the elastic tensor $\mathbf{C}$ is:

$$H_{kk'}^{mm'} = \int_V \mathbf{e}_k^{m*}(\mathbf{r}; \mathbf{r}_R) : \delta\mathbf{C}(\mathbf{r}) : \mathbf{e}_{k'}^{m'}(\mathbf{r}; \mathbf{r}_S) dV \qquad (2.5)$$

with $\mathbf{e}_k^m$ being the strain of mode (k, m), subscript R and S for the location of seismic receiver and source, "$*$" denoting complex conjugate, and ":" double dot product.

In practice, the summation is truncated below some cutoff frequency f_{max}. Since the number of modes with eigenfrequencies below a certain cutoff frequency is roughly proportional to f_{max}^2, the cost of computing one seismogram grows with frequency as f_{max}^4. For multiple sources and receivers, the computational cost goes $(N_S * N_R) * f_{max}^4$, where N_S and N_R are the number of sources and receivers, respectively.

Here we present a more efficient formalism. From the physical inspiration that the Born approximation is a single-scattering approximation, i.e., the seismic wavefield due to a heterogeneity scatterer is the convolution of a source-to-scatterer term and a scatterer-to-receiver term, we see it is possible to separate the double summation over mode pairs to two single summations (*Capdeville*, 2005). In particular, the Born seismogram can be expressed in the frequency domain as (*Tanimoto*, 1984):

$$\delta u(\omega) = \sum_k \sum_{k'} A_{kk'} \frac{1}{i\omega(\omega^2 - \omega_k^2)(\omega^2 - \omega_{k'}^2)} \qquad (2.6)$$

Upon substituting (2) in (4) and separating the terms that are indexed by (k, m) and those by (k', m'), one finds

$$\delta u(\omega) = \int_V \mathbf{R}(\mathbf{r}, \omega) : \delta\mathbf{C}(\mathbf{r}) : \mathbf{S}(\mathbf{r}, \omega) dV \qquad (2.7)$$

with

$$\mathbf{R}(\mathbf{r},\omega;\mathbf{r}_R) = \sum_k (\sum_m R_k^m \mathbf{e}_k^{m*}) \frac{1}{\omega^2 - \omega_k^2} \qquad (2.8)$$

$$\mathbf{S}(\mathbf{r},\omega;\mathbf{r}_S) = \sum_{k'} (\sum_{m'} S_{k'}^{m'} \mathbf{e}_{k'}^{m'}) \frac{1}{i\omega(\omega^2 - \omega_{k'}^2)} \qquad (2.9)$$

accounting for the scatterer-to-receiver and the source-to-scatterer contributions, respectively. Returning to the time domain, one can write

$$\delta u(t) = \int_V \mathbf{R}(\mathbf{r},t) : \delta\mathbf{C}(\mathbf{r}) \star : \mathbf{S}(\mathbf{r},t) dV \qquad (2.10)$$

with

$$\mathbf{R}(\mathbf{r},t;\mathbf{r}_R) = \sum_k (\sum_m R_k^m \mathbf{e}_k^{m*}) \frac{\sin(\omega_k t)}{\omega_k} \qquad (2.11)$$

$$\mathbf{S}(\mathbf{r},t;\mathbf{r}_S) = \sum_{k'} (\sum_{m'} S_{k'}^{m'} \mathbf{e}_{k'}^{m'}) \frac{1 - \cos(\omega_{k'} t)}{\omega_{k'}^2} \qquad (2.12)$$

and "$\star$" in (8) denoting temporal convolution.

As commented by *Capdeville* (2005), this formalism is similar to the adjoint method (e.g. *Tarantola*, 1984). Since the summations in (9) and (10) can be performed simultaneously, the cost of computing one seismogram now grows as f_{max}^2 as opposed to f_{max}^4 in the original NACT. For multiple paths, the cost is $(N_S + N_R) * f_{max}^2$, as compared to $(N_S * N_R) * f_{max}^4$. Asymptotic approximation can still be applied to collapse the integral over whole volume in (8) onto the great circle plane, as did the original NACT.

17.3 Numerical Validation

A numerical test is designed to validate the new formalism. Synthetic seismograms are computed for a path geometry shown in Figure 2.32 using the old and new formalisms, respectively. The result shows that the two synthetics agree very well in both phase and amplitude.

Table 2.2 lists the CPU time of computing a single synthetic seismogram with the two formalisms, respectively, for several cutoff frequencies. Time cost of the new formalism scales roughly as f_{max}^2, whereas that of the original NACT scales as f_{max}^3 (rather than the theoretically f_{max}^4, because in practice the mode coupling was restricted to some fixed coupling width s such that $|l' - l| \leq s$, where l is the angular order of modes). Therefore, the new formalism is computationally preferable when approaching higher frequencies. It is even more advantageous in the case of many sources and receivers, which is the reality of seismic tomography.

17.4 References

Capdeville, Y., An efficient Born normal mode method to compute sensitivity kernels and synthetic seismograms in the Earth, *Geophys. J. Int., 163,* 639-646, 2005.

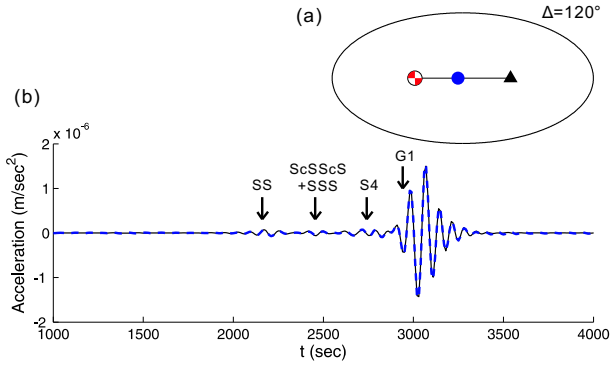

Figure 2.32: (a) Path geometry of the numerical test. A cylindrical anomaly (blue) between 0 and 1000 km depth with 2% faster V_S than PREM is located halfway between the source and the receiver. (b) Transverse component synthetic seismogram computed up to 60 sec with the original NACT (black line) versus the new formalism (blue dashed line). Major seismic phases are labeled.

Table 2.2: Time cost for computing one synthetic seismogram on a 1 GHz single CPU.

f_{max} (period)	original NACT	new formalism
60 sec	6.9 min	22 min
30 sec	56 min	72 min
10 sec	25 hr	10 hr

Deuss, A., Global observations of mantle discontinuities using SS and PP precursors, *Surv. Geophys., 30,* 301-326, 2005.

Li, X.D. and B. Romanowicz, Comparison of global waveform inversions with and without considering cross-branch modal coupling, *Geophys. J. Int., 121,* 695-709, 1995.

Li, X.D. and B. Romanowicz, Global mantle shear-velocity model developed using nonlinear asymptotic coupling theory, *J. Geophys. Res., 101(B10),* 22,245-22,272, 1996.

Mégnin, C. and B. Romanowicz, The three-dimensional shear velocity structure of the mantle from the inversion of body, surface and higher-mode waveforms, *Geophys. J. Int., 143(3),* 709-728, 2000.

Panning, M. and B. Romanowicz, A three dimensional radially anisotropic model of shear velocity in the whole mantle, *Geophys. J. Int., 167,* 361-379, 2006.

Tanimoto, T., A simple derivation of the formula to calculate synthetic long-period seismograms in a heterogeneous earth by normal mode summation, *Geophys. J. Int., 77,* 275-278, 1984.

Tarantola, A., Inversion of seismic reflection data in the acoustic approximation, *Geophysics, 49,* 1259-1266, 1984.

Woodhouse, J.H. and A.M. Dziewonski, Mapping the Upper Mantle: Three-Dimensional Modeling of Earth Structure by Inversion of Seismic Waveforms, *J. Geophys. Res., 89(B7),* 5953-5986, 1984.

Woodhouse, J.H. and T.P. Girnius, Surface waves and free oscillations in a regionalized earth model, *Geophys. J. R. Astr. Soc., 68(3),* 653-673, 1982.

18 Modeling of the Byerly's False S Phase

David Dolenc (U of Minnesota) and Doug Dreger

18.1 Introduction

Byerly's False S phase was first observed more than 70 years ago (*Byerly*, 1937) for earthquakes off the coast of Northern California. We used the recent dense station coverage in the region (USArray, Northern California Seismic Network, Berkeley Digital Seismic Network, Mendocino Array) to study the False S observations. We identified offshore events that produced the False S phase, relocated them using a double-difference algorithm, and inverted for the seismic moment tensor. With the location and source parameters constrained, we modeled the broadband waveforms using 2D and 3D velocity structures to find the origin of the False S arrivals.

18.2 History of False S

Byerly (1937) observed False S for the events located in the Mendocino Triple Junction (MTJ) at the stations to the south in the 2°-9° distance range. The speed of False S and the fact that the phase died out at distance led Byerly to believe that False S is a P wave that propagated through the sedimentary layer. However, Byerly noted that False S was not observed at Ferndale, the closest station to the MTJ at that time, and concluded that his proposed origin of the False S was open to objection. *Cameron* (1961) determined that False S is a longitudinal wave that arrives at the observing stations with a small angle of emergence. He also concluded that False S could be a P wave that propagated in the upper sedimentary layer. *Oliver and Major* (1960) suggested that False S results from the amplitude variation in the leaking-mode propagation within the near-surface wave guide. *Maulik* (1964) tried to explain the propagation of the phase through the sedimentary layer and concluded that a similar "false" phase should follow the true S wave, corresponding to S-wave propagation in the sedimentary layer. However, no such phase was observed. *Ghosh* (1964) suggested that False S resulted from the Stoneley wave propagating along the inclined continental margin. But *Auld et al.* (1969) showed that the phase was not observed at an ocean-bottom seismometer and ruled out the Stoneley-wave hypothesis.

18.3 Results

Our analysis of the offshore Mendocino events showed that (1) False S is observed for some offshore events along the Mendocino Escarpment (E of 127°W) and to the north (up to 41°N), (2) for events that generate False S, the phase is always observed on the near-coast stations north of the MTJ (up to station L02A), (3) events that generate False S always generate False S at the near shore station JCC, (4) False S is never observed at the closest stations KCT and KMPB, (5) strong False S is observed when the S phase is strong, (6) for strong False S events, the phase can be observed to the south, all the way to the San Francisco Bay region, and (7) no "false" phase after the true S wave is observed. The results support our starting hypothesis that False S is an SP phase that propagates as an S wave through the crustal layer above the Gorda plate and is refracted as a P wave back to the surface when it hits the thicker part of the subducting plate. This model can explain (1) the time delay between P and False S, (2) why a strong False S is observed when the S phase is strong, (3) why False S is never observed at the closest stations, (4) why the phase dies out at long distances, and (5) why False S phase has a small angle of emergence. We modeled the False S observations by developing a network of 2D structures to explain False S on all the stations leading to 3D modeling. The results showed that the origin of the False S phase could be explained by simple 2D modeling. The finite-difference modeling so far could not reproduce the False S observations. We are further testing the 2D and 3D models using finite-difference code to complete this work.

18.4 Acknowledgements

This project was funded by NSF grant EAR-0745803. We thank R. Allen, E. Humphreys, and A. Levander for sharing the Mendocino Array data with us.

18.5 References

Auld, B. et al., Seismicity off the coast of northern California determined from ocean bottom seismic measurements, *Bull. Seism. Soc. Am., 59*, 2001-2015, 1969.

Byerly, P., Earthquakes off the coast of northern California, *Bull. Seism. Soc. Am., 27*, 73-96, 1937.

Cameron, J. B., Earthquakes in the northern California coastal region (Part II), *Bull. Seism. Soc. Am., 51*, 337-354, 1961.

Ghosh, M. L., On a possible explanation of the PF-phase, *Bull. Seism. Soc. Am., 54*, 1417-1427, 1964.

Maulik, T. N., On the PF and other phases in the early part of seismogram, *Pure and Applied Geophysics, 58*, 49-62, 1964.

Oliver, J. and M. Major, Leaking modes and the PL phase, *Bull. Seism. Soc. Am., 50*, 165-180, 1960.

Zelt, C. A. and R. B. Smith, Seismic traveltime inversion for 2-D crustal velocity structure, *Geophys. J. Int., 108*, 16-34, 1992.

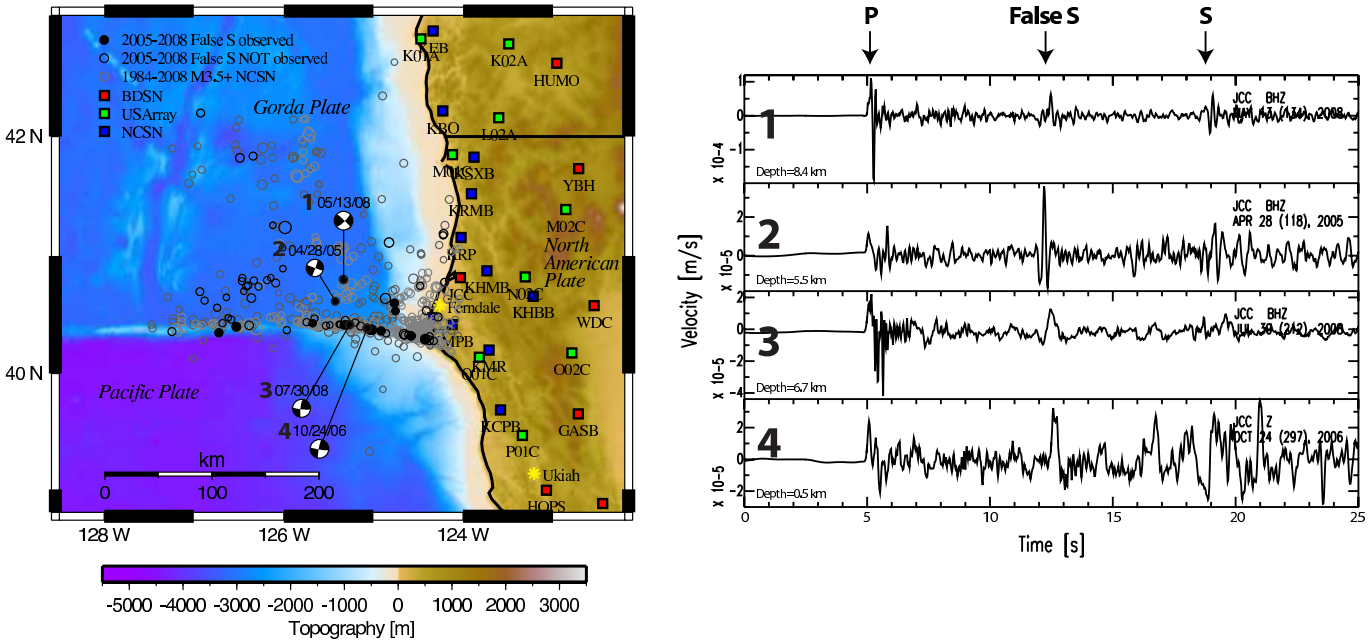

Figure 2.33: Left: Locations of the offshore events included in the study. Filled black circles are 2005-2008 events for which False S was observed on at least some stations. Open black circles are 2005-2008 events for which False S was not observed. Right: Velocity waveforms for the four numbered events. Shown is the vertical JCC component that had instrument response deconvolved.

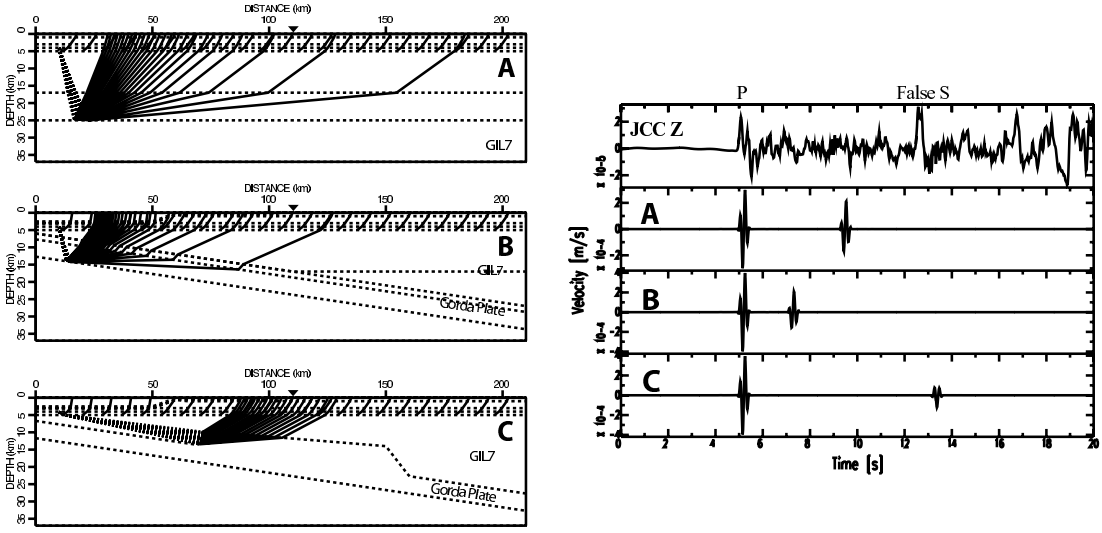

Figure 2.34: Example of 2D ray-tracing (RAYINVR; *Zelt and Smith*, 1992) used to model travel times and amplitudes. Left: (A) P-wave modeled as a head wave that propagated just below the 5 km interface. We looked for the phase that arrives at the station as a P wave, does not reflect more than once, and arrives with the largest possible delay relative to P. The resulting phase SP is shown on the right. (B) Gorda plate is modeled as a 2-layer slab with a 6° dip. The phase that has the largest delay relative to the P-wave and satisfies the above conditions is shown as an SP phase that is reflected at the bottom of the Gorda plate. (C) Gorda plate has non-uniform thickness. S wave propagates through the GIL7 crustal layer above the Gorda plate, and when it hits the thicker part of the Gorda plate, it is refracted back to the surface as a P wave. This type of model can explain the observed time delay between P and False S. Right: Synthetic seismograms for the 3 models are compared to the observations at JCC. Only model C can produce a phase that has travel-time comparable to that of the observed False S.

19 ShakeAlert: A Unified EEW System for California

Holly Brown, Richard Allen, Maren Böse (Caltech), Georgia Cua (ETH), Egill Hauksson (Caltech), Thomas Heaton (Caltech), Margaret Hellweg, Oleg Khainovski, Doug Neuhauser, Kalpesh Solanki (Caltech), Michael Fischer (ETH)

19.1 Introduction

Earthquake Early Warning (EEW) is a method of rapidly identifying an earthquake in progress and transmitting warning messages to nearby population centers before damaging ground shaking arrives. The first few seconds of the initial P-wave arrival are used to detect the event and predict magnitude and peak shaking from a single or multiple stations, and combined station detections are used to locate the event. Warnings of imminent shaking can be used to activate automatic safety measures, such as slowing down trains, isolating sensitive factory equipment, or opening elevator doors. Warnings can also be sent directly to the public via cell phone, computer, television, or radio.

The Berkeley Seismological Laboratory (BSL) worked for several years to develop the Earthquake Alarm Systems (ElarmS), an EEW system specifically for California. ElarmS was tested in conjunction with two other prototype EEW systems in a three-year proof of concept project by the California Integrated Seismic Network (CISN) to demonstrate the potential for EEW in California. In August 2009, the proof of concept project was completed and declared a success. The CISN EEW partners, the BSL, the California Institute of Technology (Caltech) and the Swiss Institute of Technology (ETH), are now collaborating again in a new three-year project, to build a single, integrated, production-grade system for testing purposes in California. The new system, called ShakeAlert, will be capable of continuous long-term operation, exhibit reliability and redundancy during extreme ground shaking, and rapidly provide warning to large numbers of users across the state. ShakeAlert is already under development and will provide warnings to a small group of test users by August 2012.

19.2 Project goals

The new ShakeAlert algorithm utilizes the best aspects of each of the three test systems from the proof-of-concept project. Caltech's OnSite algorithm uses P-wave data from the single station nearest the epicenter to provide an extremely rapid estimate of likely ground shaking. The BSL's ElarmS algorithm and ETH's Virtual Seismologist algorithm use data from multiple stations around an event epicenter to produce a slightly slower but more reliable estimate of magnitude and location. Combining these methods produces an algorithm which has the speed of a single-station method but is then promptly confirmed and adjusted by additional station data to form a more accurate description of the event.

When an event is identified and determined to be above pre-defined thresholds for magnitude, ground shaking intensity and statistical likelihood, event data is broadcast to system users. Currently, event information is only being sent to the developers while system components are being developed and refined. By 2012, event information will be sent to a small group of test users outside the seismological community. The event data will be received by a user-configurable alert program, which will sound an alarm, predict shaking at the user's specific location, and/or display a map of regional shaking. Emergency responders and regionally diverse industries (e.g. trains, utilities) may choose to display a map, showing multiple points of interest, while an individual may only be concerned with the immediate hazard at their specific location.

19.3 Current Progress

ShakeAlert will be comprised of four primary software components (Figure 2.35). The first, called the Waveform Processing Module, receives seismic waveforms from every early-warning capable seismometer or accelerometer in California (Figure 2.36), identifies P-wave arrivals, and calculates the relevant P-wave parameters necessary for EEW magnitude estimation. The second component, called the Event Monitoring Module, combines the current algorithms from OnSite, Virtual Seismologist, and ElarmS to recognize events in progress and calculate event magnitude and location. The third component, called the Decision Module, can receive event notifications from multiple systems include the existing three test systems and the new integrated system, reviews events, and determines whether to send warnings to users. The final component is the User Display, which will be installed at an EEW user's site. The User Display will receive warnings from the Decision Module and generate an alert message, a map of ground shaking intensities at various locations, or other output, as per the user's preconfigured settings.

During the last year, Caltech programmers developed an initial prototype of the User Display Module, while Berkeley programmers built an initial prototype of the Decision Module to combine output from the three original event monitoring algorithms. The three CISN EEW partners (Caltech, BSL, ETH) are working together to jointly build a new, robust Waveform Processing Module. The BSL, with significant input from the other part-

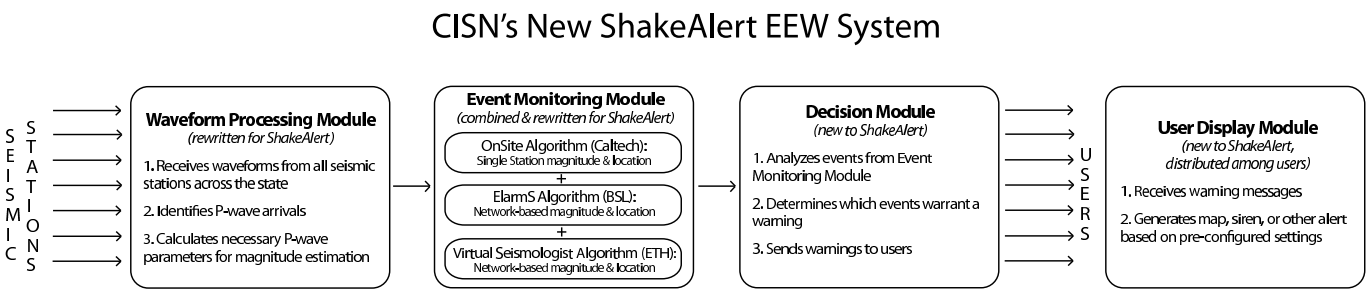

Figure 2.35: Components of the new ShakeAlert EEW System

ners, is also beginning work on the new Event Monitoring Module, combining the three original algorithms into a single, efficient algorithm that takes advantage of the best parts of each original algorithm.

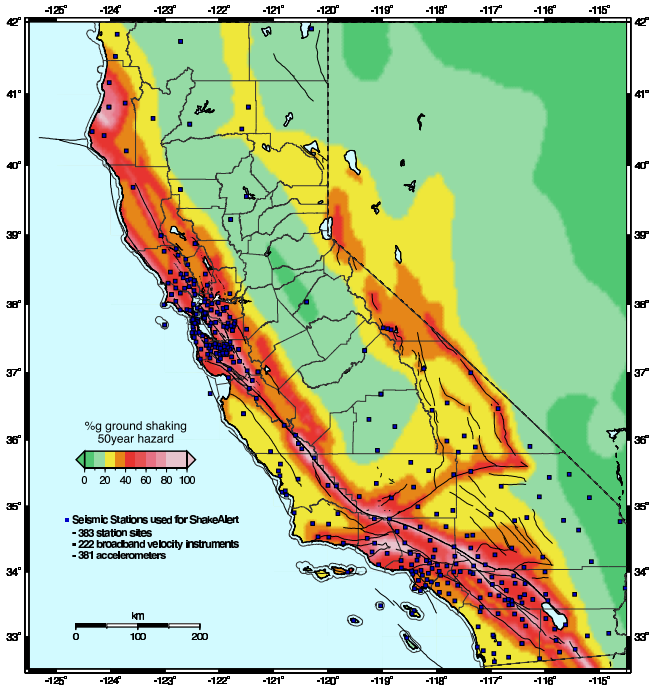

Figure 2.36: Seismic Stations used by ShakeAlert

19.4 Future Steps

During the coming year, the CISN EEW project members will connect all the new modules into a single end-to-end data flow. We will also begin sending warning messages to a few test users outside of the seismology community. Concurrently, we will continue to update and improve our new modules for speed and accuracy. The new event monitoring module in particular presents many opportunities for testing new methods and theories of EEW. While it will use the OnSite algorithm for estimating earthquake characteristics from a single station's P-wave data, and the Virtual Seismologist and ElarmS algorithms for analyzing earthquakes when three or more stations provide P-wave data, none of the three original test algorithms offer insight into how to combine data from exactly two stations. The CISN EEW group has been investigating the best method for analyzing two-station events using Bayesian statistics.

19.5 References

Allen, R.M., H. Brown, M. Hellweg, O. Khainovski, P. Lombard, D. Neuhauser, Real-time earthquake detection and hazard assessment by ElarmS across California, *Geophys. Res. Lett., 36,* L00B08, doi:10.1029/2008GL036766, 2009.

Allen, R.M., P. Gasparini, O. Kamigaichi, M. Böse, The status of earthquake early warning around the world: An introductory overview, *Seism. Res. Lett., 80(5),* 682-693, 2009.

Böse, M., E. Hauksson, K. Solanki, H. Kanamori, T.H. Heaton, Real-time testing of the on-site warning algorithm in southern California and its performance during the July 29 2008 M_w5.4 Chino Hills earthquake, *Geophys. Res. Lett., 36,* L00B03, doi:10.1029/2008GL036366, 2009.

Cua, G., M. Fischer, T. Heaton, S. Wiemer, Real-time performance of the Virtual Seismologist earthquake early warning algorithm in southern California, *Seism. Res. Lett., 80(5),* 740-747, 2009.

20 January 10, 2010 M_w6.5 Gorda Plate Earthquake: Automated Finite-Source Modeling

Douglas S. Dreger

20.1 Introduction

On January 9, 2010 at 16:27:38 (January 10, 00:27:38 UTC) a M_w6.5 Gorda Plate event occurred approximately 43 km offshore of Ferndale, California. Despite its offshore location it was well recorded by broadband, strong motion and GPS stations operated by the BSL, USGS, and CGS (California Geological Survey). Several years ago, we implemented finite-source inversion algorithms to rapidly, and automatically determine the causative fault plane of an earthquake from the automatic seismic moment tensor solution (e.g. *Pasyanos et al.,* 1996), and to solve for both line and planar models of the slip distribution (e.g. *Dreger and Kaverina*, 2000, and *Dreger et al.*, 2005).

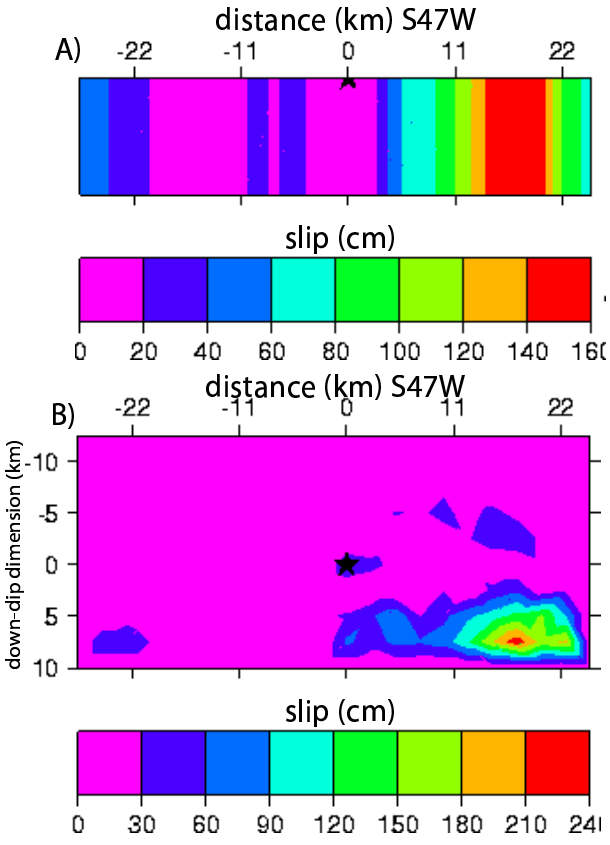

Figure 2.37: A) Line-source slip model. B) Plane-source slip model. In both cases the hypocenter is at 16.9 km depth. Both models show unilateral rupture to the SW.

20.2 Automatic Finite-Source Solutions

The moment tensor solution (Figure 2.39) is typical for this offshore region with near-vertical nodal planes and a predominant strike-slip motion. Events in the offshore region occur on both the NW and NE striking nodal planes. The November 8, 1980 M7.2 Mendocino earthquake occurred on a NE striking plane approximately 50 km NW of the 2010 event.

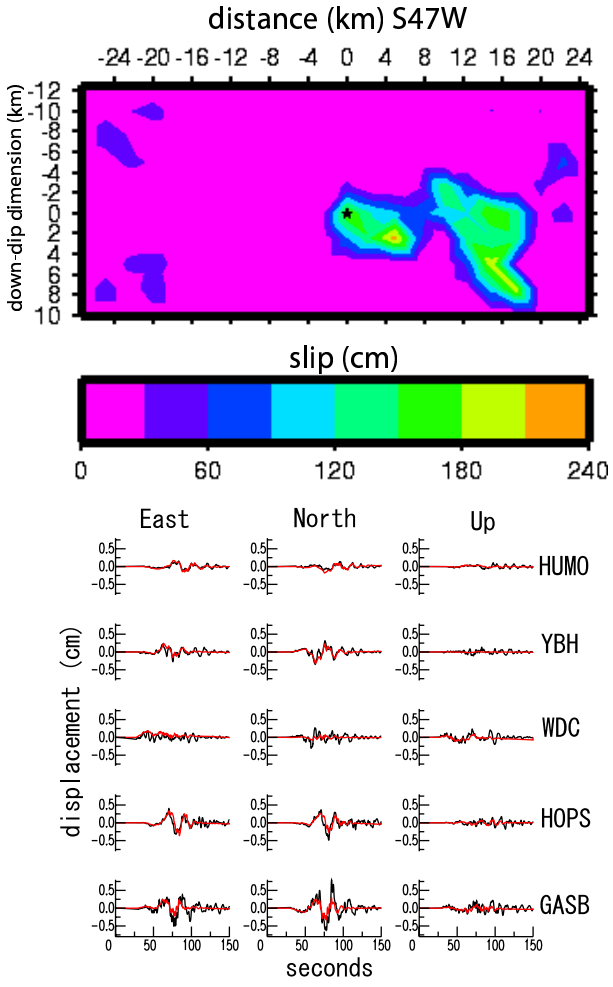

Figure 2.38: Revised slip model obtained by adjusting hypocenter depth to 21.7 km and adjusting the timing of Green's functions to align with observed S-wave arrival times. Broadband (0.01 to 10 Hz) data (black) and synthetics (red) are compared. The same amplitude scale was used for all stations.

The automatic finite-source code tested both nodal plane orientations with both line-source (Figure 2.37A and plane-source (Figure 2.37B) slip inversions of three-component broadband (0.01 to 10 Hz) displacement waveforms. Despite the poor station coverage due to the offshore location of the earthquake, the stations do sample enough of the focal sphere to capture the directivity of the event. These automatic finite-source calculations were completed within 22 minutes of the occurrence of the earthquake, and the results showed that the NE striking nodal plane was the causative structure. Furthermore, as Figure 2.37 shows, the earthquake ruptured unilaterally to the SW, away from the coast, on the NE striking fault plane. The scalar seismic moment of the plane-source model is $6.76x10^{25}$ dyne cm, corresponding to M_w6.5. A rise time of 1 second was assumed, and the best fitting rupture velocity was 2.2 km/s.

The initial hypocentral depth was 16.4 km, which was used in the finite-source calculations. Figure 2.37 suggests that the actual slip is deeper. The moment tensor solution yielded a centroid depth of 24 km. Revisions of the hypocenter location resulted in updates of the depth to 21.7, and 29.3 km.

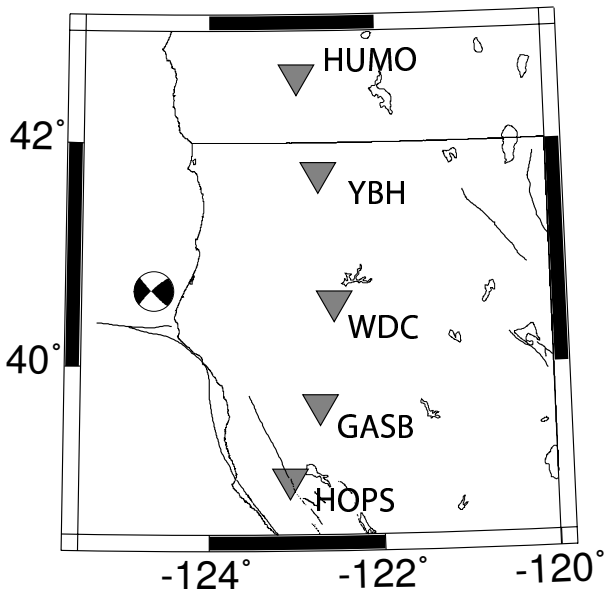

Figure 2.39: Location of event and stations (triangles). The focal mechanism was obtained from moment tensor inversion of long-period (20 to 50 seconds) three-component waveforms.

20.3 Finite-Source Model Revisions

The initial analyst review of the automatic solution updated the hypocenter to the first revised depth of 21.7 km, and a 1 second timing adjustment was applied to all stations to align the Green's functions to the observed S-wave arrivals. A rise time of 2 seconds (increased from 1 second to match the long-period character of the data) and the 2.2 km/s rupture velocity from the automatic processing were assumed. The revised solution (Figure 2.38) shows the rupture was unilateral to the SW with slip occurring in the 17 to 30 km depth range. The peak slip was 2.7m, and the scalar seismic moment increased to $9.33x10^{25}$ dyne cm (M_w6.6).

As Figure 2.38 shows, the fit to the broadband displacement waveforms is quite good. Stations GASB and HOPS have the largest amplitudes. These stations are approximately the same distance from the source as stations HUMO and YBH, which show much lower amplitudes. In fact, the small amplitudes at HUMO, YBH and WDC, and the notably larger amplitudes at GASB and HOPS illustrate the strong directivity of the source.

20.4 Implications for Ground Motion Reporting

Automated finite-source models may be used to improve ShakeMap ground motion reporting by taking the finite rupture extent into account in the computation of ground motions from empirical relations for the purpose of interpolating the observed values (*e.g. Dreger et al.,* 2005). Although the application of the finite-source model in ShakeMap for this event had minimal impact due to the distant offshore location of the event, the 22 minute processing time, and the success of the system in the identification of the causative fault, the slip distribution and the unilateral rupture characteristics, despite the poor station coverage, demonstrates that such information can be made routinely available in a time frame suitable for rapid ground motion reporting.

Ongoing efforts involve improving automated processing times and solutions as well as updating the analyst interface used to examine and revise solutions.

20.5 References

Dreger, D. S., and A. Kaverina, Seismic remote sensing for the earthquake source processes and near-source strong shaking: A case study of the October 16, 1999 Hector Mine earthquake, *Geophys. Res. Lett., 27,* 1941, 2000.

Dreger, D. S., L. Gee, P. Lombard, M. H. Murray, and B. Romanowicz, Rapid finite-source analysis and near-fault strong ground motions: Application to the 2003 Mw6.5 San Simeon and 2004 Mw6.0 Parkfield earthquakes *Seism. Soc. Am., 76*, 40, 2005.

Pasyanos, M. E., D. S. Dreger, and B. Romanowicz, Towards real-time determination of regional moment tensors, *Bull. Seism. Soc. Am., 86,* 1255, 1996.

21 Towards a Real-time Earthquake Source Determination and Tsunami Early Warning in Northern California

Aurélie Guilhem and Douglas S. Dreger

21.1 Introduction

The Mendocino Triple Junction is the most seismically active region in Northern California, with a variety of unusual seismic events in addition to regular earthquakes. It also represents the southernmost part of the Cascadia subduction zone (CSZ) where potential damaging thrust earthquakes can occur. The current real-time earthquake monitoring is a cascade-type procedure following a joint effort of the USGS Menlo Park and the Berkeley Seismological Laboratory at UC Berkeley. For offshore earthquakes occurring outside of the seismic network, as is the case in the Mendocino region, such a procedure can generate errors in the event detections and locations resulting in incorrect source determinations. With the goal of more efficiently monitoring the offshore region of Northern California, particularly for slow/low-stress-drop and large, possibly tsunamigenic earthquakes, we develop an automatic scanning of continuous long-period (> 20 sec) broadband seismic records following the method proposed by Kawakatsu (1998) and currently in use in Japan (*Tsuruoka et al.*, 2009). In addition, we are proposing an improved algorithm for great earthquakes occurring along the CSZ, that, if implemented in real-time with a continuous scanning algorithm, will provide information that could be utilized for near-source tsunami early warning.

21.2 The approach

We are implementing a continuous seismic scanning algorithm following the method proposed by Kawakatsu (1998) that makes use of continuous long-period filtered data. By using this approach, it is possible to calculate moment tensors every two seconds for each point of a spatial grid. We generated a grid of nearly 5,000 virtual sources, with each point being separated by 0.2 degrees in latitude (between 40N and 43N) and longitude (between -123E and -128E) and a 3 km interval in depth (5 to 38 km). We selected four Berkeley broadband stations (HUMO, ORV, WDC, and YBH) for which we computed a catalog of Green's functions using a 1D velocity model of Northern California. In order to detect all earthquakes of small and large magnitudes within the region, we are implementing two parallel-running systems. The first one is an inversion of 380 seconds of data filtered between 20 and 50 sec to detect earthquakes with magnitudes between 3.5 and 7. The second system considers longer records (480 sec) filtered at longer periods (100 and 200 sec) to account for M8+ earthquakes.

21.3 Detecting a M8+ earthquake

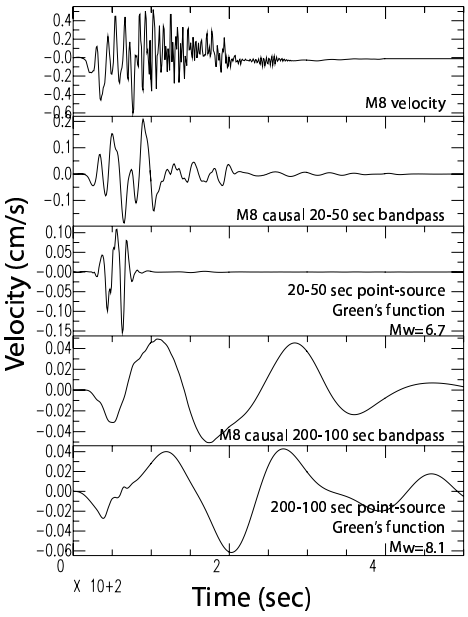

Figure 2.40: Comparison of the frequency bands (0.02-0.05 Hz and 0.005-0.01 Hz) and corresponding Green's functions for a magnitude 8 earthquake along the CSZ.

The CSZ that marks the subduction of the Pacific Plate beneath the North American Plate can produce very large and tsunamigenic earthquakes - magnitude 9.0 or greater - if rupture occurs over the entire area. The last known great earthquake in the region was in January of 1700, and geological evidence indicates that great earthquakes may have a return time of 300 to 600 years. Because there is no available seismic data for a magnitude 8+ earthquake in the study region, we performed a series of synthetic tests for such large events, defined with uniform and variable slip models along the subduction zone. Figure 2.40 illustrates the need to look for longer period data for a M8+ earthquake. Indeed we find that inversions using the 20-50 sec passband fail to recover the seismic moment and location of the tested event. The moment is underestimated, yielding only a M6.7 for a M8.2 synthetic earthquake, and our best solution is located onshore (Figure 2.41a). The narrow band processing and the point-source synthetic only fit a small portion of the record, and the inversion is not sensitive

to the total moment of the event.

However, for the 100-200 sec passband, the inversion yields a point-source location near the fault centroid (Figure 2.41), indicating that this passband works well in identifying the earthquake magnitude, mechanism and location. Furthermore, for the heterogeneous slip models, the detections show better variance reductions (VR) due to the concentration of slip that is better represented by a point-source assumption (Figure 2.41b).

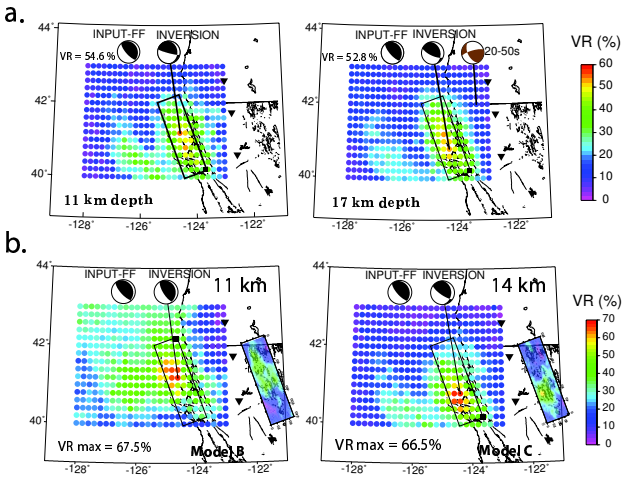

Figure 2.41: Maps of the best VRs obtained for the homogeneous slip model at 11 and 17 km depth (a.) and variable slip models (b.).

21.4 Multi-point source

For great earthquakes, the proximity of the seismic stations to the rupture segment leads to the problem of a near-field component, for which the single point-source assumption considered in the previously described method could fail. To account for the finiteness of the near-field rupture, we are testing the algorithm with multi-point sources obtained after summing together single point sources accounting for the respective distances and azimuths between source and receiver for each of the sources. By doing this, it is possible to study any type of rupture and directivity: north to south, south to north, and bilateral, depending on the grid points considered.

Figure 2.42 demonstrates that the multi-point source assumption (here a summation of three points of the grid) can deliver a better source solution of a large earthquake located off the coast of Northern California than a single point source. Indeed the VR increases from 66% (Figure 2.42b) to 75% (Figure 2.42d).

21.5 Conclusions

Such scanning will provide complete information on the events in real-time using a single stage of processing,

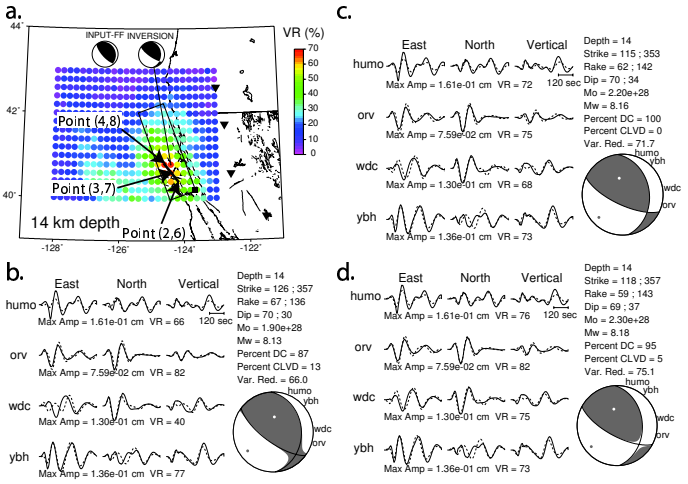

Figure 2.42: Comparison of the moment tensor (MT) using single and multi-point source assumptions. a) Map of the best VRs at 14 km depth for Model C (Figure 2.41). b) Best MT analysis obtained using a single point source. c) MT analysis after summing Points (2,6), (3,7) and (4,8). d) Same as c) but considering a south to north rupture.

and for this reason it will be faster than the current procedures. The method that we are implementing makes use of regional seismic recording stations with continuous real-time telemetry that will enable autonomous detection, location, estimation of scalar seismic moment, and determination of the mode of faulting (i.e. dip-slip versus strike-slip) within approximately 8 minutes of the earthquake occurrence and before the damaging tsunami waves reach the coastline. In the future, our efforts toward a real-time source parameter reporting system for great earthquakes may aid in the development of a tsunami early warning system in Northern California.

21.6 Acknowledgements

This project is supported by the U.S. Geological Survey through award G10AP00069 (NERHP).

21.7 References

Kawakatsu, H., On the realtime monitoring of the long-period seismic wavefield, *Bull. Earth. Res. Inst., 73*, 267-274, 1998.

Tsuruoka, H. H. Kawakatsu, and T. Urabe, GRID MT (Grid-based Realtime Determination of Moment Tensors) monitoring the long-period seismic wavefield, *Phys. Earth Planet. Int., Special issue: Earthquakes in subduction zones: A multidisciplinary approach, 175*, 8-16, 2009.

22 Seismic Constraints on Fault-Zone Frictional Properties at Seismogenic Depth on the San Andreas Fault, Parkfield

Taka'aki Taira, Robert M. Nadeau, and Douglas S. Dreger

22.1 Introduction

Probing subsurface fault-zone frictional properties is a key to improving our understanding of the mechanics of postseismic deformations following larger earthquake that will control the occurrences of subsequent aftershocks and triggered earthquakes. Geodetic measurements have revealed spatially and temporally varying postseismic deformations in the crust immediately after large earthquakes (e.g., *Johanson et al.*, 2006; *Langbein et al.*, 2006). The estimations in deformation field at depth are, however, limited by surface measurements of strain. We propose a methodology for observing subsurface frictional properties of the fault zone by exploiting cumulative seismic slips derived from repeating earthquake sequences.

22.2 Frictional Properties at Depth

Repeating earthquakes are sequences of seismic events that are believed to rupture isolated asperities in creeping sections of fault zones (*Nadeau and McEvilly*, 1999). Their seismic source characteristics have been used to probe spatiotemporal fault-zone properties such as fault healing processes (*Vidale et al.*, 1994), deep creep rate (*Nadeau and McEvilly*, 1999), and fault strength (*Taira et al.*, 2009) as well as to monitor temporal changes in the crustal structure (*Niu et al.*, 2003), by utilizing seismograms from repeating earthquakes. One major advantage of making use of source characteristics of repeating earthquake sequences is that spatial changes in time-dependent fault properties can be more easily isolated than examining spatiotemporal changes in seismicity rates. An ideal test for measuring frictional properties has been provided by the 2004 M 6 Parkfield earthquake, California, because numerous repeating earthquakes have been found in the postseismic period of the 2004 Parkfield earthquake.

We explore subsurface cumulative fault slips extracted from a set of 27 repeating earthquake sequences extending over a depth range of 10 km at the Parkfield segment of the San Andreas fault. These sequences are chosen because around 5 repeating earthquakes in individual sequences typically occurred during the first month of the postseismic period, which allows us to illuminate time evolutions of cumulative seismic slips. Additionally, we have been monitoring selected sequences since 1984. We are able to well constrain background levels of cumulative seismic slips that needed to be corrected in order to address time-dependent postseismic deformations. Parkfield repeating earthquakes have been detected from continuous HRSN borehole seismograms, and their locations were determined using a double-difference relocation approach (*Nadeau et al.*, 2004). The seismic moments also were reliably evaluated through a spectral ratio method introduced by (*Nadeau and Johnson, 1998*). Those precise determinations in source characteristics of individual sequences are crucial to identifying spatiotemporal variations of cumulative seismic slips.

We have employed rate-strengthening friction (*Perfettini and Avouac*, 2005) and viscoelastic models (*Montési*, 2004) to characterize fault-zone rheological properties from seismological observations of postseismic deformation following the 2004 Parkfield earthquake. We first show that 24 of the 27 sequences can be well-explained by the rate-strengthening friction model (Figure 2.43a). We then evaluate frictional parameter $a\sigma$ where a is a frictional coefficient and σ is effective normal stress, by combining the static Coulomb stress change based on the coseismic slip model of the mainshock (*Kim and Dreger*, 2008). Our results suggest $a\sigma$ to be 0.01-0.5 MPa (Figure 2.43b), a value that is generally consistent with previous studies (*Marone et al.*, 1991).

22.3 Conclusions

Our preliminary result suggests that cumulative seismic slips inferred from repeating earthquake sequences provide a means of observing the in-situ frictional parameter. Continuing work will explore spatial variation in frictional parameters and the slip distribution of individual repeating earthquake sequences with finite source modeling.

22.4 Acknowledgements

The present study was supported by the National Science Foundation EAR-0910322. The Parkfield High-Resolution Seismic Network is operated by University of California, Berkeley Seismological Laboratory with financial support from the U.S. Geological Survey through National Earthquake Hazards Reduction Program awards 07HQAG0014 and G10AC00093. We would like to thank A. Kim for providing us with the coseismic slip model.

22.5 References

Johanson, I.A., E.J. Fielding, R. Rolandone and R. Bürgmann, Coseismic and postseismic slip of the 2004 Parkfield earthquake from space-geodetic data, *Bull. Seism. Soc. Am.*, *96*, S269-S282, 2006.

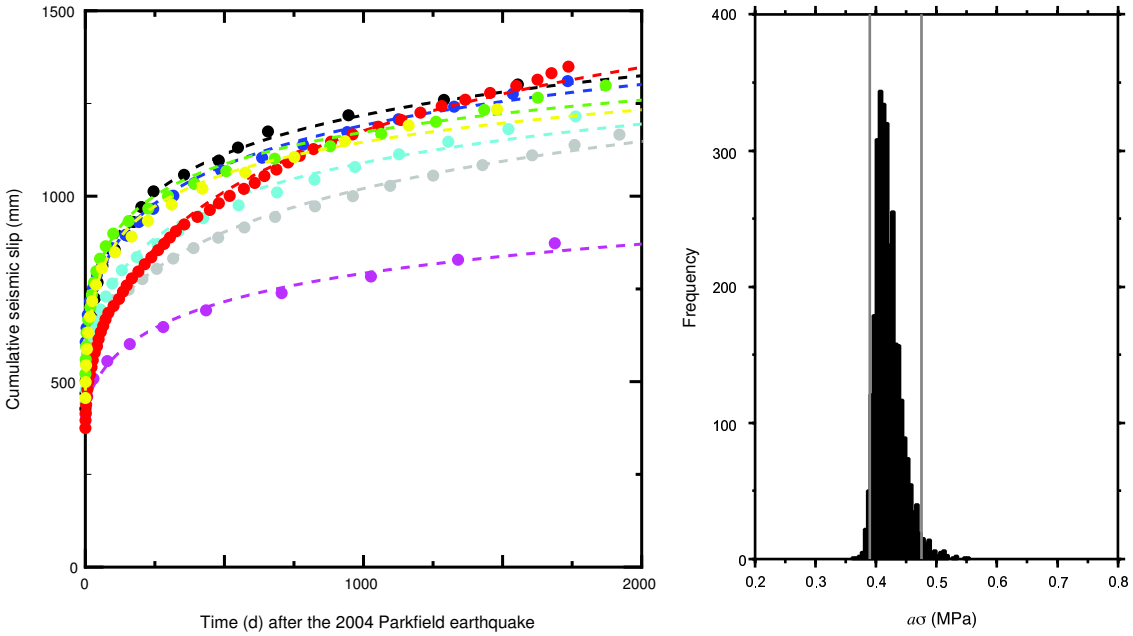

Figure 2.43: (a) Time evolutions of cumulative seismic slips derived from selected eight repeating earthquake sequences (circles) after the 2004 Parkfield earthquake. Also shown are the predicted cumulative fault slips (solid curves) from a rate-strengthening friction model. (b) Distribution of frictional parameter $a\sigma$ for one sequence. Gray vertical lines are the 95% confidence interval using a bootstrap approach with 3,000 subsample data sets.

Kim, A., and D. S. Dreger, Rupture process of the 2004 Parkfield earthquake from near-fault seismic waveform and geodetic records, *J. Geophys. Res.*, *113*, B07308, doi:10.1029/2007JB005115, 2008.

Langbein, J., J.R. Murray, and H.A. Snyder, Coseismic and initial postseismic deformation from the 2004 Parkfield, California, earthquake, observed by global positioning system, electronic distance meter, creepmeters, and borehole strainmeters, *Bull. Seismol. Soc. Am.*, *96*, S304-S320, doi 10.1785/0120050823, 2006.

Marone, C.J., C.H. Scholtz, and R. Bilham, On the mechanics of earthquake afterslip, *J. Geophys. Res.*, *96(B5)*, 8441-8452, doi:10.1029/91JB00275, 1991.

Montési, L.G., Controls of shear zone rheology and tectonic loading on postseismic creep, *J. Geophys. Res.*, *109*, doi:10.1029/2003JB002925, 2004.

Nadeau, R.M. and L.R. Johnson, Seismological studies at Parkfield VI: Moment release rates and estimates of source parameters for small repeating earthquakes, *Bull. Seismol. Soc. Am.*, *88*, 790-814, 1998.

Nadeau, R.M. and T.V. McEvilly, Fault slip rates at depth from recurrence intervals of repeating microearthquakes, *Science*, *285*, 718-721, 1999.

Nadeau, R.M., A. Michelini, R.A. Uhrhammer, D. Dolenc and T.V. McEvilly, Detailed kinematics, structure and recurrence of micro-seismicity in the SAFOD target region, *Geophys. Res. Lett.*, *31*, L12S08, doi:10.1029/2003GL019409, 2004.

Niu, F., P.G. Silver, R.M. Nadeau and T.V. McEvilly, Migration of seismic scatterers associated with the 1993 Parkfield aseismic transient event, *Nature*, *426*, 544-548, 2003.

Perfettini, H. and J.-P. Avouac, Postseismic relaxation driven by brittle creep: A possible mechanism to reconcile geodetic measurements and the decay rate of aftershocks, application to the Chi-Chi earthquake, Taiwan, *J. Geophys. Res.*, *109*, B02304, doi:10.1029/2003JB002488, 2004.

Taira, T., P.G. Silver, F. Niu and R.M. Nadeau, Remote triggering of fault-strength changes on the San Andreas Fault at Parkfield, *Nature*, *461*, 636-639, doi:10.1038/nature08395, 2009.

Vidale J.E., W.L. Ellsworth, A. Cole and C. Marone, Variations in rupture process with recurrence interval in a repeated small earthquake, *Nature*, *368*, 624-626, 1994.

23 Postseismic Variations in Seismic Moment and Recurrence Interval of Repeating Earthquakes at Parkfield

Kate Huihsuan Chen (National Taiwan Normal Univ.), Roland Bürgmann, Robert M. Nadeau, Ting Chen (Caltech), and Nadia Lapusta (Caltech)

23.1 Observations of postseismic recurrence behavior

In laboratory experiments, longer stationary contact time leads to larger seismic moment during repeated ruptures. However, not all observations in natural fault systems agree with the prediction. We analyze a subset of 34 M -0.4∼2.1 repeating earthquake sequences (RES) from 1987-2009 at Parkfield to examine the variation of their recurrence properties in space and time.

Following the 29 September 2004, M 6.0 Parkfield earthquake, a strongly accelerated rate of postseismic repeats is observed for 22 of the 34 event sequences. These repeating events have greatly reduced recurrence intervals that increase systematically with time (Figure 2.44a). The rapid event recurrences reflect increased loading of the RES asperities by coseismic stress changes and accelerated fault creep surrounding the 2004 rupture (*Johanson et al.*, 2006; *Johnson et al.*, 2006; *Murray and Langbein*, 2006). 36% of the 773 recurrence intervals are shorter than 0.1 times the average interval, and 100% of these short intervals follow the 2004 Parkfield event.

In addition to this recurrence acceleration, we also find systematic changes in seismic moment (M_o), where most sequences experienced an immediate increase in M_o and subsequent decay as T_r approached pre-quake durations. Figure 2.44 shows the temporal evolution of recurrence intervals and seismic moment for three example groups. The RES at shallower depth tend to have a larger range in both T_r and M_o (Figure 2.44a-b), whereas deeper RES show smaller variation (Figure 2.44d-e). The shallowest RES with the greatest magnitude (the M1.8-2.1 SAFOD target events) among the events we studied reveal large variation in T_r but small variation in M_o (Figure 2.44g-h).

To further explore the variability in seismic moment M_o and recurrence interval T_r, and to investigate their potential relation, we plot M_o vs. T_r, with M_o normalized by the average M_o (M_{ave}) of the whole sequence in Figure 2.44c, f, and i. To quantify the relation between M_o and T_r, we fit the postseismic data with $M_o/M_{ave} \sim qlog(T_r)$ using the least squares method, for the 26 Parkfield RES with more than four postseismic events (following *Peng et al.*, 2005). The fits are shown by dashed lines in Figure 2.44c, f, and i. Positive/negative slopes q of the M_o-T_r relation correspond to an increase/decrease in moment with increasing recurrence time. We find that 19 out of 26 RES have decreasing M_o as T_r increases.

23.2 Rate and state models of repeating sequences

These observations are qualitatively consistent with earthquake simulations in 3D continuum fault models with rate- and state-dependent friction shown in Figure 2.45. In the models, RES are produced on velocity-weakening patches surrounded by velocity-strengthening fault areas (Figure 2.45a). In the simulations, the sign of the slope for the M_o-T_r relation is controlled by the ratio $r/h\star$, where r is the radius of the velocity-weakening patch and $h\star$ is the so-called nucleation size dependent on the friction properties of the patch (*Chen and Lapusta*, 2009):

$$h\star = (\pi^2/4) \cdot \mu bL/(\pi\sigma(b-a)^2)$$

where μ is the shear modulus, σ is the effective normal stres, and a, b and L are friction parameters. Given the same nucleation size $h\star$ (i.e., the same frictional properties and effective normal stress), smaller radii, and hence smaller seismic moments, result in negative M_o-T_r slopes, whereas larger radii, and hence larger moments, lead to weak positive M_o-T_r slopes, consistent with observations. Conversely, with only a small percentage of its slip accumulated seismically, a small asperity appears to grow in M_o under high loading rate, which is contrary to the view that M_o should decrease due to a reduced strength recovery time. Our simulations show that the recurrence intervals T_r are systematically reduced for larger loading velocity, as intuitively expected and confirmed by our observations.

23.3 Conclusion

Most shallower RES (<7 km) experienced a strong reduction in T_r accompanied by an increase in M_o immediately following the 2004 Parkfield mainshock, evolving towards pre-earthquake values in subsequent years. Among the shallow RES, larger events show less variability in seismic moment than small events, even though their transient recurrence acceleration is strong. This magnitude-dependent postseismic behavior can be qualitatively explained by 3-D models using rate and state friction laws. Small asperities tend to accumulate most of their slip aseismically, with earthquakes occupying a small fraction of their area. When experiencing higher loading rates, these small events are found to rupture a larger area of the velocity-weakening asperity, producing the observed behavior of increasing moment with increasing loading rate and decreasing recurrence intervals. For

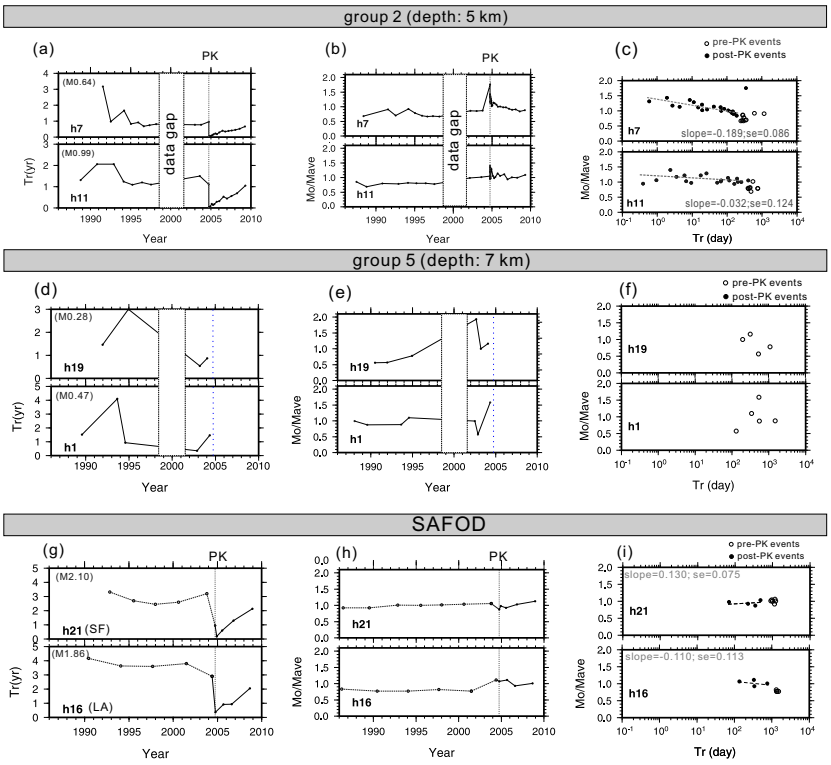

Figure 2.44: (a) Recurrence interval, (b) relative moment variation (ratio of M_o and average M_o of the sequence) as a function of time, and (c) relative moment as a function of recurrence interval for group 2 repeating sequences. Black and open circles indicate post- and pre- Parkfield events, respectively. (d-f) For group 5 repeating sequences. (g-i) For SAFOD repeating sequences.

the postseismic period, the good correlation between the observation and model predictions implies that the sudden increase in and time-variability of the loading rate on the velocity-weakening patch plays a significant role in a repeater's seismic properties. Such an inference, however, should be tested with proper laboratory-based friction experiments in the future.

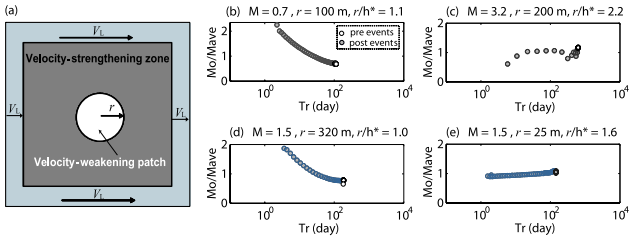

Figure 2.45: Simulation results for RES response to postseismic effects of a large nearby event using different model parameters. (a) Fault model for 3-D simulation. A vertical strike-slip fault is embedded into an elastic medium and governed by rate and state friction laws (*Chen and Lapusta*, 2009). (b-e) Computed relative seismic moment as a function of recurrence interval for varying patch radius r and nucleation size $h\star$. Open and filled circles indicate the preseismic and postseismic events, respectively.

23.4 References

Chen, T., and N. Lapusta, Scaling of small repeating earthquakes explained by interaction of seismic and aseismic slip in a rate and state fault model, *J. Geophys. Res., 114*, B01311, doi:10.1029/2008JB005749, 2009.

Johnson, K. M., R. Bürgmann, and K. Larson, Frictional properties on the San Andreas Fault near Parkfield, California, inferred from models of afterslip following the 2004 earthquake, *Bull. Seism. Soc. Am., 96(4B)*, S321-S338, doi: 10.1785/0120050808, 2006a.

Johanson, I. A., E. J. Fielding, F. Rolandone, and R. Bürgmann, Coseismic and postseismic slip of the 2004 Parkfield earthquake from space-geodetic data, *Bull. Seismol. Soc. Am., 96(4B)*, S269-S282, doi: 10.1785/0120050818, 2006b.

Murray, J., and J. Langbein, Slip on the San Andreas fault at Parkfield, California over two earthquake cycles and the implications for seismic hazard, *Bull. Seismol. Soc. Am., 96(4B)*, S283-S303, doi: 10.1785/0120050820, 2006.

Peng Z., J. E. Vidale, C. Marone, and A. Rubin, Systematic variations in recurrence interval and moment of repeating aftershocks, *J. Geophys. Res., 32* doi:10.1029/2005GL022626, 2005.

24 Identification of Nonvolcanic Tremors Triggered by Regional Earthquakes in the Parkfield, California Region

Aurélie Guilhem, Zhigang Peng (Georgia Institute of Technology), and Robert M. Nadeau

24.1 Introduction

Nonvolcanic tremor activity along the Parkfield-Cholame section of the San Andreas fault (SAF) in central California has been recorded since 2001 (*Nadeau and Dolenc*, 2005; *Nadeau and Guilhem*, 2009). In addition to ambient tremors, triggered tremors associated with the surface waves of large teleseisms have been recognized (*Gomberg et al.*, 2008; *Peng et al.*, 2009). However, no tremors triggered by regional earthquakes have been observed within the region and in other tremor regions. *Rubinstein et al.* (2009) explained the absence of tremor triggering from regional quakes in Cascadia by the similar frequency bands (i.e. 1-15 Hz) and waveform characteristics of the P and S coda waves from regional events. However *Brodsky and Prejean* (2005) showed that large earthquakes at regional and teleseismic distances have triggered microearthquakes and that the large-amplitude long-period surface waves appeared to favor the triggering more than shorter period waves of similar amplitude. To effectively separate the potential triggered tremors from the regional coda waves, we propose to examine higher frequency bands (i.e. above 15 Hz).

24.2 Detection of triggered tremors

By systematically searching the high-frequency (i.e. > 15 Hz) filtered seismograms (250 samples per second) of 99 M5+ earthquakes occurring between July 2001 and April 2010 and distributed between 100 and 1200 km from the broadband seismic station PKD located at Parkfield, we visually identified four earthquakes that triggered tremors in central California: the 15 June 2005 M7.2 Mendocino, 04 January 2006 M6.6 Baja California (BC), 03 August 2009 M6.9 BC, and 04 April 2010 M7.2 BC earthquakes. The triggered tremors constitute consecutive bursts of energy that are phase-correlated with the passing of the surface waves (Figure 2.46).

We found that between 3 and 15 Hz, which corresponds to the typical frequency band for nonvolcanic tremors, the data mainly show the emergent P and S waves without clear indication of triggered tremors. However, tremors are best observed between 15 and 30 Hz for the 2006 and 2010 earthquakes and between 25 and 40 Hz for the 2005 and 2009 events (Figure 2.46a).

We adapted the envelope-based location algorithm already used for ambient tremors to locate the four triggered tremors. Their sources, with the exception of the 2009 event, are found on or close to the main SAF segment, within the region where ambient and teleseismi-

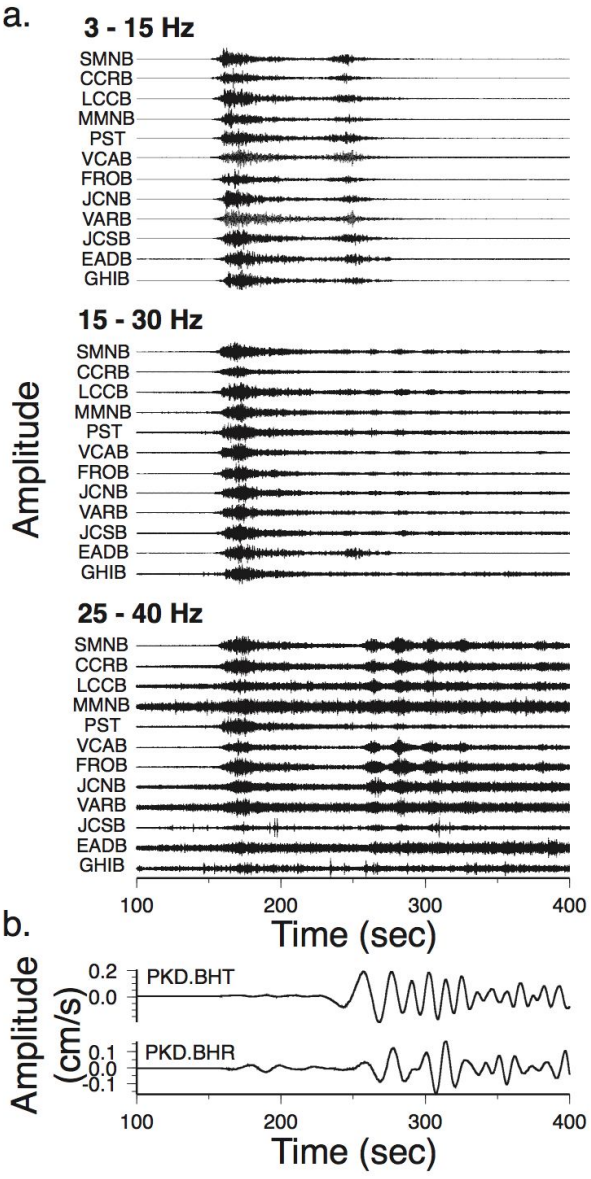

Figure 2.46: a) Velocity seismograms (relative scaling) ordered from north (top) to south (bottom) along the SAF strike recorded by the HRSN stations and the surface station PST filtered at several frequency bands for the 2005 Mendocino earthquake. The triggered tremor is seen between 250 and 350 sec. b) Unfiltered transverse (BHT) and radial (BHR) components of the station PKD from *Guilhem et al.* (2010).

cally triggered tremors have been detected. However, the 2009 BC earthquake appears to occur about 25 km NE of the fault.

24.3 Peak ground velocities

Most of tremor signals occur in phase with the surface waves, seeming to indicate a causal relationship between occurrence of tremors and surface waves. We measured the peak ground velocities (PGV) of the surface waves of the 99 earthquakes as well as of the teleseisms studied by *Peng et al.* (2009) recorded on the transverse and vertical components of the PKD station (Figure 2.47a), and we found that the events that did trigger tremors in central California have among the largest PGVs. This is emphasized after filtering the data between 30 and 200 sec (Figure 2.47b).

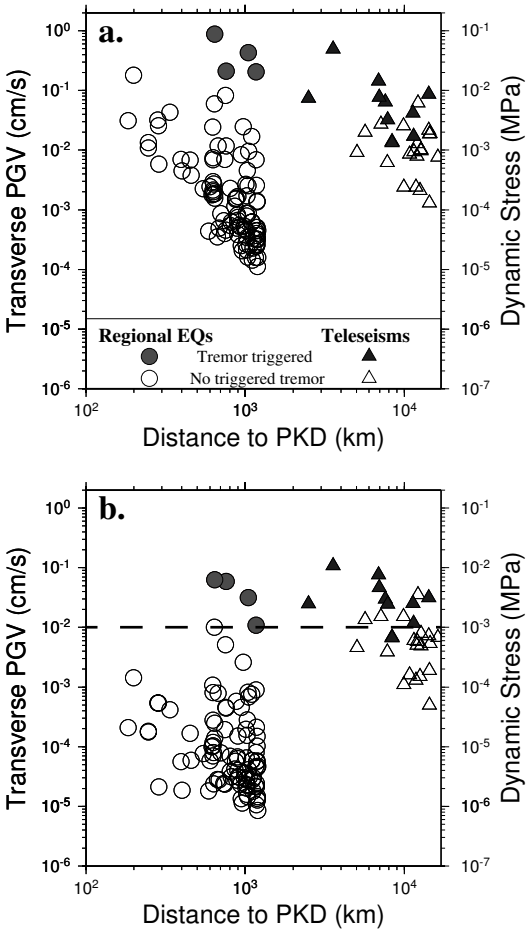

Figure 2.47: a) Peak ground velocities (PGV) recorded at PKD on unfiltered transverse components of PKD. b) PGVs recorded between 30 and 200 sec period from *Guilhem et al.* (2010).

If we consider a PGV threshold of 0.01 cm/s to separate triggering and non-triggering earthquakes at both regional and teleseismic distances and use a nominal surface wave velocity of 3.5 km/s and the elastic modulus of 35 GPa at tremor depth we found a corresponding dynamic stress of about 1 kPa (Figure 2.47b).

24.4 Conclusions

We show that tremors are not bandpass limited to 1-15 Hz but can have significant energy at higher frequencies. By searching seismic records above 15 Hz we found four triggered tremors correlating with the passage of the surface waves. High-frequency content is also observed for teleseismically triggered tremors. Finally, our calculated dynamic stress change of 1 kPa is in agreement with other findings, indicating that it is important to continue detecting and analyzing the tremor activity in central California in order to better define the fault mechanics and interactions in the deep crust.

24.5 Acknowledgements

This project is supported by the U.S. Geological Survey through award 07HQAG0014 and 08HQGR0100 and by the National Science Foundation through award EAR-0537641. Z. Peng was supported by the National Science Foundation through awards EAR-0809834 and EAR-0956051.

24.6 References

Brodsky, E. E., and S. G. Prejean, New constraints on mechanisms of remotely triggered seismicity at Long Valley Caldera, *J. Geophys. Res.*, *110*, B04302, 2005.

Gomberg, J., J. L. Rubinstein, Z. Peng, K.C. Creager, J. E. Vidale, and P. Bodin, Widespread triggering of nonvolcanic tremor in California, *Science*, *319*, 173, 2008.

Guilhem, A., Z. Peng, and R. M. Nadeau, High-frequency identification of non-volcanic tremor triggered by regional earthquakes, *Geophys. Res. Lett.*, *37*, *in press*, 2010.

Nadeau, R. M., and D. Dolenc, Nonvolcanic tremors deep beneath the San Andreas Fault, *Science*, *307*, 389, 2005.

Nadeau, R. M., and A. Guilhem, Nonvolcanic tremor and the 2003 San Simeon and 2004 Parkfield, California earthquakes, *Science*, *325*, 191-193, 2009.

Peng, Z., J. E. Vidale, K. C. Creager, A. G. Wech, R. M. Nadeau, and K.C. Creager, Remote triggering of tremor along the San Andreas Fault in central California, *J. Geophys. Res.*, *114*, B00A06, 2009.

Rubinstein, J. L., J. Gomberg, J. E. Vidale, A. G. Wech, H. Kao, K. C. Creager, and G. Rogers, Seismic wave triggering of nonvolcanic tremor, episodic tremor and slip, and earthquakes on Vancouver Island, *J. Geophys. Res.*, *114*, B00A01, 2009.

25 Locating Nonvolcanic Tremors Beneath the San Andreas Fault Using a Station-pair Double-Difference Location Method

Robert M. Nadeau, Haijiang Zhang (Massachusetts Institute of Technology), and Nafi Toksoz (Massachusetts Institute of Technology)

25.1 Introduction

It has been a challenging task to locate nonvolcanic tremors because of their lack of impulsive wave arrivals. To help overcome these difficulties, we have developed a station-pair double-difference (DD) location method to determine absolute tremor locations by directly using the station-pair travel time differences measured from cross-correlating tremor waveform envelopes. To account for velocity model inaccuracy, multiple tremors are located together to invert for station corrections. The new method is applied to tremors in the Parkfield region of central California occurring between 27 July 2001 and 21 February 2009, and the resulting locations are compared to the catalog locations of *Nadeau and Guilhem* (2009). The comparison shows that the new tremor locations more clearly delineate the spatial and temporal distribution of tremor activity in the area and improve our understanding of tremor origin and process.

25.2 Station-pair double-difference location method

The DD location method, developed by *Waldhauser and Ellsworth* (2000), has been widely used to locate earthquakes using differential arrival times at common stations from pairs of 'events'. We use the same concept applied to the case where differential times on pairs of 'stations' from common events are accurately calculated (using the station-pair differential travel times directly to locate the tremor events). In addition, because station corrections are included in our inversion, our approach is a 'multiple-event' location method. Our method uses station-pair cross-correlation delay times measured from tremor waveform envelopes between different stations. It should also be applicable for locating low frequency earthquakes (LFEs) when similar travel time difference information is available. We applied our location method to station-pair delay time measurements from nonvolcanic tremors occurring beneath the San Andreas Fault around the Parkfield and Cholame area (originally detected and located by *Nadeau and Guilhem* (2009)). More detail on the station-pair DD method can be found in *Zhang et al.* (2010).

25.3 Results and Discussion

Figure 2.48 compares station-pair DD locations with original catalog locations (*Nadeau and Guilhem,* 2010). The DD located tremors are shifted northeast and deeper (Figure 2.48C and D), relative to the original catalog. The average shift is 3.4 km in X and 3.7 km in depth. The northeast shift may be due to bias introduced by our use of a 1-D velocity model in this region of strong lateral velocity contrast. The shift in depth is likely due to the station-pair DD location method's more accurate determination of tremor depths, which avoids the coupling effect between depth and origin time. The DD locations are also more clustered, and more substructure can be seen than with the catalog locations (Figure 2.48G and H). Overall, the location uncertainties of the station-pair DD tremor locations are about half those of the catalog tremors (Figure 2.48G and H; also see Auxiliary Material in (*Zhang et al.*, 2010)).

Figure 2.48E and F show histograms of tremor depths from the catalog and station-pair DD locations. In this area, earthquakes locate in the upper ∼15 km of the Earth's crust, and the Moho depth is ∼25 km. Hence, our results suggest that tremors predominate below the seismogenic zone, in the ductile lower crust, and that a distinct gap in depth between the seismogenic and tremor zones exists.

Nadeau and Guilhem (2009) also observed periodic episodes of tremors at Cholame after the 2004 Parkfield M6 earthquake that where concentrated and more periodic in the southwestern portion of the tremor zone. Our results confirm these observations (see Figures 2c and d of *Zhang et al.*, 2010), and they indicate that the process generating tremors in this area may be structurally controlled and vary across the SAF.

25.4 Acknowledgements

Supported through USGS grants 06HQGR0167, 07HQAG0014, 08HQGR0100, and 08HQGR0101; DOE contract DE-FC52-06NA27325; NSF grants EAR-0537641 and EAR-0544730; and Chinese government executive program SinoProbe-02.

25.5 References

Nadeau, R.M. and A. Guilhem, Nonvolcanic Tremor Evolution and the San Simeon and Parkfield, California, Earthquakes, *Science, 325,* 191-193, 2009.

Waldhauser, F. and W.L. Ellsworth, A double-difference earthquake location algorithm: method and application to the Northern Hayward Fault, California, *Bull. Seism. Soc. Am. 90,* 1353-1368, 2000.

Zhang, H., R.M. Nadeau and N. Toksoz, Locating nonvolcanic tremors beneath the San Andreas Fault using a station-pair double-difference location method, *Geophys. Res. Lett., 37,* L13304, doi:10.1029/2010GL043577, 2010.

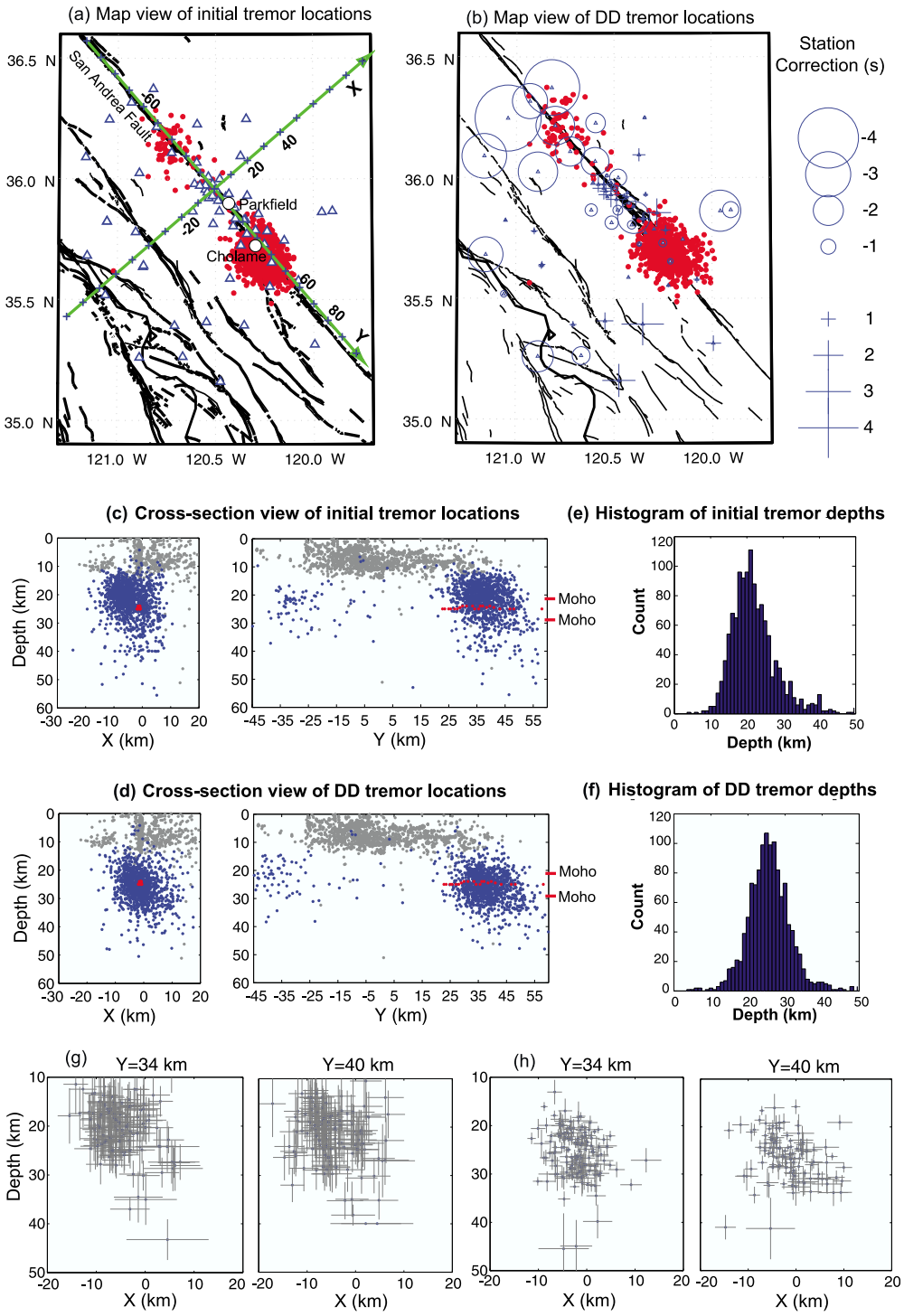

Figure 2.48: Comparison of catalog and station-pair DD tremor locations. (A) Map view of 1246 tremors (red/gray dots) and 64 stations (triangles) used in this study. Tremor catalog locations are from *Nadeau and Guilhem* (2009). The Cartesian coordinate system used in location is shown with a tick (marked as '+') interval of 10 km on X and Y axes. Faults are shown as black lines. Parkfield and Cholame are marked as white dots. (B) Map view of new tremor locations determined by station-pair DD location method. Station corrections in seconds are also shown. (C) Catalog tremor locations (blue/dark-gray) are shown in X-depth and Y-depth sections. (D) DD tremor locations are shown in X-depth and Y-depth sections. (E) Depth distribution of catalog tremor locations. (F) Depth distribution of DD tremor locations. (G) Across-fault cross sections of catalog tremor locations and the associated 95% uncertainty bounds at Y=34 and 40 km (within 1 km of both sides of the section). (H) The same as G but for DD tremor locations. In both panels (C) and (D), background seismicity from *Thurber et al.* (2006) is shown as light gray dots and the inferred LFE locations of *Shelly* (2009) are shown as the near horizontal red/light-gray dots at ~25 km depth.

Chapter 3

BSL Operations

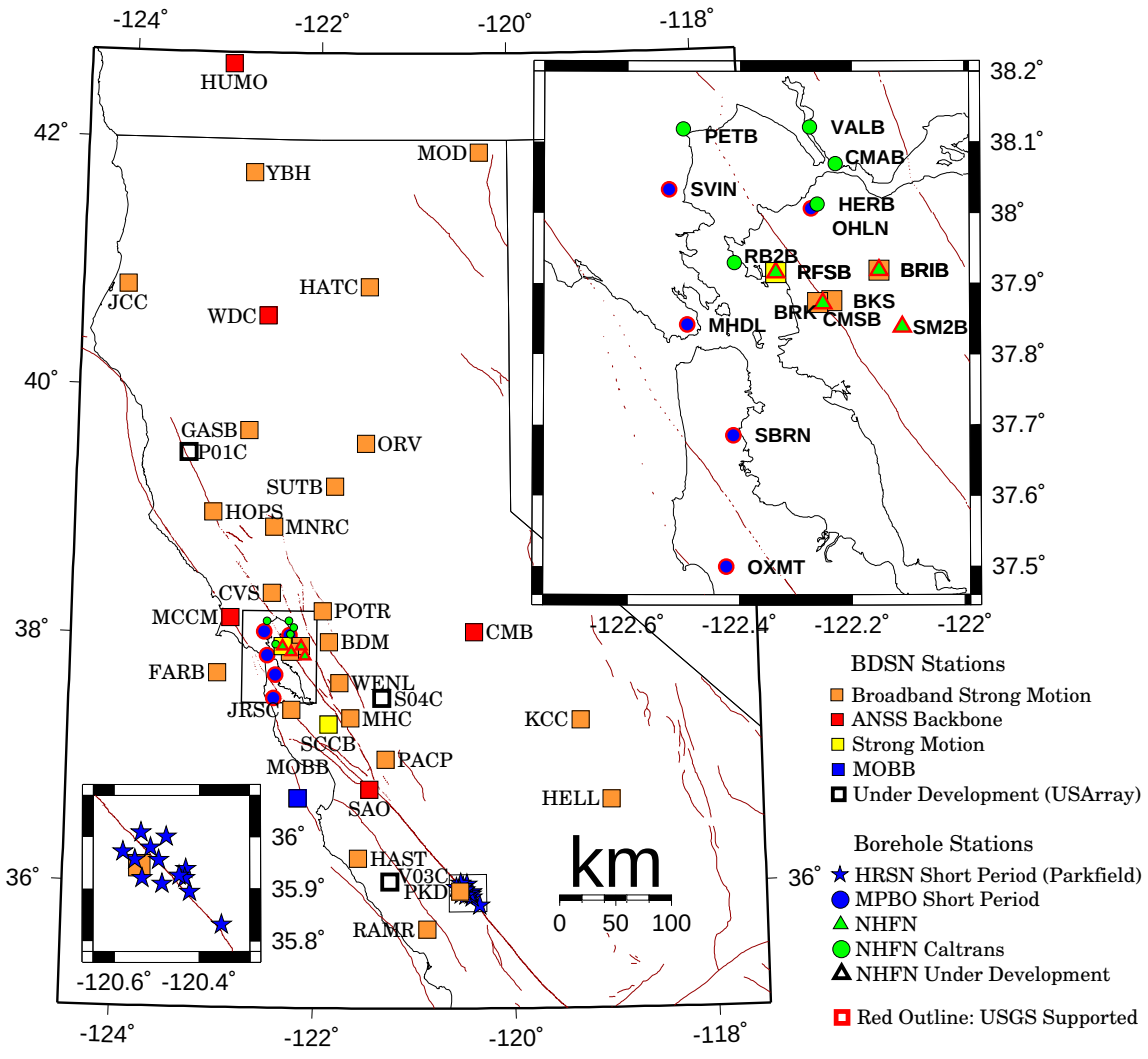

Figure 3.1: Map illustrating the distribution of BSL networks in Northern and Central California.

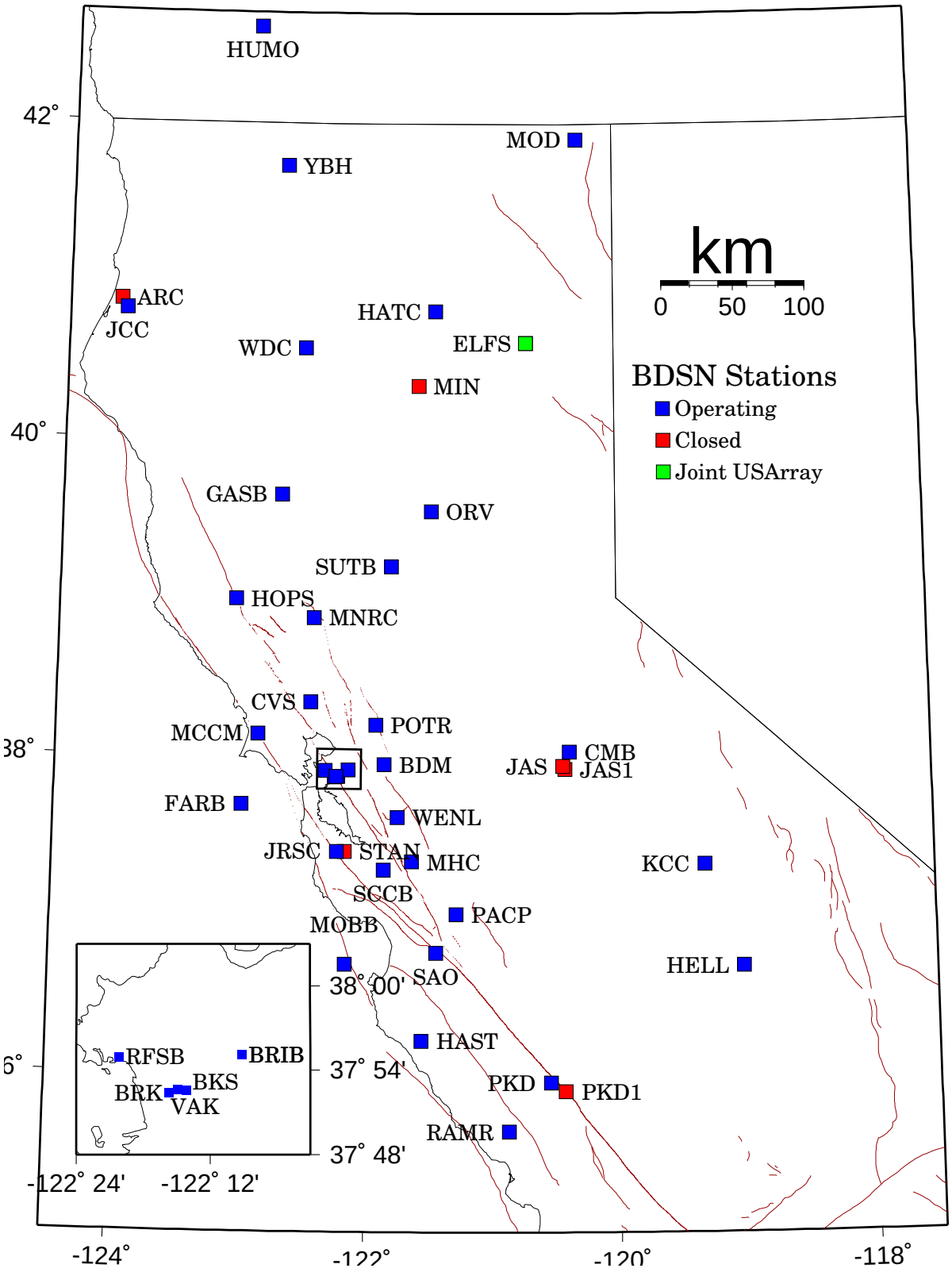

Figure 3.2: Map illustrating the distribution of BDSN stations in Northern and Central California.

1 Berkeley Digital Seismic Network

1.1 Introduction

The Berkeley Digital Seismic Network (BDSN) is a regional network of very broadband and strong motion seismic stations spanning Northern California and linked to UC Berkeley through continuous telemetry (Figure 3.2 and Table 3.3). The network is designed to monitor regional seismic activity at the magnitude 3+ level as well as to provide high quality data for research in regional and global broadband seismology.

Since 1991, the BDSN has grown from the original 3 broadband stations installed in 1986-87 (BKS, SAO, MHC) to 32 stations, including an autonomous ocean-bottom seismometer in Monterey Bay (MOBB). We take particular pride in high quality installations, which often involve lengthy searches for appropriate sites away from sources of low-frequency noise as well as continuous improvements in installation procedures and careful monitoring of noise conditions and problems. This year, most of the field and operation efforts have been directed toward station upgrades, thanks to the "American Recovery and Reinvestment Act" (ARRA). Engineering and research efforts were also devoted to several projects to develop and test new instrumentation (see Operational Section 7). We made progress in testing a new, low-cost sensor for pressure and temperature to be installed at seismic and GPS sites, and have begun testing of the Quanterra environmental add-on, the QEP. Finally, the BSL is part of a team for developing and testing a newly designed VBB sensor to replace the STS-1 seismometer.

The expansion of our network to increase the density of state-of-the-art strong motion/broadband seismic stations and improve the joint earthquake notification system in this seismically hazardous region, one of BSL's long term goals, must be coordinated with other institutions and is contingent on the availability of funding.

Equally important to network growth, data quality and the integrity of the established network must be preserved. The first generation of broadband seismometers installed by the BSL has been operating for almost 25 years. At the same time, the first generation of broadband data loggers are entering their 18th year of service. Fortunately, we received funding and equipment from the ARRA to replace data loggers at the 25 stations with older models between September 2009 and September 2011. These efforts are ongoing. In the meantime, we continue to exercise vigilance and commit time and resources to repairs and upgrades as necessary.

1.2 BDSN Overview

Twenty-eight of the BDSN sites are equipped with three-component broadband seismometers and strong-motion accelerometers, and a 24-bit digital data acquisition system or data logger. Two additional sites (RFSB and SCCB) consist of a strong-motion accelerometer and a 24-bit digital data logger. The ocean-bottom station MOBB is equipped with a three component broadband seismometer and a DPG. Data from all BDSN stations are transmitted to UC Berkeley using continuous telemetry. Continuous telemetry from MOBB was implemented early in 2009. Unfortunately, the underwater cable was trawled and damaged several times, until it finally failed in late February 2010. We are currently preparing a new cable to connect MOBB to the nearby science node. It will be buried in the seafloor, which will hopefully protect it from trawling operations. In order to avoid data loss during utility disruptions, each site has a three-day supply of battery power; many are accessible via a dialup phone line. The combination of high-dynamic range sensors and digital data loggers ensures that the BDSN has the capability to record the full range of earthquake motion required for source and structure studies. Table 3.4 lists the instrumentation at each site.

Most BDSN stations have Streckeisen STS-1 or STS-2 three-component broadband sensors (*Wielandt and Streckeisen*, 1982; *Wielandt and Steim*, 1986). A Guralp CMG-3T broadband sensor contributed by LLNL is deployed in a post-hole installation at BRIB. A Guralp CMG-1T is deployed at MOBB. The strong-motion instruments are Kinemetrics FBA-23, FBA-ES-T or Metrozet accelerometers with $\pm$ 2 g dynamic range. Thanks to the ARRA funding, we are replacing the noisier FBA-23 sensors with FBA-ES-Ts. The recording systems at all sites except MOBB are either Q330, Q680, Q730, or Q4120 Quanterra data loggers, with 3, 6, 8, or 9 channel systems. The Quanterra data loggers employ FIR filters to extract data streams at a variety of sampling rates. In general, the BDSN stations record continuous data at .01, 0.1, 1.0, 20 or 40, and 80 or 100 samples per second. However, at some sites, data at the highest sampling rate are sent in triggered mode using the Murdock, Hutt, and Halbert event detection algorithm (*Murdock and Hutt*, 1983) (Table 3.1). In addition to the 6 channels of seismic data, signals from thermometers and barometers are recorded at many locations (Figure 3.3).

As the broadband network was upgraded during the 1990s, a grant from the CalREN Foundation (California Research and Education Network) in 1994 enabled the BSL to convert data telemetry from analog leased lines to digital frame relay. The frame-relay network uses digital phone circuits which support 56 Kbit/s to 1.5 Mbit/s throughput.

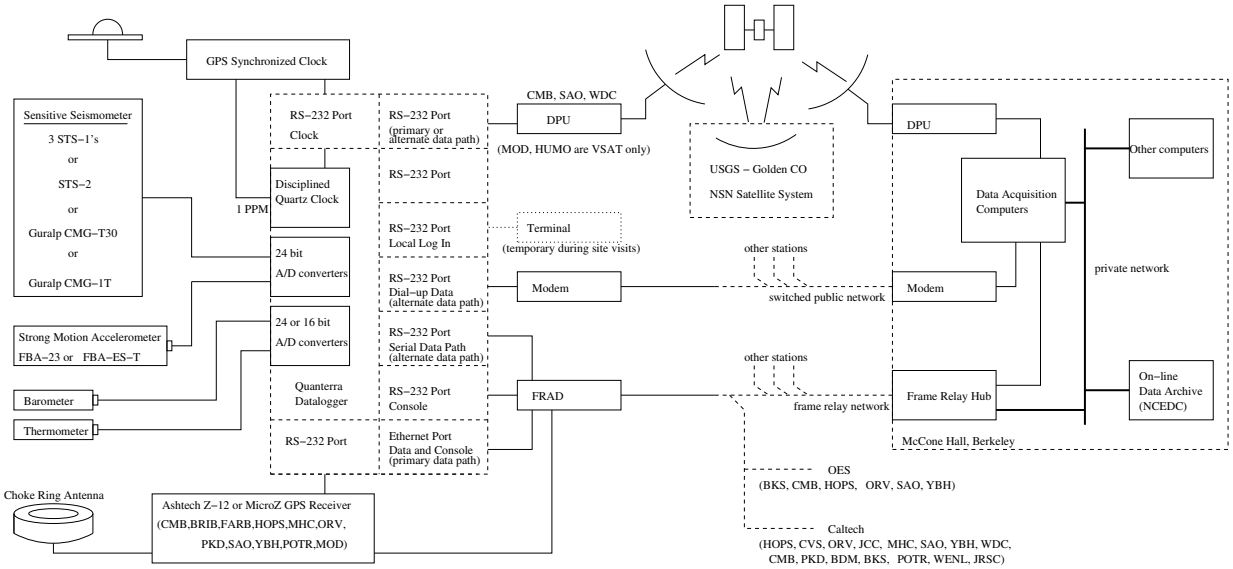

Figure 3.3: Schematic diagram showing the flow of data from the sensors through the data loggers to the central acquisition facilities of the BSL.

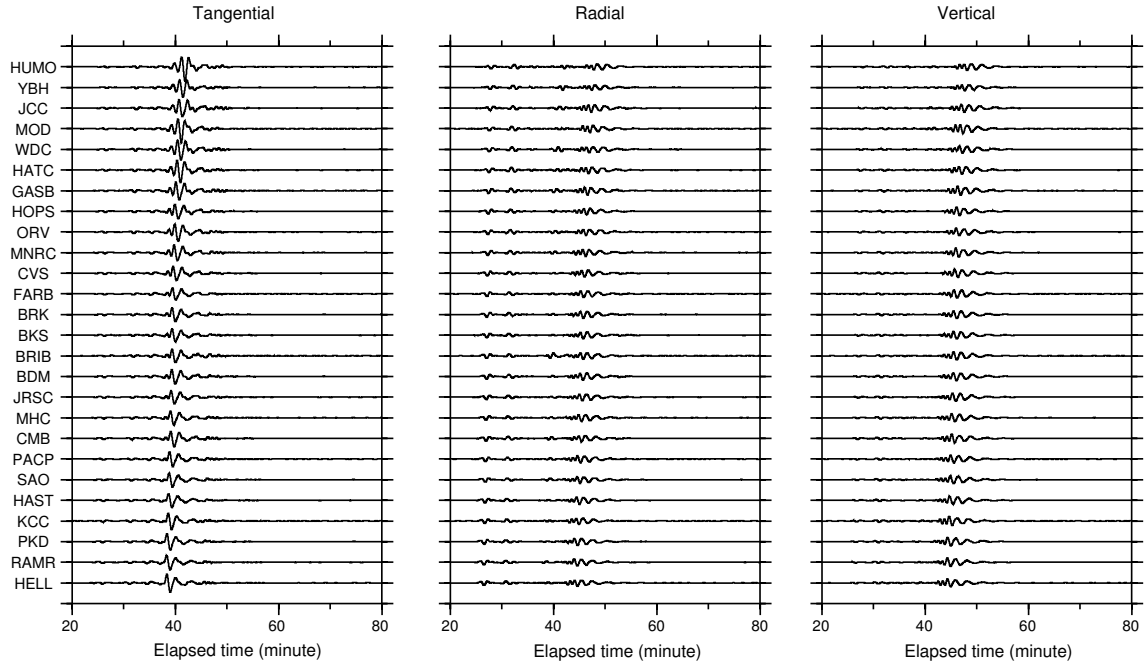

Figure 3.4: Long period (50-200 s period) waveforms recorded across BDSN from the M_w 8.8 teleseism which occurred on February 27, 2010, in Chile at 35.91 S, 72.73 W. The traces are deconvolved to ground velocity, scaled absolutely, and ordered from bottom to top by distance from the epicenter. The highly similar waveforms recorded across the BDSN provide evidence that the broadband sensors are operating within their nominal specifications. Data from MOBB, MCCM, and WENL were not available for this earthquake.

Since frame-relay is a packet-switched network, a site may use a single physical circuit to communicate with multiple remote sites through the use of "permanent virtual circuits." Frame Relay Access Devices (FRADs), which replace modems in a frame-relay network, can simultaneously support a variety of interfaces such as RS-232 async ports, synchronous V.35 ports, and ethernet connections. In practical terms, frame relay communication provides faster data telemetry between the remote sites and the BSL, remote console control of the data loggers, services such as FTP and telnet to the data loggers, data transmission to multiple sites, and the capability of transmitting data from several instruments at a single site, such as GPS receivers and/or multiple data loggers. Today, 25 of the BDSN sites use frame-relay telemetry for all or part of their communications system.

As described in Operational Section 7, data from the BDSN are acquired centrally at the BSL. These data are used for rapid earthquake reporting as well as for routine earthquake analysis (Operational Section 2 and 8). As part of routine quality control (Operational Section 7), power spectral density (PSD) analyses are performed continuously and are available on the internet (`http://www.ncedc.org/ncedc/PDF/html/`). The occurrence of a significant teleseism also provides the opportunity to review station health and calibration. Figure 3.4 displays BDSN waveforms for the great M_w 8.8 earthquake that occurred in Chile on February 27, 2010.

BDSN data are archived at the Northern California Earthquake Data Center. This is described in detail in Operational Section 6.

Sensor	Channel	Rate (sps)	Mode	FIR
Broadband	UH?	0.01	C	Ac
Broadband	VH?	0.1	C	Ac
Broadband	LH?	1	C	Ac
Broadband	BH?	20/40	C	Ac
Broadband	HH?	80/100	C	Ac/Ca
SM	LL?	1	C	Ac
SM	BL?	20/40	C	Ac
SM	HL?	80/100	C	Ac/Ca
Thermometer	LKS	1	C	Ac
Barometer	LDS	1	C	Ac

Table 3.1: Typical data streams acquired at BDSN stations, with channel name, sampling rate, sampling mode, and the FIR filter type. SM indicates strong-motion; C continuous; T triggered; Ac acausal; Ca causal. The LL and BL strong-motion channels are not transmitted over the continuous telemetry but are available on the Quanterra disk system if needed. The HH channels are recorded at two different rates, depending on the data logger. Q4120s and Q330s provide 100 sps and causal filtering; Q680/980s provide 80 sps and acausal filtering.

Electromagnetic Observatories

In 1995, in collaboration with Dr. Frank Morrison, the BSL installed two well-characterized electric and magnetic field measuring systems at two sites along the San Andreas Fault which are part of the Berkeley Digital Seismic Network. Since then, magnetotelluric (MT) data have been continuously recorded at 40 Hz and 1 Hz and archived at the NCEDC (Table 3.2). At least one set of orthogonal electric dipoles measures the vector horizontal electric field, E, and three orthogonal magnetic sensors measure the vector magnetic field, B. These reference sites, now referred to as electromagnetic (EM) observatories, are collocated with seismometer sites so that the field data share the same time base, data acquisition, telemetry, and archiving system as the seismometer outputs.

Sensor	Channel	Rate (sps)	Mode	FIR
Magnetic	VT?	0.1	C	Ac
Magnetic	LT?	1	C	Ac
Magnetic	BT?	40	C	Ac
Electric	VQ?	0.1	C	Ac
Electric	LQ?	1	C	Ac
Electric	BQ?	40	C	Ac

Table 3.2: Typical MT data streams acquired at SAO, PKD, BRIB, and JRSC with channel name, sampling rate, sampling mode, and FIR filter type. C indicates continuous; T triggered; Ac acausal.

The MT observatories are located at Parkfield (PKD1, PKD), 300 km south of the San Francisco Bay Area, and Hollister (SAO), halfway between San Francisco and Parkfield (Figure 3.2). In 1995, initial sites were established at PKD1 and SAO, separated by a distance of 150 km, and equipped with three induction coils and two 100 m electric dipoles. PKD1 was established as a temporary seismic site, and when a permanent site (PKD) was found, a third MT observatory was installed in 1999 with three induction coils, two 100 m electric dipoles, and two 200 m electric dipoles. PKD and PKD1 ran in parallel for one month in 1999, and then the MT observatory at PKD1 was closed. Starting in 2004, new electromagnetic instrumentation was installed at various Bay Area sites in cooperation with Simon Klemperer at Stanford University. Sensors are installed at JRSC (2004), MHDL (2006) and BRIB (2006/2007).

Data at the MT sites are fed to Quanterra data loggers, shared with the collocated BDSN stations, synchronized in time by GPS, and sent to the BSL via dedicated communication links.

In 2009, the BSL led a joint effort toward improving operation and maintenance of these sites with Jonathan Glen and Darcy McPhee from the USGS, and Simon Klemperer at Stanford University.

Engineers from the BSL met scientists from the USGS and Stanford at the station SAO in October of 2008 to assess the condition of the EM/MT system. At that time, the EM coils were found to be not working. They were removed and returned to the manufacturer (EMI Schlumberger). In June 2010, the EM coils had not been reinstalled at SAO. EM/MT equipment at PKD was evaluated in August of 2008. There, the data logger was removed from the PKD EM/MT system and has not yet been returned.

Since it began in 1995, the EM/MT effort has suffered from minimal funding, in part due to the misconception that the EM/MT data could be recorded on unused channels in the seismic data logger. These data loggers had no channels available, however. Thus, for each site, an additional data logger was purchased. In 2008, the BSL began in-house development of a low cost digitizing solution. While not as feature-rich as commercially available data loggers, the prototype 24 bit digitizer was developed and is being tested in the field.

1.3 2009-2010 Activities

Station Upgrades, Maintenance, and Repairs

Given the remoteness of the off-campus stations, BDSN data acquisition equipment and systems are designed, configured, and installed so that they are both cost effective and reliable. As a result, there is little need for regular station visits. Nonetheless, many of the broadband seismometers installed by BSL are from the first generation and are about 25 years old. Concurrently, the first generation of broadband data loggers is now 18 years old. Computer systems are retired long before this age, yet the electronics that form these data acquisition systems are expected to perform without interruption.

In the summer of 2009, the USGS received ARRA funds, among other things, to upgrade and improve seismic stations operated as part of the Advanced National Seismic System (ANSS). The BSL is benefitting from those funds. We are receiving the newest model of Quanterra data logger, the Q330, as government-furnished equipment (GFE) to replace the old Quanterras at 25 of the BDSN seismic stations. In addition, all remaining Kinemetrics FBA-23 accelerometers will be replaced with Kinemetrics' newer model, the FBA-ES-T. Stations for which the upgrade is complete are marked in Table 3.4. As of June 2010, we have replaced equipment at about half of the BDSN sites that will be upgraded. Finally, we have also received support through the ARRA project to investigate and implement alternative, and less expensive, telemetry options.

As always, some of the BSL's technical efforts were directed toward maintaining and repairing existing instrumentation, stations, and infrastructure. While expanding the network continues to be a long term goal of BSL, it is equally important to assure the integrity of the established network and preserve data quality.

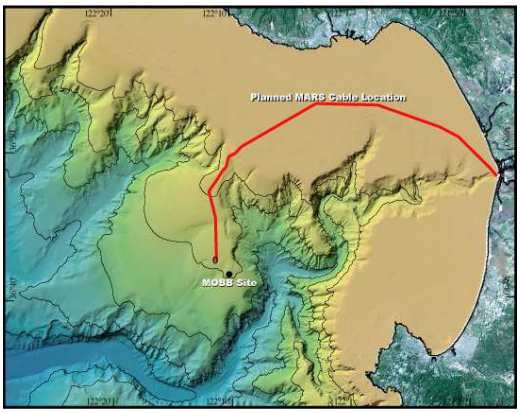

Figure 3.5: Location of the MOBB station in Monterey Bay, California, against seafloor and land topography. The path of the MARS cable is indicated by the solid line.

The Monterey Bay Ocean Bottom Seismic Observatory (MOBB)

The Monterey Ocean Bottom Broadband observatory (MOBB) is a collaborative project between the Monterey Bay Aquarium Research Institute (MBARI) and the BSL. Supported by funds from the Packard Foundation to MBARI, NSF/OCE funds, and UC Berkeley funds to the BSL, its goal has been to install and operate a long-term seafloor broadband station as a first step toward extending the onshore broadband seismic network in Northern California to the seaward side of the North-America/Pacific plate boundary, providing better azimuthal coverage for regional earthquake and structure studies. It also serves the important goal of evaluating background noise in near-shore buried ocean floor seismic systems, such as may be installed as part of temporary deployments of "leap-frogging" arrays (e.g. Ocean Mantle Dynamics Workshop, September 2002). The project has been described in detail in BSL annual reports since 2002 and in several publications (e.g. *Romanowicz* et al., 2003, 2006).

The MARS (Monterey Accelerated Research System) observatory (Figure 3.5, `http://www.mbari.org/mars/`) comprises a 52 km electro-optical cable that extends from a shore facility in Moss Landing out to a seafloor node in Monterey Bay (Figure 3.5). The cable was deployed in the spring of 2007, and node installation was completed in November 2008. It now can provide power and data to as many as eight science experiments through underwater electrical connectors. MOBB, located 3km from the node, is one of the first instruments to be connected to the cable. The connection was established on February 28,

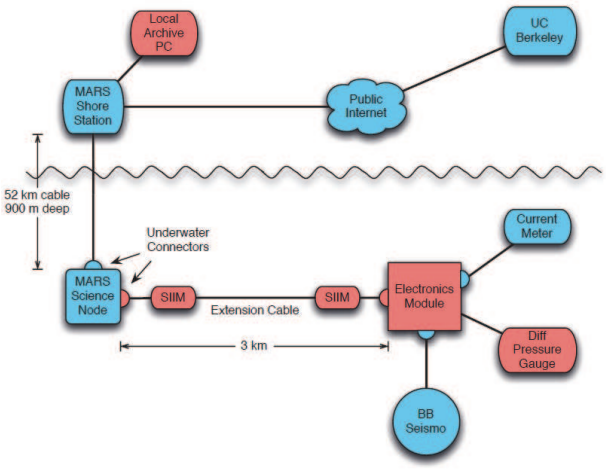

Figure 3.6: Components of the cabled observatory: the MOBB system integrated into the MARS network. MARS-provided components are shown in blue, and components installed or modified by the MOBB team are shown in pink.

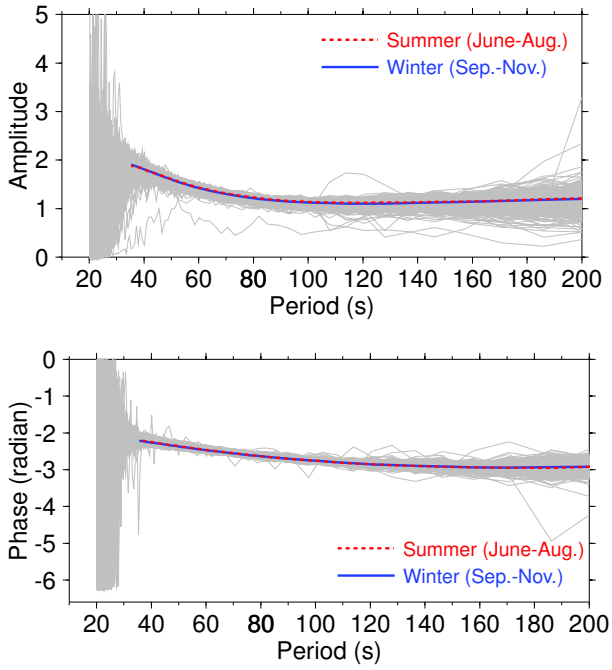

Figure 3.7: Transfer function from DPG to the vertical seismic component at MOBB, in the period range 35-200 sec, during a one year period, showing the seasonal stability both in amplitude (top) and in phase. The bold lines show that the smoothed averages in summer and winter are in good agreement across the frequency band considered (bottom).

2009, through an extension cable installed by the ROV Ventana, with the help of a cable-laying toolsled. The data interface at the MARS node is 10/100 Mbit/s Ethernet, which can directly support cables of no more than 100 m in length. To send data over the required 3 km distance, the signals pass through a Science Instrument Interface Module (SIIM) at each end of the extension cable (Figure 3.6). The SIIMs convert the MARS Ethernet signals to Digital Subscriber Line (DSL) signals, which are converted back to Ethernet signals close to the MOBB system. Power from the MARS node is sent over the extension cable at 375 VDC, and then converted to 28 VDC in the distal SIIM for use by the MOBB system. The connection to the MARS node eliminates the need for periodic exchange of the battery and data package using ROV and ship. At the same time, it allows us to acquire seismic data from the seafloor in real time (*Romanowicz* et al., 2009).

The electronics module in the MOBB system has been refurbished to support the connection to the MARS observatory. The low-power autonomous data logger has been replaced with a PC/104 computer stack running embedded Linux. This new computer runs an Object Ring Buffer (ORB), whose function is to collect data from the various MOBB sensors and forward it to another ORB running on a computer at the MARS shore station. There, the data are archived and then forwarded to a third ORB running at the UC Berkeley Seismological Laboratory. The Linux system acquires data from the various systems on the sea floor: from the Guralp digitizer included in the seismometer package (via RS232) and from a Q330 Quanterra 24 bit A/D converter which digitizes data from the DPG (via Ethernet). It also polls and receives data (via RS232) from the current meter. The data are available through the NCEDC. Procedures to include the MOBB data in the Northern California real time earthquake processing are under development.

Recently, we have been exploring ways to routinely remove low frequency noise generated by infragravity ocean waves, which are also observed on the DPG. Figure 3.7 shows the transfer function from the DPG to MOBB-Z in the period band (35 - 200 sec). The stability of the transfer function over the course of a year indicates that automatic implementation of the noise reduction procedure will allow us to more effectively use MOBB data jointly with data from other BDSN stations to constrain regional moment tensors in real time. Figure 3.8 shows the vertical component trace before and after removing the DPG correlated noise, in the case of a regional event of M_w 4.3. Unfortunately, the cable that links the MOBB instrumentation to the MARS science node was trawled several times since February 2009 leading to a failure on February 27, 2010. We have obtained funds from NSF/OCE to purchase and install a new cable. This time, the cable will be buried in the seafloor to avoid further trawling incidents. This has required the construction of a cable

burying tool for the MBARI ROV Ventana, which is in the process of being tested, for a planned installation of the new cable in early 2011.

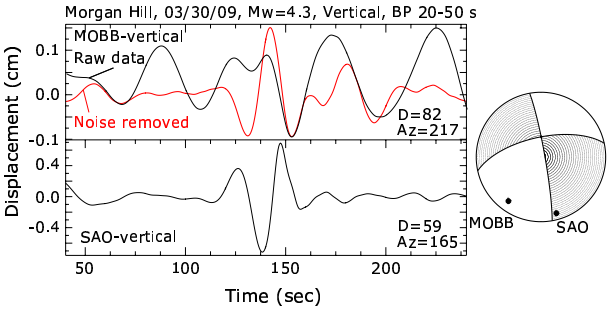

Figure 3.8: Comparison of raw and filtered traces on the vertical component at MOBB, before and after deconvolution with the DPG data to remove infragravity wave related noise, for the Morgan Hill M_w 4.3 earthquake of 03/30/09. The bottom trace shows the corresponding record at land station SAO. On the right is shown the earthquake mechanism with the azimuths of the two stations.

1.4 Acknowledgements

Under Barbara Romanowicz's general supervision, Peggy Hellweg and Doug Neuhauser oversee the BDSN data acquisition operations, and Bill Karavas heads the engineering team. John Friday, Jarrett Gardner, Rick Lellinger, Taka'aki Taira, and Bob Uhrhammer contribute to the operation of the BDSN. The network upgrades and improvements are funded through the ARRA (American Reinvestment and Recovery Act), under the USGS Award Number G09AC00487.

MOBB is a collaboration between the BSL and MBARI, involving Barbara Romanowicz, Taka'aki Taira, and Doug Neuhauser from the BSL, and Paul McGill from MBARI. The MBARI team also has included Steve Etchemendy (Director of Marine Operations), Jon Erickson, John Ferreira, Tony Ramirez, and Craig Dawe. The MOBB effort at the BSL is supported by UC Berkeley funds. MBARI supports the dives and data recovery. The MOBB seismometer package was funded by NSF/OCE grant #9911392. The development of the interface for connection to the MARS cable is funded by NSF/OCE grant #0648302.

Bill Karavas, Taka'aki Taira, and Peggy Hellweg contributed to the preparation of this section.

1.5 References

Cox, C., T. Deaton and S. Webb, A deep-sea differential pressure gauge, *J. Atm. Ocean. Tech., 1*, 237-245, 1984.

Crawford W. C., and S. C. Webb, Identifying and removing tilt noise from low-frequency (<0.1 Hz) seafloor vertical seismic data, *Bull. Seis. Soc. Am., 90*, 952-963, 2000.

Murdock, J., and C. Hutt, A new event detector designed for the Seismic Research Observatories, *USGS Open-File-Report 83-0785,* 39 pp., 1983.

Romanowicz, B., D. Stakes, R. Uhrhammer, P. McGill, D. Neuhauser, T. Ramirez, and D. Dolenc, The MOBB experiment: a prototype permanent off-shore ocean bottom broadband station, *EOS Trans. AGU*, Aug 28 issue, 2003.

Romanowicz, B., D. Stakes, D. Dolenc, D. Neuhauser, P. McGill, R. Uhrhammer, and T. Ramirez, The Monterey Bay Broadband Ocean bottom seismic observatory, Ann. Geophys., 49, 607-623, 2006.

Romanowicz, B., P. McGill, D. Neuhauser and D. Dolenc, Acquiring real time data from the broadband ocean bottom seismic observatory at Monterey Bay (MOBB), *Seismol. Res. Lett, 80,* 197-202, 2009.

Wielandt, E., and J. Steim, A digital very broadband seismograph, *Ann. Geophys., 4*, 227-232, 1986.

Wielandt, E., and G. Streckeisen, The leaf spring seismometer: design and performance, *Bull. Seis. Soc. Am., 72*, 2349-2367, 1982.

Zürn, W., and R. Widmer, On noise reduction in vertical seismic records below 2 mHz using local barometric pressure, *Geophys. Res. Lett., 22*, 3537-3540, 1995.

Code	Net	Latitude	Longitude	Elev (m)	Over (m)	Date	Location
BDM	BK	37.9540	-121.8655	219.8	34.7	1998/11 -	Black Diamond Mines, Antioch
BKS	BK	37.8762	-122.2356	243.9	25.6	1988/01 -	Byerly Vault, Berkeley
BRIB	BK	37.9189	-122.1518	219.7	2.5	1995/06 -	Briones Reservation, Orinda
BRK	BK	37.8735	-122.2610	49.4	2.7	1994/03 -	Haviland Hall, Berkeley
CMB	BK	38.0346	-120.3865	697.0	2	1986/10 -	Columbia College, Columbia
CVS	BK	38.3453	-122.4584	295.1	23.2	1997/10 -	Carmenet Vineyard, Sonoma
FARB	BK	37.6978	-123.0011	-18.5	0	1997/03 -	Farallon Island
GASB	BK	39.6547	-122.716	1354.8	2	2005/09 -	Alder Springs
HAST	BK	36.3887	-121.5514	542.0	3	2006/02 -	Carmel Valley
HATC	BK	40.8161	-121.4612	1009.3	3	2005/05 -	Hat Creek
HELL	BK	36.6801	-119.0228	1140.0	3	2005/04 -	Miramonte
HOPS	BK	38.9935	-123.0723	299.1	3	1994/10 -	Hopland Field Stat., Hopland
HUMO	BK	42.6071	-122.9567	554.9	50	2002/06 -	Hull Mountain, Oregon
JCC	BK	40.8175	-124.0296	27.2	0	2001/04 -	Jacoby Creek
JRSC	BK	37.4037	-122.2387	70.5	0	1994/07 -	Jasper Ridge, Stanford
KCC	BK	37.3236	-119.3187	888.1	87.3	1995/11 -	Kaiser Creek
MCCM	BK	38.1448	-122.8802	-7.7	2	2006/02 -	Marconi Conference Center, Marshall
MHC	BK	37.3416	-121.6426	1250.4	0	1987/10 -	Lick Obs., Mt. Hamilton
MNRC	BK	38.8787	-122.4428	704.8	3	2003/06 -	McLaughlin Mine, Lower Lake
MOBB	BK	36.6907	-122.1660	-1036.5	1	2002/04 -	Monterey Bay
MOD	BK	41.9025	-120.3029	1554.5	5	1999/10 -	Modoc Plateau
ORV	BK	39.5545	-121.5004	334.7	0	1992/07 -	Oroville
PACP	BK	37.0080	-121.2870	844	0	2003/06 -	Pacheco Peak
PKD	BK	35.9452	-120.5416	583.0	3	1996/08 -	Bear Valley Ranch, Parkfield
RAMR	BK	37.9161	-122.3361	416.8	3	2004/11 -	Ramage Ranch
RFSB	BK	37.9161	-122.3361	-26.7	0	2001/02 -	RFS, Richmond
SAO	BK	36.7640	-121.4472	317.2	3	1988/01 -	San Andreas Obs., Hollister
SCCB	BK	37.2874	-121.8642	98	0	2000/04 -	SCC Comm., Santa Clara
SUTB	BK	39.2291	-121.7861	252.0	3	2005/10 -	Sutter Buttes
WDC	BK	40.5799	-122.5411	268.3	75	1992/07 -	Whiskeytown
WENL	BK	37.6221	-121.7570	138.9	30.3	1997/06 -	Wente Vineyards, Livermore
YBH	BK	41.7320	-122.7104	1059.7	60.4	1993/07 -	Yreka Blue Horn Mine, Yreka

Table 3.3: Stations of the Berkeley Digital Seismic Network currently in operation. Each BDSN station is listed with its station code, network id, location, operational dates, and site description. The latitude and longitude (in degrees) are given in the WGS84 reference frame, and the elevation (in meters) is relative to the WGS84 reference ellipsoid. The elevation is either the elevation of the pier (for stations sited on the surface or in mining drifts) or the elevation of the well head (for stations sited in boreholes). The overburden is given in meters. The date indicates either the upgrade or installation time.

Code	Broadband	Strong-motion	Data logger	T/B	GPS	Other	Telemetry	Dial-up
BDM	STS-2	FBA-23	Q4120	X			FR	
BKS	STS-1	FBA-23	Q980	X		Baseplates	FR	X
BRIB	CMG-3T	FBA-ES-T	Q330HR*		X	Strainmeter, EM	FR	X
BRK	STS-2	FBA-ES-T	Q330HR				LAN	
CMB	STS-1	FBA-23	Q980	X	X	Baseplates	FR	X
CVS	STS-2	FBA-ES-T	Q330HR				FR	
FARB	STS-2	FBA-ES-T	Q330HR*		X		R-FR/R	
GASB	STS-2	FBA-ES-T	Q4120	X			R-FR	
HAST	STS-2	FBA-ES-T	Q330HR				R-Sat	
HATC	STS-2	FBA-ES-T	Q330HR				T-1	
HELL	STS-2	FBA-ES-T	Q330				R-Sat	
HOPS	STS-1	FBA-ES-T*	Q330HR*		X	Baseplates	FR	X
HUMO	STS-2	FBA-ES-T	Q4120	X			VSAT	X
JCC	STS-2	FBA-ES-T	Q980	X			FR	X
JRSC	STS-2	TSA-100S	Q680				FR	X
KCC	STS-1	FBA-ES-T	Q330HR			Baseplates	R-Mi-FR	X
MCCM	STS-2	FBA-ES-T	Q4120				VSAT	
MHC	STS-1	FBA-ES-T	Q980	X	X		FR	X
MNRC	STS-2	FBA-ES-T	Q330HR*				None	X
MOBB	CMG-1T		DM24			Current meter, DPG	None	
MOD	STS-1**	FBA-ES-T	Q330HR		X	Baseplates	VSAT	X
ORV	STS-1	FBA-ES-T*	Q330HR*		X	Baseplates	FR	X
PACP	STS-2	FBA-ES-T	Q330HR*				Mi/FR	
PKD	STS-2	FBA-ES-T*	Q330HR*		X	EM	R-FR	X
RAMR	STS-2	FBA-ES-T	Q330				R-FR	X
RFSB		FBA-ES-T	Q730				FR	
SAO	STS-1	FBA-ES-T*	Q330HR*		X	Baseplates, EM	FR	X
SCCB		TSA-100S	Q730		X		FR	
SUTB	STS-2	FBA-ES-T	Q330HR				R-FR	
WDC	STS-2	FBA-23	Q980	X			FR	X
WENL	STS-2	FBA-ES-T	Q330HR*				FR	
YBH	STS-1 & STS-2	FBA-ES-T	Q980	X	X	Baseplates	FR	X

Table 3.4: Instrumentation of the BDSN as of 06/30/2010. Except for RFSB, SCCB, and MOBB, each BDSN station consists of collocated broadband and strong-motion sensors, with a 24-bit Quanterra data logger and GPS timing. The stations RFSB and SCCB are strong-motion only, while MOBB has only a broadband sensor. Additional columns indicate the installation of a thermometer/barometer package (T/B), collocated GPS receiver as part of the BARD network (GPS), and additional equipment (Other), such as warpless baseplates or electromagnetic sensors (EM). The OBS station MOBB also has a current meter and differential pressure gauge (DPG). The main and alternate telemetry paths are summarized for each station. FR - frame relay circuit, LAN - ethernet, Mi - microwave, POTS - plain old telephone line, R - radio, Sat - Commercial Satellite, VSAT - USGS ANSS satellite link, None - no telemetry at this time. An entry like R-Mi-FR indicates telemetry over several links, in this case, radio to microwave to frame relay. (**) During 2009-2010, the STS-1 at this station was replaced by an STS-2. (*) Data logger and/or accelerometer replaced with ARRA provided government-furnished equipment.

2 California Integrated Seismic Network

2.1 Introduction

Advances in technology have made it possible to integrate separate earthquake monitoring networks into a single seismic system as well as to unify earthquake monitoring instrumentation. In California, this effort began in the south with the TriNet Project. There, Caltech, the California Geological Survey (CGS), and the USGS created a unified seismic system for Southern California. With major funding provided by the Federal Emergency Management Agency (FEMA), the California Governor's Emergency Management Agency (CalEMA), and the USGS, monitoring infrastructure was upgraded and expanded, combining resources in a federal, state and university partnership. In 2000, the integration effort expanded to the entire state with the formation of the California Integrated Seismic Network (CISN, see 2000-2001 Annual Report). To this end, UC Berkeley and the USGS Menlo Park and Pasadena offices joined forces with Caltech and the CGS. The CISN is now in the tenth year of collaboration and its ninth year of funding from CalEMA.

2.2 CISN Background

Organization

The organizational goals, products, management, and responsibilities of the CISN member organizations are described in the founding memorandum of understanding and in the strategic and implementation plans. To facilitate activities among institutions, the CISN has three management centers:

- Southern California Earthquake Management Center: Caltech/USGS Pasadena
- Northern California Earthquake Management Center: UC Berkeley/USGS Menlo Park
- Engineering Strong Motion Data Center: California Geological Survey/USGS National Strong Motion Program

The Northern and Southern California Earthquake Management Centers operate as twin statewide earthquake processing centers, serving information on current earthquake activities, while the Engineering Strong Motion Data Center is responsible for producing engineering data products and distributing them to the engineering community.

The Steering Committee, made up of two representatives from each core institution and a representative from CalEMA, oversees CISN projects. The position of chair rotates among the institutions; Barbara Romanowicz took over as chair of the Steering Committee in December 2009 from Rob Clayton.

An external Advisory Committee represents the interests of structural engineers, seismologists, emergency managers, industry, government, and utilities, and provides review and oversight. The Advisory Committee is chaired by Stu Nishenko of Pacific Gas and Electric Company. It last met in January 2009. Agendas from the meetings and the resulting reports may be accessed through the CISN Web site (`http://www.cisn.org/advisory`).

The Steering Committee has commissioned other committees, including a Program Management Group to address planning and coordination and a Standards Committee to resolve technical design and implementation issues.

In addition to the core members, other organizations contribute data that enhance the capabilities of the CISN. Contributing members include: University of California, Santa Barbara; University of California, San Diego; University of Nevada, Reno; University of Washington; California Department of Water Resources; Lawrence Livermore National Lab; and Pacific Gas and Electric.

CISN and ANSS

The USGS Advanced National Seismic System (ANSS) is developing along a regionalized model. Eight regions have been organized, with the CISN representing California. David Oppenheimer of the USGS represents the CISN on the ANSS National Implementation Committee (NIC).

This year, the CISN is benefiting from the America Recovery and Reinvestment Act (ARRA). The ANSS has received funds from the ARRA to improve seismic monitoring throughout the nation and the world. In California, these funds are being directed toward replacing old data loggers in both Northern and Southern California, as well as improving installations at individual stations and adding strong motion sites in the form of NetQuakes sensors. The BSL's ARRA-funded activities are described in Operational Sections 1, 4 and 3.

As the ANSS moves forward, committees and working groups are established to address issues of interest. BSL faculty and staff have been involved in several working groups of the Technical Integration Committee, including Doug Dreger, Peggy Hellweg, Pete Lombard, Doug Neuhauser, Bob Uhrhammer, and Stephane Zuzlewski. Last Fall, the BSL hosted two ANSS workshops. In October 2009, operators of ANSS Regional Seismic Networks

met in the Hearst Mining Building at UC Berkeley for NetOps IV, a workshop to learn about the new version of the ShakeMap program. The next month, November 2009, the BSL hosted a one-day ANSS workshop on the future of the ANSS catalog (`http://www.ncedc.org/anss/catalog-search.html`), followed by a meeting of the ANSS National Implementation Committee (NIC).

CISN and CalEMA

CalEMA has long had an interest in coordinated earthquake monitoring. The historical separation between Northern and Southern California and between strong-motion and weak-motion networks resulted in a complicated situation for earthquake response. Thus, CalEMA has been an advocate of increased coordination and collaboration in California earthquake monitoring and encouraged the development of the CISN. In FY01-02, Governor Gray Davis requested support for the CISN, to be administered through CalEMA. Funding for the California Geological Survey, Caltech and UC Berkeley was made available in spring 2002, officially launching the statewide coordination efforts. Following the first year of funding, CalEMA support led to the establishment of 3-year contracts to UC Berkeley, Caltech, and the California Geological Survey for CISN activities. We have just completed the second year of the third three-year contract (2008-2011). Past CISN-related activities are described in previous annual reports.

2.3 2009-2010 Activities

We have just completed the first full year of operation in the NCEMC (Northern California Earthquake Management Center) with the new suite of earthquake monitoring software. In the past, we have called this system the CISN software. In 2008, it was adopted by the ANSS as the system to be used by the regional networks for their operations and earthquake reporting, and it is now called the ANSS Quake Monitoring System, or AQMS. The NCEMC made the switch to the AQMS software package in June 2009, and the software is now operating at the BSL and in Menlo Park. CISN funding from CalEMA contributed to this transition, and has supported a number of other activities at the BSL during the past year as well.

Northern California Earthquake Management Center

As part of their effort within the CISN, the BSL and the USGS Menlo Park have completed implementation of the next generation Northern California joint earthquake information system, the AQMS software. Operational Section 8 describes the operation of this system and reports on implementation progress.

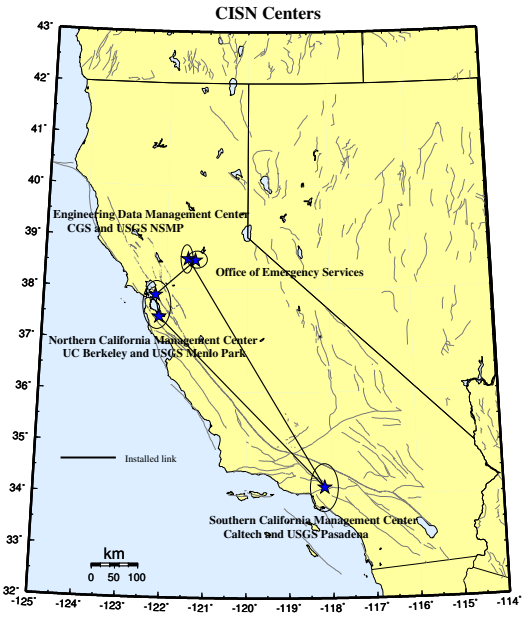

Figure 3.9: Map showing the geographical distribution of the CISN partners and centers. The communications "ring" is shown schematically with installed links (solid lines).

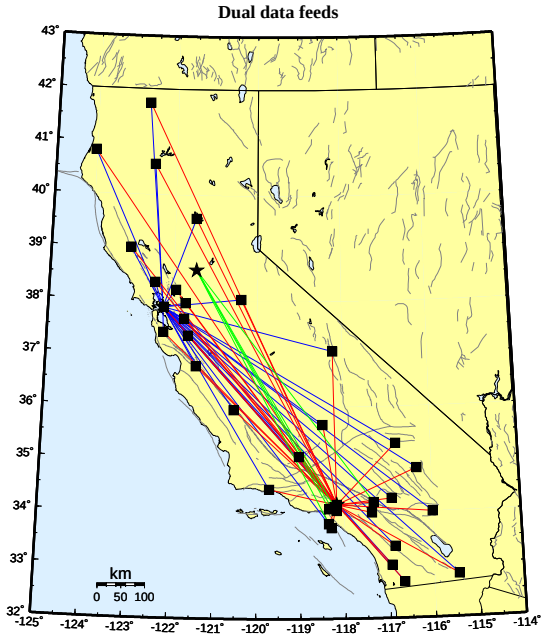

Figure 3.10: Map showing the 30 stations selected to send data directly to the Northern and Southern California processing centers, and the 5 stations that send data directly to the Engineering Data Center and the Southern California processing center.

For monitoring earthquakes in Northern California, the USGS Menlo Park and BSL have improved their commu-

nications infrastructure. The BSL and the USGS Menlo Park are currently connected by two dedicated T1 circuits. One circuit is a component of the CISN ring, while the second circuit was installed in 2004-2005 (Figure 3.11) to support dedicated traffic between Berkeley and Menlo Park above and beyond that associated with the CISN.

The installation of the second dedicated T1 between Berkeley and Menlo Park freed up a frame-relay connection deployed by the BSL as part of the CalREN project in mid-1990s. The BSL now uses this frame-relay circuit as a second data acquisition link. BDSN data acquisition is distributed between two frame-relay T1 circuits, eliminating what had been a single point of failure. An additional Permanent Virtual Circuit (PVC) has also been implemented at each BDSN site so that each station has connections to both T1s. This has improved the robustness of data acquisition at the BSL by providing redundancy in the incoming circuit.

In the long term, the BSL and USGS Menlo Park hope to be connected by high-bandwidth microwave or satellite service. Unfortunately, we have not yet been able to obtain funding for such an additional communication link.

Statewide Integration

Despite the fact that AQMS software is now operating in both Northern and Southern California, efforts toward statewide integration continue. BSL staff are involved in many elements of these efforts. The Standards Committee, chaired by Doug Neuhauser, continues to define and prioritize projects important to the ongoing development and operation of the statewide earthquake processing system and to establish working groups to address them (see minutes from meetings and conference calls at `http://www.cisn.org/standards/meetings.html`).

Dual Station Feeds: Early in the existence of CISN, "dual station feeds" were established for 30 stations (15 in Northern California and 15 in Southern California) (Figure 3.10). Because of decreases in funding and other issues, Northern California now sends data from 13 stations to Southern California in real time, and Southern California sends data from 12 to Northern California. The Northern California Earthquake Management Center (NCEMC) is using data from the Southern California stations to estimate magnitudes on a routine basis. In addition, some of the stations are used in moment tensor inversions, a computation that is sensitive to the background noise level.

Data Exchange: Part of the AQMS software allows reduced amplitude timeseries to be produced and exchanged. Currently, these timeseries are being exchanged at the NCEMC, but not yet statewide. Using a common format, the CISN partners continue to exchange observations of peak ground motion with one another following an event or a trigger. This step increases the robustness of generating products such as ShakeMap, since all CISN partners now exchange data directly with one another. This also improves the quality of ShakeMaps for events on the boundary between Northern and Southern California, such as the San Simeon earthquake, by allowing all data to be combined in a single map. Finally, this is a necessary step toward the goal of generating statewide ShakeMaps.

In the past year, we have also implemented the exchange of waveforms for event gathers. Since then, we have been working to implement statewide exchange of reduced amplitude data, including PGA, PGV, PGD and ML100 for use in real-time processing.

The Software Calibration & Standardization: CISN partners have calibrated and standardized much of the software used for automatic earthquake processing and earthquake review, now the AQMS software. The AQMS software now serves as the real-time system operating in the NCEMC. The transition was made in June 2009.

Local Magnitudes: Since the transition to the AQMS software in Northern California in June 2009, local magnitudes are calculated throughout the state using the new $logA_o$ function and the associated station-specific corrections for broadband/strong motion stations, and also for strong-motion only stations. We are now focusing magnitude development in two directions. First, we are investigating the discrepancy Southern California has discovered between M_L and M_w for events with magnitudes greater than M_L 4. Second, we are working to tie the new local magnitude system to vertical components, whether short period or broadband. A final component of the magnitude efforts is the determination of a magnitude reporting hierarchy. For the near future, each region will continue to use its own preferences for magnitude reporting.

ShakeMap: At present, ShakeMaps are generated on 5 systems within the CISN. Two systems in Pasadena generate "SoCal" Shakemaps; 2 systems in the Bay area generate "NoCal" Shakemaps; and 1 system in Sacramento generates ShakeMaps for all of California. The Sacramento system uses EIDS (Earthquake Information Distribution System) to provide the authoritative event information for Northern and Southern California.

For the past year, we have been evaluating the new release of the program, ShakeMap 3.5, before using it to publish ShakeMaps for new events and before recalculating the ShakeMaps for all events in the catalog. As part of the process to prepare for the recalculation, we have reviewed the magnitudes of many events with M 3.5 or greater in the aftershock sequence of the 2003 San Simeon earthquake.

A second goal is to improve the robustness of ShakeMap generation and delivery by taking advantage of the fact that ShakeMaps are generated in the Bay

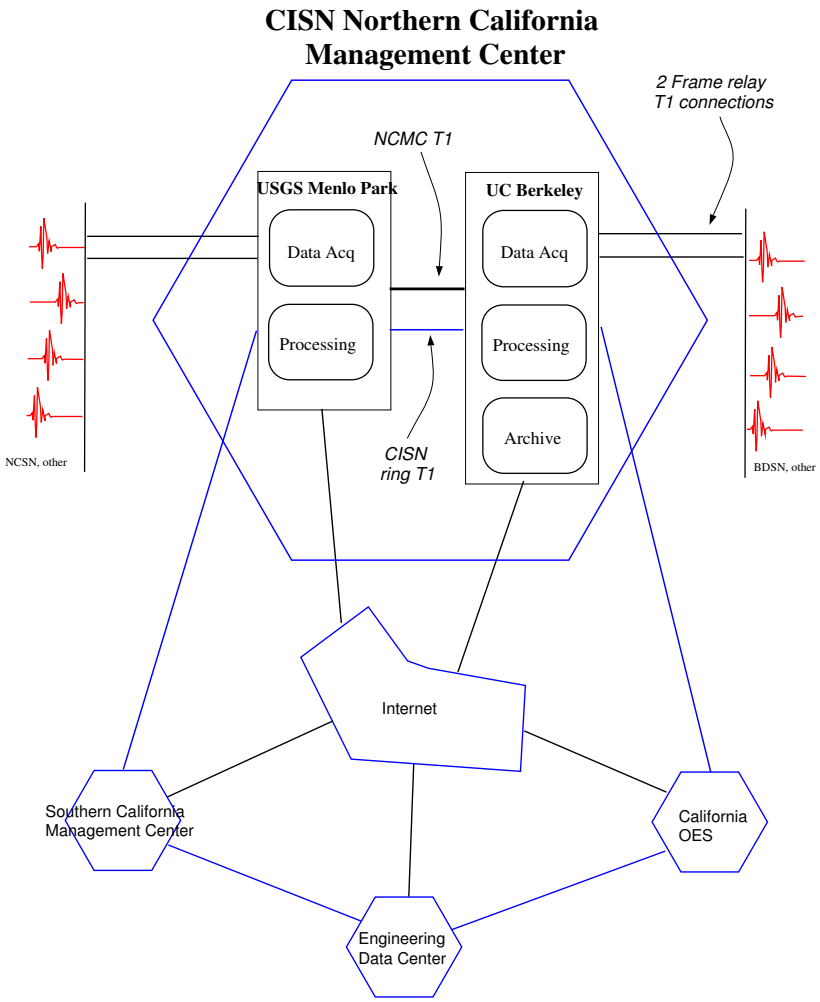

Figure 3.11: Schematic diagram illustrating the connectivity between the real-time processing systems at the USGS Menlo Park and UC Berkeley, forming the Northern California Management Center, and with other elements of the CISN.

Area, Pasadena, and Sacramento. Ongoing efforts in this direction will likely be based on the new USGS ShakeMap webpages at the National Earthquake Information Center.

Location Codes: The CISN adopted a standard for the use of "location" codes (part of the Standard for the Exchange of Earthquake Data [SEED] nomenclature to describe a timeseries based on network-station-channel-location) in the late fall of 2003. USGS and UC Berkeley developers modified the Earthworm software to support their use. After the transition at USGS Menlo Park away from the CUSP analysis system to `Jiggle` in late November 2006, all networks in the CISN implemented location codes in their systems. During the past year, as we deploy new data loggers using ARRA funding, we have begun the transition to non-blank location codes for the BDSN stations. When the data logger at a station is replaced with an ARRA-funded data logger, it receives the location code "00." Borehole seismic stations will have the location code "40."

Metadata Exchange: Correct metadata are vital to CISN activities, as they are necessary to ensure valid interpretation of data. CISN is working on issues related to their reliable and timely exchange. The CISN Metadata Working Group compiled a list of metadata necessary for data processing and developed a model for their ex-

change. In this model, each CISN member is responsible for the metadata for its stations and for other stations that enter into CISN processing through it. For example, Menlo Park is responsible for the NSMP, Tremor, and PG&E stations, while Caltech is responsible for the Anza data. At the present time, dataless SEED volumes are used to exchange metadata between the NCEMC and the SCEMC. The Metadata Working Group is developing a Station XML format for metadata exchange. This vehicle is expandable, and will probably allow exchange of a more comprehensive set of metadata than dataless SEED volumes, some of which may be necessary for other systems, for example in V0 formatted data.

Standardization: The CISN's focus on standardization of software continues. The complete system is now implemented and providing real-time earthquake information in the NCEMC (see Operational Section 8). The software is currently being implemented at other regional networks of the ANSS.

CISN Display

CISN Display is an integrated Web-enabled earthquake notification system designed to provide earthquake information for emergency response at 24/7 operations centers. First responders, organizations with critical lifelines and infrastructure, and emergency responders are invited to register for an account at `http://www.cisn.org/software/cisndisplay.htm`.

The application provides users with maps of real-time seismicity and automatically provides access to Web-related earthquake products such as ShakeMaps. CISN Display also offers an open source GIS mapping tool that allows users to plot freely available layers of public highways, roads and bridges, as well as private layers of organizational-specific infrastructure and facilities information. The current version of CISN Display is 1.4. Its primary enhancement over the previous version is the development of a kiosk mode for public display purposes.

Earthquake Information Distribution

The USGS hosted a workshop in October 2004 to develop plans for the installation and use of the EIDS software. Doug Neuhauser and Pete Lombard participated in this workshop, which resulted in a document outlining the steps necessary for the installation and migration of the earthquake notification system from the current Quake Data Distribution Services (QDDS) to EIDS. During the past year, the NCEMC transitioned to using the EIDS system for publishing earthquake information.

Outreach

Starting in FY05-06, the CISN Web site (`www.cisn.org`) was been supported by two servers located at Berkeley and Caltech. The Web servers were set up so that the load could be distributed between them, providing improved access during times of high demand. With these servers, the CISN provided access to certain earthquake products directly from `www.cisn.org`. For example, ShakeMaps are now served directly from the CISN Web site, in addition to being available from several USGS Web servers and the CGS. The design and content of `http://www.cisn.org` continues to evolve. The Web site is an important tool for CISN outreach as well as for communication and documentation among the CISN partners. Unfortunately, the Caltech server died during the past year, and only the Berkeley server is online providing information to the public and emergency responders.

The CISN supports a dedicated Web site for emergency managers. This Web site provides personalized access to earthquake information. Known as "myCISN," the Web site is available at `eoc.cisn.org`. To provide highly reliable access, the Web site is limited to registered users.

As part of the CISN, the BSL contributed to efforts in 2009-2010 to raise awareness of earthquakes and earthquake preparedness. The BSL is a member of the Earthquake Country Alliance, a state-wide organization of people, institutions and agencies associated with earthquake response and research. In the past year, we publicized the state-wide ShakeOut on October 15, 2009 and participated in it. We are now working toward a statewide California ShakeOut on October 21, 2010 at 10:21 (see `http://www.shakeout.org` for more information and to sign up).

2.4 Acknowledgements

CISN activities at the BSL are supported by funding from the California Emergency Management Agency, CalEMA.

Barbara Romanowicz and Peggy Hellweg are members of the CISN Steering Committee. Peggy Hellweg is a member of the CISN Program Management Group, and she leads the CISN project at the BSL with support from Doug Neuhauser. Doug Neuhauser is chair of the CISN Standards Committee, which includes Peggy Hellweg, Pete Lombard, Taka'aki Taira, and Stephane Zuzulewski as members.

Because of the breadth of the CISN project, many BSL staff members have been involved, including: John Friday, Jarrett Gardner, Peggy Hellweg, Bill Karavas, Oleg Khainovski, Rick Lellinger, Pete Lombard, Doug Neuhauser, Charley Paffenbarger, Taka'aki Taira, Stephen Thompson, Bob Uhrhammer, and Stephane Zuzlewski. Peggy Hellweg contributed to this section. Additional information about the CISN is available through reports from the Program Management Group.

3 Northern Hayward Fault Network

3.1 Introduction

Complementary to the regional surface broadband and short-period networks, the Hayward Fault Network (HFN) (Figure 3.12 and Table 3.5) is a deployment of borehole-installed, wide-dynamic range seismographic stations along the Hayward Fault and throughout the San Francisco Bay toll bridges system. Development of the HFN initiated through a cooperative effort between the BSL (Berkeley Seismological Laboratory) and the USGS, with support from the USGS, Caltrans, EPRI, the University of California Campus/Laboratory Collaboration (CLC) program, LLNL (Lawrence Livermore National Laboratory), and LBNL (Lawrence Berkeley National Laboratory). The project's objectives included an initial characterization period followed by a longer-term monitoring effort using a backbone of stations from among the initial characterization set. Subsequent funding from Caltrans, however, has allowed for continued expansion of the backbone station set for additional coverage in critical locations.

The HFN consists of two components. The Northern Hayward Fault Network (NHFN), operated by the BSL, consists of 30 stations in various stages of development and operation. These include stations located on Bay Area bridges, at free-field locations, and now at sites of the Mini-PBO (mPBO) project (installed with support from NSF and the member institutions of the mPBO project). The NHFN is considered part of the BDSN and uses the network code BK. The Southern Hayward Fault Network (SHFN) is operated by the USGS and currently consists of 5 stations. This network is considered part of the NCSN and uses the network code NC. The purpose of the HFN is fourfold: 1) to contribute operational data to California real-time seismic monitoring for response applications and the collection of basic data for long-term hazards mitigation, 2) to increase substantially the sensitivity of seismic data to low amplitude seismic signals, 3) to increase the recorded bandwidth for seismic events along the Hayward fault, and 4) to obtain deep bedrock ground motion signals at the bridges from more frequent, smaller earthquakes.

In addition to the NHFN's contribution to real-time seismic monitoring in California, the mix of deep NHFN sites at near- and far- field sites and the high-sensitivity (high signal-to-noise), high-frequency broadband data recorded by the NHFN also contributes significantly to a variety of scientific objectives, including: a) investigating bridge responses to stronger ground motions from real earthquakes; b) obtaining a significantly lower detection threshold for microearthquakes and possible non-volcanic tremor signals; c) increasing the resolution of the fault-zone seismic structure (e.g., in the vicinity of the Rodgers Creek/Hayward Fault step over); d) improving monitoring of spatial and temporal evolution of seismicity (to magnitudes below $M \sim 0.0$) that may signal behavior indicative of the nucleation of large, damaging earthquakes; e) investigating earthquake scaling, physics, and related fault processes; f) improving working models for the Hayward fault; and g) using these models to make source-specific response calculations for estimating strong ground shaking throughout the Bay Area.

Below, we focus primarily on activities associated with BSL operations of the NHFN component of the HFN.

3.2 NHFN Overview

The initial characterization period of HFN development ended in 1997. During that period, the NHFN sensors provided signals to on-site, stand-alone Quanterra Q730 and RefTek 72A-07 data loggers, and manual retrieval and download of data tapes was required. Also in that year, the long-term monitoring phase of the project began, involving the installation of 24-bit data acquisition and communication platforms and data telemetry to the BSL archives to create a backbone of initial NHFN stations.

Over the years, Caltrans has provided additional support for the upgrade of two non-backbone sites to backbone operational status and for the addition of several new sites to the monitoring backbone. These expansion efforts are ongoing. Also since February 1 of 2007, the 5 stations of the mPBO project have been folded into the NHFN.

Of the 30 stations considered part of the NHFN history, 10 are non-backbone stations that have not been upgraded to continuous telemetry. Though collection of monitoring data from these sites has never taken place, their borehole sensor packages are still downhole (having been grouted in), and 8 of these sites were mothballed for possible reactivation' in the future. Reactivation of two of the mothballed sites is currently in progress (W05B and E07B), and efforts to fund reactivation/upgrade of the other mothballed sites with Quanterra or Basalt data loggers and continuous telemetry are ongoing. Sixteen of the 30 stations are operational, with 15 of the sites telemetering recorded data streams that flow continuously into the BSL's BDSN processing stream with subsequent archival in the Northern California Earthquake Data Center (NCEDC) archive. These include the 5 mPBO sites. One additional site, BBEB, had previously recorded data as an active backbone site, but in August of 2007 its sensor cable was severed during retrofit work on the east span of the Bay Bridge. This site now operates only as a telemetry repeater site.

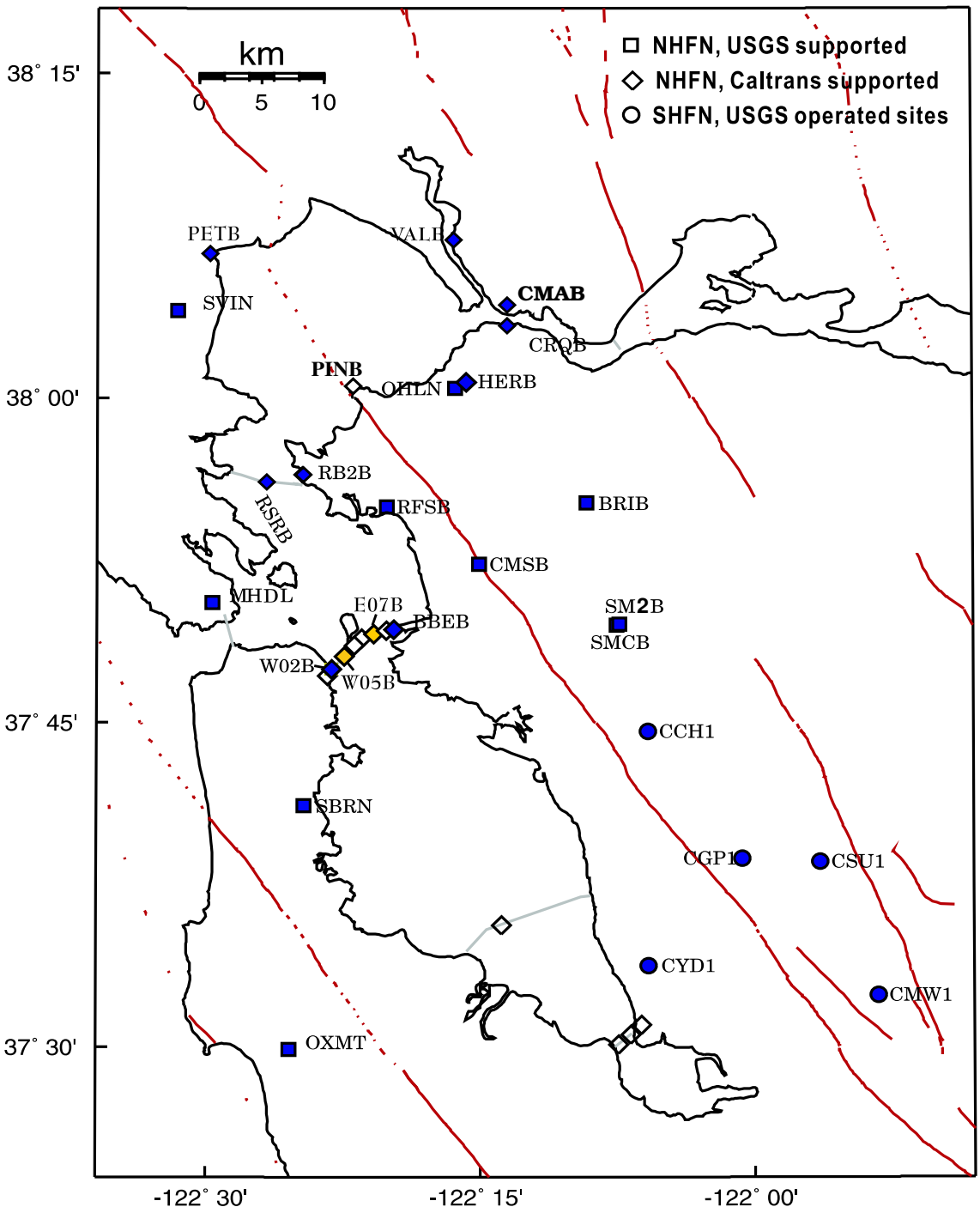

Figure 3.12: Map showing the locations of the HFN stations operated by the BSL (NHFN - squares and diamonds) and the USGS (SHFN - circles). Currently and previously active NHFN monitoring sites (i.e., those with data archived at the NCEDC) are filled blue/black. Sites CRQB and SMCB have been decommissioned in favor of replacement sites (CMAB and SM2B respectively) with higher quality data. Data prior to the termination of recording at sites RSRB and BBEB (resulting from retrofit work on the Richmond-San Rafael and Bay Bridges) is also available at the NCEDC. Sites in progress are yellow/grey. Other instrumented but currently non-operational boreholes are indicated as open symbols. PINB is non-instrumented open symbol site under consideration. Currently, station BBEB operates only as a telemetry repeater site because access to the borehole was cut off during seismic retrofit work on the eastern span of the Bay Bridge.

Sensor	Channel	Rate (sps)	Mode	FIR
Accelerometer	CL?	500.0	T	Ca
Accelerometer	HL?	200.0	C	Ca
Accelerometer	BL?	20.0	C	Ac
Accelerometer	LL?	1.0	C	Ac
Geophone	DP?	500.0	T,C	Ca
Geophone	EP?	200.0	C	Ca
Geophone	EP?	100.0	C	Ca
Geophone	BP?	20.0	C	Ac
Geophone	LP?	1.0	C	Ac

Table 3.7: Typical data streams acquired at NHFN sites, with channel name, sampling rate, sampling mode, and FIR filter type. C indicates continuous, T triggered, Ca causal, and Ac acausal. Typically, the DP1 continuous channel is archived and the remaining high sample rate data (i.e., CL and DP channels) are archived as triggered snippets. Prior to September 2004, however, only triggered data was archived for all high sample rate channels. Of the stations currently recording data, CMAB, HERB, BRIB, RFSB, CMSB, SM2B, W02B, and RB2B record at maximum sample rates of 500 Hz; VALB and PETB at maximum 200 Hz and mPBO sites (SVIN, OHLN, MHDL, SBRN, OXMT) at maximum 100 Hz.

Three additional previously active backbone sites (RSRB, SMCB, and CRQB) are no longer in service. RSRB was taken off-line during the retrofit of the Richmond-San Rafael Bridge, with the expectation that it would be reactivated upon completion of the retrofit work. Unfortunately, during the retrofit, the sensor cable to the site was inadvertently dropped into the bay by contractors and was not recoverable. Both stations SMCB (a shallow post-hole installation) and and CRQB (a shallow and very noisy installation) were replaced with nearby higher quality installations at SM2B and CMAB, respectively.

Installation of one planned new borehole site (PINB) at Pt. Pinole Regional Park is being reconsidered after unexpected environmental issues were recognized relating to the sites historical use as a dynamite manufacturing facility and the possible release of deep seated chemical contaminants from the planned drilling of the borehole.

Installation/Instrumentation: The NHFN Sensor packages are generally installed at depths ranging between 100 and 200 m, the non-backbone, non-operational Dumbarton bridge sites being exceptions with sensors at multiple depths (Table 3.5).

The five former mPBO sites that are now part of the NHFN have 3-component borehole geophone packages. Velocity measurements for the mPBO sites are provided by Mark Products L-22 2 Hz geophones (Table 3.6). All the remaining backbone and non-backbone NHFN sites have six-component borehole sensor packages. The six-component packages were designed and fabricated at LBNL's Geophysical Measurement Facility and have three channels of acceleration, provided by Wilcoxon 731A piezoelectric accelerometers, and three channels of velocity, provided by Oyo HS-1 4.5 Hz geophones.

The 0.1-400 Hz Wilcoxon accelerometers have lower self-noise than the geophones above about 25-30 Hz, and remain on scale and linear to 0.5 g. In tests performed in the Byerly vault at UC Berkeley, the Wilcoxon is considerably quieter than the FBA-23 at all periods, and is almost as quiet as the STS-2 between 1 and 50 Hz.

All 15 recording NHFN backbone sites have Quanterra data loggers with continuous telemetry to the BSL. Signals from these stations are digitized at a variety of data rates up to 500 Hz at 24-bit resolution (Table 3.7). The data loggers employ causal FIR filters at high data rates and acausal FIR filters at lower data rates.

Data Rates and Channels: Because of limitations in telemetry bandwidth and disk storage, 7 of the 10 (excluding CMAB, VALB and PETB) six-component NHFN stations transmit maximum 500 Hz data, one channel of geophone data continuously (i.e., their vertical geophone channels), and an additional 3 channels of triggered data in 90 second snippets. VALB transmits maximum 200 Hz data with one continuous geophone channel and three triggered channels. PETB transmits maximum 200 Hz data continuously on all six channels (three geophone, three accelerometer), and CMAB transmits maximum 500 Hz data continuously on all six channels. A Murdock, Hutt, and Halbert (MHH) event detection algorithm (*Murdock and Hutt*, 1983) is operated independently at each station on 500 sps data for trigger determinations. Because the accelerometer data is generally quieter, the three triggered channels are taken from the Wilcoxon accelerometers when possible. However, there is a tendency for these powered sensors to fail, and, in such cases, geophone channels are substituted for the failed accelerometers. Station VALB also transmits data from only four channels; however, all channels are transmitted continuously at a maximum of 200 Hz sampling. Continuous data for all channels at reduced rates (20 and 1 sps) are also transmitted to and archived at the BSL. The five mPBO originated sites transmit their three-component continuous geophone data streams, which are also archived at BSL, at 100, 20, and 1 sps.

Integration with the NCSS, SeisNetWatch, and SeismiQuery: The NHFN is primarily a research network that complements regional surface networks by providing downhole recordings of very low amplitude seismic

signals (e.g., from micro-earthquakes or non-volcanic tremor) at high gain and low noise. Nonetheless, we have now also completed the integration of data flow from all operating NHFN stations into the Northern California Seismic System (NCSS) real-time/automated processing stream for response applications and collection of basic data for long-term hazards mitigation. The NCSS is a joint USGS (Menlo Park) and Berkeley Seismological Laboratory (BSL) entity with earthquake reporting responsibility for Northern California, and data from networks operated by both institutions are processed jointly to fulfill this responsibility.

Through this integration, the NHFN picks, waveforms, and NCSS event locations and magnitudes are automatically entered into a database where they are immediately available to the public through the NCEDC and its DART (Data Available in Real Time) buffer. The capability for monitoring state of health information for all NHFN stations using SeisNetWatch has also now been added, and up-to-date dataless SEED formatted metadata is now made available by the NCEDC with the SeismiQuery software tool.

Station Maintenance

Ongoing network maintenance involves regular inspection of the collected seismic waveform data and spectra of nearby seismic events, and also of noise samples. Other common problems include changes to background noise levels due to ground loops and failing preamps, as well as power and telemetry issues. Troubleshooting and remediation of problems often benefit from a coordinated effort, with a technician at the BSL examining seismic waveforms and spectra while the field technicians are still on site. BSL technicians and researchers regularly review data and assist in troubleshooting.

The NHFN station hardware has proven to be relatively reliable. Nonetheless, numerous maintenance and performance enhancement measures are still carried out. In particular, when a new station is added to the backbone, extensive testing and correction for sources of instrumental noise (e.g., grounding related issues) and telemetry through-put are carried out to optimize the sensitivity of the station. Examples of maintenance and enhancement measures that are typically performed include: 1) testing of radio links to ascertain reasons for unusually large numbers of dropped packets, 2) troubleshooting sporadic problems with numerous frame relay telemetry dropouts, 3) manual power recycle and testing of hung Quanterra data loggers, 4) replacing blown fuses or other problems relating to dead channels identified through remote monitoring at the BSL, 5) repairing frame relay and power supply problems when they arise, and 6) correcting problems that arise due to various causes, such as weather or cultural activity.

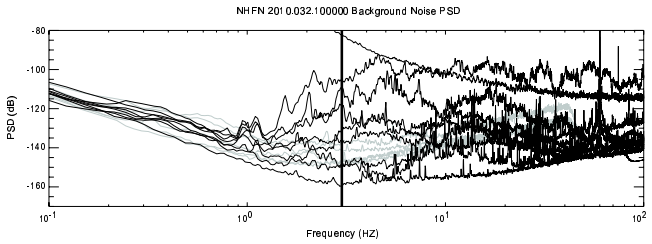

Figure 3.13: Plot showing typically observed background noise PSD for the NHFN borehole stations (including the mPBO in gray lines) as a function of frequency. The data are for a 1000 second period on February 1, 2010 beginning at 02:00 (AM) local time on a Monday morning. Note that there is considerable variation in the general level and structure of the individual station background noise PSD estimates. The signals from three of the stations (RFSB, SM2B, and VALB) have 60 Hz noise (sometimes accompanied by 120 and 180 Hz harmonics), which is indicative of the presence of ground loops that need to be addressed. The PSD ranking (lowest to highest) of the 14 stations in operation at the time (PETB was not yet recording data) at 3 Hz (near minimum PSD for most NHFN stations) is:
CMSB.BK.DP1 -159.616
SM2B.BK.DP1 -149.143
SVIN.BK.EP1 -147.990
BRIB.BK.DP1 -147.706
OXMT.BK.EP1 -147.052
OHLN.BK.EP1 -147.004
MHDL.BK.EP1 -140.832
SBRN.BK.EP1 -137.196
RFSB.BK.DP1 -136.228
HERB.BK.DP1 -130.961
CMAB.BK.DP1 -118.527
VALB.BK.EP1 -109.230
CRQB.BK.DP1 -104.792
W02B.BK.DP1 -81.926

Quality Control

Power Spectral Density Analyses: One commonly used quality check on the performance of the borehole installed network includes assessment of the power spectral density (PSD) distributions of background noise. Figure 3.13 shows PSD of background noise for vertical geophone components of the 14 NHFN stations operating at the time.

By periodically generating such plots, we can rapidly evaluate the network's recording of seismic signals across the wide high-frequency spectrum of the borehole NHFN sensors. Changes in the responses often indicate problems with the power, telemetry, or acquisition systems or with changing conditions in the vicinity of station installations that are adversely affecting the quality of the recorded seismograms. In general, background noise lev-

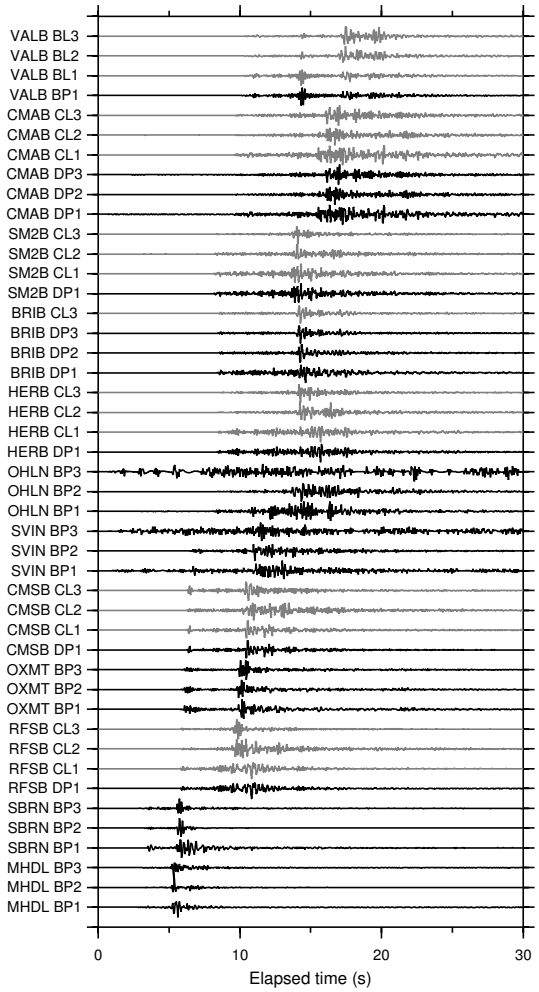

Figure 3.14: Plot of ground accelerations recorded on the geophones (black lines) and accelerometers (gray lines) of the 12 NHFN borehole stations operational at the time of a recent Bay Area earthquake (28 June 2010, M 3.25 offshore of San Francisco, CA). The traces are filtered with a 1-8 Hz bandpass filter, scaled by their maximum values, and ordered from bottom to top by distance from the epicenter

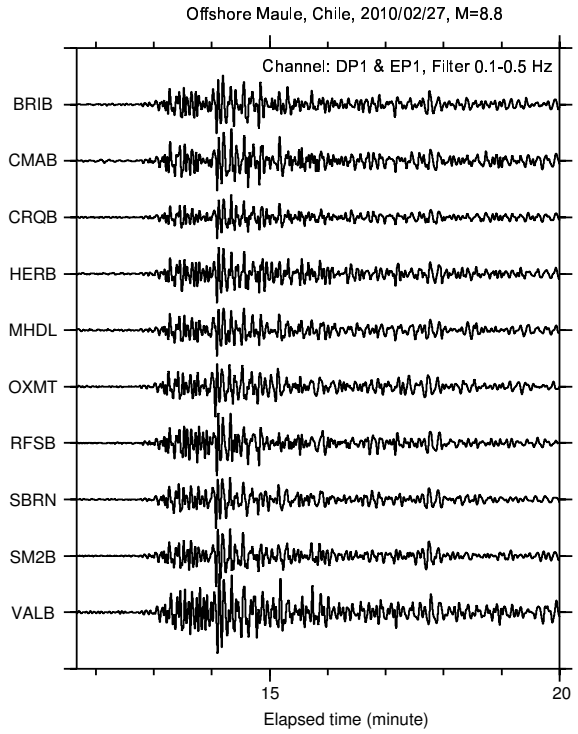

Figure 3.15: Plot of P-wave seismograms of the teleseismic M_w 8.8 earthquake in the offshore Maule, Chile (Lat.: 35.909S; Lon.: 72.733W; Depth: 35 km) occurring on February 27, 2010 at 03:34:14 (UTC), recorded on the DP1 (vertical) channels of the 10 NHFN borehole stations in operation at the time. Here, vertical component geophone (velocity) data have been 0.1-0.5 Hz bandpass filtered.

els of the borehole NHFN stations are more variable and generally higher than those of the Parkfield HRSN borehole stations (see Parkfield Borehole Network section). This is due in large part to the significantly greater cultural noise in the Bay Area and the siting of several near-field NHFN sites in proximity to bridges.

On average, the mPBO component of the NHFN sites is more consistent and somewhat quieter. This is due in large part to the greater average depth of the mPBO sensors, the locations of mPBO stations in regions with generally less industrial and other cultural noise sources, and possibly to the absence of powered sensors (i.e. accelerometers) in their borehole sensor packages.

One of the most pervasive problems at NHFN stations equipped with Q4120 data loggers is power line noise (60 Hz and its harmonics at 120 and 180 Hz). This noise reduces the sensitivity of the MHH detectors and can corrupt research based on full waveform analyses. When NHFN stations are visited, the engineer at the site and a seismologist at the BSL frequently work together to identify and correct ground-loop problems, which often generate 60, 120, and 180 Hz contamination from inductively coupled power line signals.

Real Event Displays: Another method for rapid assessment of network performance is to generate and evaluate the seismograms from moderate local and large teleseismic earthquakes recorded by the NHFN stations. This is an essential component of NHFN operations because the seismic data from local, regional, and teleseismic events is telemetered directly to the BSL and made available to the Northern California Seismic System (NCSS) real-time/automated processing stream within a few seconds of being recorded by the NHFN for seismic response applications.

Shown in Figure 3.14 is an example display of NHFN geophone and accelerometer channels for a recent local Bay Area earthquake (28 June 2010, M_L 3.25 offshore

of San Francisco, CA). It is immediately apparent from this simple display that the some components of stations OHLN and SVIN were in need of attention by field personnel.

Figure 3.15 shows seismograms of the recent teleseismic M_w 8.8 earthquake of February 27, 2010 at 03:34:14 (UTC) occurring offshore of Maule, Chile (Lat.: 35.909S; Lon.: 72.733W; Depth: 35 km) On this date and for this frequency band (0.1-0.5 Hz) network performance appears good for the 10 stations in operation at the time; however, an additional 4 sites did not record this event, for various reasons, and had to be visited by field personnel. Figures 3.14 and 3.15 serve to illustrate the value of routine evaluation of both local (higher frequency) and teleseismic (lower frequency) events when monitoring the state of health of the NHFN.

Owing to their near similar source-receiver paths, signals from teleseismic events also serve as a good source for examining the relative responses of the BK borehole network station/components to seismic ground motion, after correction for differences in instrument response among the stations. By rapidly generating such plots (particularly with correction for instrument response) following large teleseismic events, quick assessment of the NHFN seismometer responses to real events is easily done and corrective measures implemented with relatively little delay.

3.3 2009-2010 Activities

As in every year, routine maintenance, operations, quality control, and data collection have played an important part in our activities. In this year, we are fortunate to have received funds and government furnished equipment (GFE) data loggers to update equipment and improve station infrastructure from an American Recovery and Reinvestment Act award from the USGS. The equipment will be used to upgrade data loggers at 9 stations, including the mPBO stations. As the GFE data loggers did not arrive at the BSL until Summer 2010, we did not embark on any equipment upgrades at the NHFN sites in this reporting interval. Some maintenance activities, however, were funded by the award.

Other NHFN project activities have included: a) efforts to obtain additional funds for future upgrade and expansion of the network, b) leveraging NHFN activities through partnerships with various institutions outside of BSL, c) network adaptations to compensate for changing conditions associated with retrofit work on Bay Area bridges, and d) new station additions and network expansion efforts.

Additional Funding

Operation of this Bay Area borehole network is funded by the ANSS and through a partnership with the California Department of Transportation (Caltrans). ANSS (Advanced National Seismic System) provides operations and maintenance (O&M) support for a fixed subset of 9 operational stations that were initiated as part of previous projects in which the USGS was a participant. Caltrans provides support for development and O&M for an additional 10 stations that have been or are in the process of being added to the network with Caltrans partnership grants. Caltrans also continues to provide additional support for upgrade and expansion when possible.

In June of this year, our team held 2 meetings at Berkeley with our Caltrans contact and made a presentation at Caltrans in Sacramento to argue against O&M funding reductions and for further upgrade and expansion of the NHFN. These efforts resulted in a request by Caltrans for a proposal to install surface instruments at up to 6 of our borehole installations and to reactivate 3 currently mothballed NHFN sites. We submitted our proposal in September of 2010 and are awaiting a decision from Caltrans.

Partnerships

The NHFN is heavily leveraged through partnerships with various institutions, and we have continued to nurture and expand these relationships. Over the past year, we have continued our collaborative partnerships with the USGS, Caltrans, St. Mary's College, and the Cal Maritime Academy. In addition, we have coordinated with a Lawrence Berkeley National Laboratory (LBNL) project to help develop to ensure complementary placement of borehole installations at LBNL with our existing NHFN stations.

New Installations

Since reorganization of engineering support for the NHFN project this past year, significant progress has been made on activation of NHFN stations. This year, three new sites have been brought fully online (CMAB, PETB and RB2B). Two additional instrumented sites are awaiting completion of the retrofit of the Bay Bridge before being completed and brought online (E07B and W05B).

Last year, complex negotiations involving (among others) the East Bay Regional Parks District and UNAVCO were finally completed, giving us permission to create borehole site (PINB) at Pt. Pinole Regional Park. However, it has now been recognized that installation of a deep borehole at this site is potentially problematic due to environmental issues (in the past, the park had been a dynamite manufacturing facility, leaving the possibility that liberation of chemical contaminants may occur from extraction of borehole materials during drilling). We are continuing to evaluate the viability of installation at this site, given these circumstances.

3.4 Acknowledgments

Thomas V. McEvilly, who passed away in February 2002, was instrumental in developing the Hayward Fault Network, and, without his dedication and hard work, the creation and continued operation of the NHFN would not have been possible.

Under Bob Nadeau's and Doug Dreger's general supervision, Bill Karavas, Doug Neuhauser, Bob Uhrhammer, John Friday, Taka'aki Taira, and Rick Lellinger all contribute to the operation of the NHFN. Bob Nadeau prepared this section with help from Taka'aki Taira.

Support for the NHFN is provided by the USGS through the NEHRP grant program (grant numbers 07HQAG0014 and G10AC00093) and by Caltrans through grant number 65A0366. The ARRA Award to support maintance and equipment upgrades at the NHFN stations is USGS grant number G09AC00487. Pat Hipley of Caltrans has been instrumental in the effort to continue to upgrade and expand the network. Larry Hutchings and William Foxall of LLNL have also been important collaborators on the project in past years.

3.5 References

Rodgers, P.W., A.J. Martin, M.C. Robertson, M.M. Hsu, and D.B. Harris, Signal-Coil Calibration of Electromagnetic Seismometers, *Bull. Seism. Soc. Am., 85(3)*, 845-850, 1995.

Murdock, J. and C. Hutt, A new event detector designed for the Seismic Research Observatories, *USGS Open-File-Report 83-0785,* 39 pages, 1983.

Code	Net	Latitude	Longitude	Elev (m)	Over (m)	Date	Location
VALB	BK	38.1215	-122.2753	-24	155.8	2005/11 - current	Napa River Bridge
PETB	BK	38.1189	-122.5011	-30	113	2010/09 - current	Petaluma River Bridge
CMAB	BK	38.06885	-122.22909	6	148	2009/12 - current	Cal Maritime Academy
CRQB	BK	38.05578	-122.22487	-25	38.4	1996/07 - 2010/05	CB
HERB	BK	38.01250	-122.26222	-25	217.9	2000/05 - current	Hercules
PINB*	BK	38.0113	-122.3653	tbd	tbd	not recorded	Point Pinole
BRIB	BK	37.91886	-122.15179	219.7	108.8	1995/06 - current	BR, Orinda
RFSB	BK	37.91608	-122.33610	-27.3	91.4	1996/01 - current	RFS, Richmond
CMSB	BK	37.87195	-122.25168	94.7	167.6	1994/12 - current	CMS, Berkeley
SMCB	BK	37.83881	-122.11159	180.9	3.4	1997/12 - 2007/06	SMC, Moraga
SM2B	BK	37.8387	-122.1102	200	150.9	2007/06 - current	SMC, Moraga
SVIN	BK	38.03325	-122.52638	-21	158.7	2003/08 - current	mPBO, St. Vincent's school
OHLN	BK	38.00742	-122.27371	-0	196.7	2001/07 - current	mPBO, Ohlone Park
MHDL	BK	37.84227	-122.49374	94	160.6	2006/05 - current	mPBO, Marin Headlands
SBRN	BK	37.68562	-122.41127	4	157.5	2001/08 - current	mPBO, San Bruno Mtn.
OXMT	BK	37.4994	-122.4243	209	194.2	2003/12 - current	mPBO, Ox Mtn.
BBEB	BK	37.82167	-122.32867	-31	150.0	2002/05 - 2007/08	BB, Pier E23
E17B	BK	37.82086	-122.33534		160.0	1995/08 - current *	BB, Pier E17
E07B	BK	37.81847	-122.34688	tbd	134.0	1996/02 - current *	BB, Pier E7
YBIB	BK	37.81420	-122.35923	-27.0	61.0	1997/12 - current *	BB, Pier E2
YBAB	BK	37.80940	-122.36450		3.0	1998/06 - current *	BB, YB Anchorage
W05B	BK	37.80100	-122.37370	tbd	36.3	1997/10 - current *	BB, Pier W5
W02B	BK	37.79120	-122.38525	-45	57.6	2003/06 - current	BB, Pier W2
SFAB	BK	37.78610	-122.3893		0.0	1998/06 - current *	BB, SF Anchorage
RSRB	BK	37.93575	-122.44648	-48.0	109.0	1997/06 - 2001/04	RSRB, Pier 34
RB2B	BK	37.93	-122.41	-18	133	2009/11 - current	RSRB, Pier 58
SM1B	BK	37.59403	-122.23242		298.0	not recorded	SMB, Pier 343
DB3B	BK	37.51295	-122.10857		1.5	1994/09 - 1994/11 *	DB, Pier 44
					62.5	1994/09 - 1994/09 *	
					157.9	1994/07 - current *	
DB2B	BK	37.50687	-122.11566			1994/07 - current *	DB, Pier 27
					189.2	1992/07 - 1992/11 *	
DB1B	BK	37.49947	-122.12755		0.0	1994/07 - 1994/09 *	DB, Pier 1
					1.5	1994/09 - 1994/09 *	
					71.6	1994/09 - 1994/09 *	
					228.0	1993/08 - current *	
CCH1	NC	37.7432	-122.0967	226		1995/05 - current	Chabot
CGP1	NC	37.6454	-122.0114	340		1995/03 - current	Garin Park
CSU1	NC	37.6430	-121.9402	499		1995/10 - current	Sunol
CYD1	NC	37.5629	-122.0967	-23		2002/09 - current	Coyote
CMW1	NC	37.5403	-121.8876	343		1995/06 - current	Mill Creek

Table 3.5: Stations of the Hayward Fault Network. Each HFN station is listed with its station code, network id, location, operational dates, and site description. The latitude and longitude (in degrees) are given in the WGS84 reference frame. The elevation of the well head (in meters) is relative to the WGS84 reference ellipsoid. The overburden (depth of sensor package below surface) is given in meters. The start dates indicate either the upgrade or installation time. The abbreviations are: BB - Bay Bridge; BR - Briones Reserve; CMS - Cal Memorial Stadium; CB - Carquinez Bridge; DB - Dumbarton Bridge; mPBO - Mini-Plate Boundary Observatory; RFS - Richmond Field Station; RSRB - Richmond-San Rafael Bridge; SF - San Francisco; SMB - San Mateo Bridge; SMC - St. Mary's College; and YB - Yerba Buena. Installation of PINB is pending, due to environmental issues. The * in the Date column indicates stations recording data only during the premonitoring period (manually retrieved data now at LLNL). Temporary deployment data are not archived on the NCEDC, and the stations have been mothballed and are currently offline. The borehole sensors are still in place, however, and funds have been requested in a proposal to Caltrans to bring three of these sites back online (which three has yet to be determined). Note that due to Bay Bridge retrofit work, station BBEB now operates only as a telemetry relay station and no longer records seismic activity.

Site	Geophone	Accelerometer	Z	H1	h2	data logger	Notes	Telem.
VALB	Oyo HS-1	Wilcoxon 731A	TBD	TBD	TBD	Q330		FR
PETB	Oyo HS-1	Wilcoxon 731A	TBD	TBD	TBD	Q300		FR/Rad.
CMAB	Oyo HS-1	Wilcoxon 731A	TBD	TBD	TBD	Q4120		Rad./VPN
CRQB	Oyo HS-1	Wilcoxon 731A	-90	251	341	None at Present		FR
HERB	Oyo HS-1	Wilcoxon 731A	-90	TBD	TBD	Q4120		FR
PINB	Oyo HS-1	Wilcoxon 731A	TBD	TBD	TBD	TBD		TBD
BRIB	Oyo HS-1	Wilcoxon 731A	-90	79	349	Q4120	Acc. failed, Dilat.	FR
RFSB	Oyo HS-1	Wilcoxon 731A	-90	256	346	Q4120		FR
CMSB	Oyo HS-1	Wilcoxon 731A	-90	19	109	Q4120		FR
SMCB	Oyo HS-1	Wilcoxon 731A	-90	76	166	None at present	Posthole	FR
SM2B	Oyo HS-1	Wilcoxon 731A	TBD	TBD	TBD	Q4120		FR
SVIN	Mark L-22		-90	298	28	Q4120	Tensor.	FR/Rad.
OHLN	Mark L-22		-90	313	43	Q4120	Tensor.	FR
MHDL	Mark L-22		-90	TBD	TBD	Q4120	Tensor.	FR
SBRN	Mark L-22		-90	347	77	Q4120	Tensor.	FR
OXMT	Mark L-22		-90	163	253	Q4120	Tensor.	FR
BBEB	Oyo HS-1	Wilcoxon 731A	-90	TBD	TBD	None at present	Acc. failed	Radio
E17B	Oyo HS-1	Wilcoxon 731A	-90	TBD	TBD	None at present		
E07B	Oyo HS-1	Wilcoxon 731A	-90	TBD	TBD	None at present		
YBIB	Oyo HS-1	Wilcoxon 731A	-90	257	347	None at present	Z geop. failed	FR/Rad.
YBAB	Oyo HS-1	Wilcoxon 731A	-90	TBD	TBD	None at present		
W05B	Oyo HS-1	Wilcoxon 731A	-90	TBD	TBD	None at present		
W02B	Oyo HS-1	Wilcoxon 731A	-90	TBD	TBD	Q4120		Radio
SFAB	None	LLNL S-6000	TBD	TBD	TBD	None at present	Posthole	
RSRB	Oyo HS-1	Wilcoxon 731A	-90	50	140	None at present	2 acc. failed	FR
RB2B	Oyo HS-1	Wilcoxon 731A	-90	TBD	TBD	Q4120	1 acc. failed	FR
SM1B	Oyo HS-1	Wilcoxon 731A	-90	TBD	TBD	None at present		
DB3B	Oyo HS-1	Wilcoxon 731A	-90	TBD	TBD	None at present	Acc. failed	
DB2B	Oyo HS-1	Wilcoxon 731A	-90	TBD	TBD	None at present		
DB1B	Oyo HS-1	Wilcoxon 731A	-90	TBD	TBD	None at present	Acc. failed	
CCH1	Oyo HS-1	Wilcoxon 731A	-90	TBD	TBD	Nanometrics HRD24	Dilat.	Radio
CGP1	Oyo HS-1	Wilcoxon 731A	-90	TBD	TBD	Nanometrics HRD24	Dilat.	Radio
CSU1	Oyo HS-1	Wilcoxon 731A	-90	TBD	TBD	Nanometrics HRD24	Dilat.	Radio
CYD1	Oyo HS-1	Wilcoxon 731A	-90	TBD	TBD	Nanometrics HRD24	Dilat.	Radio
CMW1	Oyo HS-1	Wilcoxon 731A	-90	TBD	TBD	Nanometrics HRD24	Dilat.	Radio

Table 3.6: Instrumentation of the HFN as of 06/30/2010. Every HFN downhole package consists of collocated 3-component geophones and accelerometers, with the exception of mPBO sites which have only 3-component geophones and are also collecting tensor strainmeter data. Six HFN sites (5 of the SHFN and 1 of the NHFN) also have dilatometers (Dilat.). Currently, 15 NHFN sites have Quanterra data loggers with continuous telemetry to the BSL. The remaining backbone sites are still being developed with support from Caltrans. The 5 SHFN sites have Nanometrics data loggers with radio telemetry to the USGS. The orientation of the sensors (vertical - Z, horizontals - H1 and H2) are indicated where known or identified as "to be determined" (TBD). VPN is Virtual Private Network.

4 Parkfield Borehole Network (HRSN)

4.1 Introduction

The operation of the High Resolution Seismic Network (HRSN) at Parkfield, California began in 1987, as part of the United States Geological Survey (USGS) initiative known as the Parkfield Prediction Experiment (PPE) (*Bakun and Lindh*, 1985).

Figure 3.16 shows the location of the network, its relationship to the San Andreas fault, sites of significance from previous and ongoing experiments using the HRSN, double-difference relocated earthquake locations from 1987-1998, routine locations of seismicity from August 2002 to July 2003, nonvolcanic tremor locations from 27 July 2001 through 21 February 2009, and the epicenters of the 1966 and 2004 M6 earthquakes that motivated much of the research. The HRSN records exceptionally high-quality data, owing to its 13 closely-spaced three-component borehole sensors (generally emplaced in the extremely low attenuation and background noise environment at 200 to 300 m depth [Table 3.8], its high-frequency, wide bandwidth recordings (0-100 Hz; 250 sps), and its sensitivity to very low amplitude seismic signals (e.g., recording signals from micro-earthquakes with magnitudes below 0.0 M_L).

Several aspects of the Parkfield region make it ideal for the study of small earthquakes and nonvolcanic tremors and their relationship to tectonic processes and large earthquakes. These include the fact that the network spans the SAFOD (San Andreas Fault Observatory at Depth) experimental zone, the nucleation region of earlier repeating magnitude 6 events and a significant portion of the transition from locked to creeping behavior on the San Andreas fault; the availability of three-dimensional P and S velocity models (*Michelini and McEvilly*, 1991); a long-term HRSN seismicity catalog (complete to very low magnitudes and that includes at least half of the M6 seismic cycle); a well-defined and simple fault segment; the existence of deep nonvolcanic tremor (NVT) activity; and a relatively homogeneous mode of seismic energy release as indicated by the earthquake source mechanisms (over 90% right-lateral strike-slip).

In a series of journal articles and Ph.D. theses, the cumulative, often unexpected, results of UC Berkeley's HRSN research efforts (see: `http://seismo.berkeley.edu/seismo/faq/parkfield_bib.html`) trace the evolution of a new and exciting picture of the San Andreas fault zone responding to its plate-boundary loading, and they are forcing new thinking on the dynamic processes and conditions within the fault zone at the sites of recurring small earthquakes and deep nonvolcanic tremors.

The Parkfield area has also become an area of focus of the EarthScope Project (`http://www.earthscope.org`) through the deep borehole into the San Andreas Fault, the SAFOD experiment (`http://www.earthscope.org/observatories/safod`), and the HRSN is playing a vital role in this endeavor. SAFOD is a comprehensive project to drill into the hypocentral zone of repeating M ∼2 earthquakes on the San Andreas Fault at a depth of about 3 km. The goals of SAFOD are to establish a multi-stage geophysical observatory in close proximity to these repeating earthquakes, to carry out a comprehensive suite of down-hole measurements in order to study the physical and chemical conditions under which earthquakes occur, and to monitor and exhume rock, fluid, and gas samples for extensive laboratory studies (*Hickman et al.*, 2004).

4.2 HRSN Overview

Installation of the HRSN deep (200-300m) borehole sensors initiated in late 1986, and recording of triggered 500 sps earthquake data began in 1987. The HRSN sensors are 3-component geophones in a mutually orthogonal gimbaled package. This ensures that the sensor corresponding to channel DP1 is aligned vertically and that the others are aligned horizontally. Originally a 10 station network, completed in 1988, the HRSN was expanded to 13 borehole stations in late July 2001, and the original recording systems (see previous Berkeley Seismological Laboratory [BSL] Annual Reports) were upgraded to 24 bit acquisition (Quanterra 730s) and 56K frame relay telemetry to UCB. Properties of the sensors are summarized in Table 3.9.

The 3 newest borehole stations (CCRB, LCCB, and SCYB) were added, with NSF support, at the northwest end of the network as part of the SAFOD project to improve resolution of the structure, kinematics, and monitoring capabilities in the SAFOD drill-path and target zones. Figure 3.16 illustrates the location of the drill site and the new borehole sites, as well as locations of earthquakes recorded by the initial and upgraded/expanded HRSN.

These 3 new stations have a similar configuration to the original upgraded 10 station network and include an additional channel for electrical signals. Station descriptions and instrument properties are summarized in Tables 3.8 and 3.9. All the HRSN data loggers employ FIR filters to extract data at 250 and 20 Hz (Table 3.10).

The remoteness of the drill site and new stations required an installation of an intermediate data collection point at Gastro Peak, with a microwave link to our facility on the California Department of Forestry's (CDF) property in Parkfield. The HRSN stations use SLIP to transmit TCP and UDP data packets over bidirectional

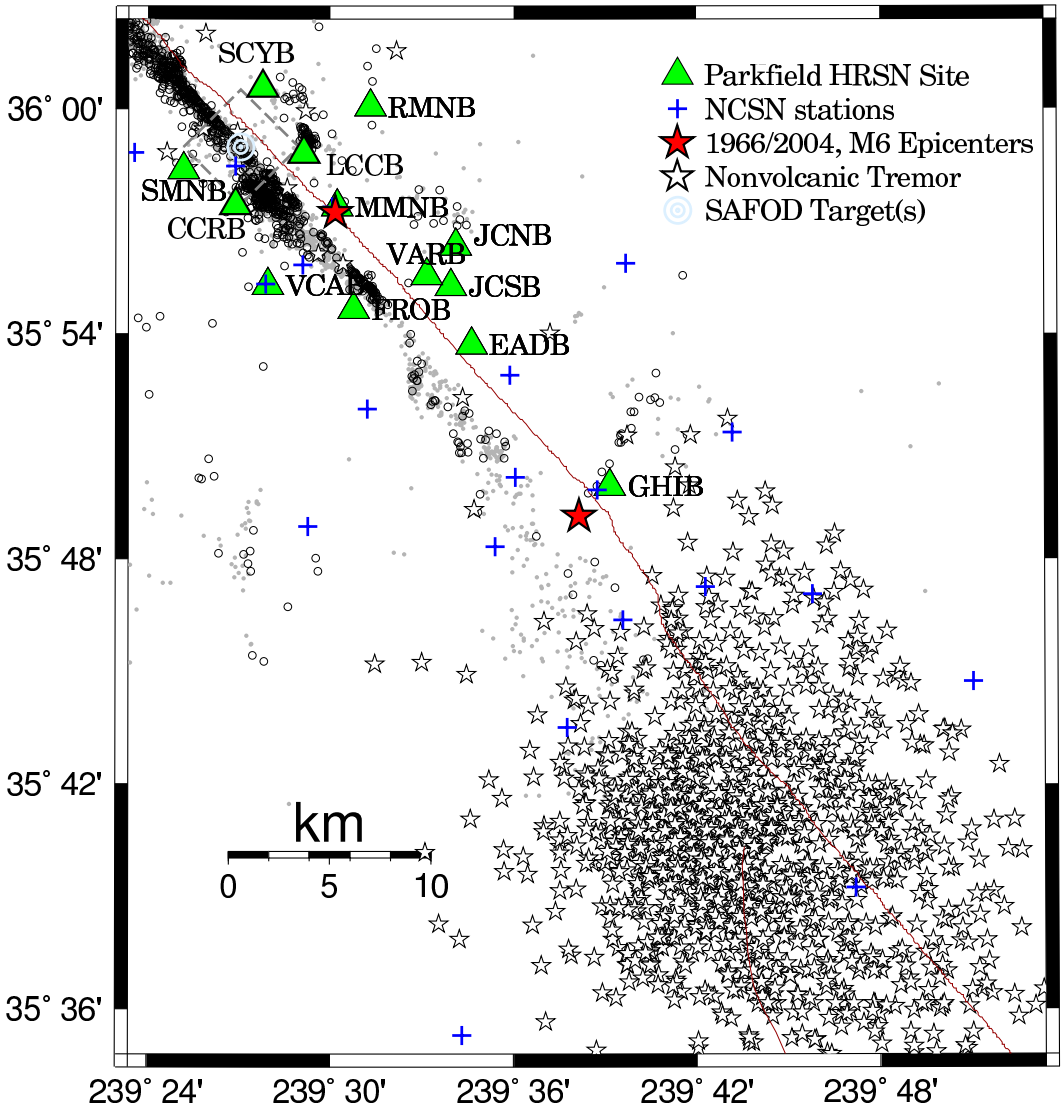

Figure 3.16: Map showing the San Andreas Fault trace and locations of the 13 Parkfield HRSN stations, the repeating M2 SAFOD targets (a 4 km by 4 km dashed box surrounds the SAFOD zone), and the epicenters of the 1966 and 2004 M6 Parkfield main shocks. Also shown are locations of nonvolcanic tremors in the Cholame, CA area (27 July 2001 through 21 February 2009), routine locations of earthquakes recorded by the expanded and upgraded 13 station HRSN (small open circles), and locations of events recorded by the earlier vintage 10 station HRSN relocated using an advanced 3-D double-differencing algorithm (gray points) applied to a cubic splines interpolated 3-D velocity model (*Michelini and McEvilly*, 1991).

Site	Net	Latitude	Longitude	Surf. (m)	Depth (m)	Date	Location
EADB	BP	35.89525	-120.42286	466	245	01/1988 -	Eade Ranch
FROB	BP	35.91078	-120.48722	509	284	01/1988 -	Froelich Ranch
GHIB	BP	35.83236	-120.34774	400	63	01/1988 -	Gold Hill
JCNB	BP	35.93911	-120.43083	527	224	01/1988 -	Joaquin Canyon North
JCSB	BP	35.92120	-120.43408	455	155	01/1988 -	Joaquin Canyon South
MMNB	BP	35.95654	-120.49586	698	221	01/1988 -	Middle Mountain
RMNB	BP	36.00086	-120.47772	1165	73	01/1988 -	Gastro Peak
SMNB	BP	35.97292	-120.58009	699	282	01/1988 -	Stockdale Mountain
VARB	BP	35.92614	-120.44707	478	572	01/1988 - 08/19/2003	Varian Well
VARB	BP	35.92614	-120.44707	478	298	08/25/2003 -	Varian Well
VCAB	BP	35.92177	-120.53424	758	200	01/1988 -	Vineyard Canyon
CCRB	BP	35.95718	-120.55158	595	251	05/2001 -	Cholame Creek
LCCB	BP	35.98005	-120.51424	640	252	08/2001 -	Little Cholame Creek
SCYB	BP	36.00938	-120.53660	945	252	08/2001 -	Stone Canyon

Table 3.8: Stations of the Parkfield HRSN. Each HRSN station is listed with its station code, network id, location, date of initial operation, and site description. The latitude and longitude (in degrees) are given in the WGS84 reference frame. The surface elevation (in meters) is relative to mean sea level, and the depth to the sensor (in meters) below the surface is also given. Coordinates and station names for the 3 new SAFOD sites are given at the bottom.

Site	Sensor	Z	H1	H2	RefTek 24	Quanterra 730
EADB	Mark Products L22	-90	170	260	01/1988 - 06/1998	03/2001 -
FROB	Mark Products L22	-90	338	248	01/1988 - 06/1998	03/2001 -
GHIB	Mark Products L22	90	failed	unk	01/1988 - 06/1998	03/2001 -
JCNB	Mark Products L22	-90	0	270	01/1988 - 06/1998	03/2001 -
JCSB	Geospace HS1	90	300	210	01/1988 - 06/1998	03/2001 -
MMNB	Mark Products L22	-90	175	265	01/1988 - 06/1998	03/2001 -
RMNB	Mark Products L22	-90	310	40	01/1988 - 06/1998	03/2001 -
SMNB	Mark Products L22	-90	120	210	01/1988 - 06/1998	03/2001 -
VARB	Litton 1023	90	15	285	01/1988 - 06/1998	03/2001 -
VCAB	Mark Products L22	-90	200	290	01/1988 - 06/1998	03/2001 -
CCRB	Mark Products L22	-90	N45W	N45E	-	05/2001 -
LCCB	Mark Products L22	-90	N45W	N45E	-	08/2001 -
SCYB	Mark Products L22	-90	N45W	N45E	-	08/2001 -

Table 3.9: Instrumentation of the Parkfield HRSN. Most HRSN sites have L22 sensors and were originally digitized with a RefTek 24 system. The WESCOMP recording system failed in mid-1998 and after an approximate 3 year hiatus the network was upgraded and recording was replaced with a new 4-channel system. The new system, recording since July 27, 2001, uses a Quanterra 730 4-channel system. Three new stations were also added during the network upgrade period (bottom) with horizontal orientations that are approximately N45W and N45E. More accurate determinations of these orientations will be made as available field time permits.

Sensor	Channel	Rate (sps)	Mode	FIR
Geophone	DP?	250.0	C	Ca
Geophone	BP?	20.0	C	Ac

Table 3.10: Data streams currently being acquired at operational HRSN sites. Sensor type, channel name, sampling rate, sampling mode, and type of FIR filter are given. C indicates continuous; Ac acausal; Ca causal. "?" indicates orthogonal, vertical, and 2 horizontal components.

spread-spectrum radio links between the on-site data acquisition systems and the central recording system at the CDF. Prior to June, 2008, six of the sites transmitted directly to a router at the central recording site. The other seven sites transmitted to a router at Gastro Peak, where the data are aggregated and transmitted to the central site over a 4 MBit/second digital 5.4 GHz microwave link. All HRSN data are recorded to disk at the CDF site. Due to disproportionately increasing landowner fees for access to the Gastro Peak site, we reduced our dependence on that site in the summer and fall of 2008 in cooperation with the USGS, and data from five of the stations previously telemetering through Gastro Peak have now been re-routed through an alternative site at Hogs Canyon (HOGS).

The upgraded and expanded system is compatible with the data flow and archiving common to all the elements of the BDSN/NHFN and the NCEDC (Northern California Earthquake Data Center), and is providing remote access and control of the system. It has also provided event triggers with better timing accuracy and is in addition now recording continuous 20 and 250 sps data for all channels of the HRSN, which flow seamlessly into both the USGS automated earthquake detection system and into Berkeley's NCEDC for archiving and online access by the community. The new system also helps minimize the problems of timing resolution, dynamic range, and missed detections, in addition to providing the added advantage of conventional data flow (the old system (1987-2001) recorded SEGY format).

Another feature of the new system that has been particularly useful both for routine maintenance and for pathology identification has been the Internet connectivity of the central site processing computer and the station data loggers with the computer network at BSL. Through this connection, select data channels and on-site warning messages from the central site processor are sent directly to BSL for evaluation by project personnel. If, upon these evaluations, more detailed information on the HRSN's performance is required, additional information can also be remotely accessed from the central site processing computer at Parkfield. Analysis of this remotely acquired information has been extremely useful for trouble shooting by allowing field personnel to schedule and plan the details of maintenance visits to Parkfield. The connectivity also allows certain data acquisition parameters to be modified remotely when needed, and commands can be sent to the central site computer and data loggers to modify or restart processes when necessary.

The network connectivity and seamless data flow to the NCEDC also provide near-real-time monitoring capabilities that are useful for rapid evaluation of significant events as well as the network's overall performance level. For example, shown in Figure 3.17 are P-wave seismograms of the teleseismic M_w 8.8 earthquake offshore of Maule, Chile (Lat.: 35.909S; Lon.: 72.733W; Depth: 35 km) occurring on February 27, 2010 03:34:14 (UTC) recorded on the DP1 (vertical) channels of the 9 HRSN borehole stations in operation at the time. The seismic data from the quake was telemetered to Berkeley and available for analysis by the Northern California Seismic System (NCSS) real-time/automated processing stream within a few seconds of being recorded by the HRSN.

This is a good signal source for examining the relative responses of the BP borehole network station/components to seismic ground motion, and these and corresponding waveform plots for the horizontal (DP2 and DP3 channels) indicate that the following stations were not responding normally to seismic ground motions at the time of this event:
FROB.BP.DP1 - anomalous, weak signal
SMNB.BP.DP1 - no seismic response, telemetry outage
SMNB.BP.DP2 - no seismic response, telemetry outage
SMNB.BP.DP3 - no seismic response, telemetry outage
MMNB.BP.DP1 - no seismic response, telemetry outage
MMNB.BP.DP2 - no seismic response, telemetry outage
MMNB.BP.DP3 - no seismic response, telemetry outage
CCRB.BP.DP1 - no seismic response, telemetry outage
CCRB.BP.DP2 - no seismic response, telemetry outage
CCRB.BP.DP3 - no seismic response, telemetry outage
JCNB.BP.DP1 - no seismic response, signal cable cut
JCNB.BP.DP2 - no seismic response, signal cable cut
JCNB.BP.DP3 - no seismic response, signal cable cut
By rapidly generating such plots following large teleseismic events, quick assessment of the HRSN seismometer responses to real events is easily done and corrective measures implemented with relatively little delay.

Data Flow

Initial Processing Scheme. Continuous data streams on all HRSN components are recorded at 20 and 250 sps on disk on the local HRSN computer at the CDF facility. These continuous data are transmitted in near-real-time to the Berkeley Seismological Laboratory (BSL) over a T1 link and then archived at the NCEDC. In addition, the near-real-time data are being transmitted over the T1 circuit to the USGS at Menlo Park, CA, where they are integrated into the Northern California Seismic System

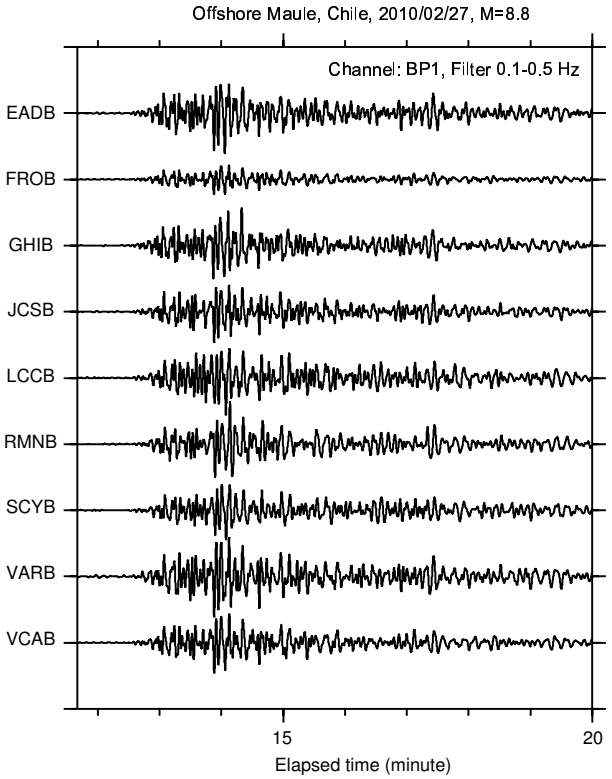

Figure 3.17: Plot of P-wave seismograms of the teleseismic M_w 8.8 earthquake in the offshore Maule, Chile (Lat.: 35.909S; Lon.: 72.733W; Depth: 35 km) occurring on February 27, 2010 03:34:14 (UTC) recorded on the DP1 (vertical) channels of the 9 HRSN borehole stations in operation at the time. Here, vertical component geophone (velocity) data have been 0.1-0.5 Hz bandpass filtered.

(NCSS) real-time/automated processing stream. This integration has also significantly increased the sensitivity of the NCSN catalog at lower magnitudes, effectively doubling the number of small earthquake detections in the critical SAFOD zone.

Shortly after being recorded to disk on the central site HRSN computer, event triggers for the individual station data are also determined, and a multi-station trigger association routine then processes the station triggers and generates a list of potential earthquakes. For each potential earthquake that is detected, a unique event identification number (compatible with the NCEDC classification scheme) is also assigned. Prior to the San Simeon earthquake of December 22, 2003, 30 second waveform segments were then collected for all stations and components and saved to local disk as an event gather, and event gathers were then periodically telemetered to BSL and included directly into the NCEDC earthquake database (dbms) for analysis and processing.

Because of its mandate to detect and record very low magnitude events in the Parkfield area, the HRSN is extremely sensitive to changes in very low amplitude seismic signals. As a consequence, in addition to detecting very small local earthquakes at Parkfield, the HRSN also detects numerous regional events and relatively distant and small amplitude nonvolcanic tremor events. For example, spot checks of aftershocks following the M6.5 San Simeon earthquake of December 22, 2003 using continuous data and HRSN event detection listings have revealed that the overwhelming majority of HRSN detections following San Simeon resulted from seismic signals generated by San Simeon's aftershocks, despite the HRSN's $\sim$50 km distance from the events. Data from the California Integrated Seismic Network (CISN) show that there were $\sim$1,150 San Simeon aftershocks with magnitudes $>$1.8 in the week following San Simeon, and during this same period, the number of HRSN event detections was $\sim$10,500 (compared to an average weekly rate before San Simeon of 115 detections). This suggests that, despite the $\sim$50 km distance, the HRSN is detecting San Simeon aftershocks well below magnitude 1.

Current Processing. Since the beginning of the network's data collection in 1987, and up until 2002, the local and regional events were discriminated based on analyst assessment of S-P times, and only local events with S-P times less than $\sim$2.5 s at the first arriving station were picked and located as part of the HRSN routine catalog. However, because of the network's extreme sensitivity to the large swarm of aftershocks from the San Simeon and M6 Parkfield earthquakes of September 2004 (e.g., in the first 5 months following the San Simeon mainshock, over 70,000 event detections were made by the HRSN system, compared to an average 5 month detection rate of 2500 prior to San Simeon) and because of ever declining funding levels, this approach has had to be abandoned.

The dramatic increase in event detections vastly exceeded the HRSN's capacity to process both the continuous and triggered event waveform data. To prevent the loss of seismic waveform coverage, processing of the triggered waveform data has been suspended to allow the telemetry and archiving of the 20 and 250 sps continuous data to continue uninterrupted. Subsequent funding limitations have precluded reactivation of the processing of triggered waveform data. Cataloging of the event detection times from the modified REDI real-time system algorithm is continuing, however, and the continuous waveform data is currently being telemetered directly to the BSL and USGS over the T1 link for near-real-time processing and archiving at the NCEDC, for access by the research community.

Funding to generate catalogs of local events from the tens of thousands of aftershock detections has not been forthcoming, and, as a consequence, major changes in our approach to cataloging events have been implemented.

The HRSN data is now integrated into NCSN automated event detection, picking, and catalog processing (with no analyst review). In addition, a high resolution procedure is now being developed to automatically detect, pick, locate, double-difference relocate, and determine magnitudes for similar and repeating events down to very low magnitudes (i.e., below magnitude -1.0M_L). These new schemes are discussed in more detail in the activities section below.

4.3 2009-2010 Activities

This year, routine operation and maintenance of the HRSN (California's first and longest operating borehole seismic network) have been augmented by funding through the USGS from the America Reinvestment and Recovery Act (ARRA). This funding is directed toward upgrading the data loggers at all sites with government furnished equipment (GFE) data loggers, and with improving and upgrading telemetry and power infrastructure at the sites. As the GFE data loggers were not delivered to the BSL until the summer of 2010, none were replaced during this reporting interval. Nonetheless, many of the routine the maintenance activities described below were funded with ARRA monies. Other project activities this year include: a) processing of ongoing similar and repeating very low magnitude seismicity and integrating this information into network SOH (state of health) monitoring, b) lowering operational (primarily landowner fee) and catalog production costs, c) monitoring non-volcanic tremor activity in the Parkfield-Cholame area, and d) SAFOD related activities.

Routine Operations and Maintenance

Routine maintenance tasks required this year to keep the HRSN in operation include cleaning and replacement of corroded electrical connections; grounding adjustments; cleaning of solar panels; re-seating, resoldering, and replacing faulty pre-amp circuit cards; testing and replacement of failing batteries; and insulation and painting of battery and data logger housings to address problems with low power during cold weather. Remote monitoring of the network's health using the Berkeley Seismological Laboratory's SeisNetWatch software is also performed to identify both problems that can be resolved over the Internet (e.g. rebooting of data acquisition systems due to clock lockups) and more serious problems requiring field visits. Over the years, such efforts have paid off handsomely by providing exceptionally low noise recordings of very low amplitude seismic signals produced by microearthquakes (below magnitude 0.0M_L) and non-volcanic tremors.

Station MMNB Failure.
Station MMNB is situated directly in the fault zone over the epicenter of the Parkfield 1996 mainshock, ∼5 km southeast of SAFOD, and plays a key role in a variety of scientific investigations, including studies of fault zone guided waves (FZGWs), monitoring of seismicity and non-volcanic tremor, seismic source and scaling studies and SAFOD related research. The station also contributes real-time data to the Northern California Seismic System (NCSS) real-time/automated processing stream for earthquake detection and location.

On August 13, 2009 (DOY 225, UTC) the flow of seismic signals from borehole sensors of the station ceased at between 16:13 and 16:14 (UTC) (local 11:13 and 11:14 AM) (Figure 3.18). It was discovered, only after inquiring about the site after observing the failure remotely, that an effort to clean-up the abandoned USGS water well gear at middle mountain took place on the same day. After the sensor failure, only instrument/pre-amp noise was recorded at the station up until Sept. 16 at 17:37 (UTC), at which time our field engineer removed the pre-amp electronics after confirming no response from the downhole sensors. Our engineer also found that what we believed to be the well head of the MMNB borehole had been demolished. This was apparently done on Sept. 15th as part of the subsequent filling-in of the USGS water well vault pit by the landowner due to safety concerns.

It is now clear that the MMNB borehole well-head was mistakenly assumed to be part of the USGS water well installation during the clean-up effort and that during this effort the scientifically important HRSN station was inadvertently disabled. Significant and scarce resources were expended to track down the cause of the MMNB failure, to assess the degree of damage, and to devise a plan for possible recovery of the station's operation. Fortunately, the recovery efforts have proven successful and data is once again being collected from this vital installation.

Nonetheless, we were disappointed at not having been notified of the clean-up plans at the Middle Mountain site, and we have asked for and received assurances from the USGS that closer coordination between USGS and Berkeley during activities of this kind will be implemented to avoid similar catastrophes in the future.

Station JCNB Status.
In the spring of 2008, signals from HRSN station JCNB began showing signs of deterioration. Shortly thereafter, data flow from this station stopped completely. Field investigation showed that the borehole sensor and cable had been grouted to within ∼34 feet of the surface and that a rodent had found itself trapped in the upper 100 foot void space and chewed through the cable, thus severing the connection to the deep borehole package. At this time, costs for reestablishing connection to the cable at depth are prohibitive, and it is also likely that the grouted-in sensor has been compromised by fluids running down the exposed cable. Hence, plans are being made to substitute either a surface seismometer or a

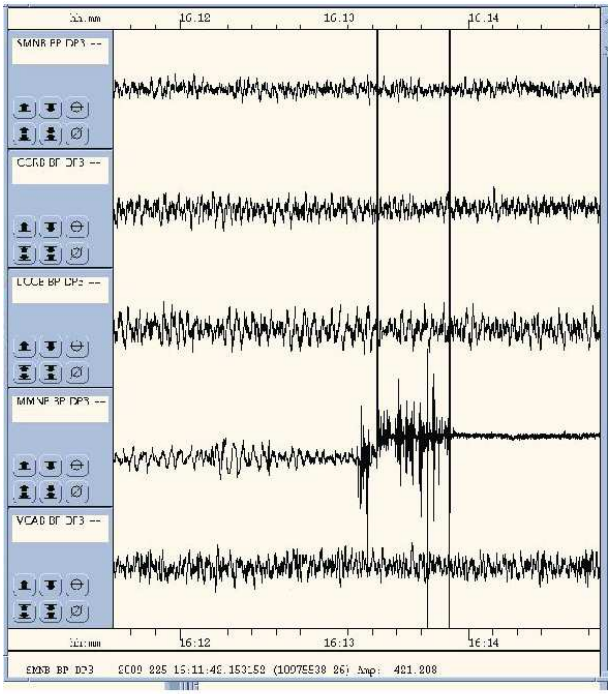

Figure 3.18: Seismograms for several HRSN stations including the period of failure of MMNB on August 13, 2009 (DOY 225, UTC) between 16:13 and 16:14 (UTC) (local 11:13 and 11:14 AM). Only after time consuming investigation and multiple inquiries with USGS personnel did we find that the failure was a result of a clean-up effort of an abandoned USGS water well site. With considerable effort by the BSL and help from the USGS, the MMNB is now back on-line. Arrangements for improved future coordination between the BSL and the USGS in the Parkfield region have been reached to avoid repeats of such circumstances.

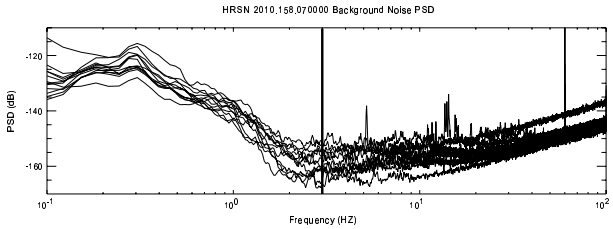

Figure 3.19: Background noise Power Spectral Density (PSD) levels as a function of frequency for the 12, 250 sps vertical component channels (DP1) of the HRSN borehole stations in operation during the 1000 second period analyzed, beginning 00:00 AM local time on 6/7/2010 (a Monday morning). The approximate 2 Hz minimum of the PSD levels occurs because of the 2 Hz sensors used at these sites. Below 2 Hz, noise levels rise rapidly, and the peak at 5 to 3 sec (.2 to .3 Hz) is characteristic of teleseismic noise observed throughout California. The PSD (dB) ranking (lowest to highest) at 3 Hz (intersection with vertical line) for the vertical channels is:
SCYB.BP.DP1 -166.377
CCRB.BP.DP1 -165.459
MMNB.BP.DP1 -162.088
FROB.BP.DP1 -161.101
JCSB.BP.DP1 -160.914
EADB.BP.DP1 -160.575
SMNB.BP.DP1 -157.109
RMNB.BP.DP1 -156.914
GHIB.BP.DP1 -154.451
LCCB.BP.DP1 -153.926
VCAB.BP.DP1 -151.044
VARB.BP.DP1 -150.921

borehole sensor package within the open 34 foot section of the borehole to provide continued seismic coverage at the JCNB site. An surplus mPBO sensor package in storage at the BSL has been identified as a possible replacement in the remaining void space of the JCNB hole and the sensor and feasibility of installation are now being assessed by BSL's engineering group.

Remote SOH Monitoring.
The network connectivity over the T1 circuit also allows remote monitoring of various measures of the state of health (SOH) of the network in near-real-time, such as background noise levels. Shown in Figure 3.19 are power spectral density (PSD) plots of background noise for the 12 operational vertical components of the HRSN for a 1000 second period beginning at 00:00 AM local time on 6/7/2010 (a Monday morning). By periodically generating such plots, we can rapidly evaluate, through comparison with previously generated plots, changes in the network's station response to seismic signals across the wide band high-frequency spectrum of the borehole HRSN sensors. Changes in the responses often indicate problems with the power, telemetry, or acquisition systems, or with changing conditions in the vicinity of station installations that are adversely affecting the quality of the recorded seismograms.

Once state of health issues are identified with the PSD analyses, further remote tests can be made to more specifically determine possible causes for the problem, and corrective measures can then be planned in advance of field deployment within a relatively short period of time.

Similar Event Catalog

The increased microseismicity (thousands of events) resulting from the San Simeon M6.5 (SS) and Parkfield M6 (PF) events, the lack of funds available to process and

catalog the increased number of micro-earthquakes, and the increased interest in using the micro-quakes in repeating earthquake and SAFOD research have required new thinking on how to detect and catalog microearthquakes recorded by the HRSN.

One action taken to help address this problem has been to integrate HRSN data streams into the NCSN event detection and automated cataloging process. This approach has been successful at detecting and locating a significantly greater number of micro-earthquakes over the previous NCSN detection and location rate (essentially doubling the number of events processed by the NCSN). However, the HRSN sensitized NCSN catalog is still only catching about 1/2 the number of local events previously cataloged by the HRSN using the old HRSN-centric processing approach. Furthermore, triggered waveforms for the additional small NCSN processed events are not typically made available; they are not reviewed by an analyst, nor do they generally have NCSN magnitude determinations associated with them.

These limitations severely hamper research efforts relying on similar and characteristically repeating microseismicity such as earthquake scaling studies, SAFOD-related research, deep fault slip rate estimation, and the compilation of recurrence interval statistics for time-dependent earthquake forecast models. They also reduce, to some degree, the use of recurring micro-seismicity as a tool for monitoring the state-of-health (SOH) of either the HRSN or NCSN.

To help overcome these limitations, this year, we have begun implementing an automated similar event cataloging scheme based on pattern matching (match filter) scans using cross-correlation of the continuous HRSN data. The method uses a set of reference events whose waveforms, picks, locations, and magnitudes have been accurately determined, and it automatically detects, picks, locates, and determines magnitudes for events similar to the reference event to the level of accuracy and precision that only relative event analysis can bring.

The similar event detection is also remarkably insensitive to the magnitude of the reference event used, allowing similar micro-events ranging over about 3 magnitude units to be fully cataloged using a single reference event, and it does a remarkably good job at discriminating and fully processing multiple superposed events.

Once a cluster of similar events has been processed, an additional level of resolution can then be achieved through the identification and classification of characteristically repeating microearthquakes (i.e., near identical earthquakes) occurring within the similar event family (Figure 3.20). The pattern scanning approach also ensures optimal completeness of repeating sequences owing to scans of the matching pattern through all available continuous data (critical for applications relying on recurrence interval information). For example, while only about half of the events shown in Figure 3.20 were picked up by the NCSN-HRSN integrated network, the pattern scanning approach we employ picked up all of the near identical events.

Figure 3.20 shows how stable the performance of the VCAB.BP.DP1 channel has remained over the 4 year period analyzed. This is not necessarily the case for all the other HRSN channels being recorded. These repeating events can generally be identified using as few as 4 of the 38 HRSN channels, so, once they are identified, assessment of the channel responses for all the remaining HRSN channels can be carried out repeatedly through time and with time resolutions dependent on the number of repeating sequences used and the frequency of their repeats. Armed with this type of information, field engineers can quickly identify and address major problems. In addition to a visual assessment, the extreme similarity of the events lends itself to the application of differencing techniques in the time and frequency domains to automatically identify even subtle SOH issues.

Repeating sequences of this magnitude typically repeat every 1 to 2 years, and we are currently monitoring 34 of these sequences. Hence, on average, evaluations of this type can be made approximately every few weeks on an automated basis. However, there are on the order of 200 such sequences known in the Parkfield area, leaving open the possibility that automated SOH analyses could take place every 2 to 3 days.

For other networks recording continuously in the Parkfield area (e.g., NCSN, BDSN) it is also a relatively simple process to extend the SOH analysis using characteristic repeating events to their stations. Furthermore, numerous repeating and similar event sequences are also known to exist in the San Francisco Bay and San Juan Bautista areas, where continuous recording takes place. Hence, application of the repeating event SOH technique to these zones should also be feasible.

We are continuing to expand the number of pattern events and resulting multi-year scans in the Parkfield area to increase the frequency of sampling of similar and repeating event sequences for SOH purposes and for expanding the catalog of very small similar and repeating microearthquakes (down to M_p of -0.5). We are also adapting the codes to take advantage of faster computing now available.

Further development of the similar event processing approach also holds promise in other applications where automated and precise monitoring of bursts of seismic activity to very low magnitudes is desirable (e.g. in aftershock zones or in volcanic regions) or where automated updates of preexisting repeating sequences and their associated deep slip estimates are desired.

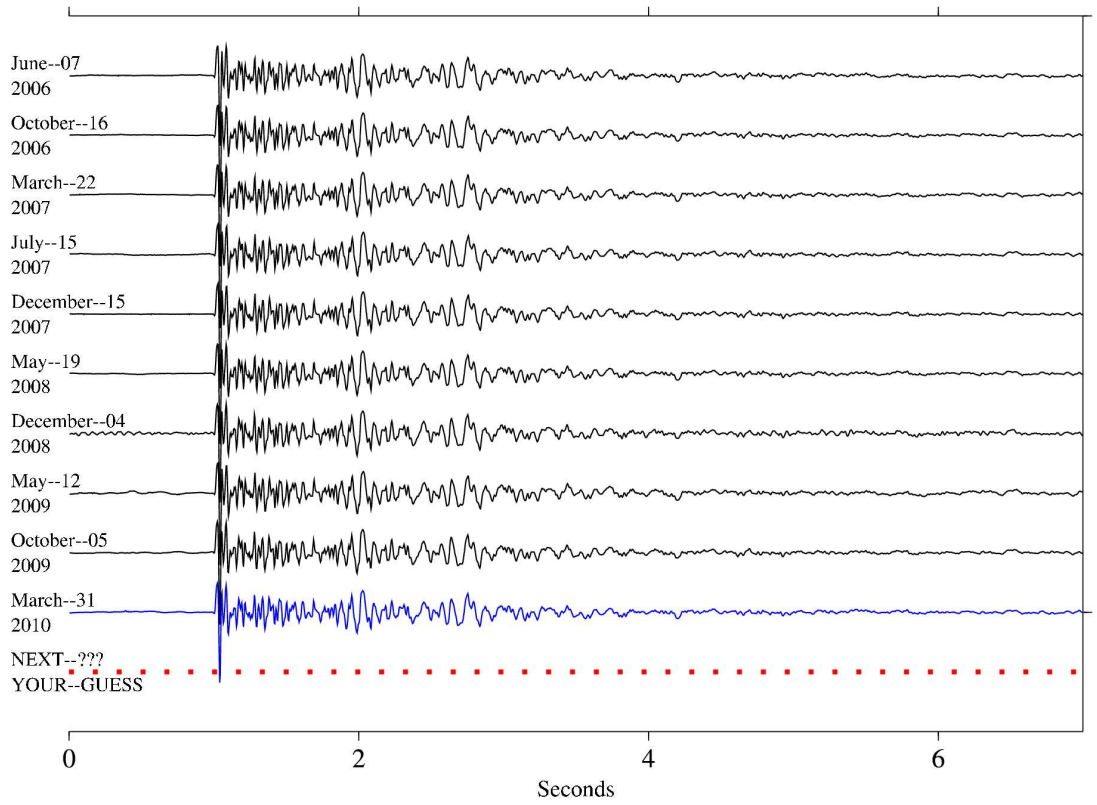

Figure 3.20: Ten most recent repeats of a characteristic sequence of repeating magnitude 0.25 (M_p, USGS preferred magnitude) microearthquakes recorded by vertical (DP1) channel of HRSN station VCAB. Waveform amplitudes are absolute scaled to the reference event (top), showing how small the variation in magnitudes of these naturally occurring events really are. High-precision location and magnitude estimates of these events show they are extremely similar in waveform (typically 0.95 cross-correlation or better), nearly collocated (to within 5-10 m) and of essentially the same magnitude (+/- 0.13 M_p units). The dashed line labeled "NEXT" serves to illustrate that events in these types of sequences continue to repeat and that they can therefore be used for monitoring ongoing channel response relative to past performance.

Reducing Operational costs

In recent years, increased scientific activity in the rural Parkfield area due to SAFOD has led to an increased demand for site access and development on privately owned property and a corresponding increase in access fees charged by private land owners. As a result, land use fees paid by the HRSN project had increased dramatically from less than $1000 annually prior to the SAFOD effort to over $14,000 over about a 3 year period . This represented over 15% of the entire HRSN budget, with no corresponding increase in support from the project's funding agency. To compensate for the increased landowner costs, maintenance efforts had to be cut back, and, as a result, network performance suffered.

To help alleviate the problem, we have completed implementation (through cooperation with the USGS) of plans to minimize our dependence on access to private lands. This primarily involved establishing alternative telemetry paths for roughly half of the HRSN sites through Gastro Peak.

To date, telemetry paths for five HRSN sites (SMNB, CCRB, MMNB, VARB, and SCYB) have been redirected from the Gastro Peak relay site to an alternative relay site at Hogs Canyon (HOGS) through an agreement with the USGS. Telemetry of GHIB data has also been redirected from Gastro Peak through an alternative path. Plans to redirect telemetry of an additional site from Gastro Peak (LCCB) are being examined and field tested for viability. Last year, the landowner also chose not to renew our access agreement for Gastro Peak, saving us approx. $9800 in annual fees. However, the owner did allow us to temporarily continue operating one station (RMNB) located at the Gastro Peak site free of charge for an unspecified period of time. This past summer the landowner had suggested that he was going to remove the RMNB site. We immediately began re-negotiations, and the site is still operating, however resolution of the issue has still not been forthcoming. Adding to the seriousness of the situation, until alternative telemetry to low lying station LCCB can be worked out (a difficult task given the lim-

ited telemetry options available), the RMNB station is also serving as a repeater for LCCB.

Tremor Monitoring

The HRSN played an essential role in the initial discovery of nonvolcanic tremors (NVT) along the San Andreas Fault (SAF) below Cholame, CA (*Nadeau and Dolenc, 2005*), and continues to play a vital role in ongoing NVT research. The Cholame tremors occupy a critical location between the smaller Parkfield (∼M6) and much larger Ft. Tejon (∼M8) rupture zones of the SAF (Figure 3.16). Because the time-varying nature of tremor activity is believed to reflect time-varying deep deformation and presumably episodes of accelerated stressing of faults, because anomalous changes in Cholame area NVT activity preceded the 2004 Parkfield M6 earthquake, and because elevated tremor activity has continued since the 2004 Parkfield event, we are continuing to monitor the tremor activity observable by the HRSN to look for additional anomalous behavior that may signal an increased likelihood of another large SAF event in the region. Some recent results of continued HRSN related NVT research are presented in the "Research Studies" chapter of this report.

Efforts in Support of SAFOD

An intensive and ongoing effort by the EarthScope component called SAFOD (San Andreas Fault Observatory at Depth) is underway to drill through, sample, and monitor the active San Andreas Fault at seismogenic depths and in very close proximity (within a few tens of kilometers or less) to a repeating magnitude 2 earthquake site. The HRSN data plays a key role in these efforts by providing low noise and high sensitivity seismic waveforms from active and passive sources, and by providing a backbone of very small earthquake detections and continuous waveform data.

As of early September 2007, SAFOD drilling had penetrated the fault near the HI repeating target sequence and collected core samples in the fault region that presumably creeps and surrounds the repeatedly rupturing HI patch. Unfortunately, due to complications during drilling, penetration and sampling of the fault patch involved in repeating rupture was not possible, though core samples and installation of seismic instrumentation in the region adjacent to the repeating patch was achieved. Current efforts are focused on long-term monitoring of the ongoing chemical, physical, seismological, and deformational properties in the zone (particularly any signals that might be associated with the next repeat of the SAFOD repeating sequences).

HRSN activities this year have contributed in three principal ways to these and longer-term SAFOD monitoring efforts:

1) Integration and processing of the HRSN data streams with those from the NCSN in the Parkfield area continues, effectively doubling the number of small events available for monitoring seismicity in the target zone and for constraining relative locations of the ongoing seismic activity.

2) Telemetry of all HRSN channels (both 20 and 250 sps data streams) continues to flow directly from Parkfield, through the USGS Parkfield T1 and the NCEMC T1, to the USGS and the BSL for near-real-time processing, catalog processing, and data archiving on the Web-based NCEDC. This also provides near immediate access of the HRSN data to the SAFOD community without the week- or month-long delay associated with the previous procedure of having to transport DLT tapes to Berkeley to upload and quality check the data.

3) We have also continued to apply our prototype similar event automated catalog approach to the primary (HI), secondary (SF), and tertiary (LA) SAFOD target zones as a continued effort to monitor the SAFOD target zone activity at very high relative location precision, and to notify the SAFOD community of repeats of M2 target events. The most recent repeats of the SAFOD HI, SF, and LA sequences occurred on (UTC): August 29, 2008; December 20, 2008; and December 19, 2008 (respectively). Of particular interest were the SF and LA repeats, which were recorded on the SAFOD main hole seismometer that had been installed in October.

4.4 Acknowledgments

Under Robert Nadeau's and Doug Dreger's general supervision, Bill Karavas, Rick Lellinger, Taka'aki Taira, Doug Neuhauser, Peter Lombard, John Friday, and Bob Uhrhammer all contribute to the operation of the HRSN. Bob Nadeau prepared this section with help from Taka'aki Taira. During this reporting period, operation, maintenance, and data processing for the HRSN project was supported by the USGS, through grants 07HQAG0014 and G10AC00093. Additional improvements in the power and telemetry systems were funded under the USGS ARRA grant G09AC00487.

4.5 References

Bakun, W. H., and A. G. Lindh, The Parkfield, California, prediction experiment, *Earthq. Predict. Res., 3*, 285-304, 1985.

Hickman, S., M.D. Zoback and W. Ellsworth, Introduction to special section: Preparing for the San Andreas Fault Observatory at Depth, *Geophys. Res. Lett., 31*, L12S01, doi:10.1029/2004GL020688, 2004.

Michelini, A. and T.V. McEvilly, Seismological studies at Parkfield: I. Simultaneous inversion for velocity structure and hypocenters using B-splines parameterization, *Bull. Seismol. Soc. Am., 81*, 524-552, 1991.

Nadeau, R.M. and D. Dolenc, Nonvolcanic Tremors Deep Beneath the San Andreas Fault, *SCIENCE, 307*, 389, 2005.

5 Bay Area Regional Deformation Network

5.1 Background

The Bay Area Regional Deformation (BARD) network is a collection of permanent, continuously operating GPS receivers that monitors crustal deformation in the San Francisco Bay Area (SFBA) and Northern California. Started in 1991 with two stations spanning the Hayward Fault, BARD has been a collaborative effort of the Berkeley Seismological Laboratory (BSL), the USGS at Menlo Park (USGS/MP), and several other academic, commercial, and governmental institutions. The BARD network is designed to study the distribution of deformation in Northern California across the Pacific-North America plate boundary and interseismic strain accumulation along the San Andreas fault system in the Bay Area for seismic hazard assessment, and to monitor hazardous faults and volcanoes for emergency response management. The BSL maintains and/or has direct continuous telemetry from 26 stations comprising the BARD Backbone (Table 3.11), while additional stations operated by the USGS, US Coast Guard and others fill out the extended BARD network. Twelve BARD Backbone sites are collocated with broadband seismic stations of the BDSN, with which they share continuous telemetry to UC Berkeley (Table 3.11).

With the completion of major construction on the Plate Boundary Observatory (PBO) portion of EarthScope, the number of GPS stations in Northern California has expanded to over 250 (Figure 3.21) and a number of BARD stations were folded into the PBO network. Together, PBO and BARD stations provide valuable information on the spatial complexity of deformation in the SFBA and Northern California, while the BARD network has the infrastructure and flexibility to additionally provide information on its temporal complexity over a wide range of time scales and in real-time. Many of the GPS stations in the BARD network are collocated with BDSN seismic instrumentation or are close to active faults where reliable access to real-time information could be critical following an earthquake.

The majority (24 of 26) of BARD Backbone stations now collect data at 1 Hz sampling frequency (Table 3.11). The data are collected continuously, as opposed to on a triggered basis, and transmitted to the BSL. The effort to expand the high-rate data collection was helped by upgrades over the past several years at 12 stations to Trimble NetRS receivers. The NetRS receivers feature a compact data stream, which has allowed us to collect high-rate data from locations with limited bandwidth telemetry. Furthermore, IP connectivity on the NetRS facilitates streaming of data over a Ntrip server to other agencies and the general public. Data streams from NetRS equipped BARD stations are currently available (`http://seismo.berkeley.edu/bard/realtime`).

The BSL has received funding through the American Reinvestment and Recovery Act (ARRA) to upgrade the remaining BARD sites with Topcon Net-G3A receivers that will provide BINEX streaming of data at 1Hz sampling over TCP/IP. The new receivers will also be capable of recording L5 data in addition to L1 and L2; L5 is a third frequency that will be added to GPS satellites in the coming years. In addition to upgrading existing sites, we have also received ARRA funding to install seven new stations at existing BDSN stations (Table 3.11), thereby taking advantage of shared telemetry. Three of these stations will be mounted on the existing seismic vaults, while the remaining four will be new, short-braced monuments.

5.2 BARD overview

BARD station configuration

Twelve BARD stations are currently equipped with high performance Trimble NetRS receivers, which have sufficient internal buffering to allow robust real-time telemetry at 1Hz. Recent upgrades include stations YBHB and SAOB in April, 2009, MODB in August, 2009, and SUTB in March, 2010. At MODB, we are able to telemeter 1Hz data using the USGS VSAT system that collects seismic broadband data as part of the National Seismic Network (NSN). Other stations are still equipped with older Ashtech Z-12 (A-Z12) and Ashtech MicroZ-CGRS (A-UZ) receivers. At these sites, the data are collected using direct serial connections and are susceptible to data loss during telemetry outages.

All BARD stations are continuously telemetered to the BSL. Many use frame relay technology, either alone or in combination with radio telemetry. Other methods include a direct radio link to Berkeley (TIBB, EBMD) and VSAT satellite telemetry (MODB). We also changed our data strategy by allowing some data to be transferred by web-based telemetry (ADSL lines). This will reduce our communication operational costs and, we hope, will not affect our ability to react in a large event. Twelve GPS stations are collocated with broadband seismometers and Quanterra data loggers. With the support of Integrated Research Institutions for Seismology (IRIS), the BSL developed software that converts continuous GPS data to MiniSEED opaque blockettes that are stored and retrieved from the Quanterra data loggers (*Perin et al.*, 1998), providing more robust data recovery from onsite disks following telemetry outages.

BARD station monumentations broadly fall into three types. Most are anchored into bedrock, either directly or via a steel-reinforced concrete cylinder. The five "mini-

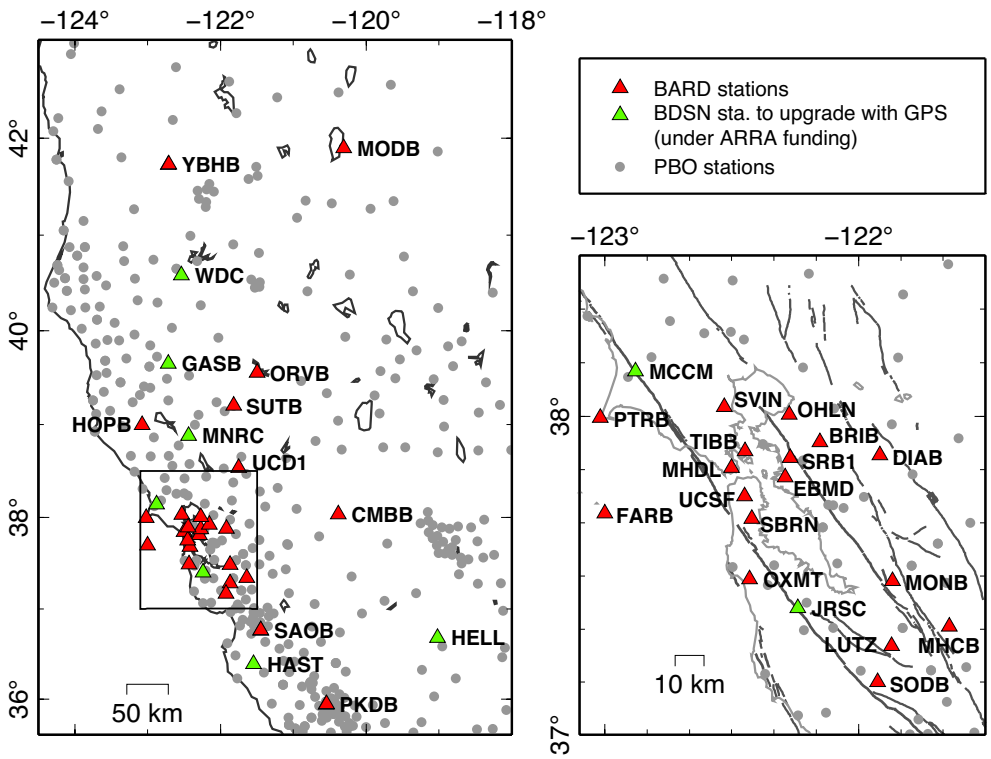

Figure 3.21: Map of the BARD network and surrounding PBO sites in Northern California.

PBO" stations that are still operated by the BSL are collocated with USGS strainmeters and the GPS antennas are bolted onto the borehole casing using an experimental mount developed at the BSL, which has since been adopted by PBO for their strainmeter sites. Four sites (UCD1, SRB1, UCSF, SBRB) are located on the roofs of buildings. Most of the last type have been installed in the past three years, and their stability over long periods of time is yet to be evaluated.

Most BARD stations use a radome-equipped, low-multipath choke-ring antenna, designed to provide security and protection from weather and other natural phenomena, and to minimize differential radio propagation delays. Four stations are equipped with Trimble Zephyr Geodetic antennas, though these are scheduled to be upgraded to choke-rings under ARRA funding. A low-loss antenna cable is used to minimize signal degradation on the longer cable setups that normally would require signal amplification. Low-voltage cutoff devices are installed to improve receiver performance following power outages.

Parkfield Stations

In September 2009, the BSL established the telemetry of high-rate data from 13 PBO stations in the Parkfield region. These stations were installed as part of the collaborative NSF/MRI program between the BSL, UC San Diego and Carnegie Institution of Washington nicknamed "mini-PBO." Since September 2009, 1 Hz GPS data from these 13 stations flow through the T1 line from Parkfield to Menlo Park and then on to Berkeley. From here it is sent back to UCSD via a NTRIP server. We plan to participate in a state-wide real-time geodetic network that will eventually be integrated with the CISN for earthquake notification purposes. The acquisition of real-time data from the Parkfield subnetwork is the first step towards linking Southern and Northern California real-time GPS networks.

Data Archival

Raw and RINEX data files from the 26 BARD Backbone stations and several other stations run by BARD collaborators are archived at the Northern California Earthquake Data Center (NCEDC). The data are checked to verify their integrity, quality, completeness, and conformance to the RINEX standard, and are then made accessible, usually within 2 hours of the end of the UTC day, to all BARD participants and other members of the GPS community through the Internet, both by anonymous FTP and through the World Wide Web (`http://ncedc.org/`). BARD data are also available to the community through GPS Seamless Archive Centers (GSAC), such as that hosted by the Scripps Orbit and Permanent Array Center (SOPAC, `http://gsac.ucsd.edu`). High-rate raw data are also decimated to create 15 s RINEX data files. 1 Hz RINEX files are available for all BARD Backbone sites after May 2010; high-rate

	Sites	Lat. (deg.)	Lon. (deg)	Receiver	Telem.	Sampling rate	Collocated Network	Location
1	BRIB	37.91	-122.15	NETRS	T1	1 Hz	BDSN	Briones Reservation, Orinda
2	CMBB	38.03	-120.39	A-UZ12	FR	1 Hz	BDSN	Columbia College, Columbia
3	DIAB	37.87	-121.92	NETRS	FR	1 Hz		Mt. Diablo
4	EBMD	37.81	-122.28	T-5700	R	1 Hz		East Bay Mud Headquarters
5	FARB	37.69	-123.00	NETRS	R-FR/R	1 Hz	BDSN	Farallon Island
6	HOPB	38.99	-123.07	T-SSI	FR	1 Hz	BDSN	Hopland Field Stat., Hopland
7	LUTZ	37.28	-121.87	A-Z12	FR	30 s	BDSN	SCC Comm., Santa Clara
8	MHCB	37.34	-121.64	A-Z12	FR	1 Hz	BDSN	Lick Obs., Mt. Hamilton
9	MHDL	37.84	-122.49	NETRS	FR	1 Hz	mini-PBO	Marin Headlands
10	MODB	41.90	-120.30	NETRS	VSAT	1 Hz	BDSN	Modoc Plateau
11	MONB	37.48	-121.87	A-Z12	FR	1 Hz		Monument Peak, Milpitas
12	OHLN	38.00	-122.27	A-UZ12	FR	1 Hz	mini-PBO	Ohlone Park, Hercules
13	ORVB	39.55	-121.50	NETRS	FR	1 Hz	BDSN	Oroville
14	OXMT	37.49	-122.42	A-Z12	FR	1 Hz	mini-PBO	Ox Mountain
15	PKDB	35.94	-120.54	NETRS	FR	1 Hz	BDSN	Bear Valley Ranch, Parkfield
16	PTRB	37.99	-123.01	A-Z12	R-FR	1 Hz		Point Reyes Lighthouse
17	SAOB	36.76	-121.45	NETRS	FR	1 Hz	BDSN	San Andreas Obs., Hollister
18	SBRN	37.69	-122.41	A-Z12	FR	1 Hz	mini-PBO	San Bruno
18	SBRB	37.69	-122.41	A-UZ12	FR	1 Hz	mini-PBO	San Bruno Replacement
19	SODB	37.17	-121.93	A-Z12	R-FR	15 s		Soda Springs, Los Gatos
20	SRB1	37.87	-122.27	T-SSE	FR	1 Hz		Seismic Replacement Building, Berkeley
21	SUTB	39.20	-121.82	NETRS	R-FR	1 Hz	BDSN	Sutter Buttes
22	SVIN	38.03	-122.53	A-UZ12	R-FR	1 Hz	mini-PBO	St. Vincents
23	TIBB	37.89	-122.45	A-UZ12	R	1 Hz		Tiburon
24	UCD1	38.53	-121.75	NETRS	WEB	1 Hz		UC Davis, Davis
25	UCSF	37.75	-122.46	NETRS	FR	1 Hz		UC San Francisco, San Francisco
26	YBHB	41.73	-122.71	NETRS	FR	1 Hz	BDSN	Yreka Blue Horn Mine, Yreka
27	GASB	39.65	-122.72				BDSN	Alder Springs, CA
28	HAST	36.39	-121.55				BDSN	UC Hastings Preserve, Carmel Valley
29	HELL	36.68	-119.02				BDSN	Rademacher Property, Miramonte
30	JRSC	37.4	-122.24				BDSN	Jasper Ridge Biol. Preserve, Stanford
31	MCCM	38.14	-122.88				BDSN	Marconi Conference Center, Marshall
32	MNRC	38.88	-122.44				BDSN	McLaughlin Mine, CA
33	WDC	40.58	-122.54				BDSN	Whiskeytown Dam, Whiskeytown

Table 3.11: List of BARD stations maintained by the BSL. Six models of receiver are operating now: Trimble NetRS, (NETRS), Ashtech Z12 (A-Z12), and Ashtech Micro Z (A-UZ12), Trimble 4000 SSE (T-SSE), Trimble 4000 SSI (T-SSI), Trimble 5700 (T-5700). The telemetry types are listed in column 6: FR = Frame Relay, R = Radio, VSAT= Satellite, WEB = DSL line. Some sites are transmitting data over several legs with different telemetry. Sites 27 to 33 are to be installed under ARRA funding.

RINEX files for earlier dates will be backfilled in the coming months.

As part of the activities funded by the USGS through the BARD network, the NCEDC has established an archive of the 10,000+ survey-mode occupations collected by the USGS since 1992. The NCEDC continues to archive non-continuous survey GPS data. The initial dataset archived is the survey GPS data collected by the USGS Menlo Park for Northern California and other locations. The NCEDC is the principal archive for this dataset. Quality control efforts were implemented by the NCEDC to ensure that raw data, scanned site log sheets, and RINEX data are archived for each survey. All of the USGS/MP GPS data has been transferred to the NCEDC, and virtually all of the data from 1992 to the present has been archived and is available for distribution. These survey-mode data are used together with data from BARD and PBO stations to produce BAVU (Bay Area Velocity Unification), a united set of continuous and survey data from the wider San Francisco Bay Area, processed under identical conditions using GAMIT (*d'Alessio et al.*, 2005).

Data from five of our sites (HOPB, MHCB, CMBB, OHLN, and YBHB) are sent to the National Geodetic Survey (NGS) in the framework of the CORS (Continuous Operating Reference Stations) project (`http://www.ngs.noaa.gov/CORS/`). The data from these five sites are also distributed to the public through the CORS FTP site.

Data Processing

Average station coordinates are estimated from 24 hours of observations for BARD stations and other nearby continuous GPS sites using the GAMIT/GLOBK software developed at MIT and SIO (*King and Bock*, 1999, *Herring*, 2005). GAMIT uses double-difference phase observations to determine baseline distances and orientations between ground-based GPS receivers. Ambiguities are fixed using the widelane combination followed by the narrowlane, with the final position based on the ionospheric free linear combination (LC or L3). Baseline solutions are loosely constrained until they are combined together. GAMIT produces solutions as H-files, which include the covariance parameters describing the geometry of the network for a given day and summarize information about the sites.

We combine daily, ambiguity-fixed, loosely constrained H-files using the Kalman filter approach implemented by GLOBK (*Herring*, 2005). They are combined with solutions from the IGS global network and PBO and stabilized under a North America-fixed reference frame. The estimated relative baseline determinations typically have 2-4 mm long-term scatter in the horizontal components and 10-20 mm scatter in the vertical. The most recent velocity solutions (*Houlié and Romanowicz*, in press, Figure 3.22) are in good agreement with previous work (e.g. *d'Alessio et al.*, 2005).

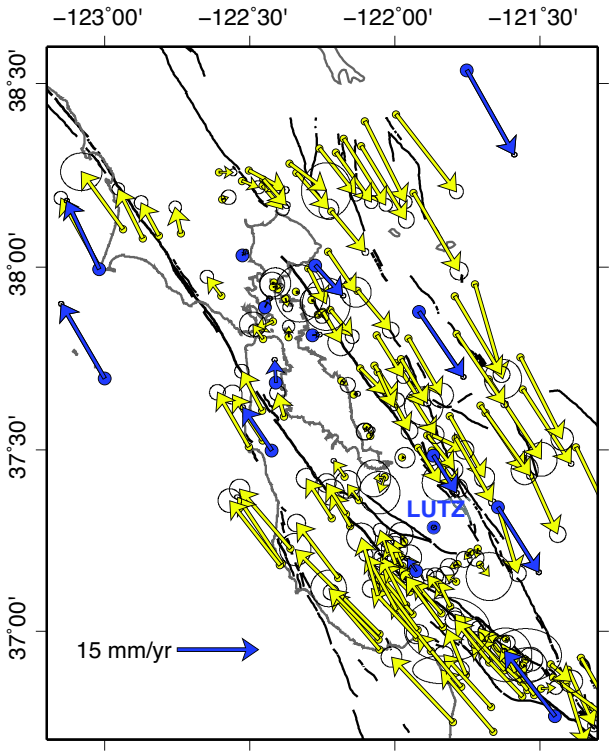

Figure 3.22: Site velocities from BAVU2 within the SFBA, including BARD (in blue), PBO and campaign stations. Shown relative to station LUTZ. BAVU website: `http://seismo.berkeley.edu/~burgmann/RESEARCH/BAVU/`

5.3 Recent developments

Real-time streaming: We have begun the process of making all our 1Hz data available in real time; a step toward our goal of integrating GPS with the Northern California Seismic System (NCSS) for use in hazard assessment and emergency response. Stations with IP connectivity (currently those that are NetRS equipped) are the first to be streamed over our NTRIP server. Stations with serial connections will be phased in over the coming months. Similarly data are currently available in BINEX format, but RTCM streams and other raw formats will be added. Data are available to the general public, but an account must first be established; see `http://seismo.berkeley.edu/bard/realtime` for details.

Time-series analysis: Testing continues to reestablish automatic time-series generation of BARD Backbone data; an activity that was funded under the ARRA program. Daily processing ensures that bad data is caught quickly and any problems can be fixed in a timely manner. Several products used in time-series gen-

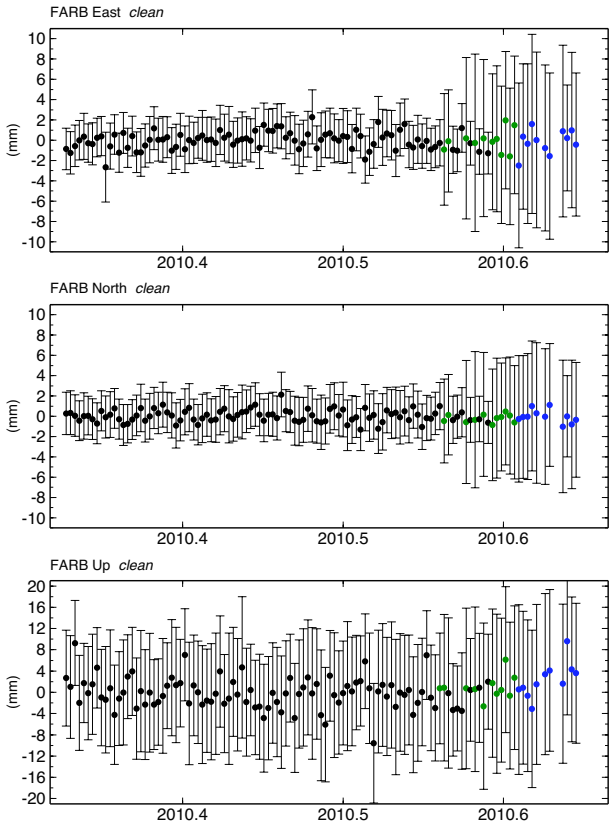

Figure 3.23: Detrended and cleaned time series for station FARB from 5/1/2010 through 8/24/2010. Blue points are for days processed with IGS rapid orbit files, green points are days that were processed with IGS final orbit files, but were not combined with PBO solutions, black points are fully processed, with final orbits and all combined solutions.

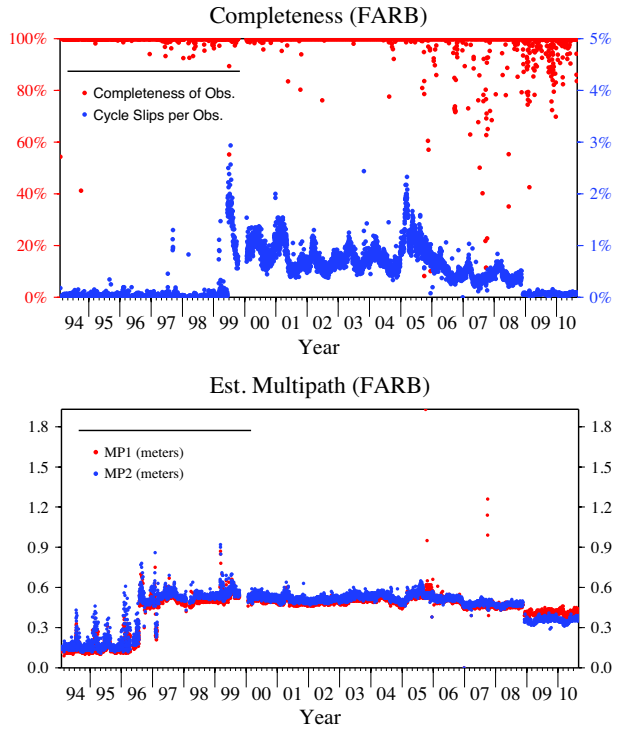

Figure 3.24: Data completeness and estimated multipath over the lifetime of BARD backbone station FARB. For estimated multipath parameters, MP1 and MP2 correspond to the L1 and L2 signals, respectively. Higher MP values indicate a greater prevalence of multipathing, i.e. objects on the ground are providing multiple reflection pathways from the satellite to the antenna.

eration are available on different time scales. Final orbit files are generally available after 7-10 days, while IGS and PBO solutions have their own lag times. Figure 3.23 shows the detrended (residual) time series for station FARB on the Farallon Islands, for 5/1/2010 through 8/24/2010, as produced on 8/27/2010. The time series has been cleaned by removing common mode errors, which were determined using all California stations (though most are in the Bay Area). Overall scatter is very low, as would be expected for a time period with no major or moderate events, with root mean square (RMS) values of 0.9 mm, 0.6 mm, and 2.9 mm for the North, East and Up directions, respectively. The scatter in the data is not dramatically affected by being processed with ISG rapid orbit files (blue points) or when not combined with PBO solutions (green points), though the calculated error bars are affected. Motions above the several mm level should be detectable within 2-3 days, while smaller motions will be evident when final orbit files are available in 1-2 weeks. Once finalized, these plots will be posted on the BARD website and updated daily.

Metadata overhaul: Another major activity of the past year has been the updating, consolidation and presentation of site metadata and quality control information. Station log files (`ftp://ncedc.org/pub/gps/site/`) are now 100% up to date and conform to the IGS standard for metadata reporting. The BARD webpage (`http://seismo.berkeley.edu/bard`) has also been redesigned and upgraded to provide more information on individual stations. The web pages also include plots of data completeness (how many epochs are present in the data files) and estimated multipath for the L1 and L2 signals (Figure 3.24). These are updated daily and provide a measure of the antenna and telemetry performance and of the effect of the surroundings on the data quality. Changes to these values correspond to equipment changes, equipment failure and changes to the environment surrounding the site. The last is particularly important, as changes such as construction or tree removal can occur near a station without the BSL's knowledge.

5.4 Acknowledgements

The BARD program is overseen by Barbara Romanowicz and Ingrid Johanson (since February 2010). Rich Clymer, Bill Karavas, Rick Lellinger, John Friday, Doug Neuhauser, Mario Aranha and Jennifer Taggart contributed to the operation of the BARD network in 2009-10. Operation of the BARD network is partially supported by funding from the USGS/NEHRP program grants #07HQAG0031 and #G10AC00141 and infrastructure upgrades were made possible by funding from the ARRA grant #G10AC00079.

5.5 References

d'Alessio, M. A., I. A. Johanson, R. Bürgmann, D. A. Schmidt, and M. H. Murray, Slicing up the San Francisco Bay Area: Block kinematics from GPS-derived surface velocities, *J. Geophys. Res., 110*, B06403, doi:10.1029/2004JB003496, 2005.

Herring, T., GLOBK: Global Kalman Filter: VLBI and GPS Analysis Program, version 10.2, 2005.

Houlié, N. and Romanowicz, B., Asymmetric deformation across the San Francisco Bay Area faults from GPS observations in northern California, *Phys. Earth Planet. In.*, in press.

King, R., and Y. Bock, Documentation of the GAMIT software, MIT/SIO, 1999.

Perin, B. J., C. M. Meertens, D. S. Neuhauser, D. R. Baxter, M. H. Murray, and R. Butler, Institutional collaborations for joint seismic and GPS measurements, *Seismol. Res. Lett., 69,* 159, 1998.

6 Northern California Earthquake Data Center

6.1 Introduction

The Northern California Earthquake Data Center, a joint project of the Berkeley Seismological Laboratory (BSL) and the U.S. Geological Survey at Menlo Park, serves as an online archive and distribution center for various types of digital data relating to earthquakes in Central and Northern California. The NCEDC is located at the Berkeley Seismological Laboratory, and has been accessible to users via the Internet since mid-1992.

The primary goal of the NCEDC is to provide a stable and permanent archival and distribution center of digital geophysical data for networks in Northern and Central California. These data include seismic waveforms, electromagnetic data, GPS data, strain, creep, and earthquake parameters. The seismic data comes principally from the Berkeley Digital Seismic Network (BDSN) operated by the Seismological Laboratory, the Northern California Seismic Network (NCSN) operated by the USGS, the Berkeley High Resolution Seismic Network (HRSN) at Parkfield, the EarthScope USArray Transportable Array stations in Northern California, the various Geysers networks, and selected stations from adjacent networks such as the University of Nevada, Reno network and the Southern California Seismic Network (SCSN). GPS data are primarily from the Bay Area Regional Deformation (BARD) GPS network and the USGS/Menlo Park GPS surveys. The collection of NCSN digital waveforms dates from 1984 to the present, the BDSN digital waveforms date from 1987 to the present, and the BARD GPS data date from 1993 to the present. The BDSN includes stations that form the specialized Northern Hayward Fault Network (NHFN) and the MiniPBO (mPBO) borehole seismic and strain stations in the SF Bay Region. Additional seismic and strain data from the EarthScope Plate Boundary Observatory (PBO) and the San Andreas Fault Observatory at Depth (SAFOD) are also archived at the NCEDC. Figure 3.27 shows the total data volume by year, as itemized in Table 3.12.

The NCEDC also provides support for earthquake processing and archiving activities of the Northern California Earthquake Management Center (NCEMC), a component of the California Integrated Seismic Network (CISN). The CISN is the California regional organization of the Advanced National Seismic System (ANSS).

Figure 3.26 shows the location of stations archived at the NCEDC (excluding EarthScope stations located outside of CA).

6.2 2009-2010 Activities

By its nature, data archiving is an ongoing activity. In 2009-2010, the NCEDC continued to expand its data holdings and enhance access to the data. Projects and activities of particular note include:

- Distributed over 1816 GB of waveform data to external users.
- Began the process of replacing waveforms rapidly collected in real-time for earthquake event analysis with QC-ed waveforms from the BK and BP networks.
- Supported the NCEMC earthquake analysis by providing real-time access to earthquake parameters and waveforms from the NCEDC for the CISN `Jiggle` earthquake review software.
- Continued the process of reading and archiving continuous NCSN seismograms from tapes for 1996-2000.
- Began real-time telemetry and data distribution for 13 Parkfield GPS stations using the Ntrip protocol.
- Began the process of archiving continuous seismic data from the EarthScope PBO borehole seismic stations to augment the borehole strain data already being archived at the NCEDC.
- Worked with the NCSN and USGS National Strong Motion Program (NSMP) to house the metadata and build dataless SEED volumes for all NSMP dialup stations.

6.3 BDSN/NHFN/mPBO Seismic Data

The BDSN (Operational Section 1), NHFN (Operational Section 3), and Mini-PBO (Operational Section 3) stations (all network code BK) telemetered data from 48 seismic data loggers in real time to the BSL These data are written to disk files, used for CISN real-time earthquake processing and earthquake early warning (EEW) development, and delivered in real-time to the DART (Data Available in Real Time) system at the NCEDC, where they are immediately available to anyone on the Internet. In September 2004, the NCEDC began to archive continuous high frequency data (80 Hz and 100 Hz) from all of the BDSN broadband, strong motion, and strainmeter sensors. Previously, only 20 Hz and lower rate data channels were archived continuously, and high frequency data was archived only for events. In December 2005, the NCEDC developed the DART, and began making all real-time BDSN data immediately available through this facility. All timeseries data from the Berkeley networks

Data Type	GBytes
BDSN/NHFN/mPBO (broadband, electric and magnetic field, strain) waveforms	6,916
NCSN seismograms	25,660
Parkfield HRSN seismograms	3,499
BARD GPS (RINEX and raw data)	2,380
UNR Nevada seismograms	1,301
SCSN seismograms	2,338
Calpine/Unocal Geysers region seismograms	38
EarthScope SAFOD seismograms	2,035
EarthScope USArray seismograms	271
EarthScope PBO strain and seismic waveforms	1,616
PG&E seismograms	489
USGS low frequency geophysical waveforms	3
Misc data	2,977
Total size of archived data	49,523

Table 3.12: Volume of Data Archived at the NCEDC by network.

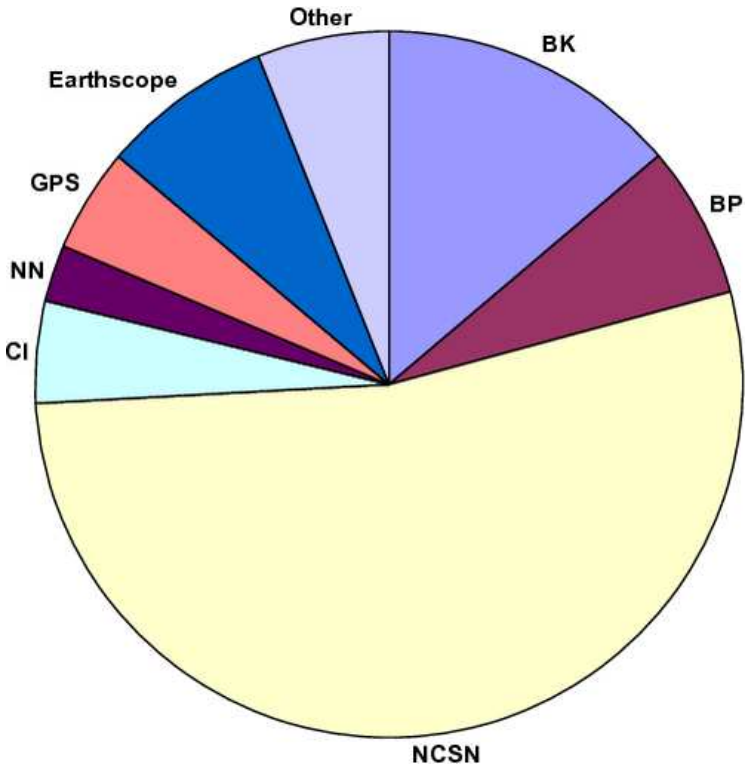

Figure 3.25: Chart showing the relative proportion of each data set at the NCEDC. (BK - Berkeley Digital Seismic Network; BP - Berkeley High-resolution Seismic Network in Parkfield; NC - Northern California Seismic Network and collaborators; CI - Southern California Seismic Network; NN - University of Nevada, Reno Seismic Network; GPS - various GPS datasets, including BARD; EarthScope - data from various EarthScope activities; Other - various small data sets.

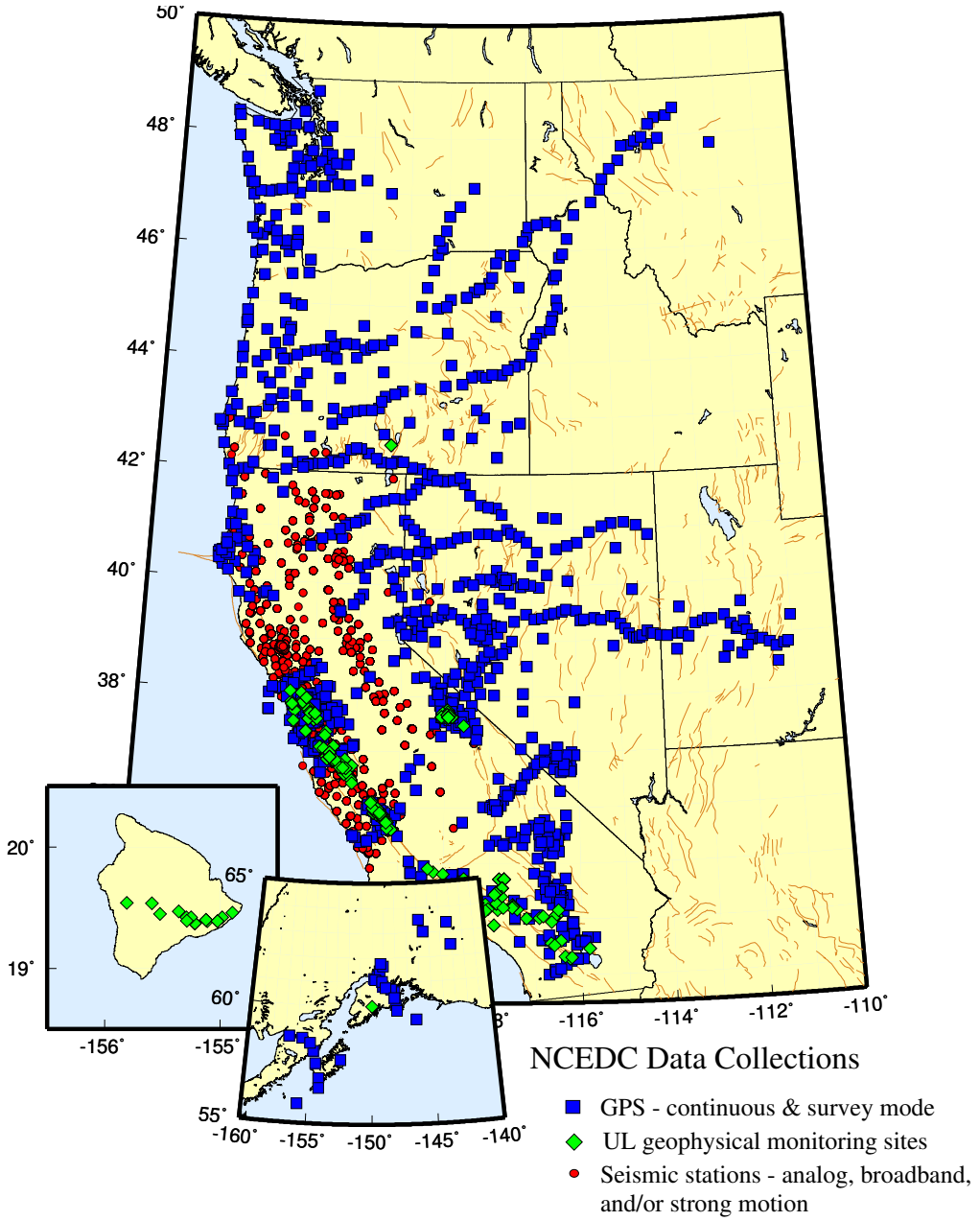

Figure 3.26: Map showing the location of stations whose data are archived at the NCEDC. Circles are seismic sites, squares are GPS sites, and diamonds are the locations of USGS low-frequency experiments.

continue to be processed and archived by an NCEDC analyst using *calqc* in order to provide the highest quality and most complete data stream to the NCEDC.

NCSN Seismic Data

NCSN continuous waveform data are transmitted from USGS/Menlo Park in real time to the NCEDC via the

Internet, converted to MiniSEED, and made available to users immediately through the NCEDC DART. NCSN event waveform data, as well as data from all other real-time BSL and collaborating networks, are automatically collected by the NCEMC waveform archiver and stored at the NCEDC for event review and analysis and for distribution to users. All NCSN and NCEMC data are archived in MiniSEED format.

The NCEDC also maintains a list of historic teleseismic events recorded by the NCSN, since these events do not appear in the NCSN catalog.

A description of the successive improvements in the acquisition of NCSN data, leading to the acquisition of complete NCSN waveform data in early 2006, can be found in the 2005-06 BSL Annual Report. We finished the first phase of the NCSN continuous waveform archiving project by reading, converting and archiving NCSN seismograms from all available NCSN tapes for mid-2001 through early 2006. We are continuing this project by processing and archiving NCSN tape data from 1996 through 2000.

Parkfield High Resolution Seismic Network Data

The history of upgrades to the acquisition and archival of HRSN data can be found in the 2005-06 BSL Annual Report. We continue to archive continuous 250 and 20 sample-per-second data from the HRSN stations.

EarthScope Plate Boundary Observatory (PBO) strain data

The NCEDC is one of two funded archives for PBO EarthScope borehole and laser strain data. Strain data are collected from all of the PBO strain sites and are processed by UNAVCO. MiniSEED data are delivered to the NCEDC using SeedLink, and raw and XML processed data are delivered to the NCEDC using Unidata's Local Data Manager (LDM). The MiniSEED data are inserted into the NCEDC DART and are subsequently archived from the DART. UNAVCO provides EarthScope funding to the NCEDC to help cover the processing, archiving, and distribution costs for these data. In early 2010, the NCEDC began receiving and archiving all of the continuous seismic waveform data from the PBO network to complement the PBO strain data. The seismic data are received from an Antelope ORB server at UNAVCO and converted from their native format to MiniSEED on a data import computer. The data are then transferred via the SEEDLink protocol to the NCEDC and inserted into the NCEDC DART and are subsequently archived from the DART.

EarthScope SAFOD

The NCEDC is an archive center for the SAFOD event data and has also processed the continuous SAFOD data. Starting with the initial data in July 2002 from the SAFOD Pilot Hole, and later data from the SAFOD Main Hole, the NCEDC converted data from the original SEG-2 format data files to MiniSEED, and developed the SEED instrument responses for this data set. Continuous 4 KHz data from SAFOD written to tape at SAFOD were periodically sent to the BSL to be converted, archived, and forwarded to the IRIS DMC (IRIS Data Management Center). SAFOD EarthScope funding to the NCEDC is to cover the processing, archiving, and distribution costs for these data. A small subset of the continuous SAFOD data channels are also incorporated into the NCSN, are available in real-time from the NCEDC DART, are archived at the NCEDC, and are forwarded to the IRIS DMC. After the failure of the SAFOD permanent instrument in September 2008, the USGS deployed a temporary network in the Main Hole, and the NCEDC continued to process and archive these data. Both the permanent and temporary seismic instruments were removed in 2010.

UNR Broadband data

The University of Reno in Nevada (UNR) operates several broadband stations in western Nevada and eastern California that are important for Northern California earthquake processing and analysis. Starting in August 2000, the NCEDC has been receiving and archiving continuous broadband data from four UNR stations. The data are transmitted in real time from UNR to UC Berkeley, where they are made available for CISN real-time earthquake processing and for archiving. Initially, some of the stations were sampled at 20 Hz, but all stations are now sampled and archived continuously at 100 Hz.

The NCEDC installed Simple Wave Server (SWS) software at UNR, which provides an interface to UNR's recent collection of waveforms. The SWS is used by the NCEDC to retrieve waveforms from UNR that were missing at the NCEDC due to real-time telemetry outages between UNR and UC Berkeley.

In early 2006, the NCEDC started to archive continuous data from the UNR short-period stations that are contributed to the NCSN. Both the broadband and short-period UNR stations contributed to the CISN are available in real-time through the NCEDC DART.

Electro-Magnetic Data

The NCEDC continues to archive and process electric and magnetic field data acquired at several UC Berkeley sites. The BSL operates both magnetic and electric field sensors at PKD and SAO. However, most of these channels have been down for repair during the 2008-2009 year. Through a collaboration with Dr. Simon Klemperer at Stanford University, we acquire magnetic and electric field channels at BSL sites JRSC and BRIB, and

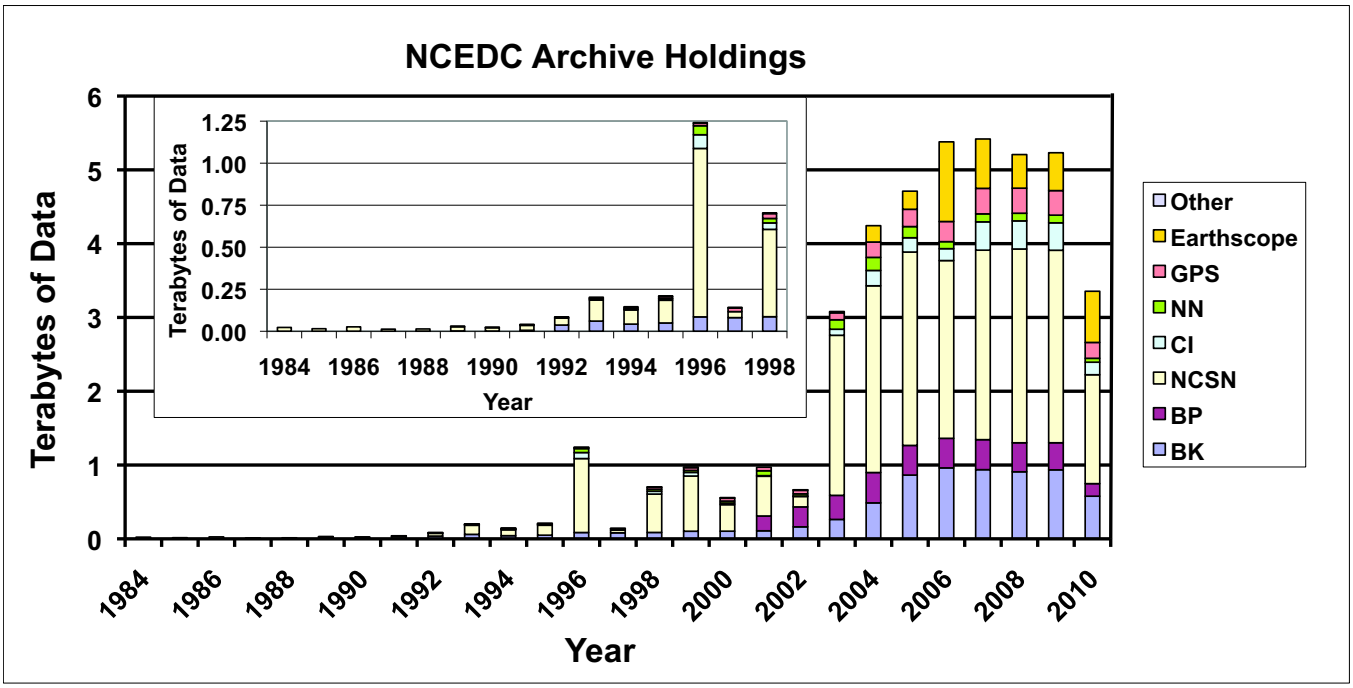

Figure 3.27: Figure showing the total volume of data archived at the NCEDC, broken down by data year.

magnetic field channels at site MHDL. The three magnetic field channels and either two or four electric field channels are digitized at 40 Hz, 1 Hz, and 0.1 Hz, and are telemetered in real-time along with seismic data to the Berkeley Seismological Laboratory, where they are processed and archived at the NCEDC in a similar fashion to the seismic data.

GPS Data

The NCEDC continues to archive GPS data through the BARD (Bay Area Regional Deformation) network of continuously monitored GPS receivers in Northern California (Operational Section 5). The NCEDC GPS archive now includes 67 continuous sites in Northern California. There are approximately 50 core BARD sites owned and operated by UC Berkeley, USGS (Menlo Park and Cascade Volcano Observatory), LLNL, UC Davis, UC Santa Cruz, Trimble Navigation, and Stanford. Data are also archived from sites operated by other agencies, including East Bay Municipal Utilities District, the City of Modesto, the National Geodetic Survey, and the Jet Propulsion Laboratory.

In addition to the standard 15 second or 30 second continuous GPS datastream, the NCEDC is now archiving and distributing high-rate 1 Hz continuous GPS data from most of the BSL-operated BARD stations. In collaboration with UCSD/SIO and USGS/MP, the BSL is now streaming real-time 1 Hz continuous data from the 13 PBO stations in Parkfield through the USGS Parkfield T1 and NCSS T1 circuits to the BSL, where it makes the data available to researchers in real-time through an Ntripcaster.

The NCEDC also archives non-continuous survey GPS data. The initial dataset archived is the survey GPS data collected by the USGS Menlo Park for Northern California and other locations. The NCEDC is the principal archive for this dataset. Significant quality control efforts were implemented by the NCEDC to ensure that the raw data, scanned site log sheets, and RINEX data are archived for each survey.

Geysers Seismic Data

The Calpine Corporation operated a micro-seismic monitoring network in the Geysers region of Northern California. Prior to 1999, this network was operated by Unocal. Through various agreements, both Unocal and Calpine have released triggered event waveform data from 1989 through 2000 along with preliminary event catalogs for the same time period for archiving and distribution through the NCEDC. This dataset represents over 296,000 events that were recorded by the Calpine/Unocal Geysers network and are available via research accounts at the NCEDC.

The Lawrence Berkeley Laboratory (LBL), with funding from the California Energy Commission, currently operates a 22 station network in the Geysers region with an emphasis on monitoring seismicity related to well water injection. The earthquake locations and waveforms from this network are sent to the NCEDC, and the locations are forwarded to the NCSN so that they can be

merged into the NCSN earthquake catalog. In August 2007, the NCSN installed an Earthworm system at the Geysers to receive continuous LBL Geysers data, and this system provides event waveforms in real-time for the NCEMC earthquake processing and the NCEDC event archives. The event data from LBL Geysers event waveforms collected from April 2004 to August 2007 will be associated with events from the NCSN catalog and will be included with the existing waveforms for these events.

USGS Low Frequency Data

Over the last 35 years, the USGS at Menlo Park, in collaboration with other principal investigators, has collected an extensive low-frequency geophysical data set that contains over 1300 channels of tilt, tensor strain, dilatational strain, creep, magnetic field, and water level as well as auxiliary channels such as temperature, pore pressure, rain and snow accumulation, and wind speed. In collaboration with the USGS, we assembled the requisite information for the hardware representation of the stations and the instrument responses for many channels of this diverse dataset, and developed the required programs to populate and update the hardware database and generate the instrument responses. We developed the programs and procedures to automate the process of importing the raw waveform data and converting it to MiniSEED format. Since these data are delivered to the NCEDC on a daily basis and immediately archived, these data are not inserted into the NCEDC DART.

We have currently archived timeseries data from 887 data channels from 167 sites, and have instrument response information for 542 channels at 139 sites. The waveform archive is updated on a daily basis with data from 350 currently operating data channels. We will augment the raw data archive as additional instrument response information is assembled by the USGS for the channels, and will work with the USGS to clearly define the attributes of the "processed" data channels.

SCSN/Statewide seismic data

In 2004, the NCEDC started to archive broadband and strong motion data from 15 SCSN (network CI) stations that are telemetered to the Northern California Management Center (NCEMC) of the California Integrated Seismic Network (CISN). These data are used in the prototype real-time state-wide earthquake processing system and also provide increased coverage for Northern California events. Since the data are telemetered directly from the stations in real-time to both the SCSN and to the NCEMC, the NCEDC archives the NCEMC's copy of the data to ensure that at least one copy of the data will be preserved. Due to reduced state funding, the SCSN has gradually reduced the number of telemetered stations to 12.

In early 2006, the NCEDC started to continuously archive all of the selected SCSN short-period stations that are contributed to the NCSN. All of these data are also available in real-time from the NCEDC DART. In 2009, the NCEMC started incorporating data from ~ 25 additional SCSN stations near the southern border of the NCEMC monitoring area in its event waveform collection to provide better azimuthal coverage of events in that area. In 2009-2010, the NCEMC also started retrieving event waveform data from the SCSN for other SCSN stations that are expected to receive signals from Northern California earthquakes. All of these event waveforms are also archived at the NCEDC.

Earthquake Catalogs

Northern California: The NCEDC provides searchable access to both the USGS and BSL earthquake catalogs for Northern and Central California. The "official" UC Berkeley earthquake catalog begins in 1910 and runs through 2003, and the "official" USGS catalog begins in 1966. Both of these catalogs are archived and available through the NCEDC, but the existence of 2 catalogs has caused confusion among both researchers and the public.

In late 2006, the NCEMC began archiving and distributing a single unified Northern California earthquake catalog in real time to the NCEDC through database replication from the NCEMC's real-time systems. The NCEDC developed and tested the required programs used to enter all previous NCSN catalog data into the NCEDC database. In 2008, we migrated all of the historic NCSN catalog, phase, and amplitude data from 1967 - 2006 into the NCEMC catalog. In addition, we spent considerable effort addressing the mapping of phase data in the BSL catalog to SEED channel names. We plan to merge the BSL catalog with the NCEMC catalog to form a single unified Northern California catalog from 1910 to the present. The BSL and the USGS have spent considerable effort over the past years to define procedures for merging the data from the two catalogs into a single Northern and Central California earthquake catalog in order to present a unified view of Northern California seismicity. The differences in time period, variations in data availability, and mismatches in regions of coverage all complicate the task.

Worldwide: The NCEDC, in conjunction with the Council of the National Seismic System (CNSS), produced and distributed a world-wide composite catalog of earthquakes based on the catalogs of the national and various U.S. regional networks for several years. Each network updates their earthquake catalog on a daily basis at the NCEDC, and the NCEDC constructs a composite world-wide earthquake catalog by combining the data, removing duplicate entries that may occur from multiple networks recording an event, and giving priority to the data from each network's *authoritative region.*

The catalog, which includes data from 14 regional and national networks, is searchable using a Web interface at the NCEDC. The catalog is also freely available to anyone via FTP over the Internet.

With the demise of the CNSS and the development of the Advanced National Seismic System (ANSS), the NCEDC was asked to update its Web pages to present the composite catalog as a product of the ANSS. This conversion was completed in the fall of 2002. We continue to create, house, distribute, and provide a searchable Web interface to the ANSS composite catalog, and to aid the regional networks in submitting data to the catalog.

6.4 NCEDC Operations

In 2005, the NCEDC relocated its archive and distribution system from McCone Hall to a new state-of-the-art computer facility in a new seismically braced building on the Berkeley campus. The facility provides seismically braced equipment racks, gigabit Ethernet network, air conditioning, and power conditioning. The entire facility is powered by a UPS with generator backup.

The currently installed NCEDC facilities consist of a mass storage environment hosted by a Sun X4150 host computer, a 100 slot LTO3 tape library with two tape drives and a 20 TByte capacity, and 60 TBytes of RAID storage, all managed with the SAM-FS hierarchical storage management (HSM) software. In 2008-2009, the tape library was upgraded from LTO2 to LTO3 drives, and all online tape data was re-archived on LTO3 tapes. DART data are collected and distributed on a Sun 280R computer and RAID storage. A Sun x4150 system provides Web services for the NCEDC, a dual Sun 280R processor provides data import and export services, and a Sun 280R computer is used for quality control procedures. Two AIT tape libraries are used to read NCSN continuous data tapes. Two 64-bit Linux systems host redundant Oracle databases. Two Sun X64 processors provide additional data processing support for the NCEDC.

The SAMFS hierarchical storage management (HSM) software used by the NCEDC is configured to automatically create multiple copies of each data file in the archive. The NCEDC creates one copy of each file on an online RAID, a second copy on LTO3 tape (of which the most recent data are stored online in the tape library), and a third copy on LTO2 tape which is stored offline and offsite. All NCEDC data are stored online and are rapidly accessible by users.

The NCEDC operates two instances of its Oracle database, one for internal operations and one for external use for user data queries and data distribution programs, and communicates with a third identical database operated offsite by the USGS in Menlo Park. These three databases are synchronized using multi-master replication.

Data Quality Control

The NCEDC developed a GUI-based state-driven system *calqc* to facilitate the quality control processing that is applied to the continuously archived data sets at the NCEDC.

The quality control procedures for these datasets include the following tasks:

- data extraction of a full day of data,
- quickcheck program to summarize the quality and stability of the stations' clocks,
- determination if there is missing data for any data channel,
- provided procedures to retrieve missing data from the stations and incorporate it into the day's data,
- optional creation of multi-day timeseries plots for state-of-health data channels,
- optional timing corrections for data,
- optional extraction of event-based waveforms from continuous data channels,
- optional repacking of MiniSEED data,
- creating waveform inventory entries in the NCEDC database,
- publishing the data for remote access on the NCEDC.

Calqc uses previously developed programs to perform each function, but it provides a graphical point-and-click interface to automate these procedures, and to provide the analyst with a record of when each process was started, whether it executed correctly, and whether the analyst has indicated that a step has been completed. *Calqc* is used to process all data from the BDSN network, and all continuous broadband data from the NCSN, UNR, SCSN, and HRSN networks that are archived by the NCEDC. The remainder of the continuously archived data are automatically archived without any analyst interaction.

The NCEDC is developing programs and procedures to replace waveforms collected for event analysis in near real-time with QC-ed waveforms from the UCB QC-ed waveform archive. This procedure will also be used to augment the NCSN event-based waveform collection from 1991 to 2006 with the appropriate waveforms from the UCB seismic networks.

6.5 Database Development

The NCEDC continues to support the Northern California Earthquake Management Center (NCEMC) by providing information and resources vital to the NCEMC's role of rapid earthquake analysis and data dissemination. The NCEDC receives earthquake parametric data in real-time from the NCEMC real-time systems and provides real-time access to the NCEDC database for *jiggle*, the CISN event analysis tool. The NCEMC continues to support the maintenance and distribution of the hardware configurations and instrument responses of the UCB, USGS/MP NCSN, and other seismic stations used by the NCEMC. During 2002-2004, the NCEDC and NCSN jointly developed a system consisting of an extensive spreadsheet containing per-channel information that describes the hardware of each NCSN data channel and provides each channel with a SEED-compliant channel name. This spreadsheet, combined with a limited number of files that describe the central-site analog digitizer, FIR decimation filters, and general characteristics of digital acquisition systems, allows the NCSN to assemble its station history in a format that the NCEDC can use to populate the hardware tracking and instrument response database tables for the NCSN. BSL staff currently chairs the CISN Schema Change working group, which coordinates all database schema changes and enhancements within the CISN.

The NCEDC instrument response schema represents full multi-stage instrument responses (including filter coefficients) for the broadband data loggers. The hardware tracking schema represents the interconnection of instruments, amplifiers, filters, and data loggers over time, and is used to describe all of the UC Berkeley and USGS stations and channels archived at the NCEDC.

The NCEDC has developed XML import and export procedures to provide better maintenance of the hardware tracking information and resulting instrument responses for stations in our database. When changes are made to either existing hardware or to station configurations, we export the current view in XML format, use a GUI-based XML editor to easily update the information, and import the changes back into the database. When adding new stations or hardware, we can easily use information from existing hardware or stations as templates for the new information. This allows us to treat the database as the authoritative source of information, and to use off-the-shelf tools such as the XML editor and XML differencing programs as part of our database maintenance procedures.

All NCSN event waveforms originally collected with the USGS CUSP processing system have been converted to MiniSEED, and are available along with the UC Berkeley data and data from the other networks archived at the NCEDC in full SEED format.

Additional details on the joint catalog effort and database schema development may be found at `http://www.ncedc.org/db`

6.6 Data Distribution

The NCEDC continues to use the World Wide Web as a principal interface for users to request, search for, and receive data from the NCEDC. In fall 2005, the NCEDC acquired the domain name *ncedc.org*. The NCEDC's Web address is now `http://www.ncedc.org/` In the 12 months from July 2009 through June 2010, the NCEDC distributed over 1816 GB of waveform data to external users.

Earthquake Catalogs

The NCEDC provides users with searchable access to Northern California earthquake catalogs and to the ANSS world-wide catalog via the Web. Users can search the catalogs by time, magnitude, and geographic region, and can retrieve either hypocenter and magnitude information or a full set of earthquake parameters including phase readings, amplitudes, and codas. Moment tensor and first motion mechanisms have been added to the NCEMC California earthquake catalog and are searchable from the NCEDC Web catalog search page.

Station Metadata

In addition to the metadata returned through the various data request methods, the NCECD provides dataless SEED volumes and SEED RESP files for all data channels archived at the NCEDC. The NCEDC currently has full SEED instrument responses for 17,985 data channels from 2,155 stations in 20 networks. This includes stations from the California Geological Survey (CGS) strong motion network that will contribute seismic waveform data for significant earthquakes to the NCEDC and SCEDC. In collaboration with the USGS NCSN and the NSMP (National Strong Motion Program), the NCEDC is building the metadata and dataless SEED volumes for over 300 stations and 2000 data channels of the NSMP dialup stations.

SeismiQuery

We ported and installed the IRIS *SeismiQuery* program at the NCEDC, which provides a common interface to query network, station, and channel attributes and query the availability of archived timeseries data.

DART (Data Available in Real Time)

The DART (Data Available in Real Time) represents the first step in the NCEDC's effort to make current and recent timeseries data from all networks, stations, and channels available to users in real time. The NCEDC

developed DART in December 2005 to provide a mechanism for users to obtain access to real-time data from the NCEDC. All real-time timeseries data streams delivered to the NCEDC are placed in MiniSEED files in a Web-accessible directory structure. The DART waveforms can be accessed by Web browsers or http command-line programs such as *wget*, a *FISSURES* waveform server, and a Berkeley-developed Simple Wave Server (SWS) which provides programmatic access to the DART data by specified SEED channel and time interval. We will be providing users with a client program to retrieve data from the SWS in the near future. The DART currently provide assess to the most recent 35 days of data.

We use the Freeorb software, an enhanced version of the open-source orb software developed by the IRIS-funded Joint Seismic Project (JSP), as the primary method for delivering real-time data to the NCEDC and into the DART. The freeorb package implements an object ring buffer (ORB) and orbserver, which provides a reliable storage ring buffer and an interface for orb client programs to read, write, and query the orbserver. Orbserver clients running at the NCEDC computer connect to remote orbservers at the BSL and USGS/Menlo Park, retrieve the MiniSEED timeseries data records, and write them to daily channel files in the NCEDC DART. Strain data from the EarthScope PBO network are delivered to the NCEDC using SeedLink and are inserted into the DART using a similar SeedLink client program.

The NCEDC developed an automated data archiving system to archive data from the DART on a daily basis. It allows us to specify which stations should be automatically archived, and which stations should be handled by the NCEDC's Quality Control program *calqc*, which allows an analyst to review the waveforms, retrieve missing data from stations or waveservers that may have late-arriving, out-of-order data, and perform timing corrections on the waveform data. The majority of data channels are currently archived automatically from the DART.

NetDC

In a collaborative project with the IRIS DMC and other worldwide datacenters, the NCEDC helped develop and implement *NetDC*, a protocol which will provide a seamless user interface to multiple datacenters for geophysical network and station inventory, instrument responses, and data retrieval requests. *NetDC* builds upon the foundation and concepts of the IRIS *BREQ_FAST* data request system. The *NetDC* system was put into production in January 2000 and is currently operational at several datacenters worldwide, including NCEDC, IRIS DMC, ORFEUS, Geoscope, and SCEDC. The *NetDC* system receives user requests via email, automatically routes the appropriate portion of the requests to the appropriate datacenter, optionally aggregates the responses from the various datacenters, and delivers the data (or FTP pointers to the data) to the users via email.

STP

In 2002, the NCEDC wrote a collaborative proposal with the SCEDC to the Southern California Earthquake Center, with the goal of unifying data access between the two data centers. As part of this project, the NCEDC and SCEDC are working to support a common set of 3 tools for accessing waveform and parametric data: *SeismiQuery*, *NetDC*, and *STP*.

The *Seismogram Transfer Program* or *STP* is a simple client-server program, developed at the SCEDC. Access to *STP* is either through a simple direct interface that is available for Sun or Linux platforms, or through a GUI Web interface. With the direct interface, the data are placed directly on a user's computer in several possible formats, with the byte-swap conversion performed automatically. With the Web interface, the selected and converted data are retrieved with a single FTP command. The *STP* interface also allows rapid access to parametric data such as hypocenters and phases.

The NCEDC has continued work on *STP*, working with the SCEDC on extensions and needed additions. We added support for the full SEED channel name (Station, Network, Channel, and Location), and are now able to return event-associated waveforms from the NCSN waveform archive.

EVT_FAST

In order to provide Web access to the NCSN waveform before the SEED conversion and instrument response for the NCSN has been completed, the NCEDC implemented *EVT_FAST*, an interim email-based waveform request system similar to the *BREQ_FAST* email request system. Users email *EVT_FAST* requests to the NCEDC and request NCSN waveform data based on the NCSN event ID. *EVT_FAST* event waveforms can be delivered in either MiniSEED or SAC format, and are now named with their SEED channel names.

FISSURES

The *FISSURES* project developed from an initiative by IRIS to improve earth scientists' efficiency by developing a unified environment that can provide interactive or programmatic access to waveform data and the corresponding metadata for instrument response, as well as station and channel inventory information. *FISSURES* was developed using CORBA (Common Object Request Broker Architecture) as the architecture to implement a system-independent method for the exchange of this binary data. The IRIS DMC developed a series of services, referred to as the *Data Handling Interface (DHI)*, us-

ing the *FISSURES* architecture to provide waveform and metadata from the IRIS DMC.

The NCEDC has implemented the *FISSURES Data Handling Interface (DHI)* services at the NCEDC, which involves interfacing the DHI servers with the NCEDC database schema. These services interact with the NCEDC database and data storage system and can deliver NCEDC channel metadata as well as waveforms using the *FISSURES* interfaces. We have separate *FISSURES DHI* waveform servers to serve archived and DART data streams. Our *FISSURES* servers are registered with the IRIS *FISSURES naming services*, which ensures that all *FISSURES* users have transparent access to data from the NCEDC.

GSAC

Since 1997, the NCEDC has collaborated with UNAVCO and other members of the GPS community on the development of the *GPS Seamless Archive Centers (GSAC)* project. This project allows a user to access the most current version of GPS data and metadata from distributed archive locations. The NCEDC is participating at several levels in the *GSAC* project: as a primary provider of data collected from core BARD stations and USGS MP surveys, and as a wholesale collection point for other data collected in Northern California. We helped to define database schema and file formats for the *GSAC* project and have produced complete and incremental monumentation and data holdings files describing the data sets that are produced by the BARD project or archived at the NCEDC so that other members of the *GSAC* community can provide up-to-date information about our holdings. Currently, the NCEDC is the primary provider for over 138,000 data files from over 1400 continuous and survey-mode monuments. The data holdings records for these data have been incorporated into the *GSAC* retailer system, which became publicly available in late 2002.

In addition, the NCEDC is archiving and distributing high-rate 1 Hz GPS data from most BSL-operated BARD stations in addition to the normally sampled 15 second or 30 second data. These high-rate data are now publicly available to the entire community.

6.7 Acknowledgements

The NCEDC is a joint project of the BSL and the USGS Menlo Park and is funded primarily by the BSL and the USGS Cooperative Agreements 07HQAG0013 and G10AC00093. Additional funding for the processing and archiving of the EarthScope PBO and SAFOD data were provided by EarthScope subawards EAR0732947-07-06 through UNAVCO.

Doug Neuhauser is the manager of the NCEDC. Stephane Zuzlewski, Rick McKenzie, Mario Aranha, Ingrid Johanson, Taka'aki Taira, Jennifer Taggart,and Peggy Hellweg of the BSL and David Oppenheimer, Hal Macbeth, Lynn Dietz, and Fred Klein of the USGS Menlo Park contribute to the operation of the NCEDC. Doug Neuhauser, Peggy Hellweg, and Stephane Zuzlewski contributed to the preparation of this section.

7 Data Acquisition and Quality Control

7.1 Introduction

Stations from the networks operated by the BSL transmit data continuously to the BSL facilities on the UC Berkeley campus for analysis and archival. In this section, we describe activities and facilities which pertain to the individual networks described in Operational Sections 1, 3, and 4, including procedures for data acquisition and quality control, and sensor testing capabilities and procedures. Some of these activities are continuous from year to year and have been described in prior BSL annual reports. In this section, we describe changes or activities which are specific to 2009-2010.

7.2 Data Acquisition Facilities

The computers and the associated telemetry equipment are now located in the campus computer facility in Warren Hall at 2195 Hearst Avenue. This building was constructed to current "emergency grade" seismic codes and is expected to be operational even after a M 7 earthquake on the nearby Hayward Fault. The hardened campus computer facility within was designed with special attention for post-earthquake operations. The computer center contains state-of-the art seismic bracing, UPS power and air conditioning with generator backup, and extensive security and equipment monitoring.

7.3 Data Acquisition

Central-site data acquisition for data from the BDSN/HRSN/NHFN/mPBO networks is performed by two computer systems in the Warren Hall data center (Figure 3.28). These acquisition systems also collect data from the Parkfield-Hollister electromagnetic array and the BARD network. A third system is used primarily for data exchange with the USNSN (U.S. National Seismograph Network) and transmits data to the USNSN from HOPS, CMB, SAO, WDC, HUMO, MOD, MCCM, and YBH. Data for all channels of the HRSN are now telemetered continuously from Parkfield to the BSL over the USGS T1 from Parkfield to Menlo Park, and over the NCEMC T1 from Menlo Park to Warren Hall.

The BSL uses the programs `comserv` and `qmaserv` developed by Quanterra for central data acquisition. These programs receive data from remote Quanterra data loggers and redistribute it to one or more client programs. The clients include `datalog`, which writes the data to disk files for archival purposes, `wdafill`, which writes the data to the shared memory region for processing with the network services routines, and other programs such as the seismic alarm process, the DAC480 system, and the feed for the Memento Mori Web page.

The two computers performing data acquisition are also "network services" computers that reduce waveforms for processing with the CISN software (Figure 3.29). To facilitate processing, each system maintains a shared memory region containing the most recent 30 minutes of data for each channel.

BDSN data loggers which use frame relay telemetry are configured to enable data transmission simultaneously to two different computers over two different frame relay T1 circuits to UCB. Normally, only one of these circuits is enabled. The `comserv/qmaserv` client program `cs2m` receives data and multicasts it over a private ethernet. The program `mcast`, a modified version of Quanterra's `comserv` program, receives the multicast data from `cs2m`, and provides a comserv-like interface to local comserv clients. Thus, each network services computer has a `comserv/qmaserv` server for every station, and each of the two systems has a complete copy of all waveform data.

We have extended the multicasting approach to handle data received from other networks such as the NCSN and UNR (University of Nevada, Reno). These data are received by Earthworm data exchange programs and are then converted to MiniSEED and multicast in the same manner as the BSL data. We use `mserv` on both network services computers to receive the multicast data and handle it in the same way as the BSL MiniSEED data.

In 2006, the BSL established a real-time data feed of all BSL waveforms between the BSL acquisition systems and the NCEDC computers using the open source Freeorb software. This allows the NCEDC to provide near-real-time access to all BSL waveform data through the NCEDC DART (Data Availabile in Real Time) system.

We monitor seismic stations and telemetry using the program `seisnetwatch`. This program extracts current information such as time quality, mass positions, and battery voltage and allows it to be displayed. If the parameter departs from the nominal range, the station is marked with yellow or red to indicate a possible problem.

7.4 Seismic Noise Analysis

BSL seismic data are routinely monitored for state-of-health. An automated analysis is computed regularly to characterize the seismic noise level recorded by each broadband seismometer.

PSD Noise Analysis

The estimation of the Power Spectral Density (PSD) of the ground motion recorded at a seismic station, as documented in the 2000-2001 BSL annual report

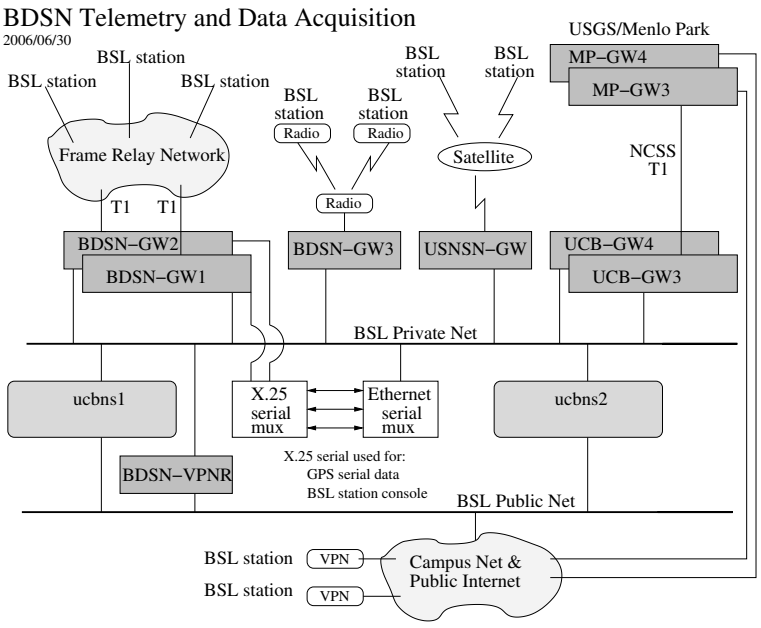

Figure 3.28: Data flow from the BDSN, NHFN, mPBO, HRSN, and BARD networks into the BSL central processing facility.

(`http://seismo.berkeley.edu/annual_report/`), provides an objective measure of background seismic noise characteristics over a wide range of frequencies. It also provides an objective measure of seasonal and secular variation in noise characteristics and supports early diagnoses of instrumental problems. In the early 1990s, a PSD estimation algorithm was developed at the BSL for characterizing the background seismic noise and as a tool for quality control. The algorithm generates a bar graph output in which all the BDSN broadband stations can be compared by component. We also use the weekly PSD results to monitor trends in the noise level at each station. Cumulative PSD plots are generated for each station and show the noise level in 5 frequency bands for the broadband channels. The plots make it easier to spot certain problems, such as failure of a sensor. In addition to the station-based plots, a summary plot is produced for each channel. The figures are presented as part of a noise analysis of the BDSN on the web at `http://www.seismo.berkeley.edu/seismo/bdsn/psd/`.

PDF PSD Noise Analysis

In addition to the PSD analysis developed by Bob Uhrhammer, the BSL has implemented the Ambient Noise Probability Density Function (PDF) analysis system developed by *McNamara and Buland* (2004). This system performs its noise analysis over all the data of a given time period (week or year), including earthquakes, calibration pulses, and cultural noise. This is in contrast to Bob Uhrhammer's PSD analysis, which looks at only the quietest portion of data within a day or week. Pete Lombard of the BSL extended the McNamara code to cover a larger frequency range and support the many different types of sensors employed by the BSL. Besides the originally supported broadband sensors, our PDF analysis now includes surface and borehole accelerometers, strain meters, and electric and magnetic field sensors. These enhancements to the PDF code, plus a number of bug fixes, were provided back to the McNamara team for incorporation in their work. The results of the PDF analysis are presented on the web at `http://www.ncedc.org/ncedc/PDF/`. One difficulty with using these plots for review of station quality is that it is necessary to look at data from each component separately. To provide an overview, we have developed summary figures for all components in two spectral bands, 32 - 128 s and 0.125 - 0.25 s (Figure 3.30). The figures are also available on the web at `http://seismo.berkeley.edu/~taira/NCEDC/NCEDC_PSD.html`.

7.5 Sensor Testing Facility

The BSL has an Instrumentation Test Facility in the Byerly Seismographic Vault where the characteristics of up to eight sensors can be systematically determined and compared. The test equipment consists of an eight-channel Quanterra Q4120 high-resolution data logger and a custom interconnect panel. The panel provides isolated power and preamplification, when required, to facilitate the connection and routing of signals from the sensors to the data logger with shielded signal lines. The vault also has a GPS rebroadcaster, so that all data loggers in the Byerly vault operate on the same time base. Upon acqui-

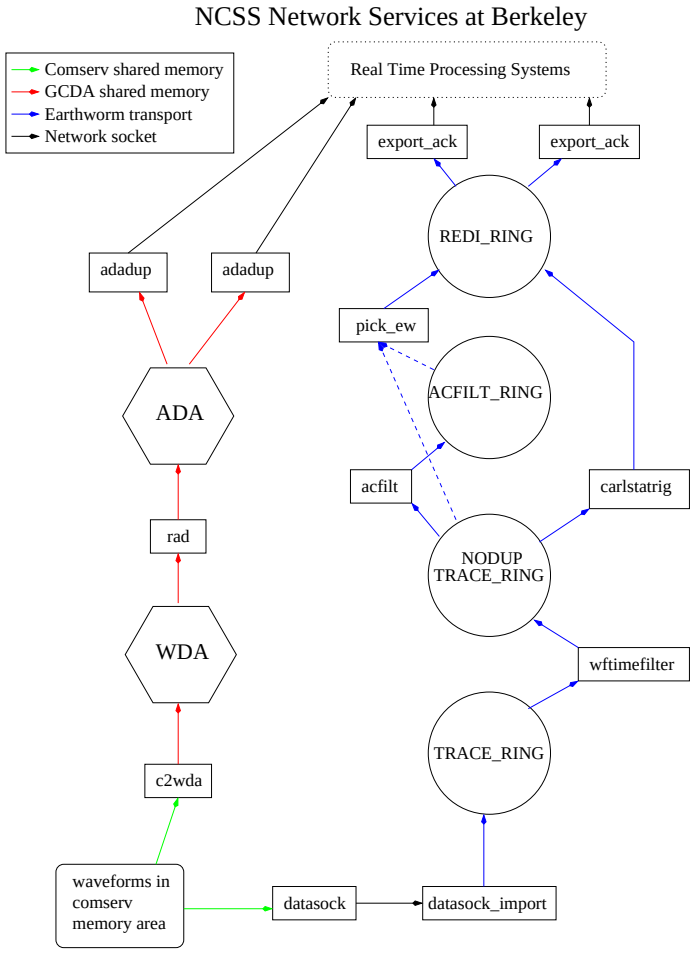

Figure 3.29: Flow of data from `comserv` areas through network services processing. One stream of the network services provides picks (and currently still provides codas) determined using the programs shown in the right flow path. Every 5 seconds, ground motion parameters are also determined, including PGA, PGV, PGD, and ML100 (left flow column). Parameters from the network services are available to the CISN software for event detection and characterization. Data are also logged to disk (via `datalog`), distributed to other computers (`mserv`), and spooled into a trace ring for export.

sition of data at up to 200 sps from the instruments under test, PSD analysis, coherence analysis, and other analysis algorithms are used to characterize and compare the sensor performance. Tilt tests and seismic signals with a sufficient signal level above the background seismic noise are also used to verify the absolute calibration of the sensors. A simple vertical shake table is used to assess the linearity of a seismic sensor. The sensor testing facility of the BSL is described in detail in the 2001-2002 Annual Report (`http://www.seismo.berkeley.edu/`).

Several projects made use of the sensor testing facility in 2009-2010. This included testing of the STS-1 type sensors being developed jointly by Metrozet and the BSL.

Enhanced Pressure Vessels for STS-1 Seismometers

As part of the NSF (National Science Foundation) funded STS-1 development grant, BSL has been working on the design, fabrication and testing of an enhanced pressure vessel for the original STS-1 seismometers. Originally, these seismometers were deployed on a glass base plate and covered with a glass dome that could be evacuated. Later the glass base plate was replaced by a warpless base plate developed by the Albequerque Seismological Laboratory (ASL). For either base plate, the dome was sealed against a rubber gasket only by the weight of the glass dome and atmospheric pressure, once air had been evacuated through a rubber stopper and glass stopcock. Vacuum leaks, and the resulting intrusion of atmo-

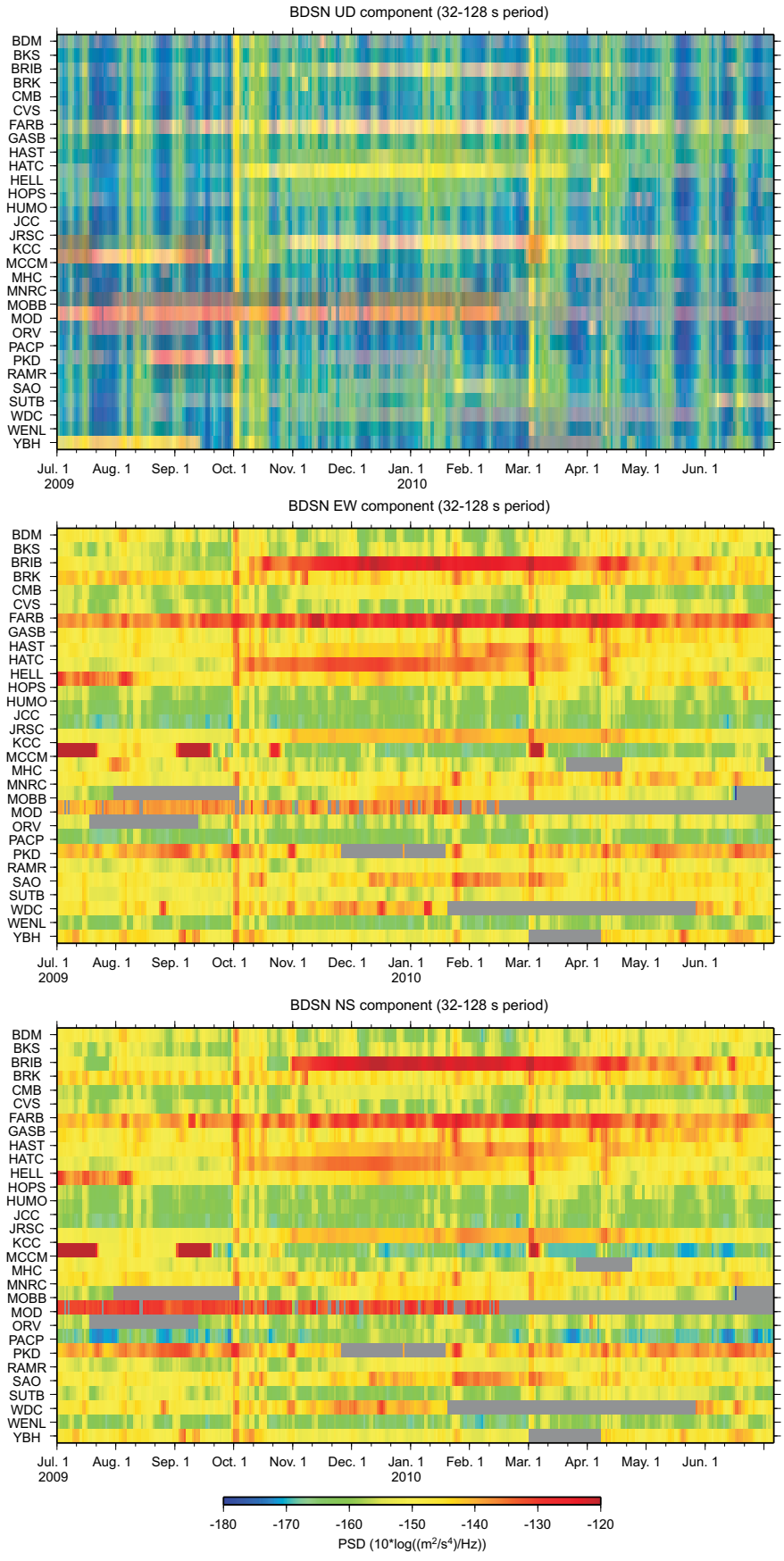

Figure 3.30: Annual summary of noise on all components of the broadband sensors of the BDSN for the band from 32 s to 128 s.

Figure 3.31: STS-1 seismometers in the Byerly Vault installed in a new pressure vessel (left) and on a warpless baseplate with a glass bell (right).

spheric humidity/moisture are believed to be the principal source of the long term degradation of the sensors.

The enhancements designed by the BSL are based on the pressure vessel design for the new MetroZet very broadband seismometers. The glass dome is replaced by an aluminum cover vessel, complete with a mounting flange and holes for bolting the cover in place. The cover is attached to a newly designed mounting ring, that attaches to the warpless baseplate. O-rings replace the flat gaskets used on both the original glass base plates and the later ASL warpless base plates. In addition, the BSL design eliminates the glass stopcock for the vacuum port. Two threaded holes were added to the mounting ring: one for a ball valve through which the vessel is evacuated, the second so that a vacuum gauge can be attached. If a solid state sensor were used in place of the vacuum gauge, the vacuum could be monitored continuously by sampling its output at a low rate. Figure 3.31 shows the test setup in the Byerly Vault.

One advantage of the newly designed vessel is that all seismometer components at a single site can be plumbed together to achieve a single, consistent level of pressure. Individual pressure differences seen by the seismometers would be eliminated and the vacuum within monitored by a single solid state pressure device.

BSL engineers have installed the enhanced pressure vessel and mounting ring at Byerly vault and are performing evaluation and comparison testing.

7.6 Acknowledgements

Doug Neuhauser, Bob Uhrhammer, Taka Taira, Peggy Hellweg, Pete Lombard, Rick McKenzie, and Jennifer Taggart are involved in the data acquisition and quality control of BDSN/HRSN/NHFN/MBPO data. Development of the sensor test facility and analysis system was a collaborative effort of Bob Uhrhammer, Tom McEvilly, John Friday, and Bill Karavas. IRIS (Incorporated Research Institutions for Seismology) and DTRA (Defense Threat Reduction Agency) provided, in part, funding for and/or incentive to set up and operate the facility, and we thank them for their support. Bob Uhrhammer, Taka Taira, Peggy Hellweg, Pete Lombard, Doug Neuhauser, and Barbara Romanowicz contributed to the preparation of this section.

7.7 References

Ekström, G. and M. Nettles, `http://www.seismology.harvard.edu/~ekstrom/Projects/WQC.html`, 2005.

Gardner, W. A., A unifying view of coherence in signal processing, Signal Processing, 29, p. 113-140, 1992.

Ingate, S. et al, Workshop Report from Broadband Seismometer Workshop, Lake Tahoe, CA, `http://www.iris.edu/stations/seisWorkshop04/report.htm`, 2004.

McNamara, D. and R. Buland, Ambient Noise Levels in the Continental United States *Bull. Seism. Soc. Am.*, 94, 4, 2004.

Scherbaum, Frank. Of Poles and Zeros: Fundamentals in Digital Seismology, Volume 15 of Modern Approaches in Geophysics, G. Nolet, Managing Editor, Kluwer Academic Press, Dordrecht, xi + 257 pp., 1996.

Tapley, W. C. and J. E. Tull, SAC - Seismic Analysis Code: Users Manual, *Lawrence Livermore National Laboratory*, Revision 4, 388 pp., March 20, 1992.

Wielandt, E. and G. Streckeisen, The leaf spring seismometer: design and performance, *Bull. Seis. Soc. Am., 72*, 2349-2367, 1982.

Wielandt, E. and Steim, J. M., A digital very broad band seismograph, *Annales Geophysicae*, 4 B(3), 227-232, 1986.

8 Northern California Earthquake Monitoring

8.1 Introduction

Routine earthquake analysis in Northern California has been unified since June 2009, with mirrored systems at the BSL and at the USGS in Menlo Park (see Operational Section 2). Processing begins as the waveforms arrive at the computers operating the real-time software, or AQMS software, and ranges from automatic processing for earthquake response to analyst review for earthquake catalogs and quality control.

In the mid 1990s, the BSL developed an automated earthquake notification system (*Gee et al.,* 1996; 2003a) called Rapid Earthquake Data Integration (REDI). This system determined earthquake parameters rapidly, producing near real-time locations and magnitudes of Northern and Central California earthquakes, estimates of the rupture characteristics and the distribution of ground shaking following significant earthquakes, and tools for the rapid assessment of damage and estimation of loss. Then, in 1996, a collaboration began between the BSL and the USGS for reporting on Northern and Central California earthquakes. Programs in Menlo Park and Berkeley were merged into a single earthquake notification system using data from the NCSN and the BDSN. The USGS and the BSL now form the Northern California Earthquake Management Center (NCEMC) of the California Integrated Seismic Network (Operational Section 2). Since June 2009, the AQMS software is the production software for earthquake reporting in the NCEMC.

With partial support from the USGS, the BSL is also participating in the development and assessment of a statewide prototype system for warning of imminent ground shaking in the seconds after an earthquake has initiated but before strong motion begins at sites that may be damaged. (See Research Study 19.)

8.2 Northern California Earthquake Management Center

In this section, we describe how the Northern California Earthquake Management Center fits within the CISN system. Figure 3.11 in Operational Section 2 illustrates the NCEMC as part of the the CISN communications ring. The NCEMC is a distributed center, with elements in Berkeley and in Menlo Park. The 35 mile separation between these two centers is in sharp contrast to the Southern California Earthquake Management Center, where the USGS Pasadena is located across the street from the Caltech Seismological Laboratory. As described in Operational Section 2, the CISN partners are connected by a dedicated T1 communications link, with the capability of falling back to the Internet. In addition to the CISN ring, the BSL and the USGS Menlo Park have a second dedicated communications link to provide bandwidth for shipping waveform data and other information between their processing systems.

Figure 3.32 provides more detail on the system operating at the NCEMC since mid-June, 2009. Now, complete earthquake information processing systems operate in parallel in Menlo Park and Berkeley. Incoming data from each network are processed locally at each of the two data centers in network services computers. The continuous reduced data, which include picks, codas, ground motion amplitudes, and ML100, are exchanged between the data centers and fed into both processing streams. Real time analysis is coordinated using up-to-date information from the local real-time database, which is replicated to the local data center database. Event review and automatic downstream processes such as computation of fault plane solutions access the internal data center databases. To maintain redundancy, robustness, and completeness, these two databases replicate each other across the Bay. They also replicate with the public database from which information is made available to the outside. The system includes the production of location and origin time as well as estimates of M_d, M_L, and M_w. For events with $M > 3.5$, ShakeMaps are also calculated on two systems, one in Menlo Park and one in Berkeley. Finite fault calculation is not yet integrated into the new processing system. It is only calculated at the BSL at this time.

This new system combines the advantages of the NCSN with those of the BDSN. The dense network of the NCSN provides rapid and accurate earthquake locations, low magnitude detection thresholds, and first-motion mechanisms. The high dynamic range data loggers, digital telemetry, and broadband and strong-motion sensors of the BDSN provide reliable magnitude determination, moment tensor estimation, calculation of peak ground motions, and estimation of source rupture characteristics. Robust preliminary hypocenters, or "Quick Looks" are published within about 25 seconds of the origin time. Event information is updated when preliminary coda magnitudes are available, within 2-4 minutes of the origin time. Estimates of local magnitude are generally available 30 seconds later, and other parameters, such as the peak ground acceleration and moment magnitude, follow within 1-4 minutes (Figure 3.33).

Earthquake information is now distributed to the web through EIDS and is available through the USGS Earthquake Notification Service (`http://ssleearthquake.usgs.gov/ens`). Organizations with the need for more rapid earthquake information should use CISN Display (`http://www.cisn.org/software/cisndisplay.`

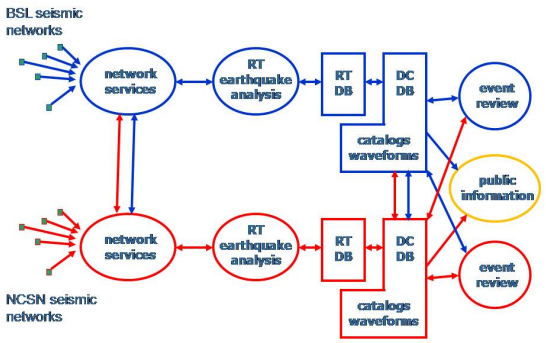

Figure 3.32: Details of the new Northern California processing system, which has been operational since mid-June, 2009. Network service processing, that is, production of picks, ground motion amplitudes, and other reduced information, occurs at both datacenters, and the information is exchanged. Complete earthquake information processing systems exist on both sides of the Bay, and up-to-date information is exchanged by database replication.

`htm`). The *recenteqs* site has enjoyed enormous popularity since its introduction and provides a valuable resource for information which is useful not only in the seconds immediately after an earthquake, but in the following hours and days as well.

8.3 2009-2010 Activities

Completed Transition to New Production System: AQMS Software

In June, 2009, we began operating the ANSS Quake Monitoring System (AQMS) software, formerly CISN Software, as the production system in the Northern California Seismic System (NCSS) for monitoring and reporting on Northern California earthquakes. This came as the result of a long effort to adapt and test software developed for the Trinet system and operating in Southern California. Over the course of the summer of 2009, systems at the USGS and UC Berkeley were updated, step-by-step. Now, nearly identical systems are operating at both locations. Very similar systems function in Southern California.

Data flow in the new Northern California system (Figure 3.34) has been modified to allow for local differences (such as very different forms of data acquisition and variability in network distribution). In addition, the BSL and the USGS want to minimize use of proprietary software in the system. One exception is the database program, Oracle. The NCEDC Oracle database hosts all earthquake information and parameters associated with the real time monitoring system. It is the centerpoint of the new system, providing up-to-date information to all processing modules. Reliability and robustness are achieved by continuously replicating the databases. The public, read-only, database provides event and parametric information to catalog users and the public.

During the last few years, BSL staff members, particularly Pete Lombard, have become extremely familiar with elements of the TriNet software. The software is now adapted for Northern California, with many adjustments and modifications completed along the way. For example, Pete Lombard adapted the TriNet magnitude module to Northern California. Pete made a number of suggestions on how to improve the performance of the magnitude module and has worked closely with Caltech and the USGS/Pasadena on modifications.

The BSL and the USGS Menlo Park are exchanging "reduced amplitude timeseries." One of the important innovations of the TriNet software development is the concept of continuous processing (*Kanamori et al.*, 1999). Waveform data are constantly processed to produce Wood Anderson synthetic amplitudes and peak ground motions. A program called `rad` produces a reduced timeseries, sampled every 5 seconds, and stores it in a memory area called an "Amplitude Data Area" or ADA. Other modules can access the ADA to retrieve amplitudes to calculate magnitude and ShakeMaps as needed. The BSL and the USGS Menlo Park have collaborated to establish tools for ADA-based exchange. The next step in improving reliability and robustness is to implement ADA exchange with Southern California as well.

Moment Tensor Solutions with `tmts` and Finite Fault Analysis

The BSL continues to focus on the unique contributions that can be made from the broadband network, including moment tensor solutions and finite fault analysis. `tmts` is a Java and web-based moment tensor processing system and review interface based on the complete waveform modeling technique of *Dreger and Romanowicz* (1994). The improved, web-based review interface has been operating in Northern California since July 2007. The automatically running version for real time analysis was extensively tested and updated by Pete Lombard, and has been running since June 2009. Reporting rules now allow automatically produced solutions of high quality to be published to the web.

From July 2009 through June 2010, BSL analysts reviewed many earthquakes in Northern California and adjoining areas of magnitude 2.9 and higher. Reviewed moment tensor solutions were obtained for 68 of these events (through 6/30/2010). Figure 3.35 and Table 3.13 display the locations of earthquakes in the BSL moment tensor catalog and their mechanisms. During this year,

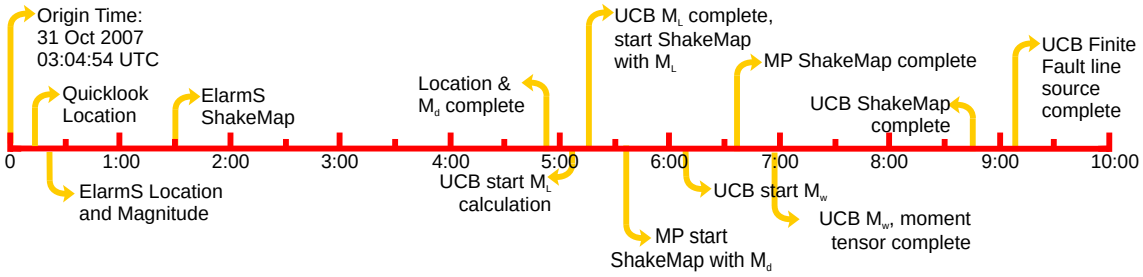

Figure 3.33: Illustration of the earthquake products timeline for the M_w 5.4 Alum Rock earthquake of October 30, 2007. Note that all processing was complete within 10 minutes of the origin time.

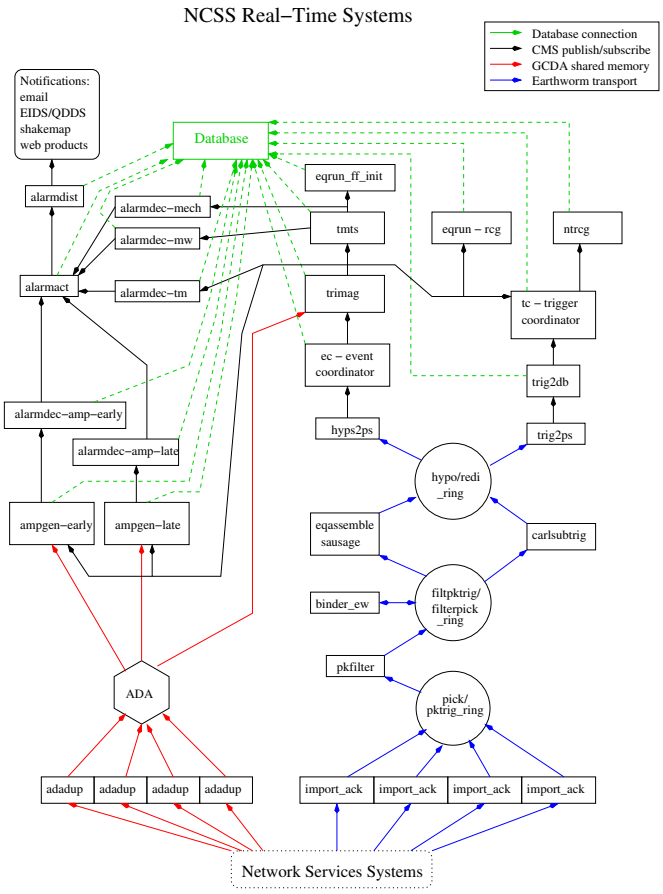

Figure 3.34: Schematic diagram of processing in the NCSS system. The design combines elements of the Earthworm, TriNet, and REDI systems

a finite fault inversion was produced for the January 9, 2010, offshore Ferndale earthquake which had a moment magnitude of M_w 6.5. For a report on the finite fault solution for that event, see Research Section 20.

8.4 Routine Earthquake Analysis

In fiscal year 2009-2010, more than 25,000 earthquakes were detected and located by the automatic systems in Northern California. This compares with over 21,500 in 2008-2009, 26,000 in 2007-2008, 23,000 in 2006-2007,

30,000 in 2005-2006 and 38,800 in 2004-2005. Many of the large number of events in 2004-2005 are aftershocks of the 2003 San Simeon and 2004 Parkfield earthquakes. Of the more than 25,000 events, about 124 had preliminary magnitudes of three or greater. Fourteen events had M_L or M_w greater than 4. The largest event recorded by the system occurred offshore of Ferndale on 09 January 2010. It had M_w 6.5.

Although BSL staff are no longer reading BDSN records for local and regional earthquakes (see Annual Report of 2003-2004), they are now participating in timing and reviewing earthquakes with `Jiggle`, mainly working on events from past sequences that have not yet been timed. This work contributes to improving the earthquake catalog for Northern California, but also ensures robust response capabilities, should the Menlo Park campus be disabled for some reason.

8.5 Acknowledgements

Peggy Hellweg oversees our earthquake monitoring system and directs the routine analysis. Peter Lombard and Doug Neuhauser contribute to the development of software. Rick McKenzie, Taka'aki Taira, Doug Dreger, Holly Brown, Sanne Cottaar, Shan Dou, Kelly Grijalva, Aurelie Guilhem, Ved Lekic, Rob Porritt, Jennifer Taggart, Amanda Thomas, Gilead Wurman, and Zhao Zheng contribute to the routine analysis of moment tensors. Peggy Hellweg, Doug Neuhauser, and Bob Uhrhammer contributed to the writing of this section. Partial support for the development, implementation and maintenance of the AQMS software is provided by the USGS.

8.6 References

Dreger, D., and B. Romanowicz, Source characteristics of events in the San Francisco Bay region, *USGS Open File Report 94-176*, 301-309, 1994.

Gee, L., J. Polet, R. Uhrhammer, and K. Hutton, Earthquake Magnitudes in California, *Seism. Res. Lett., 75(2)*, 272, 2004.

Gee, L., D. Neuhauser, D. Dreger, M. Pasyanos, R. Uhrhammer, and B. Romanowicz, The Rapid Earthquake Data Integration Project, *Handbook of Earthquake and Engineering Seismology*, IASPEI, 1261-1273, 2003a.

Gee, L., D. Dreger, G. Wurman, Y, Gung, B. Uhrhammer, and B. Romanowicz, A Decade of Regional Moment Tensor Analysis at UC Berkeley, *Eos Trans. AGU, 84(46)* , Fall Meet. Suppl., Abstract S52C-0148, 2003b.

Gee, L., D. Neuhauser, D. Dreger, M. Pasyanos, B. Romanowicz, and R. Uhrhammer, The Rapid Earthquake Data Integration System, *Bull. Seis. Soc. Am., 86,* 936-945, 1996.

Pasyanos, M., D. Dreger, and B. Romanowicz, Toward real-time estimation of regional moment tensors, *Bull. Seis. Soc. Am., 86,* 1255-1269, 1996.

Romanowicz, B., D. Dreger, M. Pasyanos, and R. Uhrhammer, Monitoring of strain release in central and northern California using broadband data, *Geophys. Res. Lett., 20,* 1643-1646, 1993.

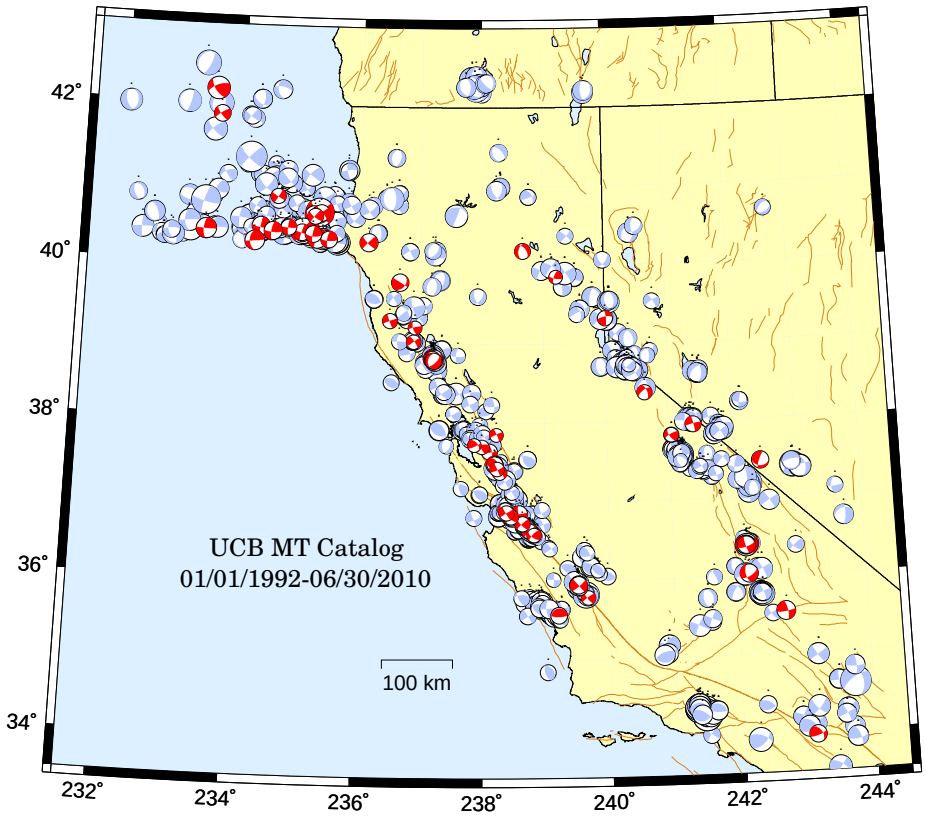

Figure 3.35: Map comparing reviewed moment tensor solutions determined by the BSL from past years (gray) with those from the fiscal year 2009-2010 (red/dark).

Location	Date	UTC Time	Lat.	Lon.	MT Depth	M_L	M_w	Mo	Str.	Dip	Rake
The Geysers, CA	7/7/2009	00:29:33.33	38.83	-122.81	5	3.26	3.76	8.00E+21	355	84	-150
The Geysers, CA	7/7/2009	05:03:30.30	38.84	-122.8	5	3.38	3.74	5.01E+21	351	87	-164
Ferndale, CA	7/7/2009	14:54:50.50	40.84	-125.39	11	3.27	3.55	2.66E+21	32	87	-6
Petrolia, CA	7/9/2009	19:24:34.34	40.3	-124.57	18	3.17	3.45	1.88E+21	185	89	-28
Petrolia, CA	7/12/2009	04:11:38.38	40.38	-125.48	5	3.29	3.63	3.43E+21	97	74	-150
Petrolia, CA	8/7/2009	10:49:35.35	40.31	-124.64	21	4.42	4.92	2.94E+23	286	88	-176
Qualeys Camp, NV	8/30/2009	19:21:22.22	37.95	-118.62	5	3.96	3.74	5.04E+21	256	84	-6
Templeton, CA	9/6/2009	03:20:56.56	35.56	-120.8	5	4.05	3.81	6.51E+21	89	75	94
Hollister, CA	9/6/2009	09:47:15.15	36.85	-121.41	8	4.17	3.87	8.01E+21	260	89	8
Aromas, CA	9/9/2009	18:45:52.52	36.9	-121.63	8	3.65	3.56	2.37E+21	239	69	28
Brentwood, CA	9/13/2009	22:53:17.17	37.85	-121.77	14	3.13	3.21	8.18E+20	336	81	-169
Talmage, CA	9/14/2009	04:33:08.8	39.03	-123.11	8	3.04	3.34	1.29E+21	234	88	-11
Willits, CA	9/17/2009	00:52:55.55	39.29	-123.5	8	3.16	3.45	1.84E+21	159	86	176
Pleasanton, CA	10/14/2009	03:27:41.41	37.64	-121.88	8	3.72	3.71	4.64E+21	84	83	25
Alum Rock, CA	10/15/2009	02:57:24.24	37.37	-121.72	8	3.31	3.39	1.51E+21	55	80	20
Spring Garden, CA	10/18/2009	15:47:30.30	39.85	-120.79	5	3.18	3.11	5.68E+20	102	72	159
The Geysers, CA	10/31/2009	06:52:24.24	38.79	-122.77	5	3.41	3.58	2.93E+21	192	84	141
Pinnacles, CA	11/1/2009	14:55:34.34	36.63	-121.25	11	3.75	3.55	2.63E+21	226	88	12
Petrolia, CA	11/4/2009	02:16:56.56	40.46	-125.66	18	3.4	4.17	2.23E+22	190	85	18
The Geysers, CA	11/24/2009	11:59:53.53	38.82	-122.79	8	3.36	3.67	3.96E+21	129	81	-163
Parkfield, CA	12/11/2009	03:50:44.44	35.94	-120.49	11	3.31	3.3	1.11E+21	325	86	161
The Geysers, CA	12/20/2009	12:26:26.26	38.79	-122.77	5	3.62	3.77	5.71E+21	274	86	34
Covelo, CA	12/22/2009	23:40:44.44	39.78	-123.34	11	3.65	3.96	1.09E+22	302	87	127
Incline Village, NV	12/23/2009	04:59:55.55	39.32	-119.99	11	3.54	3.49	2.11E+21	355	80	20
Redway, CA	1/4/2010	14:24:54.54	40.28	-123.87	30	3.67	4.12	1.91E+22	225	86	9
Milpitas, CA	1/7/2010	18:09:35.35	37.48	-121.8	8	4.35	4.05	1.65E+22	80	84	14
Milpitas, CA	1/8/2010	19:48:50.50	37.48	-121.79	8	3.81	3.73	4.83E+21	325	55	124
Ferndale, CA	1/10/2010	00:27:39.39	40.65	-124.69	24	5.82	6.5	7.06E+25	230	86	11
Ferndale, CA	1/10/2010	02:21:39.39	40.61	-124.78	11	4.23	4.41	5.13E+22	229	77	50
Ferndale, CA	1/10/2010	03:07:02.2	40.62	-124.7	11	3.51	3.97	1.11E+22	251	73	18
Petrolia, CA	1/10/2010	06:32:17.17	40.31	-124.63	21	3.64	4.12	1.91E+22	198	86	-8
Ferndale, CA	1/10/2010	11:48:32.32	40.64	-124.66	11	3.53	3.91	9.00E+21	231	84	-9
Petrolia, CA	1/11/2010	06:44:38.38	40.46	-124.85	11	3.51	4.05	1.50E+22	207	86	8
The Geysers, CA	1/30/2010	09:32:33.33	38.83	-122.8	5	3.4	3.61	3.28E+21	35	50	-66
Petrolia, CA	2/4/2010	20:20:22.22	40.41	-124.96	24	5.8	5.88	8.23E+24	215	82	9
Petrolia, CA	2/6/2010	04:05:05.5	40.37	-124.97	18	3.44	3.63	3.43E+21	115	73	153
Shandon, CA	2/7/2010	02:01:24.24	35.78	-120.34	8	3.55	3.39	1.54E+21	234	81	14
Tres Pinos, CA	2/8/2010	19:56:24.24	36.72	-121.36	8	3.56	3.5	2.20E+21	227	83	14
Parkfield, CA	2/11/2010	08:33:42.42	35.91	-120.47	11	3.16	3.43	1.71E+21	141	86	-174
Alum Rock, CA	3/3/2010	20:36:34.34	37.42	-121.76	8	3.37	3.37	1.43E+21	335	87	169
Petrolia, CA	3/4/2010	12:22:31.31	40.39	-124.98	24	3.4	3.9	8.84E+21	107	84	174
Cobb, CA	3/4/2010	17:47:02.2	38.84	-122.76	5	3.18	3.41	1.62E+21	51	61	-43
Petrolia, CA	3/6/2010	08:46:24.24	40.32	-124.73	18	4.28	4.53	7.71E+22	104	84	169
San Juan Bautista, CA	3/7/2010	06:14:12.12	36.81	-121.54	5	3.69	3.55	2.66E+21	221	84	19
Petrolia, CA	3/17/2010	00:05:17.17	40.45	-125.2	24	3.3	3.74	5.01E+21	93	85	171
Almanor, CA	3/17/2010	16:41:38.38	40.18	-121.33	11	3.72	3.71	4.56E+21	324	52	-122
Ferndale, CA	3/19/2010	23:10:40.40	40.6	-124.76	24	3	3.7	4.38E+21	219	82	15
Gold Beach, OR	3/22/2010	08:11:47.47	41.86	-126.39	24	3.55	3.88	8.17E+21	236	80	15
Parkfield, CA	3/25/2010	22:44:49.49	35.95	-120.51	11	3.38	3.4	1.59E+21	327	87	174
The Geysers, CA	3/28/2010	09:39:27.27	38.81	-122.82	5	2.96	3.65	3.70E+21	152	57	-119
Bridgeport, CA	4/2/2010	06:00:39.39	38.37	-119.38	11	3.91	3.56	2.75E+21	234	65	-34
Parkfield, CA	4/7/2010	22:40:30.30	35.94	-120.49	8	4.04	3.99	1.19E+22	140	89	-170
Pinnacles, CA	4/12/2010	11:37:46.46	36.58	-121.18	8	3.5	3.37	1.43E+21	224	74	29
Petrolia, CA	4/12/2010	15:10:05.5	40.31	-124.53	27	3.28	3.91	9.05E+21	93	75	161
Petrolia, CA	4/15/2010	08:36:07.7	40.27	-125.76	24	3.83	4.52	7.42E+22	85	87	139
The Geysers, CA	4/27/2010	23:07:21.21	38.82	-122.8	5	3.02	3.49	2.11E+21	155	68	-147
Fairview, CA	5/15/2010	17:54:43.43	37.7	-122	8	3.35	3.28	1.03E+21	156	78	154
Anderson Springs, CA	5/21/2010	03:18:45.45	38.79	-122.74	5	2.91*	3.02	4.22E+20	273	87	6
Lee Vining, CA	5/22/2010	17:06:07.7	37.82	-118.97	5	3.51	3.45	1.88E+21	67	62	34
Mammoth Lakes, CA	5/23/2010	04:45:44.44	37.82	-118.97	5	3.07	3.32	1.19E+21	242	75	23
Talmage, CA	5/28/2010	15:22:26.26	39.21	-123.09	8	3.01	3.18	7.30E+20	257	82	25
San Leandro, CA	5/30/2010	06:59:57.57	37.72	-122.12	5	3.18	3.2	7.75E+20	65	78	44
The Geysers, CA	6/1/2010	07:20:40.40	38.79	-122.81	5	2.92	3.3	1.13E+21	66	71	-29
Petrolia, CA	6/5/2010	09:05:26.26	40.4	-125.46	11	4.22	4.25	2.91E+22	94	77	164
Petrolia, CA	6/5/2010	21:28:04.4	40.37	-124.79	14	3.32	3.81	6.43E+21	189	82	23
Aromas, CA	6/12/2010	06:05:14.14	36.86	-121.61	11	3.84	3.57	2.79E+21	239	87	7
The Geysers, CA	6/14/2010	11:39:03.3	38.79	-122.78	5	3.35	3.66	3.82E+21	47	66	-74
San Francisco Zoo, CA	6/28/2010	14:47:04.4	37.74	-122.55	8	3.43	3.25	9.29E+20	308	79	141

Table 3.13: Moment tensor solutions for significant events from July 1, 2009 through June 30, 2010 using a complete waveform fitting inversion. Epicentral information is from the UC Berkeley/USGS Northern California Earthquake Management Center. Moment is in dyne-cm and depth is in km. The M_L marked with * is actually M_d.

9 Outreach and Educational Activities

9.1 Introduction

The BSL is involved in a variety of outreach activities ranging from lectures to lab tours and educational displays. Recorded information on current earthquake activity is updated regularly on our information tape (510-642-2160). Additional basic information on earthquakes and seismic hazards for northern and central California, as well as other information about seismology and our research, can be found on our extensive set of web pages at `http://seismo.berkeley.edu/`.

9.2 Highlights of 2009-2010

Michelle Bachelet Visit

Michelle Bachelet, President of Chile from 2006 to March 2010, visited UC Berkeley en route from Expo 2010 Shanghai China with a stop at the BSL, where Professors Barbara Romanowicz and Richard Allen briefed her on earthquake monitoring in California and the BSL's earthquake early warning project (Research Section 19).

Lawson Lecture

In this year's Lawson Lecture, Dr. Carol Prentice of the USGS spoke on "The Haiti Earthquake of 12 January 2010: A Geologic Perspective." Dr. Prentice discussed the tectonic setting and continuing seismic hazard of Hispaniola before moving on to some unusual results from her team's geological investigations of this complex event: They found only minor surface rupture along a short section of the major fault in southern Haiti, and they documented several areas of coastal uplift. She also touched on the tremendous damage and number of fatalities given the size of the event, caused largely by poor construction practices. The Lawson Lectures are webcast at `http://seismo.berkeley.edu/news/lawson_lecture`.

Vigilance 2010

Each year, the Office of Emergency Preparedness organizes an emergency preparedness and response exercise. This year's scenario "Vigilance 2010," involved a magnitude 5.5 earthquake on the Hayward Fault that lead to a hazardous material spill on campus. The BSL worked with staff at the Office of Emergency Preparedness to contribute damage descriptions for four UC Berkeley buildings affected in the scenario.

October 15, 2009: The Great California Shakeout

In addition to crouching under their desks at 10:15 AM shortly before the 20th anniversary of the Loma Prieta quake, BSL students, researchers, and staff were encouraged to review or make emergency preparedness plans and to pass on the seismic safety message to their friends, families, and communities.

Teacher Training

Earth science, and earthquakes, are studied in 6th and 9th grades, but are always of interest when the topic comes up in the news. The BSL has often contributed to and participated in training programs for teachers, to let them know about our current understanding of the earthquake hazard in the Bay Area and to impart to them some of the excitement we feel about our studies. A full day teacher training program on earthquakes was jointly organized by the BSL and the California State University East Bay (Hayward) geology program. On July 28, 2009, about 30 teachers listened to lectures on tectonics and earthquakes, with particular emphasis on the Bay Area. In the afternoon, the group went on a field trip to see where the Hayward Fault runs through downtown Hayward and Cal Memorial Stadium.

9.3 On-Going Activities

As in every year, tours and presentations formed an important part of BSL's public relations activities. Each year, several groups, ranging from middle-school students to scientists and engineers, tour our laboratory under the guidance of a graduate student or a member of the staff.

During 2009-2010 the BSL conducted several tours, with audiences ranging from local summer campers to undergraduates from Vancouver. In addition to the tours, Drs. Hellweg and Nadeau presented talks on earthquakes and related phenomena to public groups. Dr. Hellweg, Rick McKenzie, and graduate students Ana Luz Acevedo-Cabrera and Patrick Statz-Boyer also gave presentations to UC Berkeley's own ASUC senate.

Open House

The BSL again participated in *Cal Day*. This year, the lab was a designated stop in the Cal Day Passport, so young visitors received passport stickers as well as sample seismograms. Guests found their house or school amidst a Google Earth display of seismicity, viewed computer displays showing real-time seismic data and illustrating earthquake statistics and science concepts, jumped up and down to "make a quake," and played with the stick-slip model "earthquake machine." Graduate student volunteers were on hand to explain our exhibits and talk with visitors about UC Berkeley's role in earthquake monitoring.

Displays

The BSL provides local waveform feeds for helicorders at visitor centers associated with BDSN stations (CMB and MHC). Organizations such as LHS, KRON, and KPIX receive feeds from BKS via dedicated phone lines for display, while the USGS Menlo Park uses data from CMB for display in the lobby of the seismology building.

BSL on the Web

We continue to maintain and update our presence on the Internet. The Web pages are intended to provide a source of earthquake information for the public. They also present information about the networks we operate, including station profiles. This benefits the research community as well. The BSL Web pages publicize seminar schedules, advertise courses, and describe our research, as well as our operations. They offer updates on recent earthquake activity, details on Bay Area seismicity and hazards, and links to other earthquake and earth science servers. We also use the web server to distribute information internally among BSL personnel, with such details as the computing and operational resources, rosters, and schedules for various purposes.

Since September, 2008 the BSL has hosted its own blog, written by Horst Rademacher (`http://seismo.berkeley.edu/seismo.blog`). These pages are full of fascinating examples of geophysical science written with a clarity that can be appreciated by all. Many of this year's blog entries highlighted research and reconnaissance findings related to the offshore Ferndale, Haiti, and Chile quakes.

In the summer and fall of 2009, undergraduates Sam Peach, Matt DeMartini, and Chris Rawles, working under Dr. Kevin Mayeda, finished editing several outreach videos. New movies posted to the BSL outreach site include Dr. Peggy Hellweg's seismometer and model demonstrations, Dr. Richard Allen's discussion of the Earthscope project, and an updated film showing the Lawrence Hall of Science shake table in action. These videos are available at `http://seismo.berkeley.edu/outreach`

Earthquake Research Affiliates Program

The UC Berkeley Earthquake Research Affiliates (ERA) Program is an outreach project of the BSL. The purpose is to promote the support of earthquake research while involving corporations and governmental agencies in academic investigation and education activities such as conferences and field trips. The ERA program provides an interface between the academic investigation and practical application of earthquake studies.

9.4 Acknowledgements

Peggy Hellweg oversees the outreach activities at the BSL. Barbara Romanowicz, Bob Uhrhammer, Rick McKenzie, Jennifer Taggart, and many other faculty, staff, and students at the BSL contribute to the outreach activities. Jennifer Taggart and Peggy Hellweg contributed to the preparation of this section.

Glossary of Common Acronyms

Table 3.14: Standard abbreviations used in this report.

Acronym	Definition
ADA	Amplitude Data Area
ANSS	Advanced National Seismic System
ANSS NIC	ANSS National Implementation Committee
AQMS	ANSS Quake Monitoring System
ARRA	American Recovery and Reinvestment Act
BARD	Bay Area Regional Deformation
BAVU	Bay Area Velocity Unification
BDSN	Berkeley Digital Seismic Network
BSL	Berkeley Seismological Laboratory
CalEMA	California Emergency Management Agency
Caltrans	California Department of Transportation
CDF	California Department of Forestry
CGS	California Geological Survey
CISN	California Integrated Seismic Network
DART	Data Available in Real Time
EEW	Earthquake Early Warning
ElarmS	Earthquake Alarm Systems
EM	Electromagnetic
FACES	FlexArray along Cascadia Experiment for Segmentation
FEMA	Federal Emergency Management Agency
HRSN	High Resolution Seismic Network
InSAR	Interferometric Synthetic Aperture Radar
IRIS	Incorporated Research Institutions in Seismology
LBL	Lawrence Berkeley National Laboratory
LLNL	Lawrence Livermore National Laboratory
MARS	Monterey Accelerated Research System
MBARI	Monterey Bay Aquarium Research Institute
MOBB	Monterey Ocean Bottom Broadband Observatory
mPBO	Mini-Plate Boundary Observatory
MT	Magnetotelluric
MT	Moment Tensor
NCEDC	Northern California Earthquake Data Center
NCEMC	Northern California Earthquake Management Center
NCSN	Northern California Seismic Network
NCSS	Northern California Seismic System
NHFN	Northern Hayward Fault Network
NVT	Non-volcanic Tremor
PBO	Plate Boundary Observatory
PDF	Probability Density Function
PGV	Peak Ground Velocity

continued on next page

Table 3.14: *continued*

Acronym	Definition
PSD	Power Spectral Density
QDDS/EIDS	Quake Data Distribution System/Earthquake Information Distribution System
REDI	Rapid Earthquake Data Integration
RES	Repeating Earthquake Sequence
SAF	San Andreas Fault
SAFOD	San Andreas Fault Observatory at Depth
SEED	Standard for Exchange of Earthquake Data
SEM	Spectral Element Method
SHFN	Southern Hayward Fault Network
SOH	State of Health
SCSN	Southern Canifornia Seismic Network
UNAVCO	University NAVSTAR Consortium
USGS/MP	United States Geological Survey/ Menlo Park
USNSN	United States National Seismic Network

Appendix I: Publications, Presentations, Awards, and Panels 2009-2010

Publications

Abt, D., K. M. Fischer, S. W. French, H. A. Ford, H. Y. Yuan, and B. Romanowicz, North American Lithospheric Discontinuity Structure Imaged By Ps and Sp Receiver Functions, *J. Geophys. Res.*, in press, doi:10.1029/2009JB006914, 2010.

Allen, R.M., H. Brown, M. Hellweg, O. Khainovski, P. Lombard, D. Neuhauser, Real-time earthquake detection and hazard assessment by ElarmS across California, *Geophys. Res. Lett., 36*, L00B08, doi:10.1029/2008GL036766, 2009.

Allen, R.M., P. Gasparini and O. Kamigaichi (eds), Earthquake Early Warning, Special Issue, *Seism. Res. Lett., 80(5)* 682-782, 2009.

Allen, R.M., P. Gasparini, O. Kamigaichi, M. Böse, The Status of Earthquake Early Warning around the World: An Introductory Overview, *Seism. Res. Lett., 80(5)*, 682-693, doi: 10.1785/gssrl.80.5.682, 2009.

Audet, P., Temporal variations in crustal velocity structure near Parkfield, California, using receiver functions, *Bull. Seis. Soc. Am., 100*, doi:10.1785/0120090299, 2010.

Audet, P., M.G. Bostock, D.C. Boyarko, M.R. Brudzinski, R.M. Allen, Slab morphology in the Cascadia forearc and its relation to episodic tremor and slip, *J. Geophys. Res., 115* B00A16, doi:10.1029/2008JB006053, 2010.

Brown, H., R.M. Allen, V. Grasso, Testing ElarmS in Japan, *Seism. Res. Lett., 80(5)*, 727-739, doi: 10.1785/gssrl.80.5.727, 2009.

Brown, H., R.M. Allen, M. Hellweg, O. Khainovski, D. Neuhauser, and A. Souf, Development of the ElarmS methodology for earthquake early warning: Realtime application in California and offline testing in Japan, *Soil Dyn. and Earthquake Engin.* (in press), 2010.

Cammarano, F., B. Romanowicz, L. Stixrude, C. Lithgow-Bertelloni and W. Xu, Inferring the thermochemical structure of the upper mantle from seismic data, *Geophys. J. Int., 179(2)*, 1169-1185, 2009.

Cannata, A., M. Hellweg, G. Di Grazia, S. Ford, S. Alparone, S. Gresta, P. Montalto, D. Patanè, Long Period and Very Long Period events at Mt. Etna volcano: characteristics, variability and causality, and their implications for their sources. *J. Volc. Geotherm. Res., 187*, 227-249, 2009.

Chen, K-H., R. Bürgmann, and R.M. Nadeau, Triggering Effect of M 4-5 Earthquakes on the Earthquake Cycle of Repeating Events at Parkfield, California, *Bull. Seism. Soc. Am., 100(2)*, 522-531, doi:10.1785/0120080369, 2010.

Chen, K-H., R. Bürgmann, R.M. Nadeau, T. Chen and N. Lapusta, Postseismic variations in seismic moment and recurrence interval of small repeating events following the 2004 Parkfield earthquake, *Earth Planet. Sci. Lett.*, doi:10.1016/j.epsl.2010.08.027, in press, 2010.

Cupillard, P., and Y. Capdeville, On the amplitude of surface waves obtained by noise correlation and the capability to recover the attenuation: a numerical approach, *Geophys. J. Int., 181(3)*, 1687-1700, doi: 10.1111/j.1365-246X.2010.04586.x, 2010.

Cupillard, P., L. Stehly, and B. Romanowicz, The one-bit noise correlation: a theory based on the concepts of coherent and incoherent noise, *Geophys. J. Int.* (submitted).

Dziewonski, A. M., V. Lekic and B. Romanowicz, Mantle Anchor Structure: an Argument for Bottom up Tectonics, *Earth Planet. Sci. Lett.*, doi:10.1016/j.epsl.2010.08.013, 2010.

Eakin, C. M., Obrebski, M., Allen, R. M, Porritt, R., Brudzinski, M. R. and Boyarko, D. C., Seismic Anisotropy of Cascadia and the Mendocino Triple Junction: Interaction of the Subducting Slab with Mantle Flow, *Earth Planet. Sci. Lett.*, in press.

Farrell, J., R.B. Smith, T. Taira, W.-L. Chang, and C.M. Puskas, Dynamics and rapid migration of the energetic 2008-2009 Yellowstone Lake earthquake swarm, *Geophys. Res. Lett.*, doi:10.1029/2010GL044605, in press, 2010.

Ford, S. R., D. S. Dreger, and W. R. Walter, Source Analysis of the Memorial Day Explosion, Kimchaek, North Korea, *Geophys. Res. Lett., 36(21)*, L21304, 2009.

Ford, S. R., D. S. Dreger, and W. R. Walter, Identifying isotropic events using a regional moment tensor inversion, *J. Geophys. Res., 114(B1)*, B01306, 2009.

Guilhem, A., Z. Peng, and R.M. Nadeau, High-frequency signature of triggered non-volcanic tremors, *Geophys. Res. Lett., 37*, L16309, doi:10.1029/2010GL044660, 2010.

Johanson, I.A. and Bürgmann, R., Coseismic and postseismic slip from the 2003 San Simeon earthquake and their effects on backthrust slip and the 2004 Parkfield earthquake, *J .Geophys. Res., 115*, B07411, doi:10.1029/2009JB006599, 2010.

Jolivet, R., Bürgmann, R., and N. Houlié, Geodetic exploration of the elastic properties across and within the northern San Andreas fault zone, *Earth and Planetary Science Letters, 288(1-2)*, doi:10.1016/j.epsl.2009.1009.1014, 2009.

Kim, A., D. S. Dreger, and S. Larsen, Moderate earthquake ground motion validation in the San Francisco Bay Area, *Bull. Seism. Soc. Am., 100(2)*, 819-825, 2010.

Korneev, V.A. and R.M. Nadeau, Active Seismic Monitoring of the San Andreas Fault at Parkfield, in Active Geophysical Monitoring, Vol 40, Handbook of Geophysical Exploration: Seismic Exploration, Klaus Helbig and Sven Treitel, edited by Junzo Kasahara, Valeri Korneev and Michael Zhdanov, pp. 449-462, Elsevier, The Netherlands, 2010.

Lekic, V., J. Matas, M. Panning and B. Romanowicz, Reply to Comments on "Measurement and implications of frequency dependence of attenuation" by I. Morozov, *Earth Planet. Sci. Lett., 293(1-2)*, 216-217, doi:10.1016/j.epsl.2010.02.039, 2009.

Lekic, V., M. Panning and B. Romanowicz, A simple method for improving crustal corrections in waveform tomography, *Geophys. J. Int. 82(1)*, 265-278, 2010.

Malagnini, L., S. Nielson, K. Mayeda and E. Boschi, Self-similarity breakdown in seismic sources and implications for dynamic fault weakening, *J. Geophys. Res.*, doi:10.1029/2009JB006786, 2010.

Mayeda, K., and L. Malagnini, Source radiation invariant property of local and near-regional shear-wave coda: Application to source scaling for the Mw 5.9 Wells, Nevada sequence, *Geophys. Res. Lett. 37*, L07306, doi:10.1029/2009GL042148.

Nadeau, R.M. and A. Guilhem, Nonvolcanic Tremor Evolution and the San Simeon and Parkfield, California Earthquakes, *Science, 325*, 191-193, doi:10.1126/science.1174155, 2009.

Nadeau, R.M, F. Niu, and T. Taira, Seismic imaging of fault zone processes on the San Andreas Fault near Parkfield, *EarthScope OnSite Newsletter*, Winter 2010.

Panet, I., F. Pollitz, V. Mikhailov, M. Diament, P. Banerjee, K. Grijalva, Upper mantle rheology from GRACE and GPS postseismic deformation after the 2004 Sumatra-Andaman earthquake, *Geochem. Geophys. Geosys., 11*, Q06008, doi:10.1029/2009GC002905, 2010.

Panning, M., V. Lekic and B. Romanowicz, The importance of crustal corrections in the development of a new global model of radial anisotropy, *Geophys. J. Int.*, in press, 2010.

Rhie, J., and D. Dreger, A simple method for simulating microseism H/V spectral ratio in 3D structure, *Geosciences Journal, 13(4)*, 401-406, DOI 10.1007/s12303-009-0036-y, 2009.

Rhie, J., D. S. Dreger, M . H. Murray, and N. Houlie, Peak ground velocity shakemaps from geodetic slip models, *Geophys. Journ. Int.*, doi: 10.1111/j.1365-246X.2009.04327.x, 2009.

Rolandone, F., Bürgmann, R., Agnew, D.C., Johanson, I.A., Templeton, D.C., d'Alessio, M.A., Titus, S.J., DeMets, C., and Tikoff, B., Reply to Comment by J.C. Savage on "Aseismic slip and fault-normal strain along the creeping section of the San Andreas Fault", *Geophys. Res. Lett., 36(L13306)*, doi:10.1029/2009GL039167, 2009.

Roult, G., J. P. Montagner, B. Romanowicz et al., GEOSCOPE: Program progress and challenges in the last 30 years, *Seismolog. Res. Lett.*. in press, 2010.

Ryder, I., Bürgmann, R. and Sun, J., Tandem afterslip on connected fault planes following the 2008 Nima-Gaize (Tibet) earthquake, *J. Geophys. Res., 114(B03404)*, doi:10.1029/2009JB006423, 2010.

Shen, Z.-K., Sun, J., Zhang, P., Wan, Y., Wang, M., Bürgmann, R., Zeng, Y. , Gan, W., Liao, H., and Wang, Q., Slip maxima at fault junctions and rupturing of barriers during the 2008 Wenchuan earthquake, *Nat. Geosci., 2*, doi:10.1038/NGEO1636, 2009.

Shearer, P.M. and Bürgmann, R., Lessons learned from the 2004 Sumatra-Andaman megathrust rupture, *Ann. Rev. Earth Plan. Sci., 38*, doi:10.1146/annurev-earth-040809-152537, 2010.

Taira, T., P.G. Silver, F. Niu, R.M. Nadeau, Remote triggering of fault-strength changes on the San Andreas fault at Parkfield, *Nature, 461*, 636-639, doi:10.1038/nature08395, 2009.

Taira, T., R. B. Smith, and W.-L. Chang, Seismic evidence for dilatational source deformations accompanying the 2004-2008 Yellowstone accelerated uplift episode, *J. Geophys. Res., 115*, B02301, doi:10.1029/2008JB006281, 2010.

Tkalcic, H., D. S. Dreger, G. R. Foulger, and B. R. Julian, The puzzle of the 1996 Bardarbunga, Iceland, Earthquake: No volumetric component in the source mechanism, *Bull. Seism. Soc. Am., 99*, 3077-3085, doi:10.1785/0120080361, 2009.

Thomas, A.M., R.M. Nadeau, and R. Bürgmann, Tremor-tide correlations and near-lithostatic pore pressure on the deep San Andreas fault, *Nature, 462*, 1048-1051, doi:10.1038/nature08654, 2009.

Toh, A. and B. Romanowicz, Finite frequency effects on global S diffracted travel times, *Geophys. J. Int.*, doi:10.1111/j.1365-246X.2009.04359.x, 2009.

Walter, F., J. F. Clinton, N. Deichmann, D. S. Dreger, S. E. Minson, M. Funk, Moment tensor inversions of icequakes on Gornergletscher, Switzerland, *Bull. Seism. Soc. Am., 99(2A)*, doi:10.1785/0120080110, 2009.

Walter, F., D. S. Dreger, J. F. Clinton, N. Deichmann, M. Funk, Publications Evidence for near-horizontal tensile faulting at the base of Gornergletscher, a Swiss alpine glacier, *Bull. Seism. Soc. Am., 100(2)*, 458-472, 2010.

Xue, M. and R.M. Allen, Mantle Structure Beneath the Western US and its Implications for Convection Processes, *J. Geophys. Res., 115*, B07303, doi:10.1029/2008JB006079, 2010.

Yoo, S.-H., J. Rhie, H. Choi, K. Mayeda, Evidence for non-self-similarity and transitional increment of scaled energy in the 2005 West Off Fukuoka seismic sequence, *J. Geophys. Res.* doi:10.1029/2009JB007169, 2010.

Yuan, H., and K. Dueker, Relict Slab and Young Plume: Seismic View of the Present Time Wyoming Lithosphere, *Earth Science Frontiers (Chinese), 17(3)*, 127-138, 2010.

Yuan, H., and B. Romanowicz, Lithospheric layering in the North American craton, *Nature, 466(7310)*, 1063-1068, 2010a.

Yuan, H., B. Romanowicz, K. Fisher, and D. Abt, 3-D shear wave radially and azimuthally anisotropic velocity model of the North American upper mantle, *Geophys. J. Int.*, in revision, 2010.

Zhang, H., R. M. Nadeau, and M. N. Toksoz, Locating nonvolcanic tremors beneath the San Andreas Fault using a station-pair double-difference location method, *Geophys. Res. Lett., 37*, L13304, doi:10.1029/2010GL043577, 2010.

Presentations

5th APRU/AEARU Research Symposium on Multi-Hazards around the Pacific Rim, National Taiwan Normal University, Taipei, Taiwan, August 17-18, 2009.

Allen, R.M. Building and prototype advances earthquake alert system for California.

3rd International Conference on Advances in Experimental Structural Engineering and 2009 PEER Annual Meeting, San Francisco, CA, October 15-16, 2009

Hellweg, M., R. Allen, M. Böse, H. Brown, G. Cua, M. Fischer, D. Given, E. Hauksson, T. Heaton, T. Jordan, O. Khainovski, P. Maechling, D. Neuhauser, D. Oppenheimer, K. Solanki, ShakeAlert: Developing the Earthquake Early Warning System for California.

2009 Geological Society of America Annual Meeting: From Volcanoes to Vineyards: Living with Dynamic Landscapes, Portland, OR, October 18-21, 2009

Allen, R.M., D. Boyarko, M. Brudzinski, C. Eakin, M. Obrebski, R. Porritt, Structure and seismicity along Cascadia, Paper No. 18-7, *Geological Society of America: Abstracts with Programs, 41(7)*, 64, 2009.

Allen, R.M., M. Böse, H. Brown, G. Cua, D. Given, M. Fischer, E. Hauksson, T. Heaton, M. Hellweg, T. Jordan, O. Khainovski, P. Maechling, D. Neuhauser, D. Oppenheimer, K. Solanki, Warning California: Development of a statewide advanced earthquake alert prototype, Paper No. 164-2, *Geological Society of America: Abstracts with Programs, 41(7)*, 429, 2009.

Ticci, M., K. Kelson, C. Amos, A. Streig, and C. Brossy, Applications of LiDAR data and GIS derivatives for fault analysis and evaluation: Examples from three studies in California, paper 261-1, 2009.

3rd Annual ALOS PI Symposium, Hawaii, November 9-13, 2009

Ryder I., Bürgmann, R., and Fielding, E., Investigation of Normal Faulting Earthquakes in Tibet From ALOS PALSAR Data

Ryder I., Hartnett, A., Bürgmann, R., and Fielding, E., ALOS PALSAR Measurements of Deformation in the San Francisco Bay Area, California

FRINGE 2009 Workshop, Frascati, Rome, November 30 - December 3, 2009

Ryder, I., and Bürgmann, R., Inferences of normal fault structure and properties for six earthquakes in Tibet from InSAR

American Geophysical Union Fall Meeting, San Francisco, CA, December 14-18, 2009

Allen, R.M. The current status of earthquake early warning around the world, *Eos Trans. AGU, 90(52)*, Fall Meet. Suppl., Abstract S21C-01, 2009.

Allen, R.M., P. Audet, C. M. Eakin, S. Hung, M. J. Obrebski, F. F. Pollitz, R. W. Porritt Structure and process beneath the western US: Integrating disparate geophysical datasets, *Eos Trans. AGU, 90(52)*, Fall Meet. Suppl., Abstract U51D-02, 2009.

Alvarez, M., R. M. Allen, J. C. Fowler, B. C. Beaudoin, Then and Now, 25 Years of Progress Using Portable Arrays: The IRIS-PASSCAL Program, *Eos Trans. AGU, 90(52)*, Fall Meet. Suppl., Abstract U51C-0020, 2009.

Audet, P., Temporal variations in crustal scattering structure near Parkfield, California, using receiver functions, *Eos Trans., AGU, 90(52)*, Fall Meet. Suppl., Abstract S21A-1696, 2009.

Böse, M., R. M. Allen, H. Brown, G. B. Cua, D. Given, M. Fischer, E. Hauksson, T. H. Heaton, M. Hellweg, T. H. Jordan, O. Khainovski, P. J. Maechling, D. S. Neuhauser, D. H. Oppenheimer and K. Solanki, CISN ShakeAlert - Towards a Prototype Earthquake Early Warning System for California, *Eos Trans. AGU, 90(52)*, Fall Meet. Suppl., Abstract S21C-03, 2009.

Bostock, M.G., Audet, P., Christensen, N.I., Hyndman, R.D., Peacock, S.M. and Rondenay, S., The fate of water in the Cascadia unveiled by teleseismic imaging, *Eos Trans., AGU, 90(52)*, Fall Meet. Suppl., Abstract DI14A-01, 2009.

Boyarko, D., M. R. Brudzinski, R. M. Allen, R. W. Porritt, Non-volcanic tremor in Cascadia: Segmented along strike, anti-correlated with earthquakes, and offset from the locked zone, *Eos Trans. AGU, 90(52)*, Fall Meet. Suppl., Abstract T11C-1827, 2009.

Bürgmann, R., K-H. Chen, and R.M. Nadeau, Triggering Effect of 2004 M6 Parkfield Event on Earthquake Cycle of Small Repeating Events, *Eos Trans. AGU, 90(52)*, Fall Meet. Suppl., Abstract S51C-1446, 2009.

Brown, H., R.M. Allen, M. Böse, G. Cua, D. Given, E. Hauksson, M. Fischer, T. Heaton, M. Hellweg, T. Jordan, O. Khainovski, P. Maechling, D. Neuhauser, D. Oppenheimer, and K. Solanki, CISN ShakeAlert: Specification of the Prototype Earthquake Early Warning System, *Eos Trans., AGU, 90(52)*, Fall Meet. Suppl., Abstract 213A-1719, 2009.

Cottaar, S., Cupillard, P., McNamara, A.K., Romanowicz, B.A., Wenk, H.-R., Forward modeling the origin of seismic anisotropy at the base of the mantle, *Eos Trans., AGU, 90(52)*, Fall Meet. Suppl., Abstract DI41B-1800, 2009.

Cua, G.B., R. M. Allen, M. Böse, H. Brown, D. Given, M. Fischer, E. Hauksson, T. H. Heaton; M. Hellweg, T. H. Jordan, O. Khainovski, P. J. Maechling, D. S. Neuhauser, D. H. Oppenheimer and K. Solanki, CISN ShakeAlert: Three Years of Comparative Real-Time Earthquake Early Warning Testing in California, *Eos Trans. AGU, 90(52)*, Fall Meet. Suppl., Abstract S13A-1718, 2009.

Cupillard, P., Y. Capdeville, L. Stehly, J.-P. Montagner and B. Romanowicz, Spectral Element simulation of waveforms obtained by correlation of ambient seismic noise, *Eos Trans., AGU, 90(52)*, Fall Meet. Suppl., Abstract S42A-01, 2009 (invited).

Dolenc, D., Romanowicz, B.A., Ocean-bottom Broadband Seismic Stations as Tools to Identify and Montitor Seismic Hazard in Coastal Zones, *Eos Trans., AGU, 90(52)*, Fall Meet. Suppl., Abstract NH51B-1056, 2009 (invited).

Dou, S. and B.A. Romanowicz, Toward a 3D Global Attenuation Model in the Lower Mantle from the Earth's Free Oscillations, *Eos Trans., AGU, 90(52)*, Fall Meet. Suppl., Abstract DI23A-1655, 2009.

Dreger, D. S., S. R. Ford, and W. R. Walter, Moment tensor source analysis of the May 25, 2009 Nuclear test Kimchaek, North Korea, *EOS Trans. AGU, 90(52)*, Fall Meeting Suppl., Abstract S34D-01, 2009.

Dziewonski, A.M., V. Lekic, B.A. Romanowicz, Deep Earth Geopoetry: a Permanent Megastructure Above the Core-Mantle Boundary?, *Eos Trans., AGU, 90(52)*, Fall Meet. Suppl., Abstract U23D-0065, 2009.

Eakin, C.M., M. J. Obrebski, R. M. Allen, D. C. Boyarko, M. R. Brudzinski, E. Humphreys, A. Levander, L. O'Driscoll, R. W. Porritt, Y. Zhai, Seismic Anisotropy beneath Cascadia and the Mendocino Triple Junction: Interaction of the Subducting Slab with Mantle Flow, *Eos Trans., AGU, 90(52)*, Fall Meet. Suppl., Abstract DI52A-06, 2009.

Fischer, K.M., D.L. Abt, H. Yuan, B.A. Romanowicz, Lithospheric Discontinuities Beneath North America, *Eos Trans., AGU, 90(52)*, Fall Meet. Suppl., Abstract T44B-01, 2009 (invited).

Flanagan, M.P., S. Chang, S. van der Lee, H. Bedle, E. Matzel, M.E. Pasyanos, F. Marone, B.A. Romanowicz, C. Schmid, A.J. Rodgers, Three-Dimensional P- and S-velocity Structures and Radial Anisotropy in the Mantle along the Tethyan Margin, *Eos Trans., AGU, 90(52)*, Fall Meet. Suppl., Abstract T51B-1508, 2009.

Ford, S. R., D. S. Dreger and W. R. Walter, Network sensitivity solutions for regional moment tensor inversions, *EOS Trans. AGU, 90(52)*, Fall Meeting Suppl. Abstract S21B-1712, 2009.

Graveleau, F., J. Suppe, M. Ustaszewski, K. Chang, D. Stephane, and M.-H. Huang, Coseismic growth of the Tungshih anticline during the 1999 Chi-Chi Earthquake, Taiwan, *Eos Trans., AGU, 90(52)*, Fall Meet. Suppl., Abstract T23D-03, 2009.

Grijalva, K., R. Bürgmann, P. Banerjee, Using postseismic geodetic data to constrain the Sunda downdip transition zone, *Eos Trans., AGU, 90(52)*, Fall Meet. Suppl., Abstract T13E-01, 2009.

Grijalva, K., R. Bürgmann, K. Sieh, P. Banerjee, C. Vigny, D. Natawidjaja, I. Meilano, Impacts of the 2009 Sumatran earthquake and its relation to the great megathrust events, *Eos Trans., AGU, 90(52)*, Fall Meet. Suppl., Abstract U22B-06, 2009.

Guilhem, A., D. S. Dreger, and R. Uhrhammer, Towards continuous seismic scanning in the region of the Mendocino Triple Junction, California, *Eos Trans. AGU, 90(52)*, Fall Meet. Suppl., Abstract S33D-05, 2009.

Guilhem, A., Z. Peng, and R. M. Nadeau, Systematic search of non-volcanic tremor triggered by regional earthquakes along the Parkfield-Cholame section of the San Andreas Fault, *Eos Trans. AGU, 90(52)*, Fall Meet. Suppl., Abstract T23E-05, 2009.

Hellweg, M., D. S. Dreger and B. A. Romanowicz. Comprehensive Test Ban Monitoring: Contributions from Regional Moment Tensors to Determine Source Type and Depth, *Eos Trans., AGU, 90(52)*, Fall Meet. Suppl., Abstract S34C-03, 2009.

Huang, M.-H., Suppe, J., Kuo, Y.-T., Chen, Y.-G., and Hu, J.-C., The 3D Coseismic Deformation of the 1999 Mw 7.6 Chi-Chi Taiwan Earthquake, Obtained from Sub-Pixel Cross Correlation, *Eos Trans., AGU, 90(52)*, Fall Meet. Suppl., Abstract T23D-04, 2009.

Johanson, I. A., R. Bürgmann, A. Ferretti, and F. Novali, Variable Creep on the Concord fault from PS-InSAR and SBAS, *Eos Trans. AGU, 90(52)*, Fall Meet. Suppl., Abstract G23B-0693, 2009.

Khainovski, O., H. Brown, R.M. Allen, D. Neuhauser, and M. Hellweg, ElarmS: Big earthquakes in Japan and realtime testing in California, *Eos Trans., AGU, 90(52)*, Fall Meet. Suppl., Abstract S13A-1721, 2009.

Kim, A., D.S. Dreger, and T. Taira, Empirical Green's function waveform inversion method applied to the Parkfield SAFOD repeating earthquakes, *Eos Trans., AGU, 90*(52), Fall Meet. Suppl., Abstract S23B-1748, 2009.

Konter, J.G., J. Kellogg, S.R. Hart, L.H. Kellogg, B.A. Romanowicz, T.W. Becker, Mantle Heterogeneity: Length Scales and Correlations, *Eos Trans., AGU, 90(52)*, Fall Meet. Suppl., Abstract U42A-05, 2009.

Lekic, V. and B. Romanowicz, Joint inversion of long period waveform and surface wave dispersion data for crust and upper mantle structure using the Spectral Element Method, *Eos Trans., AGU, 90(52)* Fall Meet. Suppl., Abstract U23D-0060, 2009.

Lei, L., Bürgmann, R., TerraSAR-X InSAR Investigation of Active Crustal Deformation, *Eos Trans., AGU, 90(52)*, Fall Meet. Suppl., Abstract G23A-0670, 2009.

Milluzzo, V., S. Alparone, L. Cammarata, A. Cannata, S. Gambino, S. Gresta, M. Hellweg, P. Montalto Volcano-seismic events during 2004-2008 at Vulcano (Aeolian Islands, Italy): clues to the dynamics of the hydrothermal system, *Eos Trans., AGU, 90(52)*, Fall Meet. Suppl., Abstract V23D-2110, 2009.

Nadeau, R.M. and A. Guilhem, Nonvolcanic Tremor Evolution and the San Simeon and Parkfield, California Earthquakes, *Eos Trans. AGU, 90(52)*, Fall Meet. Suppl., Abstract T13D-1915, 2009.

Neuhauser, D.S., P. N. Lombard, L. D. Dietz, S. Zuzlewski, J. H. Luetgert, W. Kohler, M. Hellweg, D. H. Oppenheimer and B. A. Romanowicz, Robust Distributed Earthquake Monitoring with CISN software in Northern California, *Eos Trans. AGU, 90(52)*, Fall Meet. Suppl., Abstract S11B-1700, 2009.

Obrebski, M., R. M. Allen, S.-H. Hung, F.F. Pollitz, Cenozoic Plume-Slab Interaction Beneath the Pacific Northwest, *Eos Trans. AGU, 90(52)*, Fall Meet. Suppl., Abstract V41B-2179, 2009.

Panning, M.P., V. Lekic, B.A. Romanowicz, The importance of crustal corrections in global anisotropic modeling, *Eos Trans. AGU, 90(52)*, Fall Meet. Suppl., Abstract DI51A-04, 2009.

Peacock, S.M., Christensen, N.I., Bostock, M.G. and Audet, P., Pore fluid pressures, porosity, and permeability of the Cascadia subduction zone plate boundary, *Eos Trans., AGU, 90(52)*, Fall Meet. Suppl., Abstract DI14A-03, 2009.

Porritt, R. W., Allen, R. M., Moschetti, M. P., Lin, F., Ritzwoller, M. H., Shaprio, N. M., Brudzinski, M. R., Boyarko, D. C., O'Driscoll, L., Humphreys, G., Zhai, Y., Levander, A., Segmentation of the Cascades Volcanic Arc Revealed Through Ambient Noise Based Surface Wave Tomography, *Eos Trans. AGU, 90(52)*, Fall Meet. Suppl., Abstract V41B-2178, 2009.

Romanowicz, B.A., Progress and challenges in global mantle attenuation tomography, *Eos Trans. AGU, 90(52)*, Fall Meet. Suppl., Abstract S44A-01, 2009 (invited).

Romanowicz, B.A., T. Taira, D. Dolenc, P.R. McGill, and D.S. Neuhauser, Exploiting real time data from the Monterey Ocean Floor Broadband Observatory (MOBB), *Eos Trans., AGU, 90*(52), Fall Meet. Suppl., Abstract S51D-04, 2009.

Rowe, C., M. Maceira, R. M. Allen, M. J. Obrebski, L. Steck, Validation of 3D Ray-Theoretical and Finite-Frequency Tomographic Images of the Western U.S. Lithosphere: Comparison of Synthetic Seismograms Generated via the Spectral Element Method, *Eos Trans. AGU, 90(52)*, Fall Meet. Suppl., Abstract S33B-1763, 2009.

Scognamiglio, L., E. Tinti, A. Michelini, D. S. Dreger, A. Cirella, M. Cocco, L. Faenza, S. Mazza, Fast determination of moment tensors and rupture history: Application to the April 6, 2009 L'Aquila earthquake, *EOS Trans. AGU, 90(52)*, Fall Meeting Suppl. Abstract U23A-0028, 2009.

Statz-Boyer, P., T. Taira, R.M. Nadeau, and D.S. Dreger, Developing a Methodology for Observing Fault-Zone Frictional Properties from Repeating Earthquakes at Depth: Application to Postseismic Deformation Following the 2004 Parkfield Earthquake, *Eos Trans. AGU, 90(52)*, Fall Meet. Suppl., Abstract G23B-0695, 2009.

Stehly, L., P. Cupillard, B.A. Romanowicz, Numerical simulation of seismic Ambient noise in the 10-50s period band using the Spectral Element Methods, *Eos Trans. AGU, 90(52)*, Fall Meet. Suppl., Abstract S33A-1739, 2009.

Taira, T., P.G. Silver, F. Niu, and R.M. Nadeau, Remote Triggering of Fault-Strength Changes on the San Andreas Fault at Parkfield, *Eos Trans. AGU, 90(52)*, Fall Meet. Suppl., Abstract S14A-07, 2009 (invited).

Taira, T., R.B. Smith, and W.-L. Chang, Seismic evidence for dilatational source deformations accompanying the 2004-2008 Yellowstone accelerated uplift episode, *Eos Trans., AGU, 90*(52), Fall Meet. Suppl., Abstract S21B-1708, 2009 (invited).

Thomas, A., R. Bürgmann, and D. Dreger, The birth of a fault?: The nature of deformation at Lake Pillsbury, CA, *Eos Trans. AGU, 90(52)*, Fall Meet. Suppl., Abstract T23C-1937, 2009.

Tkalcic, H., D. S. Dreger, G. R. Foulger, B. R. Julian, and A. Fichtner, A seismological portrait of the anomalous 1996 Bardarbunga volcano, Iceland, earthquake, *EOS Trans. AGU, 90(52)*, Fall Meeting Suppl. Abstract S21B-1710, 2009.

Vinci, M., M. Hellweg, L. M. Jones, O. Khainovski, K. Schwartz, D. Lehrer, R. M. Allen and D. S. Neuhauser, CISN ShakeAlert: Using early warnings for earthquakes in California, *Eos Trans. AGU, 90(52)*, Fall Meet. Suppl., Abstract S13A-1720, 2009.

Walter, F., D. S. Dreger, J. F. Clinton, and N. Deichmann, Full and constrained moment tensor inversion of basal icequakes beneath Gornergletscher, Switzerland, *EOS Trans. AGU, 90(52)*, Fall Meeting Suppl. Abstract S21B-1709, 2009.

Yuan, H., B. Romanowicz, D. Abt, K. Fischer, Anisotropic domains in the North American upper mantle, *Eos Trans. AGU, 90(52)*, Fall Meet. Suppl., Abstract T44B-03, 2009.

Zhai, Y.; A. Levander; L. O'Driscoll; B. Schmandt; C. P. Ryan; E. Humphreys; R. W. Porritt; R. M. Allen, The Crust, the Slab Gap, the LAB, and the Mantle Wedge in the Mendocino Triple Junction Region, *Eos Trans. AGU, 90(52)*, Fall Meet. Suppl., Abstract U51D-08, 2009.

Zheng, Z. and B. Romanowicz, Efficient Computation of NACT Seismograms, *Eos Trans., AGU, 90(52)*, Fall Meet. Suppl., Abstract S33B-1775, 2009.

USGS/NEHRP Northern California Earthquake Hazards Workshop, USGS Menlo Park, January 26-27, 2010

Brown, H., M. Hellweg, R. Allen, O. Khainovski, D. Neuhauser, CISN Earthquake Early Warning.

Guilhem, A. and D. S. Dreger, Development and implementation of continuous moment tensor scanning for offshore seismicity and tsunami early warning.

Nadeau, R.M. and D.S. Dreger, UCB Borehole Network: Northern Hayward Fault Network (NHFN), High Resolution Seismic Network (HRSN-Parkfield).

Romanowicz, B., M. Hellweg and D. Neuhauser, Operation of the Northern California Earthquake Management Center (NCEMC): Collaboration between UC Berkeley and the USGS Menlo Park, CA.

Romanowicz, B.A., T. Taira, D. Dolenc, P.R. McGill, and D.S. Neuhauser, Exploiting real time data from the Monterey Ocean Floor Broadband Observatory (MOBB).

Taira, T., R.M. Nadeau and D.S. Dreger, Collaborative Research with UCB Borehole Network: Developing a Methodology for Observing Fault-Zone Frictional Properties from Repeating Earthquakes at Depth: application to Postseismic Deformation Following the 2004 Parkfield Earthquake.

Ninth International Workshop on Seismic Microzoning and Risk Reduction, Cuernavaca, Mexico, February 21-24, 2010

Hellweg, M., R.M. Allen, M. Böse, H. Brown, G.B. Cua, D. Given, M. Fischer, E. Hauksson, T.H. Heaton, T.H. Jordan, O. Khainovski, P.J. Maechliing, D.S. Neuhauser, D.H. Oppenheimer, K. Solanki, CISN ShakeAlert - Towards a Prototype Earthquake Early Warning System for California.

USGS Workshop on real-time GPS, Boulder, CO, March 12, 2010

B. Romanowicz and I. Johanson, Integration of geodetic and seismic data (invited)

2010 Annual Graduate Student Meeting, Paris, France, March 15-19, 2010

Guilhem, A. and D. S. Dreger, A Continuous Moment Tensor Analysis in the Region of the Mendocino Triple Junction, California.

Workshop on Innovative Approaches to Planetary Seismology, KISS, Caltech, Pasadena, CA, March 15-19, 2010

Romanowicz, B.A., Planetary seismology: Inspiration from recent Earth studies.

EarthScope workshop, North American Cratonic Interior in the U.S. Midcontinent, Urbana-Champaign Illinois, April 11-13, 2010

Yuan, H., B. Romanowicz, Anisotropic stratification in the North American upper mantle.

Seismological Society of America, Annual Meeting, Portland, OR, April 21-23, 2010

Dreger, D. S., A. Kim, and S. Larsen, Moderate earthquake ground motion validation in the San Francisco bay area, *Seism. Res. Lett, 81(2)*, 310, 2010.

Dreger, D. S., J. Murray-Moraleda, and J. Svarc, Slip-distribution and kinematic rupture process of the January 9, 2010 Mw 6.5 Gorda Plate event, *Seism. Res. Lett, 81(3)*, 538-546, DOI: 10.1785/gssrl.81.3.538, 2010.

Dreger, D.S., R.M. Nadeau, A. Kim, P. Statz-Boyer and A. Acevedo-Cabrera, Finite-Source Parameters and Scaling of Micro-Repeating Earthquakes at Parkfield, *Seism. Res. Lett., 81(2)*, 374, 2010.

Guilhem, A., D. S. Dreger, and R. Uhrhammer, A continuous moment tensor analysis in the region of the Mendocino Triple Junction, California, *Seism. Res. Lett., 81(2)*, 289, 2010.

Hellweg, M., R. Darragh, W. Silva, Exploring the lower limits of the NGA using data from California, *Seismol. Res. Lett., 81(2)*, 291, 2010.

Hellweg, M., R. McPherson, D.S. Dreger, L. Dengler, J.C. Rollins, R.S. Stein, The 2010 M 6.5 and M 5.9 Offshore Ferndale Earthquakes: Seismicity, Seismic History and Stress., *Seismol. Res. Lett., 81(3)*, page TBA, 2010.

Mayeda, K. and L. Malagnini, Regional Variations in Apparent Stress Scaling from Coda Envelopes, *Seism. Res. Lett., 81(2)*, 253, 2009.

McPherson,R., M.A. Hemphill-Haley, D.S. Dreger, M. Hellweg, J.S. Rollins, Geodetic and Seismologic Evidence for a Locked Southern Margin of the Cascadia Subduction Zone. *Seismol. Res. Lett., 81(3)*, page TBA, 2010.

Obrebski, M.J., Allen, R., Pollitz, F., Hung, S.-H., Lithosphere-Asthenosphere Interaction Beneath the Pacific Northwest From the Integrated Analysis of Body and Surface Waves, *Seism. Res. Lett., 81(2)*, 363, 2010.

Porritt, R. W., Allen, R. M., Shaprio, N. M., Brudzinski, M. R., Boyarko, D. C., O'Driscoll, L., Humphreys, G., Zhai, Y., Levander, A., Imaging Shallow Cascadia Structure with Ambient Noise Tomography, *Seism. Res. Lett., 81(2)*, 336, 2010.

Romanowicz, B. A., Storms, infragravity waves and possible sources of the Earth's vertical and horizontal hum, *Seism. Res. Lett., 81(2)*, 363, 2010 (invited).

Thomas, A., Burgmann, R, and D. Dreger., The birth of a fault?: The nature of deformation at Lake Pillsbury, CA, *Seism. Res. Lett., 88(2)*, 338, 2010.

Zechar, J.D. and R.M. Nadeau, Forecasts of repeating microearthquakes near Parkfield, California, *Seism. Res. Lett., 81(2)*, 363, 2010.

European Geoscience Union, 2010 General Assembly, Vienna, Austria, May 2-7, 2010

Audet, P. and Burgmann, R., Effective elastic thickness, mechanical anisotropy and the supercontinent cycle, *Geophysical Research Abstracts, 12*, EGU2010-12381.

Geologic Society of America Cordilleran Section Meeting 2010, May 27-29, Anaheim, CA

Amos, C.B., K.I. Kelson, D.H. Rood, D.T. Simpson, R.S. Rose, Active Internal Deformation of the Sierra Nevada Microplate on the Kern Canyon Fault at Soda Spring, Tulare County, California, paper 20-7, 2010.

IRIS 2010 Workshop, Snowbird, UT, June 9-11, 2010

Allen, R.M., M.J. Obrebski, F. Pollitz, S. Hung, Lithospheric-asthenospheric interactions beneath the western US: Modification of the North American Craton.

Cottaar, S., McNamara, A.K., Romanowicz, B.A., Wenk, H.-R., Forward modeling the origin of seismic anisotropy at the base of the mantle.

CIDER 2010 Summer Program, Santa Barbara, CA, June 12- July 23, 2010

Cottaar, S., McNamara, A.K., Romanowicz, B.A., Wenk, H.-R., Forward modeling the origin of seismic anisotropy at the base of the mantle.

Dou, S., and B.A. Romanowicz, Towards a three-dimensional attenuation model of the lower mantle from the normal modes of the Earth's free oscillations.

Speaking Engagements

Allen, R.M., M. Obrebski, M. Xue, S.-H. Hung, Plume vs. plate: Convective interactions in the mantle beneath North America, Department of Geosciences, National Taiwan University, Taipei, Taiwan, August 2009.

Allen, R.M., Earthquake early warning: Status and opportunities, Presentation to the BART Board at the Berkeley Seismological Laboratory, UC Berkeley, Berkeley, CA, September 2009.

Allen, R.M., Earthquake early warning for High Speed Rail, Presentation to the California High Speed Rail Planning Group, San Francisco, CA, September 2009.

Allen, R.M., Making, shaping and breaking a continent: Structure and evolution of North America, Earthscope Science Planning Workshop, Salt Lake City, UT, October 2009.

Allen, R.M. Warning California: Developing ShakeAlert, seminar at KIGAM (Korea Institute of Geoscience and Mineral Resources), Daejeon, South Korea, November 2009.

Allen, R.M., Warning California: Developing ShakeAlert, Northern California Chapter meeting of the Earthquake Engineering Research Institute, San Francisco, CA, November 2009.

Allen, R.M., Warning California: Developing ShakeAlert, Earth Section seminar, Scripps Institution of Oceanography, San Diego, CA, November 2009.

Allen, R.M., First Jolt: ShakeAlert for the next big earthquake in California, Los Alamos National Laboratory, Los Alamos, CA, January 2010.

Allen, R.M., First Jolt: ShakeAlert for the next big earthquake in California, Department of Earth Science, UC Santa Barbara, Santa Barbara, CA, January 2010.

Allen, R.M., and M. Hellweg, First Jolt: ShakeAlert for the next big earthquake in California, San Francisco Planning and Urban Research Association (SPUR), March 2010.

Allen, R.M., and M. Hellweg, First Jolt: ShakeAlert for the next big earthquake in California, San Francisco Disaster Council, San Francisco, CA, April 2010.

Allen, R.M., and M. Hellweg, First Jolt: ShakeAlert for the next big earthquake in California, San Francisco Lifelines Council, San Francisco, CA, April 2010.

Amos, C.B., Geomorphic insights into active thrust faults: New Zealand examples, University of Nevada, Reno, NV, March 23, 2010.

Audet, P., The seismic signature of water in the forearc of Cascadia, Department of Terrestrial Magnetism Seminar, Carnegie Institution of Washington, Washington, D.C., November 4, 2009.

Audet, P., The supercontinent cycle: A role for plate strength?, Berkeley Seismological Laboratory Seminar, UC Berkeley, Berkeley, CA, March 9, 2010.

Bürgmann, R., Active Tectonics and Non-Tectonics of the San Francisco Bay Area from Space Geodesy, "Frontiers in Earth Sciences" Lecture Series, Ludwig Maximillian Univ., Munich, Germany, July 13, 2009.

Bürgmann, R., Active Tectonics and Non-Tectonics of the San Francisco Bay Area from PS-InSAR, Tele-Rilevamento Europa, Milano, Italy, July 21, 2009.

Bürgmann, R., Lithosphere and Fault Rheology from Earthquake Cycle Deformation, INGV Bologna, Bologna, Italy, July 23, 2009.

Bürgmann, R., New Insights into the San Andreas Fault System from Space Geodesy and the next Generation of Crustal Deformation Models, Loma Prieta Earthquake Commemorative Symposium, San Francisco, CA, October 19, 2009.

Bürgmann, R., Probing The Rheology And Localization Of Deformation In The Lower Crust: Evidence From Postseismic Relaxation And Tremor, Caltech, Pasadena, CA, November 23, 2009.

Bürgmann, R., Postseismic Relaxation, Slow Slip and Tremor: Rheology of the Lithosphere and Faults, EOS Nanyang Technological University, Singapore, June 26, 2010.

Dreger, D., Realtime Operations at the Berkeley Seismological Laboratory, University of Chile, Santiago, Chile, November 16, 2009.

Dreger, D., Source-Type Identification using Regional Moment Tensors, University of Chile, Santiago, Chile, November 18, 2009.

Dreger, D., Regional Moment Tensor Analysis for Source-Type Identification, Air Force Technical Applications Center (AFTAC), Satellite Beach, Florida, January 14, 2010.

Dreger, D., Multi-Scale Observations of Earthquake Rupture Kinematics at Parkfield, National Central Taiwan University, Taipei, Taiwan, March 22, 2010.

Dreger, D., Seismic Source-Type Identification and Moment Tensors of Exotic Events, National Central Univerity, Taipei, Taiwan, March 26, 2010.

Dreger D.S. and R.M. Nadeau, Berkeley Seismological Laboratory Hayward Fault Network / Caltrans Borehole Bridge Network, California Department of Transportation, Sacramento, CA, June 25, 2010 (invited).

Guilhem, A., Detection de seismes en temps reels avec tenseurs des moments en Californie, Commissariat a l'energie atomique (CEA), Laboratoire de Sismologie Operationnelle, Bruyeres le Chatel, France, March 5, 2010.

Guilhem, A., Detection de seismes en temps reels avec tenseurs des moments en Californie, Ecole et Observatoire des Sciences de la Terre, EOST seminar, Strasbourg, France, March 9, 2010.

Guilhem, A., Detection de seismes en temps reels avec tenseurs des moments en Californie, University of Nice, Seismological Laboratory, Nice, France, March 11, 2010.

Guilhem, A., Detection et analyse de seismes lents et reguliers en Californie a l'aide des tenseurs des moments, Institut de Physique du Globe de Paris (IPGP), Seismological Laboratory, Paris, France, March 30, 2010.

Hellweg, M., Listening Carefully: What can we learn from earthquakes?, Annual Meeting of the American Academy of Opthamology, San Francisco, CA, October 23-28, 2009.

Hellweg, M., Just a Moment: From Regional Seismograms to Earthquake (and Other) Sources, Instituto Nazionale de Geofisico e Vulcanologia, Catania, July 2, 2009.

Hellweg, M., Just a Moment: From Regional Seismograms to Earthquake (and Other) Sources, Instituto Nazionale de Geofisico e Vulcanologia, Rome, July 7, 2009.

Hellweg, M., A tectonic timebomb: The Hayward Fault, UC Berkeley ASUC, Berkeley, CA, November 18, 2009.

Hellweg, M., Earthquakes in our backyards, San Ramon Rotary Club, San Ramon, CA, November 18, 2009.

Huang, M.-H., The 3D Coseismic Deformationof the 1999 Mw 7.6 Chi-Chi Taiwan Earthquake, Obtained from Sub-Pixel Cross Correlation, Earthquake Science Center Seminars, USGS, Menlo Park, CA, June 2, 2010.

Johanson, I.A., Stable and transient motion on Kilauea's south flank from InSAR Persistent Scatterers, Berkeley Seismological Lab Seminar, UC Berkeley, Berkeley, CA, September 1, 2009.

Nadeau, R.M., Repeating Earthquakes: Scaling, Fault Mechanics, Forecasting, and Monitoring, National Taiwan Normal University, Taipei, Taiwan, November 10, 2009 (invited).

Nadeau, R.M., Nonvolcanic Tremor Evolution and the San Simeon and Parkfield, California Earthquakes, Institute of Earth Sciences, Academia Sinica, Taipei, Taiwan, November 11, 2009 (invited).

Nadeau, R.M., Nonvolcanic Tremor Evolution and the San Simeon and Parkfield, California Earthquakes, Berkeley Seismological Laboratory Seminar Series, UC Berkeley, Berkeley, CA, November 24, 2009 (invited).

Nadeau, R.M., Science presentation: The 2009 Haiti Earthquake and related topics on earthquakes, Ecole Bilingue de Berkeley, K1 class, Berkeley, CA, January 20, 2010 (invited).

Nadeau, R.M., Seismic Indicators of Deep Fault Process on the San Andreas Fault: Repeating Earthquakes and Non-volcanic Tremor, Symposium on Lithospheric Deformation–Turning Observations Into Models, Bochum, Germany, May 25-28, 2010 (invited).

Nadeau, R.M., Nonvolcanic Tremor Response to Moderate Earthuakes and Earth-Tides along the San Andreas Fault, California, Fachrichtung Geophysik Seminar, Freie Universitaet, Berlin, Germany, May 31, 2010 (invited).

Nadeau, R.M., Repeating Earthquakes: Persistent Asperities through Creep Rates High and Low, Special Seminar, ETH Swiss Seismological Service, Zurich, Switzerland, June 2, 2010 (invited).

Porritt, R. W., From Iris Intern to PhD Candidate, IRIS Internship Orientation, Socorro, NM, June 1st, 2010.

Porritt, R. W., Intro to Shells and GMT, IRIS Internship Orientation, Socorro, NM, June 2nd, 2010.

Porritt, R. W., Introduction to Broadband Processing with Matlab, IRIS Internship Orientation, Socorro, NM, June 3rd, 2010.

Romanowicz, B.A., Resolving the lithosphere-asthenosphere under cratons: The case of North America, Institute of Geophysics, China Academy of Sciences, Beijing, China, October 12, 2009.

Romanowicz, B.A., New insights from seismic waveform tomography, National Taiwan University, Taipei, Taiwan, October 13, 2009.

Romanowicz, B.A., Women in Science: My own case study, Tongji University, Shanghai, China, October 17, 2009.

Romanowicz, B.A., The Earth's Hum: Bridging the gap between seismology and oceanography, Tongji University, Shanghai, China, October 18, 2009.

Romanowicz, B.A., Women in Science: My own case study, Shantou University, Shantou, Guangdong Province, China, October 20, 2009.

Romanowicz, B.A., Shantou University, Seismic signal processing for imaging of the earth's mantle, Shantou University, Shantou, Guangdong Province, China, October 21, 2009.

Romanowicz, B.A., Continental lithospheric structure and formation: New insights from seismic anisotropic waveform tomography, University of Science and Techonology of China, Hefei, China, October 21, 2009.

Romanowicz, B.A., Continental lithospheric structure and formation: New insights from seismic anisotropic waveform tomography, Department of Geophysics, Stanford University, Stanford, CA., January 17, 2010.

Romanowicz, B.A., Continental lithospheric structure and formation: New insights from seismic anisotropic waveform tomography, Brown University, Providence, RI, February 25, 2010.

Romanowicz, B.A., Introduction to normal modes and surface waves, CIDER 2010 Summer Program, UC Santa Barbara, Santa Barbara, CA, July 1, 2010.

Ryder, I., The secret life of faults: New observations across the spectrum of fault phenomena, The Earth's Crazy Paving: A 21st Century Perspective on Plate Tectonics, University of Leicester, UK, March 13, 2010.

Thomas, A., Tremor-tide correlations and near-lithostatic pore pressure on the deep San Andreas fault, USGS Earthquake Science Center, Menlo Park, CA, April 7, 2010.

Awards

Barbara Romanowicz

2009 Inge Lehmann Medal
Li Ka Shing Foundation Fellowship for Women, Fall 2009
Miller Professor, Spring 2010

Panels and Professional Service

Richard M. Allen

Chair, Amphibious Array Steering Committee (for the NSF Cascadia Initiative)
providing guidance to NSF for the onshore-offshore community seismic experiment
Chair, IRIS PASSCAL Standing Committee
Co-Chair, Community Workshop "Earth Dynamics: Experiments with Portable
Ocean Bottom Seismometers," September 2010
Guest Editor, Seismological Research Letters, Special Issue: Application of earthquake
early warning around the world. Published September 2009.

Roland Bürgmann

Associate Editor, Bulletin of the Seismological Society of America
Editorial Advisory Board, Eos
Editorial Board, Earth and Planetary Science Letters
Member, SSA Board Of Directors
Member, EarthScope PBO Standing Committee
Vice-chair, WInSAR Standing Committee
Co-chair, EarthScope Thematic Working Group on Crustal Strain and Deformation

Douglas S. Dreger

Reviewer for Journal of Geophysical Research
Reviewer for Bulletin of the Seismological Society of America
Reviewer for Physical Review Letters
Cosmos Board of Directors

Margaret Hellweg

Member, CISN Program Management Committee
Member, CISN Standards Committee
Member, CISN Steering Committee
Member, CISN Outreach Committee
Member, ANSS Performance Standards Committee
Member, 1868 Commemoration Committee
Member, 1868 Commemoration Executive Committee
Chair, 1868 Committee for Developing Education and Outreach Materials and Programs
Member, Bay Area Earthquake Alliance Committee
Member, Bay Area Earthquake Alliance Executive Committee
Member, Editorial Board of Journal of Volcanology and Geothermal Research

Douglas S. Neuhauser

Chair, Standards Group, California Integrated Seismic Network (CISN)
Acting Member, CISN Program Management Committee

Barbara Romanowicz

Chair, AGU Fellows Committee in December 2009
Chair, CISN Steering Committee
Member, National Earthquake Prediction Evaluation Council
Member, CIDER Steering Committee
Reviewing Editor, Science
Member, Advisory Committee, Institute of Geophysics, Academia Sinica, Taiwan
Member, Scientific Advisory Committee, Geoscope Program (France)
Member, Organizing team, CIDER Summer program at KITP, Santa Barbara (CA), June 12-July 17, 2010
Panelist, USGS Northern California Workshop, Menlo Park, CA, January 27, 2010
Panelist, IRIS Workshop, Snowbird, UT, June 8, 2010

Taka'aki Taira

Member, California Integrated Seismic Network, Standards Committee
Member, California Integrated Seismic Network, ShakeMap Working Group
Member, Plate Boundary Observatory, Data Working Group

Appendix II
Seminar Speakers 2009-2010

LOWELL MIYAGI
UC Berkeley
"Deformation and Texture Development in Lower Mantle Mineral Phases: Implications for Deep Earth Anisotropy and Dynamics"
Tuesday, August 25, 2009

INGRID JOHANSON
UC Berkeley
"Stable and transient motion on Kilauea's south flank from InSAR Persistent Scatterers"
Tuesday, September 1, 2009

DAVID GUBBINS
UC Berkeley
"Is the inner core melting?"
Tuesday, September 8, 2009

SUSAN SCHWARTZ
UC Santa Cruz
"Slow Slip and Tremor in the Northern Costa Rica Seismogenic Zone"
Tuesday, September 15, 2009

ANTHONY SLADEN
California Institute of Technology
"The 2007 Pisco earthquake and the new data generation – Exploring the various stages of a seismic cycle"
Tuesday, September 22, 2009

JOHN HERNLUND
UC Berkeley
"Melt Buoyancy and Retention in Earth's Upper Mantle"
Tuesday, September 29, 2009

WENDY MAO
Stanford University
"Anisotropy of materials in the Earth's core and core-mantle boundary"
Tuesday, October 6, 2009

No seminar
Tuesday, October 13, 2009

AARON WECH
University of Washington
"Cascadia Tremor"
Tuesday, October 20, 2009

TAKA UCHIDE
UC San Diego
"Scaling of Earthquake Rupture Growth in Parkfield Area"
Tuesday, October 27, 2009

YEHUDA BOCK
UC San Diego
"California Real Time (GPS) Network: Earthquake Early Warning and Detection of Strain Transients"
Tuesday, November 3, 2009

Ben Andrews
University of Texas at Austin
"Magmatic Recharge Events and Long-Term Storage Conditions at El Chichón Volcano, Chiapas, Mexico"
Tuesday, November 10, 2009

CHUCK WICKS
USGS Menlo Park
"L-Band Interferometry Studies of Two Remote Volcanic Centers in Chile and Papua New Guinea"
Tuesday, November 17, 2009

BOB NADEAU
Berkeley Seismological Laboratory
UC Berkeley
"Nonvolcanic Tremor Evolution and the San Simeon and Parkfield, California Earthquakes"
Tuesday, November 24, 2009

PAUL SEGALL
Stanford University
"Mechanical Models of Slow Slip Events and the Controls on Fast Versus Slow Slip"
Tuesday, December 1, 2009

JEANNE HARDEBECK
USGS Menlo Park
"Seismotectonics of the California Central Coast"
Tuesday, December 8, 2009

No seminar
Tuesday, January 26, 2010

STUART RUSSELL
UC Berkeley (EECS)
"Treaty Monitoring by Vertically Integrated Seismic Analysis"
Tuesday, February 2, 2010

FRED POLLITZ
USGS Menlo Park
"Tectonics of the Western United States Illuminated by Seismic Surface Wave Tomography"
Tuesday, February 9, 2010

CHRIS KINCAID
University of Rhode Island
"Modeling the Evolution of Mantle Circulation and Transport in the Cascades-Yellowstone Subduction System: The Search for the Magic Bullet of Plumes"
Tuesday, February 16, 2010

ELIZABETH HEARN
University of British Columbia
"Postseismic and Interseismic Deformation Along the North Anatolian Fault: The Possible Role of Transient Rheology"
Tuesday, February 23, 2010

YINGCAI ZHENG
UC Santa Cruz
"Imaging Small-scale Heterogeneities by Transmitted Seismic Body Waves"
Tuesday, March 2, 2010

PASCAL AUDET
UC Berkeley
"Supercontinent Cycle: The Role of Plate Strength"
Tuesday, March 9, 2010

CHAINCY KUO
Caliper Life Sciences
"Imaging Biological Function with Bioluminescence and Fluorescence Tomography"
Tuesday, March 16, 2010

NO SEMINAR
Tuesday, March 23, 2010

NO SEMINAR
Tuesday, March 30, 2010

JIE (JACKIE) LI
University of Michigan
Compres distinguished speaker
"Viewing deep inside the Earth with synchrotron X-rays"
Tuesday, April 6, 2010

HERBERT HUPPERT
University of Cambridge
"The Fluid Mechanics of Carbon Dioxide Sequestration"
Tuesday, April 13, 2010

NO SEMINAR
Tuesday, April 20, 2010

ANNIE KAMMERER
US Nuclear Regulatory Commission
"Assessing Seismic Hazard and Risk for US Nuclear Power Plants"
Tuesday, April 27, 2010

GISELA VIEGAS FERNANDES
LBNL
"Source scaling of eastern North America earthquakes"
Tuesday, May 4, 2010

Berkeley Seismological Laboratory
Organizational Chart
2009-2010

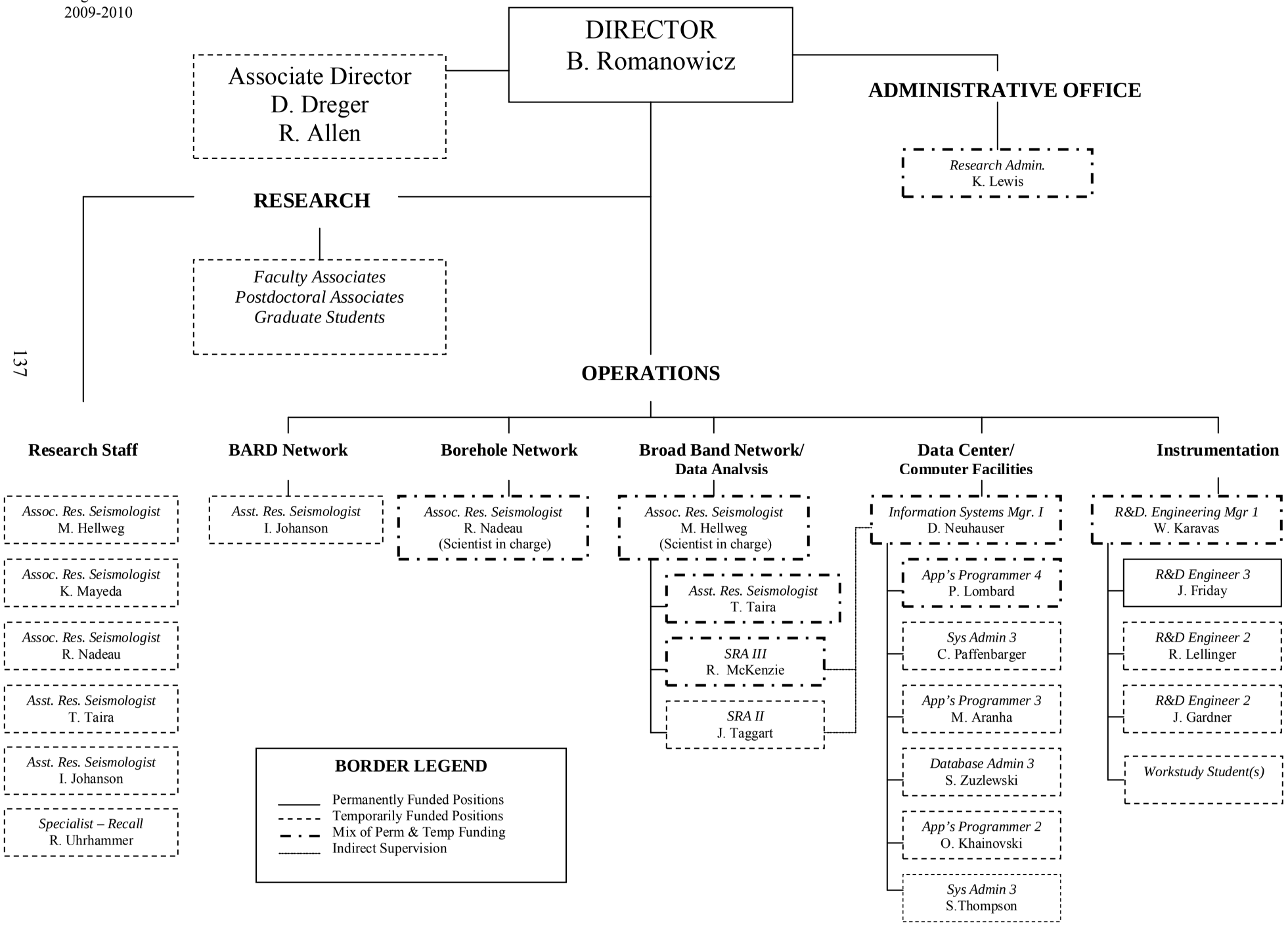

Revised 6/17/10